



TECHNISCHE UNIVERSITÄT MÜNCHEN

Fakultät Chemie

Lehrstuhl für Biotechnologie

**Sip1, a Unique Small Heat Shock Protein
of the Nematode *Caenorhabditis elegans***

- a Structural and Functional Characterization

Tilly Thea Fleckenstein

Vollständiger Abdruck der von der Fakultät für Chemie der Technischen Universität München zur Erlangung des akademischen Grades eines

Doktors der Naturwissenschaften (Doctor rerum naturalium)

genehmigten Dissertation.

Vorsitzender : Univ.-Prof. Dr. Tobias Gulder

Prüfer der Dissertation : 1. Univ.-Prof. Dr. Johannes Buchner

2. Univ.-Prof. Dr. Michael Groll

Die Dissertation wurde am 10.09.2014 bei der Technischen Universität München eingereicht und durch die Fakultät für Chemie am 17.10.2014 angenommen.

ZUSAMMENFASSUNG

Sip1 ist ein kleines Hitzeschock-Protein aus dem Modellorganismus *Caenorhabditis elegans*, welches nur in Oozyten und Embryonen des Fadenwurms gebildet wird. Seine *in vivo*- und *in vitro*-Charakterisierung soll den Einblick in Mechanismus, Regulierung und Substrat-Präferenzen dieser speziellen, klinisch bedeutsamen Klasse an molekularen Chaperonen vertiefen, die die korrekte Faltung von Proteinen in der Zelle gewährleisten.

Im Zuge der Doktorarbeit wurde die Kristallstruktur des Sip1-32-mers bestimmt, sowie die 3D-Strukturen von Sip1 als 32-mer, 28-mer und 24-mer mittels Kryoelektronenmikroskopie rekonstruiert. Durch Negativkontrast-Elektronenmikroskopie, analytische Ultrazentrifugation und Circular dichroismus-Spektroskopie konnte gezeigt werden, dass die Größenverteilung von Sip1 sowie seine Stabilität gegenüber erhöhten Temperaturen pH-abhängig sind. Bei aziden pH-Bedingungen, wie sie in Nematoden-Eiern vorkommen, dissoziiert Sip1 zu kleineren Oligomeren. Gleichzeitig nimmt seine Aktivität als molekulare Chaperone zu, entfaltende Proteine in Lösung zu halten und ihre unspezifische Aggregation zu verhindern. Sip1 bindet eine Vielzahl verschiedener Proteine, viele davon mit wichtiger Funktion für den Embryo. Die nächsten Verwandten von Sip1, die Kerngruppe der Hsp16-Familie in *C. elegans*, sind nur durch Stressbedingungen induzierbar. Sie werden nicht im Frühstadium der Embryonalentwicklung exprimiert und weisen ein Aktivitäts-Optimum bei den neutralen bis leicht basischen pH-Werten vor, die im Larven- und adulten Stadium des Fadenwurms auftreten. Da sich zudem ihr Substratspektrum mit dem von Sip1 nur zum Teil überschneidet, können sie das Fehlen von *sip1* im Deletionsstamm nicht kompensieren, was sich in dessen kurzlebigen und Hitze-sensitiven Phänotyp widerspiegelt.

Sip1 sichert somit das Überleben von Stresssituationen und gewährleistet Protein-Homöostase als einziger präsender Vertreter seiner Klasse in einem Umfeld rapider Zellteilungen und intensiver Proteinbiosynthese.

Diese Arbeit stellt die erste detaillierte Untersuchung eines auf ein einziges Entwicklungsstadium beschränkten Hitzeschock-Proteins dar. Meine Resultate offenbaren neue Aspekte der strukturellen Organisation von kleinen Hitzeschock-Proteinen im Allgemeinen und erweitern das Repertoire an regulatorischen Konzepten innerhalb eines vielzelligen Organismus'.

ABSTRACT

Sip1 is a small heat shock protein (sHsp) from the model organism *Caenorhabditis elegans* which is only produced in the oocytes and embryos of the nematode. It was characterized *in vivo*- and *in vitro* in order to afford insight into mechanism of action, regulation and substrate preferences of this special, clinically relevant class of molecular chaperones which safeguard the correct fold of proteins in the cell.

In the course of this Doctoral Thesis, the crystal structure of 32-meric Sip1 was solved and the 3D structures of the Sip1 32-mer, 28-mer, and 24-mer were reconstructed via cryo-electron microscopy. Using negative stain electron microscopy, analytical ultracentrifugation and circular dichroism spectroscopy, the size distribution as well as thermostability of Sip1 were demonstrated to be dependent on pH. Under acidic pH conditions, such as occur in nematode eggs, Sip1 dissociates into smaller oligomers. Simultaneously, its chaperone activity of keeping unfolding proteins soluble and preventing their unspecific aggregation increases. Sip1 binds a variety of proteins, many of which have an important function in the embryo. The closest homologues of Sip1, the core representatives of the Hsp16 family in *C. elegans*, are solely stress-inducible. They are not expressed in the early embryo and display optimum activity at the neutral to slightly alkaline pH values found in the larval and adult stages of the worm. Since additionally, their substrate spectrum overlaps only partially with that of Sip1, they cannot compensate for the loss of *sip1* in the deletion strain, as evidenced by the strain's short-lived and thermosensitive phenotype.

Thus, Sip1 ensures stress survival and protein homeostasis as the sole member of its class present in an environment characterized by rapid cell divisions and intensive protein biosynthesis.

This work represents the first detailed analysis of a sHsp dedicated to a single developmental stage. My results reveal new aspects of structural organization of sHsps in general and expand the repertoire of regulatory mechanisms within a multicellular organism.

Table of Contents

<u>1. Introduction.....</u>	<u>1</u>
1.1 Protein Folding.....	2
1.2 Molecular Chaperones	4
1.2.1 ATP-Dependent HSPs.....	5
1.2.2 Small Heat Shock Proteins.....	7
1.2.2.1 sHsp Function	7
1.2.2.2 sHsp Structure and Activation	8
1.2.2.3 sHsp Implication in Diseases	11
1.2.2.4 sHsp Appearance in Nature.....	12
1.3 The Model Organism <i>Caenorhabditis elegans</i>.....	12
1.3.1 Anatomy and Life Cycle	12
1.3.2 Advantages and Scientific Uses as Model Organism	15
1.4 Stress Response and sHsps of <i>C. elegans</i>	17
1.4.1 UPR, Skn1, Hsf1 and TOR.....	17
1.4.2 The Daf2/Daf16 Pathway.....	19
1.4.3 sHsps in <i>C. elegans</i>	25
1.4.3.1 Hsp12 Family and Related sHsps.....	25
1.4.3.2 Hsp16 Family	27
1.4.3.3 Sip1	30
<u>2. Objective</u>	<u>32</u>
<u>3. Results</u>	<u>33</u>
3.1 Alignment of the sHsps of <i>C. elegans</i>.....	33
3.2 Expression and Purification of Hsp16 Proteins.....	35
3.3 Buffer Screen.....	36
3.4 Structural Characterization	39
3.4.1 Secondary Structure and Stability Analyses	39
3.4.2 Quaternary Structure of Sip1	43
3.4.3 Crystallization of Sip1	47

3.4.3.1	Seleno-Methionine Substitution	47
3.4.3.2	Truncated Sip1	48
3.4.3.3	Full-Length Sip1	49
3.5	Investigation of the Oligomerization Switch	53
3.5.1	Sip1 H111/139 Double Mutant	53
3.5.2	Sip1-ACD and Sip1/ α B-Crystallin Chimaera	55
3.6	Functional Characterization	59
3.6.1	Chaperone Activity Assays – Comparison of sHsps	59
3.6.2	Refolding of MDH by Sip1	67
3.7	Expression Patterns of Sip1 and Hsp16	68
3.7.1	Western Blot	68
3.7.2	Fluorescence Microscopy	70
3.8	<i>in vivo</i> Importance of Sip1	72
3.8.1	Thermotolerance in <i>E. coli</i>	72
3.8.2	Lifespan Determination of <i>sip1</i> Deletion Nematodes	74
3.8.3	Thermotolerance Analysis	74
3.9	<i>in vivo</i> Substrates of Sip1 and Hsp16.2	75
<u>4.</u>	<u>Discussion</u>	<u>81</u>
4.1	pH-dependent Structure of Sip1	81
4.2	Function of Sip1, pH-Dependency, and Comparison with Other sHsps	87
4.3	<i>in vivo</i> Substrates of Sip1 vs. Hsp16.2	90
<u>5.</u>	<u>Summary and Outlook</u>	<u>95</u>
<u>6.</u>	<u>Materials and Methods</u>	<u>99</u>
6.1	Materials	99
6.1.1	Chemicals	99
6.1.2	<i>C. elegans</i> Strains and Media	99
6.1.3	<i>E. coli</i> Strains and Media	100
6.1.4	Cloning	101
6.1.5	Protein Purification and Buffers	102
6.1.6	Proteins	103
6.1.7	Gel-Electrophoresis and Immunodetection	104
6.1.8	Liquid Chromatography - Mass Spectrometry	105

6.1.9	Crystallography	105
6.1.10	Microscopy	105
6.1.11	Spectroscopy	106
6.1.12	Centrifuges	106
6.1.13	Further Equipment and Materials.....	106
6.1.14	Software and Online Databases.....	107
6.2	Methods.....	107
6.2.1	Molecular Biology Methods	107
6.2.2	Protein Expression and Purification	108
6.2.3	Crystallography	110
6.2.4	Electron Microscopy.....	112
6.2.5	Analytical Ultracentrifugation	112
6.2.6	<i>in vitro</i> Protein Analyses	113
6.2.6.1	UV/Vis-Spectroscopic Analyses.....	113
6.2.6.2	Circular Dichroism Analyses of Secondary Structures	114
6.2.6.3	Chaperone Activity Assays.....	115
6.2.6.4	Holdase Function of Sip1.....	116
6.2.6.5	Interaction of Sip1 and the Hsp70/40 System.....	116
6.2.7	Co-Immunoprecipitation	116
6.2.8	<i>C. elegans</i> Handling.....	118
6.2.9	SDS-PAGE and Western Blots	119
6.2.10	Fluorescent Reporter Injection	120
6.2.11	Life Span Assay	120
6.2.12	<i>C. elegans</i> Thermotolerance Assay.....	121
6.2.13	<i>E. coli</i> Thermotolerance Assays.....	121
7.	<u>Acknowledgments</u>	<u>122</u>
8.	<u>Publication</u>	<u>123</u>
9.	<u>References.....</u>	<u>124</u>



Image: <http://wormclassroom.org/>

1. INTRODUCTION

Since the dawning of mankind, human lifespan has greatly increased, slowly at first due to evolutionary favoritism of reproductive success rather than longevity, then explosively within the last century due to man's ingenuity in improving hygiene, medicine and nourishment (Fig. 1.1).

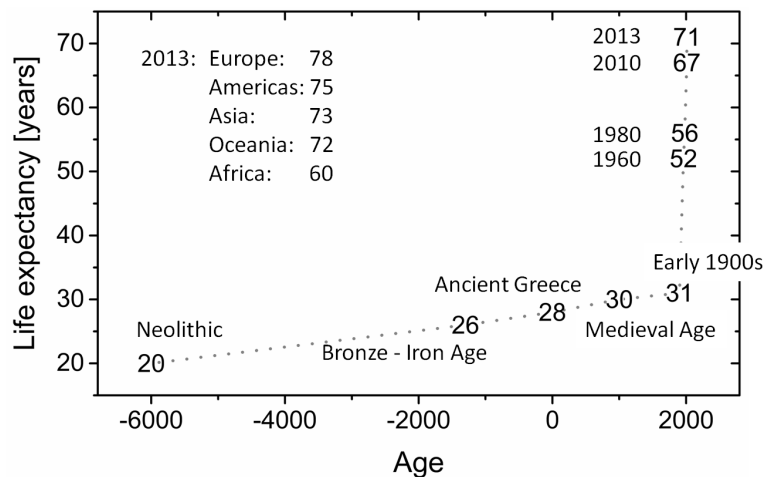
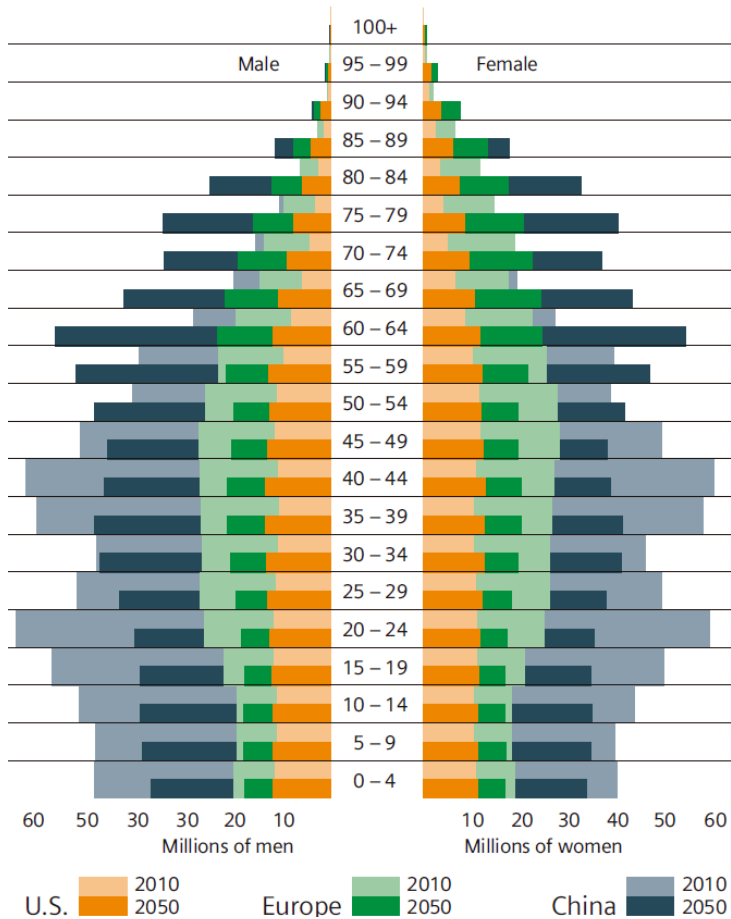


Fig. 1.1: Estimates of mankind's global life expectancies throughout the ages. Data according to [1-3].

In developed countries, the age pyramid is being turned upside down. For instance, in 1985, Federal President von Weizsäcker sent 899 congratulatory letters to German centenarians, while his successor Köhler had to pen 4.360 jubilee greetings in 2005 [4]. Today, there are more than 13,000 Germans of 100 or more years of age. The number of people aged 80 or more has increased by 122 % from 2000 to 2010, and is estimated to further rise by 51 % until 2030. Every second child born in Germany after 2000 stands a fair chance of turning 100 [5].

This demographic change (Fig. 1.2) is accompanied by much-feared, diverse pathologies like senile dementia, creating an urgent need for therapies.

While old age is the greatest risk factor of fatal neurodegenerative diseases such as Alzheimer's (AD), lifespan enhancement need not come at the cost of debilitating tradeoffs. There are mutant strains of worms, flies, and mice that are long-lived and remain youthful and healthy for far longer than normal [6]. Drugs of a corresponding effect could conceivably alleviate various diseases simultaneously, by combating aging. For instance, the immunosuppressant rapamycin extends the lifespan of mice even when administered late in life, and insulin/IGF1 pathway antagonists are anti-cancer drugs which could also prolong youthfulness and lifespan [6].



Age-related diseases as well as many other human ailments are caused by the accumulation of misfolded, aggregated proteins within cells, which results in loss of function and creates cell-toxic waste. Ensuring proper protein folding, and thus, function, even during cellular stress may well be the key to keep these pathologies at bay [7].

Fig. 1.2: Population distribution in 2010, prognosis for 2050 [8].

1.1 PROTEIN FOLDING

In order to fulfill their role within the cellular network, most proteins must adopt a defined 3D shape, i.e. their native conformation. Dictated by their amino acid (aa) composition [9], the linear polypeptide chains (“primary structure”) form α -helices, β -sheets, β -turns, etc., which are stabilized by hydrogen bonds. The relative orientation of these secondary structure elements is designated tertiary structure.

The native fold of a protein represents the minimum in free energy and a thermodynamically stable state (Fig. 1.3). Thus, most newly translated proteins fold spontaneously [10]. The possible folding trajectories can encompass population of intermediate states, nuclear growth (a slow formation of a secondary structure core followed by a rapid, concerted step to attain full native state), hydrophobic collapse (hydrophobic, tertiary contacts between remote residues preceding secondary structure adoption), or nucleation-condensation (initial nucleus, then simultaneous secondary and tertiary structure formation) [11-13].

However, molecules can become trapped as folding intermediates, i.e. local minima in the folding energy landscape, and unspecific interactions during physiological protein folding may entail irreversible misfolding [14, 15]. Proteins unable to attain their correct tertiary structure usually expose hydrophobic residues to the surface and the polar surroundings, and are prone to aggregate [16].

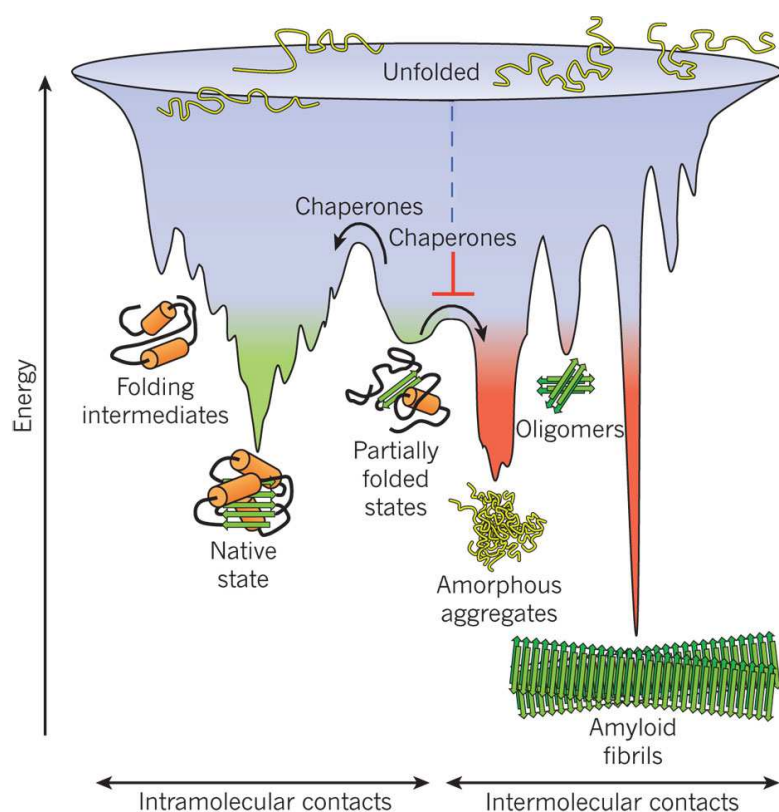


Fig. 1.3: Scheme of the funnel-shaped free-energy surface that proteins explore as they move towards the native state (green) by forming intramolecular contacts. The ruggedness of the free-energy landscape results in the accumulation of kinetically trapped conformations that need to traverse free-energy barriers to reach a favourable downhill path. *In vivo*, these steps may be accelerated by chaperones. When several molecules fold simultaneously in the same compartment, the free-energy surface of folding may overlap with that of intermolecular aggregation, resulting in the formation of amorphous aggregates, toxic oligomers or ordered amyloid fibrils (red). Fibrillar

aggregation typically occurs by nucleation-dependent polymerization. It may initiate from intermediates populated during *de novo* folding or after destabilization of the native state (partially folded states) and is normally prevented by molecular chaperones. Figure and caption taken from [15].

Degradation of these non-functional proteins – up to 30 % of all newly synthesized proteins – exacts of the cell a high toll in terms of energy [17]. Also, proteins retain the conformational flexibility needed for their functionality at the cost of low thermodynamic stability. Even mild cellular stresses, e.g. a few degrees above the physiological temperature, put them at risk to unfold and precipitate, and in some cases, form toxic fibrillar aggregates [18]. Thus, the cell employs molecular chaperones to assist the folding process in order to maintain proteostasis (protein homeostasis) [15, 19, 20].

1.2 MOLECULAR CHAPERONES

Molecular chaperones pertain to an evolutionary old, ubiquitous family of proteins. Besides folding of polypeptide chains directly at the ribosome, many chaperones maintain vital functions for their organisms even after protein biosynthesis [21, 22]: They preserve the native structure of their substrates and keep them soluble, aid the refolding of denatured proteins, target irreversibly damaged proteins for degradation and are capable of dissolving protein aggregates even when already precipitated [23].

Conversely, over-expression of chaperones is mainly induced by situations of stress, which are a persistent threat to life [24-29]. This critical, rapid cellular defensive mechanism is called the heat-shock response. Besides the unfolding of proteins, heat shock is detrimental to nuclear processes such as RNA processing, and decreases translation [30, 31]. It damages the cytoskeleton to the point of actin, tubulin and intermediary network collapse [31]. Heat shock further effects mis-localization of organelles, Golgi and endoplasmic reticulum (ER) fragmentation, the breakdown of intracellular transport, and a decline in the number of lysosomes as well as mitochondria [29-31]. This leads to the depletion of ATP levels. Moreover, an increased membrane permeability results in acidification and ion homeostasis disturbances [29]. These combined insults cause cell cycle arrest, growth stagnation and, ultimately, even cell death [29, 32]. However, chaperones induced by milder stresses can contribute to an acquired tolerance towards otherwise lethal stresses (which need not be caused by the same stressor), in what is called hormesis [29].

Hsps are essential for constant prevention of aggregation and precipitation under physiological conditions, as well. In an eukaryotic cells, the rate of protein synthesis can amount to 60,000 proteins per minute, and cytosolic protein concentration to 400 mg/ml [33]. Under these “molecular crowding” conditions, especially large, multidomain proteins would not fold on a biologically relevant timescale without the help of molecular chaperones [15, 34]. This strategy for surmounting cellular stress is apparent in almost all living beings [35].

1.2.1 ATP-DEPENDENT HSPTS

According to their molecular weight, molecular chaperones are categorized into highly conserved families: Hsp100, Hsp90, Hsp70/Hsp40, Hsp60/Hsp10 and small heat shock proteins (sHsps) [15, 18, 25, 36-38]. Frequently, Hsps form part of multi-chaperon complexes, such as the Hsp70/Hsp90 system [39]. Herein, Hsp70 (DnaK in prokaryotes) with the help of nucleotide exchange factors (NEFs), co-chaperones and Hsp40 (DnaJ) facilitates the transfer of substrates onto Hsp90 [40]. With an abundance of 1-2 %, members of the Hsp90 chaperone family range among the most abundant of all cellular proteins, and are even further upregulated by stress [18, 41, 42]. After processing by Hsp90 and its co-chaperones, a natively folded target protein leaves the ATP-dependent catalytic cycle (Fig. 1.4). Substrates of Hsps show a considerable variety of characteristics, both in sequence and structure, which implies a low binding specificity. For instance, Hsp90 is a hub for the control of many eminent signalling pathways. Its ample client range includes important regulator proteins such as (cancer-relevant) kinases, transcription factors (including its own, heat shock factor-1, Hsf1), and steroid hormone receptors (like the major therapeutic target glucocorticoid receptor) [15, 43, 44].

Hsp70 proteins display an even greater promiscuousness in clients, interacting with nascent and newly synthesized, as well as stress-damaged polypeptides, and assisting in translocation and secretion [45-48]. They recognize a motif consisting of seven, mainly hydrophobic amino acids, which occurs every 50 - 100 residues in an average protein, and whose surface exposure indicates the protein's risk of aggregation [15]. The delivery of non-native clients by Hsp40 to Hsp70 and their subsequent processing in the ATPase cycle are described in Fig. 1.4. Hsp70's many clients include clathrin [49], kinases (e.g., c-Raf, involved in signal transduction and a target for anticancer drugs)[50], enzymes instrumental in DNA replication [51], and various transcription factors (e.g., the tumor-suppressor p53 and Hsf1) [52, 53].

Downstream of this system, the cylindrical, cage-like chaperonins (Hsp60 in mitochondria, GroEL in bacteria with the lid proteins Hsp10/GroES, and TRiC/CCT in eukaryotic cytosol) enclose and fold individual substrates that are still unfolded after the Hsp70 cycle, such as actin and tubulin [15].

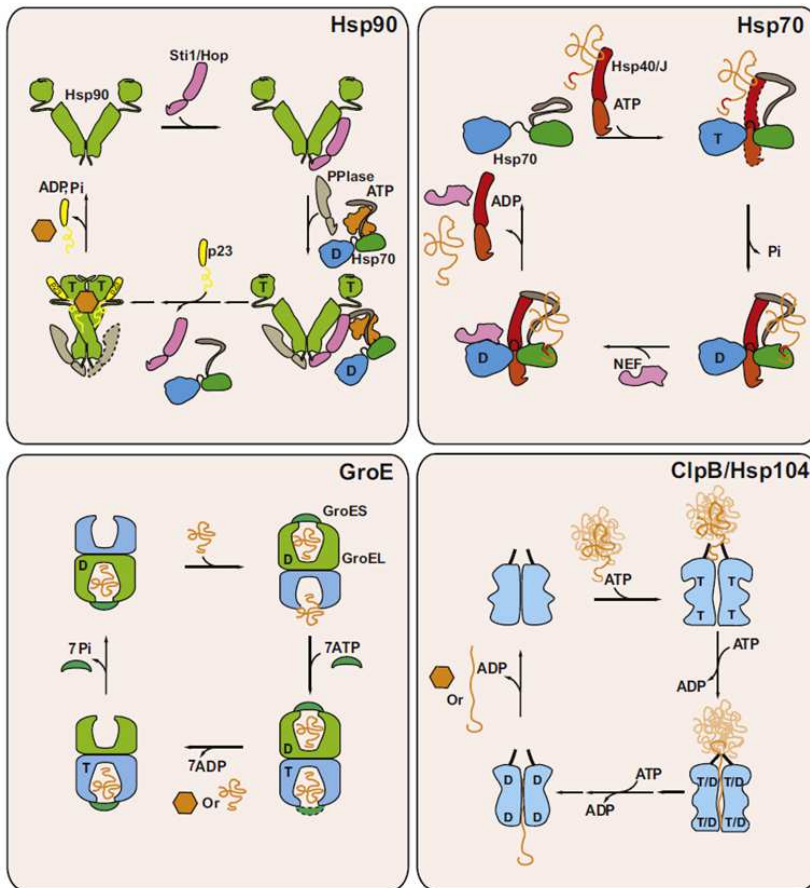


Figure 1.4: Molecular Chaperone Mechanisms

Molecular chaperones bind proteins in nonnative conformations. The shift from the high-affinity binding state to the low-affinity release state is often triggered by ATP binding and hydrolysis.

Hsp90: More than a dozen cochaperones of Hsp90 exist in eukaryotes, which seem to modulate the system. One of them, Sti1/Hop, binds both Hsp70 and Hsp90 and at the same time inhibits Hsp90s ATPase (in yeast). In this complex, which also contains an additional PPIase cochaperone, the substrate protein is transferred from Hsp70 to Hsp90. Sti1/Hop is released once Hsp90 binds nucleotide and a further cochaperone (p23). In

contrast to other chaperones, the protein in complex with Hsp90 is assumed to be bound and released as a structured intermediate.

Hsp70: The activating Hsp40/J-protein can bind the nonnative protein and deliver it to Hsp70. Hsp40 forms a complex with Hsp70 and stimulates its ATPase. It may also modulate the conformation of Hsp70 to stabilize a substrate protein-accepting state. The NEF will induce the exchange of nucleotide. This further accelerates the ATPase cycle. The substrate protein is released presumably in a nonnative form.

GroE/Hsp60: The GroE machinery in bacteria, mitochondria, and chloroplasts consists of two identical rings that enclose a central cavity each. Nonnative protein is bound by the apical domains of the rings, and upon binding of ATP and the cochaperone GroES, the protein is encapsulated and released into the cavity. ATP hydrolysis in one ring results in the release of GroES and substrate protein from the opposite ring. During encapsulation the protein may fold partially or completely.

ClpB/Hsp104: In bacteria and yeast, this chaperone is able to dissolve aggregates by actively pulling proteins through a central channel of the hexameric structure. During passage through the chaperone complex, the substrate protein is unfolded. Refolding can occur upon release, and, to some extent, in cooperation with other chaperones.

T = ATP, D = ADP. Figure and legend taken from [18].

Hsp100 superfamily members (Clp proteins in bacteria) re-solubilize proteins from aggregates, which then are either refolded into their functional conformation by means of the Hsp70/40- [54] and sHsps systems [55], or degraded by proteases [56]. As of now, no representative of the Hsp100 family is known in *Caenorhabditis elegans*. Instead, members of the Hsp70/40 superfamilies function as disaggregation machinery, as well

[57]. *C. elegans* encodes only one Hsp90 protein, Daf21, but at least 13 Hsp70 homologues, including the cytosolic, constitutive Hsc70 [58].

An overview of the different chaperone cycles is shown in Fig. 1.4, and also in [15].

1.2.2 SMALL HEAT SHOCK PROTEINS

sHsps are distinguished from the aforementioned chaperones by virtue of their diminished monomeric size (12-43 kDa), ATP-independency and structural diversity within the family [24, 59].

1.2.2.1 SHSP FUNCTION

Small heat-shock proteins recognize and bind to hydrophobic protein patches resulting from amino acid side chains exposed to the surface of non-native proteins, keeping them in a refolding-competent state [60-62]. Thus, sHsps initially prevent irreversible aggregation by way of stable complexation. They act as holdases, rather than foldases: On their own, they cannot effect refolding of bound proteins, for they lack ATPase activity [63]. It is only in concerted action with Hsp70/40 [64, 65] or Hsp100 [23, 55, 66] that release and ATP-catalyzed re-naturation is facilitated (Fig. 1.5).

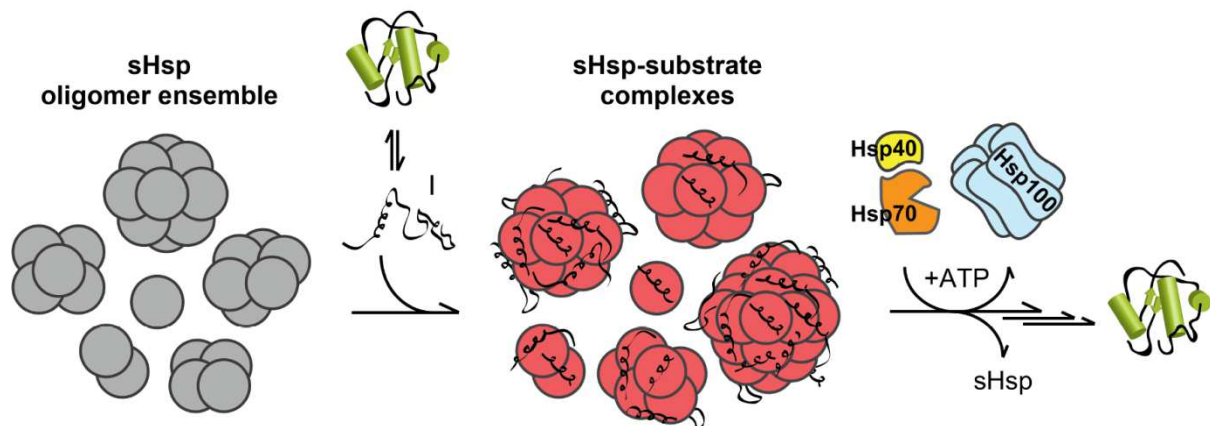


Figure 1.5: Model of chaperone function of small heat-shock proteins. Proteins that are (partially) unfolded by proteotoxic stress (I: folding intermediate) risk aggregation unless they are bound by activated heat shock proteins. By means of complexation, sHsps keep their stress-denatured substrates soluble and transfer them to the Hsp70/40 system or Hsp100 for ATP-driven refolding. Being dynamic in nature, sHsps can form oligomers and exchange subunits. Taken from Haslbeck et al. (2014), in press.

Their diverse substrates are basically any proteins which have lost their tertiary structure, ranging from unfolded to molten globule states [60, 62]. Substrates can be 3 -

100 kDa in mass [60, 65, 67], including peptides and oligomeric enzymes [65, 68]. In experiments with yeast [68, 69] and cyanobacteria [70], approximately one third of the cytosolic proteins was found in sHsps-substrate complexes upon stress.

Most organisms encode more than one sHsp [35], and it is not uncommon for two or more sHsps to be expressed in the same tissue or compartment, like many of the 16 *C. elegans* sHsps (see Chapter 1.4.3), the two α -crystallin isoforms in the eye lens or the typical bacterial two component sHsps system [35, 71, 72]. The substrate portfolio of sHsps may overlap, but need not be identical to that of other sHsps present, as demonstrated for the two *S. cerevisiae* sHsps, Hsp26 and Hsp42 [73]. Compared to the processing capacity of other molecular chaperones, sHsps are more efficient, binding up to one substrate molecule per sHsp subunit [68, 74, 75]. However, sHsps have been found to precipitate alongside their substrates [76-78]. For instance, the aptly named inclusion body-associated protein IbpB from *E. coli* [71] enters into an insoluble complex with non-native substrates when overloaded, which occurs frequently *in vivo* [78]. In this manner, sHsps are capable of promoting the elimination of protein aggregates, as well. Unfortunately, the enhanced survival due to the clearing of aggregates by sHsps has been implicated in causing drug resistance, e.g. in multiple myeloma patient treatment with the proteasome inhibitor Velcade [79].

1.2.2.2 SHSP STRUCTURE AND ACTIVATION

Common to all small heat shock proteins is a central α -crystallin domain (ACD, Fig. 3.1), named after α -A- and α -B-crystallin (CRYAA/CRYAB), the sHsps of the mammalian eye lens [80]. This sequence of 80-100 amino acids is relatively highly conserved considering the typically low homology between sHsps [81]. The flanking N- and C-terminal regions (NTR/CTR) exhibit a broad diversity in length and sequence [25, 35, 72, 82]. For instance, the NTR of *C. elegans* Hsp12.2 is 24 residues long [83], as opposed to 247 aa in *S. cerevisiae* Hsp42 [73].

The crystal structures of 11 sHsps are available to date. In only two of the five X-ray structures that were obtained from the full-length proteins, most of the terminal extensions are fully resolved, which indicates their flexibility. Only five crystal structures were solved of sHsps in an oligomeric state (see Fig. 4.1), even though some of the others are also known to oligomerize [84, 85]. However, all high-resolution structures feature a dimer of two α -crystallin domains. Two super-positioned anti-parallel β -sheets form the

conserved secondary structure of the ACD (Fig. 1.6) [86, 87]. Except for the α -crystallins, HspB1 and HspB6, all sHsp X-ray structures described previously are non-mammalian in origin and share a characteristic arrangement of the monomers [72, 86, 88-96].

In “non-mammalian-like” sHsp monomers, one layer (called here β -sheet 1) is spanned by the β -strands designated no. 2, 3, 9, and 8, and β -strands 4, 5, and 7 combine to form the β -sheet 2. Numbering starts at β 2, since some sHsps contain a short N-terminal β 1-strand. The β -strands are indicated in Fig. 1.6 and in the sHsp alignment (Fig. 3.1); for a scheme, see [97]. Non-mammalian-like ACDs consist of twisted β -strands within uneven β -sheets. Two ACDs combine, one upside-down, along the short side of the β -sheet 2 (“head-to-head”) to form the dimer. Non-mammalian sHsps all possess a flexible linker sequence between their β 6- and β 7-strands. This allows the short β 6-strand to latch alongside, and thus expand, the neighboring monomer’s β 2-sheet [97]. The resulting dimer occupies three roughly parallel planes, with the β 1-sheets forming a central plane and the two β 2-sheets on either side of it.

In contrast, „mammalian-type“ sHsps feature one long β 6+7 strand as part of the extended β -sheet 2 (Fig. 1.6). For dimerization, two ACDs meet, side-by-side, along their β 6+7 strands. This contact surface between two monomers is called the AP (antiparallel) interface. In a highly parallel, planar architecture, both β 1-sheets are on the same side of the β 2-layer spanned by the two adjacent monomers.

The ACD dimer represents the general building block for oligomerization [25, 98-101]. Many sHsps assemble to dynamic oligomers, often dodecamers and 24-mers of 100-200 Å outer diameter (Fig. 4.1), that permanently exchange subunits [25]. Even hetero-oligomer formation has been reported for human CRYAA and -B, HspB1 and *E. coli* IbpA and IbpB [101-103].

The ACD is critical for dimerization, but *per se* is insufficient for oligomerization [88, 104]. For this, (part of) the CTR and the NTR are required [105]. The short CTR contains a conserved I/L-X-I/L (“IXI”) motive, which binds into the hydrophobic groove formed by the β 4- and β 8-strands of an adjacent ACD, tethering the dimers together [106], see also Fig. 3.12. In several of the cited structures, at least some of the NTRs are directed into the sHsps’ cavities, where they as well contribute to oligomer stabilization by way of hydrophobic interactions. Moreover, truncation studies of *C. elegans* Hsp16.2 revealed a loss of chaperone activity together with a failure to oligomerize [105]. The same was

observed for crystallins and HspB1, pointing to the NTR as a requirement for sHsp functionality [101, 107]. While the NTR is widely recognized as pivotal in substrate recognition [108-110], some findings indicate that the CTR is involved in facilitating substrate binding, as well [111, 112].

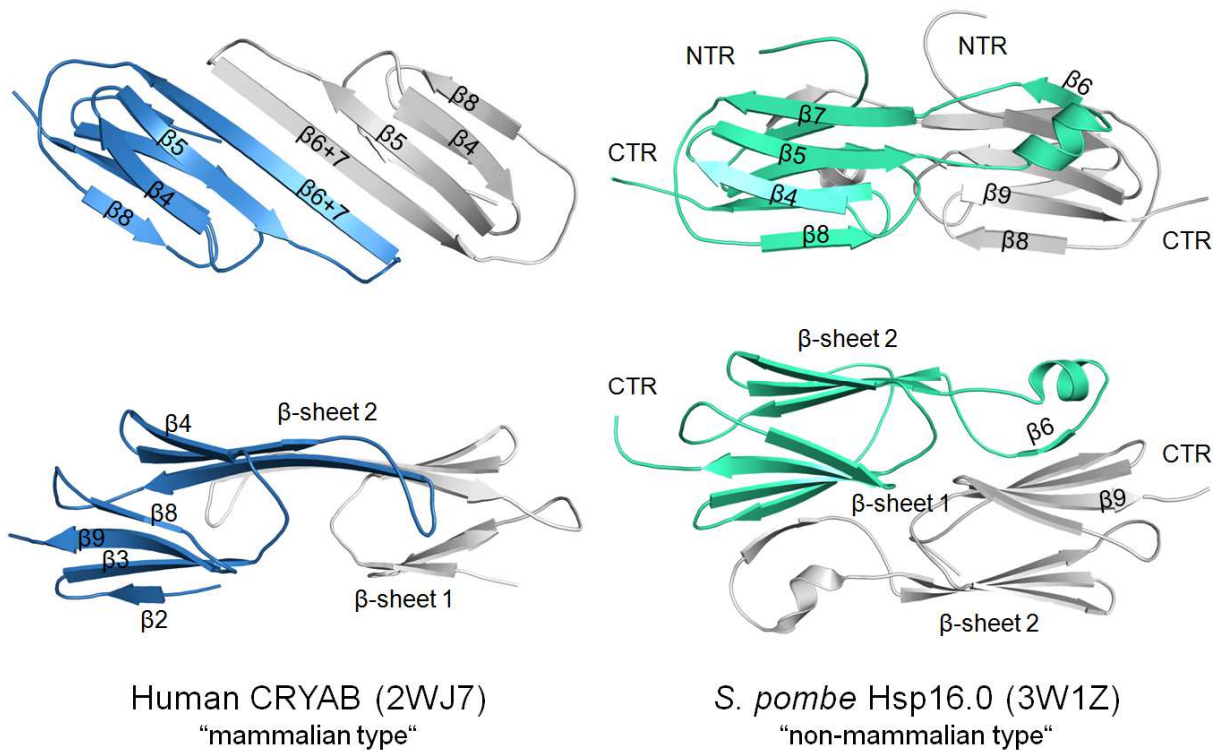


Fig. 1.6: The two structural types of sHsp dimers, represented by α B-crystallin [88] and SpHsp16.0 [90]. Loops are smoothed and termini truncated.

The variable terminal regions steer association to determine the distinct quaternary structures that effect the sHsps' particular properties [113]. As depicted in Fig. 4.1, the results are highly symmetric structures, mainly shaped like hollow spheres or double-ringed barrels [86, 89, 90, 96, 112, 114, 115].

Whereas some sHsps populate one oligomeric state only, others, like α B-crystallin, are polydisperse [92, 98, 112]. According to studies on human Hsp27 [116], α -crystallin [117] and yeast Hsp26 [74, 118, 119]), large ensembles are postulated to act as low-affine, inactive storage forms. Increases in temperature [74, 119, 120], post-translational modifications like phosphorylation [84, 121, 122], or the presence of non-native proteins can prompt the spontaneous re-arrangement of the complex [117, 118] and/or its dissociation into smaller oligomers [116] to become chaperone-active. Substrate binding could thus be facilitated by exposition of affine sites previously buried in the sHsps

complex [116, 123-126], which is consistent with a reported elevated hydrophobicity of several sHsps when stressed [124, 125, 127].

1.2.2.3 SHSP IMPLICATION IN DISEASES

Proteotoxic stress situations evoked by extrinsic or intrinsic factors, i.e. genetic alterations, may exceed the refolding capacities of chaperones. Moreover, Hsps can be rendered non-functional by mutations or posttranslational modifications. If chaperones malfunction, aggregated proteins accumulate to cytotoxic, insoluble plaques. These co-precipitate heat shock proteins, ubiquitin, and other components of the proteasome system, and eventually cause cell death [128]. A plethora of grave diseases is attributed to protein misfolding and aggregation [7, 98, 129, 130]: Prion diseases such as bovine spongiform encephalopathy (BSE) or Alzheimer's disease (AD) are indicated by the gradual death of neurons due to the formation of fibrils in the brain. Plaques in (motor)neurons give rise to muscle function deterioration, e.g. in Chorea Huntington, amyotrophic sclerosis and Morbus Parkinson. Primarily, the ten human sHsps, HspB1 – 10, have been analyzed in this context [131]. sHsp are upregulated in the brains of AD patients [130, 132], and HspB1, -5 and -8 have been shown to interact *in vitro* with amyloid- β proteins, which in the form of A β fibrils in cerebrovascular cells cause AD [133]. Interestingly, three of the four central representatives of the Hsp16 family from *C. elegans* are induced by, and also bind to, the human A β_{42} peptide [134]. High concentrations of Hsp16.2 could suppress toxicity of the A β_{42} peptide in the worm AD model [135].

CRYAA and -B (HspB4 and -5) suppress protein agglomeration in the eye lens, preserving its transparency [136]. Decreases in their chaperone activity or solubility cause cataract and, eventually, blindness [137]. HspB8 is induced by cardiomyopathies, ischaemia and hibernating myocardium, as well as rheumatoid arthritis and autoimmune diseases [7]. Furthermore, sHsps can act as oncoproteins (e.g. HspB8, CRYAB in breast cancer) and are taken into consideration as tumor marker [138]. For a review of sHsp-related ailments, see Sun and MacRae (2005).

While some sHsps (e.g. α -crystallins and HspB1) are also expressed at low levels at ambient conditions, the majority are induced by biological and physical stresses like the eponymous unphysiologically high temperatures, ethanol, acids, heavy metals, oxidants,

endotoxins, interleukin-1, ATP depletion, and hyperosmolarity [139-145]. This permits their use as both potential pharmacological targets and biomarkers.

1.2.2.4 SHSP APPEARANCE IN NATURE

sHsps are ubiquitous. They occur in all organisms except some pathogenic bacteria like *Helicobacter pylori* [25, 35, 107, 146]. In general, higher eukaryotes and plants possess more sHsps than protozoa, prokarya and archaea. Single-cell organisms usually contain one or two sHsps. In the bacterium *Escherichia coli* and the yeasts *Saccharomyces cerevisiae* and *Schizosaccharomyces pombe*, for instance, two sHsps are reported, four sHsps are found in the fruit fly *Drosophila melanogaster* and the zebrafish *Danio rerio*, whereas man has ten, and the nematode *Caenorhabditis elegans* even 16 sHsps [25, 35]. Notably, plants tend to encode the most sHsps. 21, 22, 45, and 50 putative sHsps are found in *Oryza sativa* (rice), *Arabidopsis thaliana* (mouse-ear cress), *Vitis vinifera* (grape wine), and *Populus trichocarpa* (black cottonwood), respectively [35].

Why are there so many sHsps in plants and a small worm compared to other eukaryotes? It may play a role that they cannot escape stress by moving (far) away. In any case, it is unlikely that this many sHsps would share the same expression pattern and substrate profile. Rather, some intriguing specialized niche and functional non-redundancy might be discovered among these organisms' sHsp sets. This notion was put to the test for some of the *C. elegans* sHsps in the present work.

1.3 THE MODEL ORGANISM *CAENORHABDITIS ELEGANS*

1.3.1 ANATOMY AND LIFE CYCLE

C. elegans is a nematode (roundworm) that feeds on microbes in decaying organic matter. It is found in the soil of temperate climate zones [147]. The ~1 mm long nematode is a bilaterally symmetrical, unsegmented pseudocoelomate, i.e. its tube-like body wall consisting of a collagenous cuticle and underlying hypodermis is supported by the internal hydrostatic pressure of a fluid-filled body cavity, the pseudocoelom. While lacking a skeleton, circulation and respiration, this eumetazoon is one of the simplest organisms to possess a nervous system (encompassing 302 head and tail neurons) [147, 148]. Four bands of striated body wall muscles run along the length of the worm to

facilitate its sinuous movement, and nonstriated muscles are located at the pharynx, intestine, rectum and vulva [147]. *C. elegans* feeds through a pharynx, a muscular food grinder and pump connected to the intestine and the excretory system [148].

C. elegans is mainly a hermaphrodite, but male worms (containing only one X-chromosome, X0) exist to ensure genetic variability (Fig. 1.7). They are very rare (0.1 %) [147]. Male nematodes are composed of exactly 1031, and hermaphrodites of 959 somatic cells of well-known, invariant lineage and fate [147, 148]. Males have one gonad, a *vas deferens* for sperm transport, and a tail for holding onto, and mating, with hermaphrodites. This more than triples the number of eggs laid, as opposed to self-insemination of hermaphrodites [148]. Hermaphrodites (XX) produce both oocytes and spermatozoa, and thus can generate genetically identical progeny by self-fertilization. Their two female, somatic, U-shaped gonads comprise the ovaries containing the germ line and oviducts leading to the spermathecae, where the own or male sperm is stored for the fertilization of passing, maturing oocytes. Zygotes are then held in the central uterus where an impermeable eggshell is formed around them, and are expelled thorough the vulva at ~30-cell stage, i.e. at gastrulation, before embryogenesis is completed [147, 148].

Embryogenesis in the nematode progresses in an invariant spatial and temporal pattern over a course of 14 h [147, 149]. Its first phase encompasses zygote cleavages to establish the five somatic founder lineages and the germline founder cell, cell divisions, rearrangements, migrations, and gastrulation. This proliferation results in a spheroid embryo of ~550 cells, organized into the endo-, meso-, and ectoderm germ layers, which give rise to germline and intestine, muscle and pharynx, and hypodermis and neurons, respectively. In the subsequent organogenesis and morphogenesis phase, proliferation ceases almost entirely as development and elongation into a ~560 cell larva with fully differentiated tissues and organs ensues [148-150].

After hatching, the invariant post-embryonic development starts if food is available. The larva proceeds through four larval stages, L1 – L4, which are separated by moults [147, 148]. Gonadogenesis, which starts at ~7 h after hatching, is finished during L4. At the same stage, hermaphrodites produce and store sperm, and only oocytes afterwards [147]. At 45-50 h posthatch (at 22°C), the mature, fertile adult starts laying ~300 eggs over the following 4 days (>1000 eggs if male sperm is available), and then lives for 10-15 more days (Fig. 1.8).

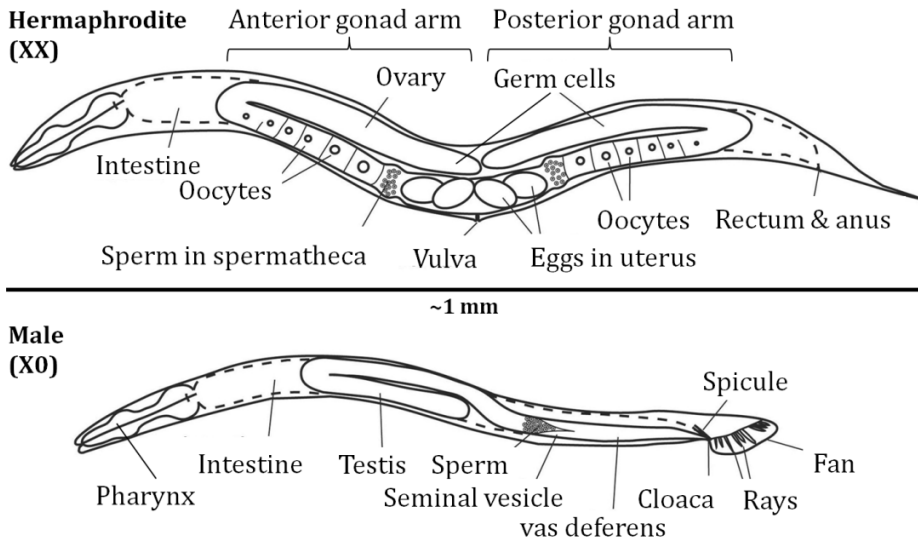


Fig. 1.7: The two sexes of *C. elegans*.

The hermaphrodites and males differ strikingly in overall body size and structures such as the somatic gonad and tail. In both cases, a large part of the nematode is taken up by the reproductive system. Adapted from [151].

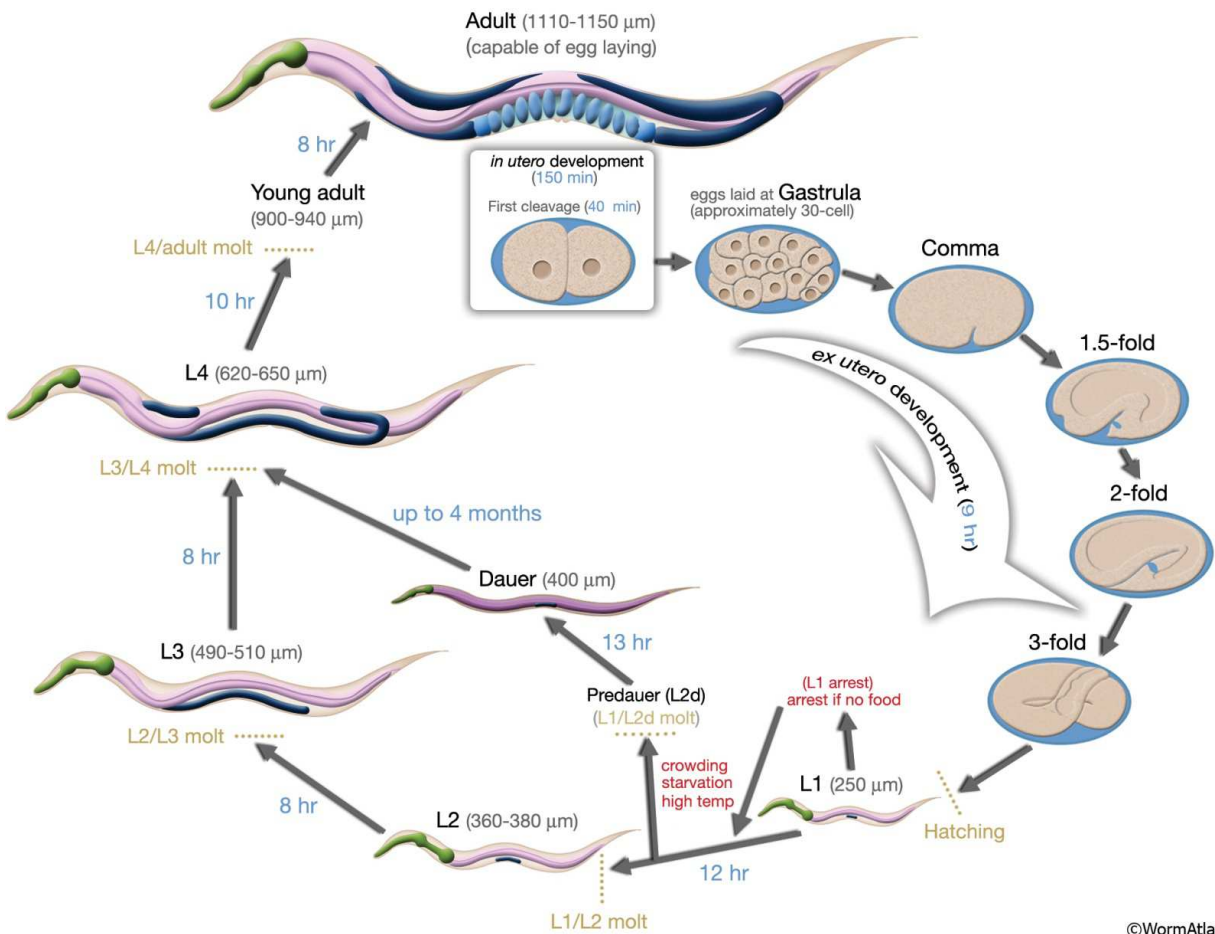


Fig. 1.8: Life cycle of *C. elegans* at 22°C. Taken from [148].

Wt adults carry ~15 eggs inside their uterus constantly [152]. At 20 °C, the wt strain N2 (a 1951 wild isolate from Bristol, UK) has an average life span of 2 - 3 weeks and a life cycle of ~3 days [148, 153].

When challenged by adverse conditions, the tiny worms have little chance of escaping to a more hospitable environment. Therefore, *C. elegans* can arrest development at two checkpoints. Embryos hatching in the absence of food survive up to 10 days as arrested L1, until they can resume feeding [154]. As a primary response to reduced sustenance, elevated temperatures, low levels of oxygen, or a pheromone indicating high population density, late L1 larvae enter an quiescent juvenile stage called dauer [155]. An impermeable cuticle contributes to the stress-resistance of dauer larvae, which survive starvation and desiccation for up to 3 months, expanding normal lifespan by 4 – 10 times [156]. Dauers show reduced movement, respiration and ATP expenditure, and cease feeding. When conditions are again favorable, they re-enter normal development at L4 [157]. Dauers are considered non-aging because diapause duration neither affects their post-dauer lifespan, nor egg production [158]. The propensity to undergo dauer is mediated by 'abnormal dauer formation' (*daf*) genes, particularly those of the insulin/IGF-1 signalling (IIS) pathway [159]. Strong mutations in *Daf2*, an ortholog of the mammalian insulin/IGF-1 receptor (IIR), induce dauer entry, as do low insulin levels in starving early larvae in nature [160]. Notably, weak reduction-of-function mutations of *daf2* or downstream IIS components do not trigger dauer formation but rather increase adult lifespan more than twofold [161]. See Chapter 1.4.2 for details.

1.3.2 ADVANTAGES AND SCIENTIFIC USES AS MODEL ORGANISM

C. elegans was first described in Algeria in 1899 [162], and suggested for genetic research because of its eutely (fixed cell number) and structural simplicity as early as 1948 [163]. In 1963, Sydney Brenner started a first mutagenesis screen on the nematode, which soon established the worm as a widely used model system for animal genetics, (neural and organ) development, apoptosis and behavior [153]. For this, he was awarded the 2002 Physiology Nobel Prize together with John Sulston and Robert Horvitz.

The 100 Mb genome of *C. elegans* consists of 6 chromosomes and a mitochondrial genome. It was sequenced in 1998 as the first multicellular organism and as the second eukaryote after *S. cerevisiae* [164]. Of *C. elegans'* 20,470 protein-coding genes, 60-80 % have human homologs [165]. Findings and protocols are amassed in dedicated online databases such as wormbase.org, wormbook.org, and wormatlas.org.

Caenorhabditis briggsae sequencing was finished in 2003 and more genomes from other related nematodes are under way, allowing for comparative genomics [166]. *C. elegans* can be used as a model system for parasitic worms (albeit with a simple life cycle) since pharmacology and physiology are comparable within the *Nematoda*, and most anthelmintic drugs target the neuromusculature. Parasitic worm infections affect crops, livestock and 2 billion people, i.e. ten times and almost 60 times the number of people suffering from malaria and HIV in 2012, respectively, according to WHO estimates [167]. With its small size, short generation time and large number of offspring, the nematode is easy to propagate. Several million worms per day can be produced in liquid culture with OP50 *E. coli* as nutrient. Animals are maintained on NGM (nematode growth medium) agar plates [153] and can be assayed in 96-well plates. Researchers capitalize on the nematode's compact genome, stereotypical development and simple, yet differentiated anatomy. Another advantage is its transparency, enabling the *in vivo* study of processes by fluorescence markers. Martin Chalfie's work on green fluorescent protein in *C. elegans*, among others, was honored with the Nobel Prize in Chemistry 2008. Furthermore, *C. elegans* is amenable to mutagenesis by chemical mutagens, ionizing radiation, etc. and an ever-increasing number of deletion strains are archived as frozen stocks. While mutations can generally be introduced without killing the diploid animal, essential genes can be reversibly knocked-down by RNA interference. RNAi, discovered by Andrew Fire and Craig Mello (2006 Nobel Prize in Physiology), is a method of gene silencing and a natural defense mechanism against viral double-stranded RNA. In order to suppress a specific gene of interest, worms are injected with or soaked in dsRNA complementary to the sequence of a target gene. *C. elegans* is one of the few nematodes that can also uptake dsRNA by feeding on transformed, dsRNA-expressing *E. coli*, which allows for large-scale gene function screens [168].

As a model for metazoans, *C. elegans* has been extensively studied with regard to various human diseases, which are listed elsewhere [165]. To name but a few, it also serves to research nicotine dependence [169], the response to volatile anaesthetics [170], and sleep, as it is the most primitive organism to display lethargus, before each moult [171]. For investigation of muscle atrophy and micro-gravity effects on physiology, specimen were also taken aboard the International Space Station, and some individuals in aluminum canisters survived the Columbia disaster [172, 173].

The behavioral palette of nematodes encompasses foraging, sensory responses to touch, taste, smell and temperature, and even social behavior, memory and learning, as well as the aforementioned dauer larva formation [174, 175]. Dauers and *daf2* mutant animals display a stunning longevity and show metabolic shifts analogous to those in humans with low insulin levels or fasting mammals, such as energy conservation and utilization of stored fat reservoirs [161, 176].

C. elegans is thus also employed in investigating metabolism, obesity and diabetes, and has contributed more than any other model organism to our understanding of biogerontology [6, 176].

A deteriorating proteostasis network in aging cells leads to the accumulation of damaged proteins, and subsequently, protein misfolding diseases like morbus Alzheimer and Huntington. *C. elegans* is utilized as a model for both of these aggregation diseases [135, 177]. Human amyloid β_{42} peptide, responsible for plaque formation in Alzheimer's disease, was found to induce CeHsp16 proteins, which suppress its toxicity in transgenic nematodes [134, 135]. The increased Hsp16 expression upon various stresses has also led to the nematode being used as a monitor for ecotoxicologic studies since the late 1980s [178].

1.4 STRESS RESPONSE AND SHSPS OF *C. ELEGANS*

1.4.1 UPR, SKN1, HSF1 AND TOR

C. elegans senses detrimental environmental changes such as elevated temperatures or toxins through specialized thermo- and chemo-responsive neurons [148, 155]. The various neurosensory inputs control (evasive) behavior and temperature-dependent growth, and elicit different stress responses, like the heat shock response (HSR), even across multiple tissues next to the affected cells [179]. The HSR is also induced cell-autonomously by the accumulation of misfolded and aggregated proteins which results from acute and chronic stress. Conserved across eukaryotes, the HSR is mediated by the heat shock transcription factor Hsf1. Invertebrates typically have only one HSF, whereas vertebrates possess four isoforms [180, 181]. The constitutively expressed Hsf1 is found in the cytosol as an inactive monomer. Upon heat shock (HS), Hsf1 trimerizes, localizes to the nucleus and acquires DNA binding affinity for heat shock elements (HSE) located in

the promoters of HS genes including Hsps, thereby inducing their transcription [182], see Fig. 1.9. In a negative feedback loop, the cytoplasmic chaperone concentration, as well as various post-translational modifications (PTMs), regulate Hsf1 activity [183].

Another transcription factor (TF), Skn1, functions in the p38 MAPK signaling pathway to convey oxidative damage tolerance. This homolog of mammalian Nrf transcription factors mobilizes the phase II detoxification in the intestine by inducing the expression of UDP-glucuronosyltransferases, glutathione S-transferases (GST), superoxide dismutases (SOD) and catalases [184]. These conserved enzymes defend against reactive oxygen species (ROS) produced in the oxidative stress response' first phase, which relies heavily on cytochrome P₄₅₀S (CYP₄₅₀)[185, 186].

Unsurprisingly, there is notable crosstalk between various stress response and growth pathways. Recently, Skn1 was shown to also directly regulate core components of the endoplasmic reticulum (ER) unfolded protein response (UPR): the *C. elegans* homologues of ATF4 and ATF6, IRE1, XBP1, PERK, and BiP [187]. The UPR is a eukaryotic compartmental signaling program (an analogous stress response exists in mitochondria) which counteracts proteotoxic conditions by inducing chaperones, inhibiting translation, and degrading misfolded proteins [179, 187]. In turn, Ire1 and Xbp1 are required for the stress tolerance and adult longevity phenotypes associated with reduced insulin/insulin-like growth factor 1-like signaling (IIS), which are predominantly effected by Daf16 and, to some extent, by Skn1. Skn1's nuclear accumulation and thus, transcription of its target genes, is prevented by phosphorylation by the IIS kinases Akt1/2 and Sgk1 [184, 185, 188].

Moreover, Daf16 and Skn1 are implicated in longevity induced by low oxygen environments, as mediated by hypoxia-inducible factor (Hif1) [189].

Like IIS, attenuation of target of rapamycin (TOR) signalling extends nematode (as well as yeast and mice) lifespan and increases resistance to environmental stress. The Tor kinases gauge the abundance of amino acids and then stimulate growth independently of IIS. However, Torc1 (Tor complex, containing the Daf16 target Daf15) can also block Daf16 and Skn1 expression and activity, and Torc2 hinders Skn1 nuclear localization in a nutrient-dependent manner [190]. For a graphical summary, see Fig. 1.9.

1.4.2 THE DAF2/DAF16 PATHWAY

Of the stress resistance-affecting neuroendocrine pathways, such as steroid hormone receptor (SHR) and transforming growth factor β (TGF- β) signaling, the Daf2 insulin/insulin-like growth factor 1 (IGF-1)-like signaling (IIS) pathway has received most attention, ever since *daf2* mutants were shown to live twice as long as wt nematodes [161]. The evolutionarily conserved IIS/TOR network determines lifespan in budding yeast, fruit flies, mice and humans, as well [6].

In *C. elegans*, IIS is initiated by insulin-like peptides (ILP) binding to the receptor tyrosine kinase and *C. elegans* insulin/IGF-1 receptor ortholog Daf2, indicating conditions supportive of growth and reproduction (Fig. 1.9). This prompts the phosphatidylinositol-3 (PI3) kinase Age1/Aap1 to generate PIP3 (phosphatidylinositol-3, 4, 5-trisphosphate) from PIP2, plasma membrane lipid (opposed by Daf18 /Pten lipid phosphatase), which in turn potentiates the activity of four downstream Ser/Thr kinases: Pdk1 (PI3 K-dependent kinase), Sgk1 (serum-glucocorticoid kinase), and Akt1/2 [159, 191]. By way of phosphorylation, the latter sequester the forkhead box O (FOXO)/winged-helix family transcription factor Daf16 to the cytoplasm [159]. A 14-3-3 protein further prevents nuclear entry or causes expulsion [191]. Thus, the response to ample ILP suppresses the emergency cytoprotective and maintenance protocols which would be instigated by active Daf16, in favor of growth and reproduction [159].

At low IIS, conversely, e.g. in response to starvation, heat or ROS, monomeric Daf16 accumulates in the nucleus to activate the stress response [160, 192]. There, Daf16 either activates or represses transcription of its many targets, which feature promoters that contain the consensus Daf16-binding element (DBE) TTG/ATTTAC [193] or the Daf16-associated element (DAE) CTTATCA [194]. Recent evidence suggests that Daf16 only induces the expression of DBE-associated stress response genes directly, while it controls the transcription of development, growth and reproduction genes by antagonizing (i.e. forcing the nuclear exit of) the DAE-binding TF Pqm1 [195].

The precise regulation (cytosolic retention or nuclear translocation, binding to and release from DNA, relocalization to the cytoplasm) of Daf16 is achieved by signalling from neurons or the germline as well as other pathways, via posttranslational modifications (PTMs): inhibitory phosphorylation of Daf16 by the aforementioned kinases or stress-induced, translocation-enhancing phosphorylation by Jun kinase 1

(Jnk1), methylation by an arginine methyltransferase (Prmt1), polyubiquitination by an E3 ubiquitin ligase, and acetylation by proteins like the sirtuin family deacetylase Sir2.1, within the nucleus [192, 196, 197]. For a schematic of the Daf2/Daf16 signalling cascade and an overview of its most important co-regulators, see Fig. 1.9.

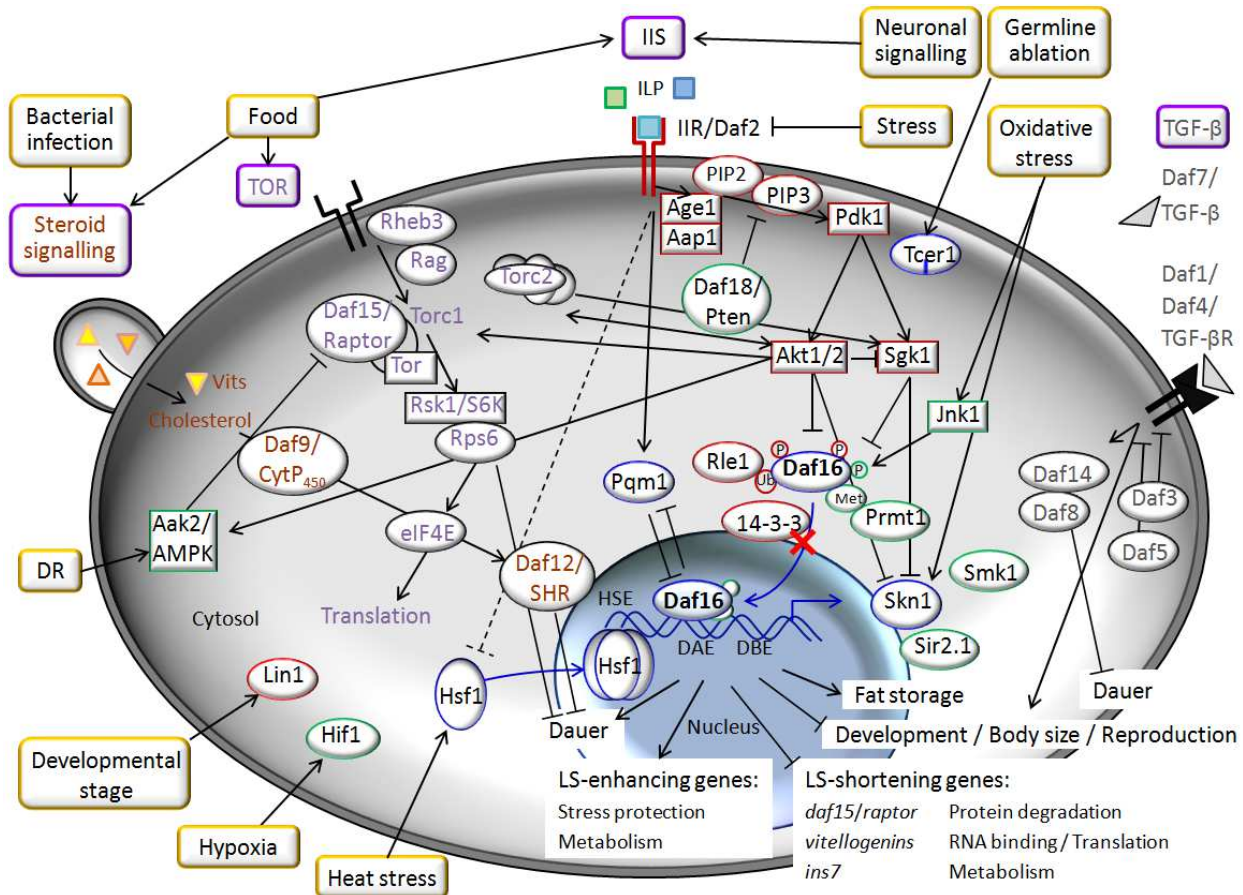


Fig 1.9: Summary of IIS and related pathways that influence Daf16 activity.

Daf2 IIS opposes the FOXO TF Daf16 by inducing its phosphorylation and nuclear exclusion through a conserved PI3K/protein kinase cascade (Aga1, Aap1, Pdk1, Akt1/2, Sgk1). Conversely, low IIS induces nuclear translocation of Daf16, where it regulates the expression of cell-protective genes that cumulatively mediate dauer formation (in early larvae), fat metabolism, stress survival and longevity [159]. Various pathways control Daf16 localization and activity posttranscriptionally, including neuronal or germline signal inputs. Although distinct from IIS, lifespan extension resulting from germline loss requires functional Daf16 as well [198].

Daf16-dependent longevity is achieved by inhibition of Daf2 or downstream IIS components, or overexpression of the heat-shock TF Hsf1, the sirtuin Sir2.1 (which acetylates Daf16 in the nucleus), the developmental-timing microRNA Lin4, the predicted transcription elongation factor Tcer1, Aak2 (a subunit of AMP kinase), or Jun kinase 1 (Jnk1). The latter two activate Daf16 by phosphorylation [6]. A number of co-regulators steers the expression of specific, independent subsets of the Daf16 transcriptome, in response to varying environmental stressors [199, 200]. For instance, Smk1 modulates the transcriptional output of *sod3*, *ctl1* and *lys8*, thus effecting the defense against microbial, oxidative and UV-stress [200]. The oxidative stress-responsive TF Skn1 acts in parallel to Daf16, however, they are partially interdependent in effecting lifespan enhancement. Both are antagonized by the Akt1/2 and Sgk1 kinases, and the transcriptome of detoxification and antioxidant genes overlaps (cf. Text). Hsf1 is required for thermotolerance in

daf2 mutants, as it regulates the transcription of heat shock genes together with Daf16 [199]. Hsf1 is further involved in larval development as well as the innate immune response (cf. Text). Survival in hypoxic environments (≤ 1 % oxygen) of wild-type *C. elegans* necessitates hypoxia-induced factor (Hif1), but also Daf16 and Skn1 to some extent [189].

The nuclear localization of Daf16 is mutually antagonistic with that of the IIS-controlled transcription activator Pqm1, which, at permissive conditions, promotes development but concomitantly transcribes marginal levels of stress response proteins in order to combat mild stresses. This anticorrelation enables Daf16 to indirectly steer the expression of DAE-associated growth and reproduction genes. Loss of Pqm1 abrogates *daf2* longevity [195].

Vitellogenins (Vit) are egg yolk proteins which transport cholesterol from the intestine to oocytes. *Vits* are among the Daf16-repressed gene set. Vitellogenins were shown to prolong the lifespan of bees, which has been attributed to their metal-binding, and thus, antioxidative capacity. Also, *Vits* reportedly enhance the immunological response of *C. elegans* to the bacterium *P. luminescens*, which requires their cholesterol transport [201]. When taken up by receptor-mediated endocytosis, cholesterol triggers the steroid-signaling pathway: Daf9/CYP₄₅₀ produces a lipophilic hormone ligand for Daf12. This nuclear steroid hormone receptor (SHR) then promotes reproductive development and hinders dauer formation. IIS and transforming growth factor β (TGF- β), the major dauer-regulating pathways, likely converge upon Daf9 and further integration of the three pathways occurs at the level of Daf12 [202].

Daf7 (TGF- β) ligand binds to the cellular receptor Daf4, if chemosensory neurons signal favorable environmental conditions. This recruits and phosphorylates another TGF- β R, Daf1, which activates the anti-dauer Smads Daf8/14. They antagonize the pro-dauer Daf3/5, thus committing to reproductive growth. An alternate Daf4/Smad pathway determinates body size of *C. elegans* [191].

The *C. elegans* TOR pathway responds to high nutrient levels by increasing translation and metabolism. Simultaneously, IIS impedes Daf16 downregulating *let363* (*tor*) and *daf15* (*raptor*). Suppression of the TOR complex would lead to fat storage and dauer formation. AMPK, which interacts with TOR, slows the consumption of lipid reserves while in the dauer stage [191].

Another dauer-regulating pathway has been omitted in the schematic. cGMP signaling relies on Daf11 (a transmembrane guanylyl cyclase) and Daf21 (Hsp90), and crosstalks by regulating *daf7* and *daf28* (an insulin) expression, and by functioning upstream of Daf12 [203, 204].

Ⓢ: Phosphorylation, (Met): methylation, (Ub): ubiquitinylation, boxes: kinases, blue: TFs, red: Daf16 antagonists, green: Daf16 activators, grey: components of TGF- β signaling, violet: TOR pathway, brown: steroid signaling. Figure modified from [6, 191, 192].

Daf16 activation by way of scarce ILP or strong loss-of-function mutations in Daf2 results in dauer entry in early larvae. In contrast, low IIS in adult animals (e.g. via weak mutations in the Daf2 pathway) extends *C. elegans'* lifespan at least 2-fold, while feeding and reproducing continue, albeit slowly [161]. Thus, ageing is controlled hormonally in *C. elegans*. In flies and mammals, as well, disruption of the IIS cascade causes longevity [6]. Furthermore, IIR, AKT and FOXO gene variants are overrepresented in several human centenarian cohorts throughout the world [6]. Intriguingly, low IIS concomitantly delays the onset, and reduces the severity of age-related diseases in many organisms, keeping them youthful and active much longer than is usual [6, 159]. Why is that?

The causes of aging have been subject to much discussion [6, 186]. In various organisms, an acquired tolerance against physiological stressors has been correlated with longevity

[205]. Long-lived *daf2* *C. elegans* mutants were also found to be resistant to oxidative and osmotic stress, bacterial infection, heat, radiation, heavy metals, anoxia and proteotoxicity in general [186, 205]. Findings in *C. elegans* and *Drosophila* established that increased activity of Daf16 is responsible for the IIS-associated longevity phenotype [6, 159]. The most eminent transcriptional targets of *Drosophila* and mammalian FOXO proteins are genes implicated in metabolism (PEPCK, glucose-6-phosphatase), cell-cycle arrest (e.g., cyclins), apoptosis (BIM1, BCL6), DNA repair and the oxidative stress response (MnSOD, catalase) [192, 206]. Among the first identified targets of *C. elegans* Daf16 were superoxide dismutase (*sod3*), transmembrane tyrosine kinase (*old1*), metallothionein (*mtl1*), SCP-like extracellular protein (*scl1*), raptor (*daf15*, a TOR regulator) and small heat shock proteins, particularly *hsp12.6*, *hsp16* and *sip1* [192, 199]. The promoters of *sod3*, *daf15*, *mtl1*, and several *shsp* genes contain the DBE or DBE-like sequences. 22 % of all *C. elegans* genes encode either the DBE or the DAE within the first 1000 bp of their promoters, and thus might also be direct Daf16 targets [207]. Indeed, genome-wide analyses have now identified many further putative Daf16 targets, and these display a significant overrepresentation of the Daf16 consensus binding sites [194, 206].

Confirmed Daf16-upregulated genes protect from many different kinds of stresses [206]. The oxidative damage adaptation class includes thioreductins, a glutathione S-transferase (*gst4*), catalases (*ctl1/2*), and, as mentioned, superoxide dismutases. Saposin-like proteins (*spp1/12*), c-type lectins and lysozymes (*lys7*) are antimicrobial effectors, cytochrome P450s and UDP-glucuronosyltransferases function in detoxification, while trehalose 6-phosphate synthases (*tps1/2*) convey hypertonic stress tolerance. Xenobiotic metabolism proteins are overexpressed in both *daf2* mutants and dauer larvae. The nematode's two metallothioneins (*mtl1/2*), which function in heavy metal detoxification, are both (differentially) regulated by Daf16 [194, 206]. Apparently, rather than the overexpression of entire sets of stress response gene categories upon heat shock or encountering toxins, Daf16 favors the specific selection of individual class members [206]. Moreover, Daf16 controls transcription of genes in the gene ontology (GO) categories ageing, adult lifespan, and development [208].

One of the 40 *C. elegans* insulin/IGF-1-like peptides, Ins7, is a Daf2 agonist resulting in normally short lifespan. Ins7 is repressed by Daf16 [194]. An analogous feedback control of IIR exists in *Drosophila* and mammals [209].

Other genes known to be repressed by Daf16 are guanylate cyclases (*gcy*, involved in neuronal signaling), and vitellogenins (*vit*, apolipoprotein-binding yolk components). Furthermore, the following GO classes are down-regulated in the long-lived *daf2* mutant in a Daf16-dependent manner: ribosome and (m)RNA-binding, translation (translation initiation and elongation factors), DNA replication (*pcn1*, *mcm* genes), protein degradation (*skr* genes, proteases, proteasome), and protein metabolism (lipid-binding proteins, phosphoenol pyruvate kinases, glyoxylate cycle/ gluconeogenesis enzymes, acyl coenzyme A dehydrogenases, alcohol dehydrogenases, esterases, and *fat* genes which function in fatty acid desaturation [206, 208]. Reduction of these processes may indicate an overall decrease in protein turnover in *daf2* mutants. [208]. Together with the increased stress resistance conveyed by over-expression of stress response proteins, this could go far in explaining the longevity phenotype of *daf2* (-) / *daf16* (+) mutants. Indeed, the majority of downstream genes whose function was tested using RNAi affected lifespan as expected from their being up- or down-regulated by Daf16 [194, 206]. Lists of the many confirmed Daf16 targets can be found elsewhere [195, 206].

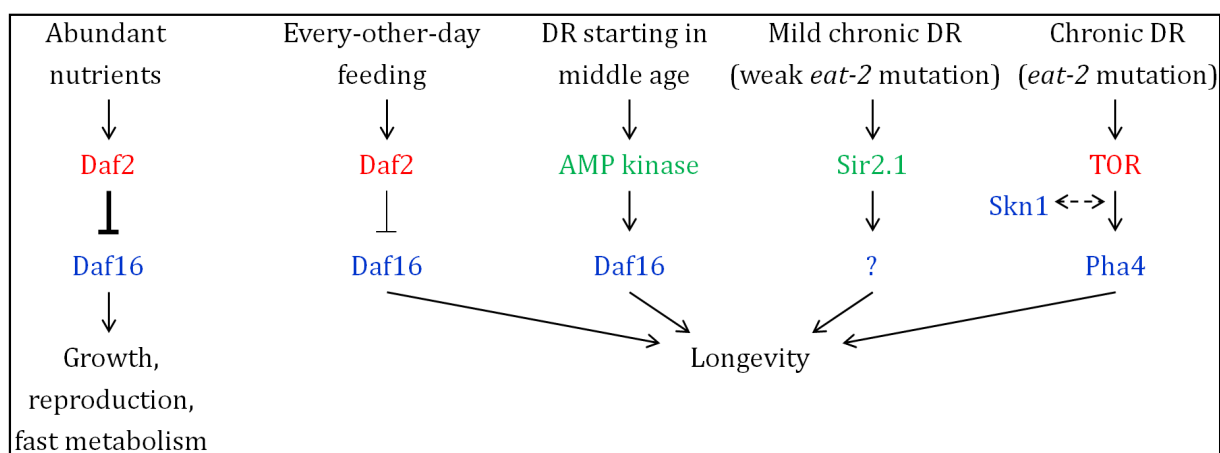


Figure 1.10: Different modes of dietary restriction (DR) convey longevity in *C. elegans* by varying pathways (modified from [6]).

Nutrients induce Daf2 signalling to inactivate Daf16, thus promoting growth and reproduction within a normally short life span. Daf16 activity triggers dauer formation in early larvae, whereas low levels of endocrine signalling (e.g. as achieved by weak mutations in Daf2) are sufficient to bypass the dauer checkpoint. In adult worms, reducing sustenance by way of every-other-day feeding down-regulates IIS, which reduces the rate of reproduction and shifts metabolism towards fat storage in a Daf16-dependent manner. Concomitantly, adult lifespan is enhanced.

Rheb1, and to some extent its target TOR, are apparently also necessary for this phenotype, however, the TOR pathway (via the Pha4 TF) is predominantly linked to longevity resulting from chronic DR, as achieved by mutating *eat2*, an ion channel subunit which acts in pharyngeal muscle to time pumping frequency.

Skn1 is involved in prolonging lifespan in chronic DR as well. Surprisingly, Sir2.1 seems to be needed to increase lifespan in weak but not strong *eat2* mutations. AMP kinase and Daf16 are necessary for longevity when middle-age nematodes suffer DR [6, 176].

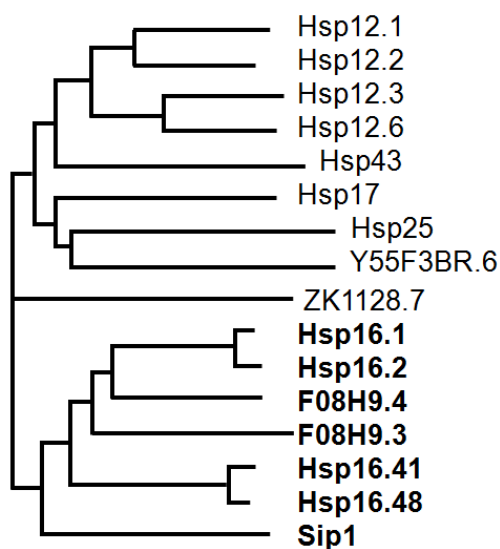
While Daf2 directly controls ageing in the adult nematode, it is also implicated in dietary restriction (DR)-dependent longevity. DR is defined as reduced feeding without malnutrition. Interestingly, the temporal aspects of the caloric limitation (life-long DR vs. DR beginning in middle age vs. every-other-day feeding) dictate whether IIS, the nutrient-sensitive TOR pathway, AMP kinase or sirtuins play the decisive role in this [6], see Fig. 1.10.

Thus, Daf16 controls growth and reproduction, lipid metabolism and dauer entry, stress resistance and ageing. Intriguingly, reducing IIS by mutating *daf2* also improves memory in young adults and maintains the ability to learn, which declines with age in *C. elegans* as it does in elderly humans. DR was also found to alleviate cognitive decline, in older animals [210].

Ageing and age-related mortality are largely correlated to the effectiveness of the heat-shock response, namely, the cells' capacity to produce Hsps. Long-lived *Drosophila* strains overexpress sHsps [211, 212]. Likewise, the aforementioned longevity and stress-tolerance of *C. elegans daf2* mutants is greatly due to the induction of sHsps such as Sip1 [194], since RNAi of *shsp* (including *sip1*) genes shortens the life span of *daf2* mutants, animals overexpressing Hsf1, and wt nematodes [199]. Conversely, overexpression of Hsp16 extends nematode life span [213].

Activated by elevated temperatures, Hsf1 appears to be the only Daf16 co-regulator necessary for heat shock gene transcription. In this vein, adaptation to a brief, mild heat pretreatment before a harsher heat shock, i.e. hormesis, induces enhanced thermotolerance and prolongs the lifespan of wild type worms, as does overexpression of Hsf1 [199, 214]. Conversely, RNAi of *hsf1* shortens wt lifespan, and deletion of *hsf1* abrogates the longevity phenotypes of *daf2* mutants and calorically deprived animals [199, 215]. Hsf1 is further required for the improved survival of *daf2* nematodes infected by microbes. Various *C. elegans* pathogens, such as *Enterococcus faecalis*, *Staphylococcus aureus* and *Pseudomonas aeruginosa*, cause protein aggregation in the intestine and may produce ROS to weaken their host. Overexpression of Hsf1 or a hormetic thermo-shock inducing transcription of *shsp* genes by Hsf1, in parallel to antioxidant and antibacterial genes by Daf16, conveys further protection [199, 214]. This also ties immunity to aging [191].

1.4.3 SHSPS IN *C. ELEGANS*



A BLAST (Basic Local Alignment Search Tool) query based on the α -crystallin ACD identifies 16 sHsps in *C. elegans*, ranging from 12 to 46 kDa in molecular mass. According to their size and sequence similarity, four of these cluster to make up the Hsp12 family, while 7 can be compartmentalized into the greater Hsp16 family (Fig. 1.11).

Fig. 1.11: Phylogram of the *C. elegans* small heat shock proteins, according to Clustal W (real branch length). The Hsp16 family is highlighted in bold.

A summary of gene locus, expression patterns and protein properties is represented in Table 1.1.

1.4.3.1 HSP12 FAMILY AND RELATED SHSPS

Hsp12.1 and Hsp12.2, and Hsp12.3 and Hsp12.6 form pairs of 42 % and 67 % identity, respectively, within the Hsp12 family. They are the smallest sHsps described to date. Their CTRs are essentially missing, and their NTRs consist of only 24-25 aa. The lack of sufficiently long termini could explain the apparent inactivity of the Hsp12 proteins towards established aggregation models, such as actin, insulin, lysozyme and citrate synthase (CS) [83]. This leads to questions as to their functionality, since they are expressed at significant levels (most highly and throughout most tissues in L1 larvae, and in vulva and spermatheca in adults). As mentioned above, Hsp12.6 is a target of Daf16, its transcription also requires Hsf1, but not Smk1. Hsp12.6 is necessary for normal lifespan since *hsp12.6* (RNAi) animals are short-lived, and may contribute to the longevity of dauer larvae, as it is over-expressed in *daf2* mutants [194, 199, 216]. So far, various stressors (captan, Ca^{2+} , alcohol, HS) could not elicit an overexpression of any Hsp12 proteins [83]. Also unusual for sHsps is the fact that recombinant Hsp12 proteins do not oligomerize beyond tetramers, and Hsp12.6 exists only as a monomer over a wide concentration range [217].

Table 1.1: CesHsp characteristics. MM: molecular mass, E: extinction coefficient, HS: heat shock, v.s.: vide supra, as above, n.d.: not determined.

Protein	Gene	Chromo- some	Tissue-specific expression	Stage-specific	Stress- inducible	# aa	MM [kDa]	pI	# Cys/Trp	E [M ⁻¹ cm ⁻¹]
Hsp12.1	T22A3.2	I	L1: ubiquitous, Adult: reproductive tissue	no, but highest in L1, decreases afterwards	no	112	12.528	5.6	0/2	13980
Hsp12.2	C14B9.1	III	v.s.	v.s.	no	110	12.264	6.3	1/2	12490
Hsp12.3	F38E11.1	IV	v.s.	v.s.	no	109	12.293	6.3	1/2	13980
Hsp12.6	F38E11.2	IV	v.s.	v.s.	no / slightly	110	12.620	5.6	1/2	12490
Hsp17	F52E1.7	V	n.d.	n.d.	n.d.	148	17.442	6.2	0/1	12950
Hsp25	C09B8.6	X	Body wall muscle, pharynx reproductive tissue,	no	no	219	25.256	6.3	0/0	16390
Hsp43	C14F11.5	X	contact regions between muscle cells and hypodermis	no	no	368	43.241	8.8	1/11	79870
Y55F3BR.6	Y55F3BR.6	IV	n.d.	n.d.	n.d.	180	19.539	6.2	0/0	5960
ZK1128.7	ZK1128.7	III	n.d.	n.d.	n.d.	205	22.988	5.6	0/2	24410
Hsp16.11	T27E4.2/8	V	ubiquitous, L4/adult: reproductive tissue	not in early embryos, highest in L1, decreases during development	yes: HS, heavy metals, pesticides, etc.	145	16.253	5.4	1/0	4470
Hsp16.2	Y46H3.3	V	v.s.	v.s.	v.s.	145	16.242	5.3	1/0	4470
Hsp16.41	Y46H3.2	V	v.s.	v.s.	v.s.	143	16.252	5.9	0/1	9970
Hsp16.48	T27E4.3/9	V	v.s.	v.s.	v.s.	143	16.299	5.5	0/1	8480
F08H9.3	F08H9.3	V	pharynx	no	slightly: HS	147	16.747	4.7	2/0	2980
F08H9.4	F08H9.4	V	anus, neurons, upon HS in intestine	no	slightly: HS	147	16.418	5.2	2/0	0
Sip1	F43D9.4	III	no	in developing oocytes and embryos only	no	159	17.839	7.9	2/1	8480

Neither does Hsp12.6 form mixed complexes with Hsp16.2, nor is Hsp16.2's chaperone activity influenced by its presence [83]. It may be that the Hsp12s only cater to few, specific substrates, or that they require special PTMs or co-factors in order to become activated [83], or that they have a different function altogether.

Hsp25 is polydisperse, forming mainly tri- and tetramers. In all stages, it localizes to dense bodies and M lines in body wall muscles, to the pharynx, and to cell-cell junctions in the spermatheca. It is not further induced upon HS. Because of its spatial expression pattern, *in vitro* chaperone-activity and binding to the dense body components α -actinin and vinculin, Hsp25 has been hypothesized to act in myofibril organization and maintenance of focal adhesion structures. However, *hsp25* RNAi did not result in a conclusive phenotype [83].

The same is true for Hsp43. The largest CesHsp is constitutively, un-inducibly expressed throughout development in (hemi)desmosomes of body wall muscles, the spermatheca and the vulva. This expression pattern is reminiscent of that of Hsp25, which suggests that Hsp25 and Hsp43 could function in parallel. The recombinant protein is poorly soluble, but appears to oligomerize to at least a 16-mer [83].

So far, little data exists on the other CesHsps not pertaining to the Hsp12 or -16 families. According to wormbase.org, Hsp17 is among the gene set differentially expressed in a Sir2.1-overexpressing strain, and is regulated by HS, induced upon microbial infection and irradiation, depleted in muscle like ZK1128.7, while Y55F3BR.6 is upregulated in muscle.

1.4.3.2 HSP16 FAMILY

The CeHsp16 family consists of seven proteins, which by sequence comparison can be compartmentalized into subfamilies: the developmentally regulated Stress-induced protein-1, Sip1, the tissue-specific F08H9.3 and F08H9.4, and the solely stress-inducible “core family” containing Hsp16.1, Hsp16.2, Hsp16.41, and Hsp16.48 (Fig. 1.11).

The gene products of *hsp16.1/hsp16.2*, and *hsp16.41/hsp16.48* form highly homologous pairs, with 93 % sequence identity to the respective partner. All *hsp16* genes are localized on chromosome V, save for *sip1*, which is encoded on chromosome III (wormbase). The core Hsp16 genes are arranged as inversely oriented tandem pairs: the duplicated pair encoding *hsp16.1/hsp16.48* and the identical *hsp16.11/hsp16.49* (T27E4.2/T27E4.3 and T27E4.8/T27E4.9, respectively), as well as *hsp16.2/hsp16.41*

(Y46H3A.3/Y46H3A.2). Their overlapping inverted promoter regions contain two heat shock elements (HSEs) in either direction between the two ORFs, directly upstream of the TATAA boxes, see [83] for an illustration. Each of the two HSEs can induce bidirectional expression of the core *hsp16* gene pairs, and the number of HSEs is correlated to the strength of the heat-induced transcription [141]. Hsu *et al.* also report Daf16-binding sites upstream of the core *hsp16* genes [199].

All four core Hsp16 proteins are fully repressed in *C. elegans* at ambient environment conditions [83, 218, 219]. When subject to stress, however, they are quickly and strongly induced in almost all somatic tissues in larvae and adults and can still be detected two hours after the stress incident [83, 220]. Specifically, Hsp16s are expressed upon heat shock (27-35 °C), oxidative stress, e.g. by the superoxide-producing herbicides paraquat, juglone, and H₂O₂, as well as some fungicides [221], by hyperbaric oxygen-induced stress, upon contact with alcohols, As³⁺, Pb²⁺, Hg²⁺, Cu²⁺ and Cd²⁺ [83, 221-223], also by bacterial infection [224], the afore-mentioned human amyloid β peptide₄₂ [134, 135], and even by electro-magnetic fields [225]. In contrast to the generic expression pattern upon heat stress, chemical inducers activate *hsp16* transcription predominantly in contact tissue, namely the pharynx and intestine [142].

The core Hsp16 proteins are not inducible in the germline and during early embryogenesis, at least not before 12 cell-stage [226], but become and remain so after gastrulation [83]. Similar to the Hsp12 family, their levels are highest in L1 and then decrease during development [83, 141]. Since the transcription in response to stressors is mediated by Daf16 and Hsf1, differential regulation of Hsp16s and subsequent changes in phenotypes are also effected by mutations in those pathways: Heat shock genes, in particular the core *hsp16s*, *sip1* and *hsp12.6* are increased in animals with reduced Daf2 activity (*daf2* pathway mutants and dauers), and decreased in animals with reduced Daf16 activity [194, 199, 216]. As stated above, *hsf1* RNAi reportedly reduces the mRNA levels of *hsp16.2* as well as *sip1* under both unstressed and stressed conditions, in both a wt and *daf2* mutant background [199]. Inhibition of Hsp16 and Sip1 shortens the lifespan of wt, *age1* and *daf2* mutants and animals overexpressing Hsf1 [199, 215]. Conversely, overexpression of Hsp16s extends nematode life span [213].

In vitro chaperone activity has been demonstrated for all core Hsp16s using citrate synthase, glutamate dehydrogenase and luciferase as aggregation-prone model

substrates ([83, 220] and Chapter 3.6.1). Hsp16.2 interacts with denatured, but not native tubulin and actin [227]. Sip1 has not been assayed for holdase function before, but was shown to convey thermotolerance when expressed in *E. coli* [228], as reproduced in this work (see Chapter 3.8.1). *In vivo*, Hsp16s were shown to suppress amyloid β_{42} toxicity [135] and to delay the onset of polyglutamine aggregation, the cause of Huntington's disease, in *C. elegans* [199].

Thus, the principal role of Hsp16 isoforms is to provide a protective system that is switched on in response to stress and contributes to longevity by preventing aggregation of oxidized or otherwise damaged aged proteins, facilitating their being refolded or degraded.

Hsp16 proteins exist as oligomers *in vivo* [229], and *in vitro*, see Table 1.2, [105, 220].

Table 1.2: Oligomeric size of Hsp16 proteins.

Protein	Weinfurtner (2008)	
	HPLC-SEC, pH 7.0 (± 50 kDa) / subunits	AUC, pH 8.5 [kDa] / subunits
Hsp16.1	500 / 27-30	n.d.
Hsp16.2	500 / 27-30	360 / 22
Hsp16.41	400 / 22-27	360 / 22
Hsp16.48	415 / 23-29	325 / 20
Sip1 (pH 6.3)	415 / 20-26	430 / 24
Hsp16.2, pH 7.5 Leroux (1997)	500 / 30	239 / 14 and 394 / 24

Electron microscopic (EM) 3D-structures which could be reconstructed for three of the core Hsp16s show a hollow spherical architecture with an average diameter of 12 nm (Fig. 1.12). Class-averaged images of Hsp16.2, -41, and -48 particles that correspond in size to the AUC results all reveal the 24-mer, composed of 12 dimers [220].

Comparatively little data is available on F08H9.3 and F08H9.4, the two Hsp16 proteins that are still named after their ORFs. They are expressed constitutively and tissue-specifically (in pharynx resp. neurons and anus, upon stress in intestine as well), and seem to be slightly heat-inducible [230]. Both F08H9.3 and -4 are upregulated in *daf7*, *daf8* and *daf14*, i.e. TGF β pathway mutants which form dauers instead of L2 larva at 25 °C [231]. F08H9.3 and -4 (RNAi) animals are sensitive towards heat shock, however, no *in*

in vitro chaperone activity for these two Hsp16 proteins has been observed so far [230], see also Chapter 3.6.1).

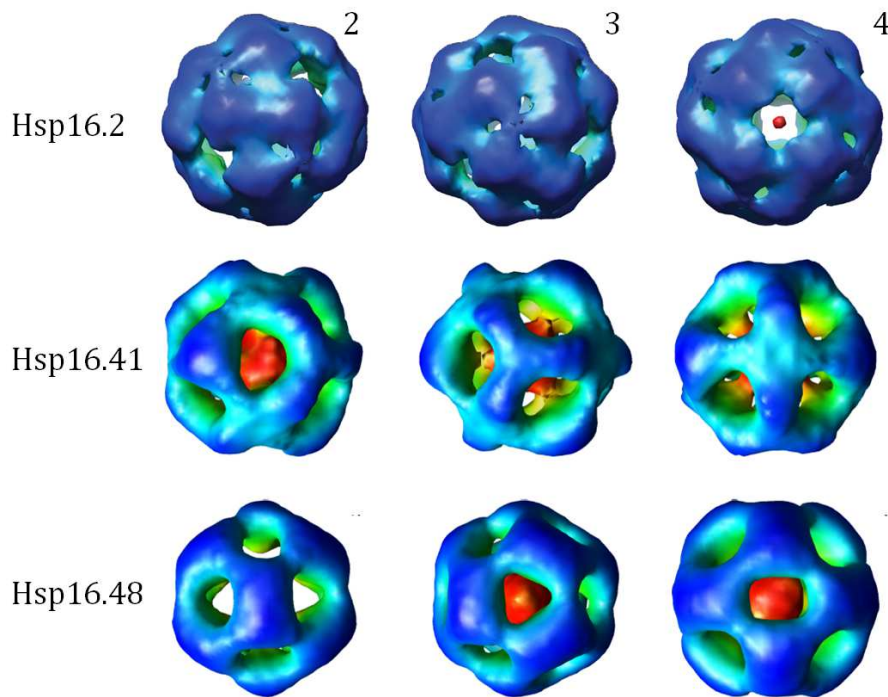


Fig. 1.12:
3D-Reconstructions
of Hsp16 oligomers.
 Class-averaged images of Hsp16.2 (top row), Hsp16.41 (middle), and Hsp16.48. Each 24mer is shown with a possible 2-, 3-, or 4-fold symmetry (indicated). 10,000 middle-sized single particles were used for the statistical analysis of Hsp16.2, and 8,000 particles for both Hsp16.41 and -48 [220].

1.4.3.3 SIP1

The *sip1* locus shares the general *hsp16* gene organization: Start codon, exon 1 (275 bp long in the case of *sip1*), short intron (56 bp), exon 2 (200 bp), stop codon, and a 3' untranslated region (3' UTR, 57 bp) that contains a polyadenylation signal and ends with a ~70 bp poly(A)tail. The intron of the core *hsp16s* separates the variable NTR and conserved ACD region of the encoded heat shock polypeptides (exon 1 is 126 bp long in *hsp16.2*). In contrast, the intron in *sip1* interrupts codon 93 (i.e. the β 7-strand in Sip1's ACD). The *sip1* and *hsp16* genes could thus have evolved from an intron-free ancestor [228].

In *sip1*, a classical TATAA box precedes the 5'UTR (47 bp upstream of the ATG) by 27 bp. Two closely spaced Daf16-binding sites [199] (-111 and -119 bp) are located upstream of the *sip1* ORF, as well as a score of farther away heat-inducible promoters (-421, -1315, -2010, -3040, -3363 bp upstream of the ATG). Hsu *et al.* (2003) identified one HSE quite far upstream of *sip1*. Using reverse transcriptase polymerase chain reaction (RT-PCR), they reported *sip1* mRNA to be upregulated in *daf2* or heat-shocked nematodes, but found wt-like levels if Hsf1 expression was downregulated by RNAi in addition to heat

stress or the *daf2* mutation [199]. However, the notion of stress- (and thus, Hsf1-) dependent Sip1 expression is challenged by Linder *et al.* (1996) observing no heat- or cadmium-inducibility, but rather a drop in *sip1* mRNA under heat stress conditions, determined by Northern blot. They deemed this conclusive with the absence of *cis* heat-inducible promoter elements or metal regulatory elements (MRE) close to the ORF [228, 232]. Fittingly, Stress-induced protein-1 was called Sec1, Small embr**y**onic chaperone-1, in this first paper on Sip1. By mass spectrometry, another group also observed the core Hsp16 proteins to be increased, but Sip1 protein levels to be downregulated in heat-stressed nematodes [233]. A fourth report concurs with Hsp16 -, but not Sip1 expression being stimulated by Cd²⁺ [234]. Thus, most data on Sip1 indicates that this sHsp is expressed constitutively.

Unique among the CesHsps, Sip1 is expressed development-specifically in oocytes within the adult gonad and embryos only. Whether Sip1 is a maternally derived transcript is subject to discussion [235]. Sip1 first becomes abundant at a time characterized by transcriptional silence [147]. Therefore, Sip1 protein could likely be produced in the oocytes by translation of *sip1* mRNA that has been synthesized in the hermaphrodite's gonad and has then been packed into germ cells [228, 236]. The abundant constitutive *sip1* mRNA and protein levels drop sharply at mid gastrulation/post-proliferation stage, before morphogenesis begins. They are basal at ventral enclosure stage (421-560 cells) at the latest [237], and remain undetectable throughout larval development, only reappearing in the developing gonad [218, 228, 238]. Sip1 is probably the only sHsp present during the intense protein synthesis of early embryogenesis, since the core Hsp16 proteins are absent in the germline, becoming inducible only after gastrulation [83], Hsp12s are absent before ventral enclosure stage (421-560 cell stage), and microarray data reveals no presence of the remaining CesHsps in oocytes [237]. No tissue-specificity within the embryo is apparent [228].

While the *sip1* deletion strain is viable and non-sterile, *sip1* antisense DNA oligonucleotides injected into gonads to inhibit the Sip1 expression resulted in dysplastic, arrested embryos [228].

However, the only evidence of Sip1 acting as a chaperone is inferred from few *in vivo* findings so far. It conveys thermotolerance onto *E. coli* [228], and resistance against the pathogenic bacteria *Enterococcus faecalis* onto *C. elegans* overexpressing Sip1 [239].

2. OBJECTIVE

The above-mentioned implies a special role for the embryo-specific small heat shock protein Sip1 that is non-redundant with that of the other *C. elegans* sHsps. However, few biochemical data on Sip1 have been published so far. As part of the endeavor to describe more about the function and regulation of molecular chaperones in nature, I set out to characterize this enigmatic sHsp.

Objective of this Doctoral Thesis was the structural and functional elucidation of the little-investigated small heat shock protein Sip1 from the Hsp16 family of the model organism *Caenorhabditis elegans*. Its contribution to the nematode's stress response was to be investigated both *in vitro* and *in vivo*. This entailed verification of the expression pattern, phenotypical analysis, determination whether Sip1 was chaperone-active, and, if so, investigation of interaction with other chaperone systems and the identification of *in vivo* substrates. Any differences to the other Hsp16 proteins were to be documented. For structural characterization, circular dichroism spectroscopy (CD), analytical ultracentrifugation (AUC), electron microscopy (EM, in cooperation with Prof. Dr. S. Weinkauf), and crystallography (Prof. Dr. M. Groll, both Technische Universität München) were employed. Sip1 proved a fascinating choice, as its physiological role and regulation are singular indeed - not only among *C. elegans* sHsps.

Insights into the complex system of small heat shock proteins in *C. elegans* will further knowledge of entire sHsp chaperone systems in more highly developed eukaryotes, especially in the hope of better understanding protein aggregation diseases and the aging processes in man.

3. RESULTS

3.1 ALIGNMENT OF THE SHSPS OF *C. ELEGANS*

According to a BLAST search and subsequent phylogenetic analysis, seven of the 16 small heat shock proteins found in *C. elegans* pertain to the Hsp16 family. Sharing the typical architecture of small heat shock proteins, all Hsp16s consist of a conserved α -crystallin domain (ACD, red in Fig. 3.1) which is flanked by a poorly homologous N-terminal region (NTR) and a shorter CTR. All *C. elegans* Hsp16s lack the short linker that divides the β 6- and β 7-strands in tapeworm Tsp36 and in all known non-metazoan sHsp structures, as represented in the alignment by SpHsp16.0. Instead, Hsp16s feature the long $\beta(6+7)$ -strand typical of mammalian sHsps such as α B-crystallin (see Fig. 1.6, Chapter 3.4.3.1). Located at the beginning of the CTR or, depending on definition, at the very C-terminal end of the ACD is the IXI motive, a conserved trait of sHsps implicated in oligomerization by binding into a hydrophobic groove in an adjacent ACD [86, 96, 106, 107, 240]. The core family's IPI is mutated to LPI in Sip1 (over-lined in purple in Fig. 3.1). Sip1 diverges notably from the "core Hsp16s" (Hsp16.1, Hsp16.2, Hsp16.41, Hsp16.48) and the relatively uncharacterized F08H9.3 and F08H9.4. A sequence alignment reveals Sip1's poor identity to its closest relatives, especially in the termini. Sip1 is larger (17.8 kDa vs. 16.2 – 16.7 kDa), and also differs in being enriched in His (10 vs. 2 – 5 His in all other Hsp16s) and Thr (18 vs. 2 – 7), but depleted in Ser (9 vs. 13 – 19). Sip1 sports a pI of 7.9, whereas all other CesHsps save Hsp43 are acidic proteins. The Asp- and Glu-rich Hsp16s have pIs of 4.7 – 5.9. Sip1 would thus be positively charged *in vivo*, since the intracellular pH (pH_i) in larval and adult *C. elegans* is 7.5 – 7.6 [241]. In contrast, all other Hsp16s should exhibit a net negative charge.

3.2 EXPRESSION AND PURIFICATION OF HSP16 PROTEINS

For their subsequent *in vitro* characterization, Sip1, F08H9.3 and F08H9.4 were natively purified. Various *E. coli* strains were tested for optimal over-production of the recombinant proteins at different growth conditions. While these expression tests showed at least moderate protein production in all strains tested, the best parameters for recombinant, soluble Sip1 over-expression were BL21 DE3 Codon+ cells transfected with *sip1* in the pET21a(+) vector, induced with 1 mM IPTG at an optical density (OD) at 595 nm of 0.7, and then grown overnight at 37 °C at 130 rpm. F08H9.3 and F08H9.4 showed the highest soluble expression in JM109 DE3 cells, also after overnight incubation at 37 °C. Exemplary expression test gels and the purification results are depicted for the F08H9 proteins in Fig. 3.2, Sip1 in BL21 DE3+ showed a similar pattern. Sip1, F08H9.3 and F08H9.4-containing *E. coli* were harvested and lysed in buffer A (see Materials and Methods, M&M 6.1.5). The proteins were purified by anion exchange and size exclusion chromatography. When >95 % pure, the proteins were concentrated and stored at -80 °C in standard buffer: 10 mM MES, 10 mM MOPS, 141 mM KCl, 1 mM CaCl₂, pH 7.5. Yields were >80 mg of F08H9.3 and F08H9.4, and 125 mg of crystal-grade pure Sip1 per 7.5 l of LB_{amp}, IPTG (Figs. 3.2, 3.3). This far surpassed the 20 mg of Sip1 obtained from 4 l of inoculated LB medium reported previously [220].

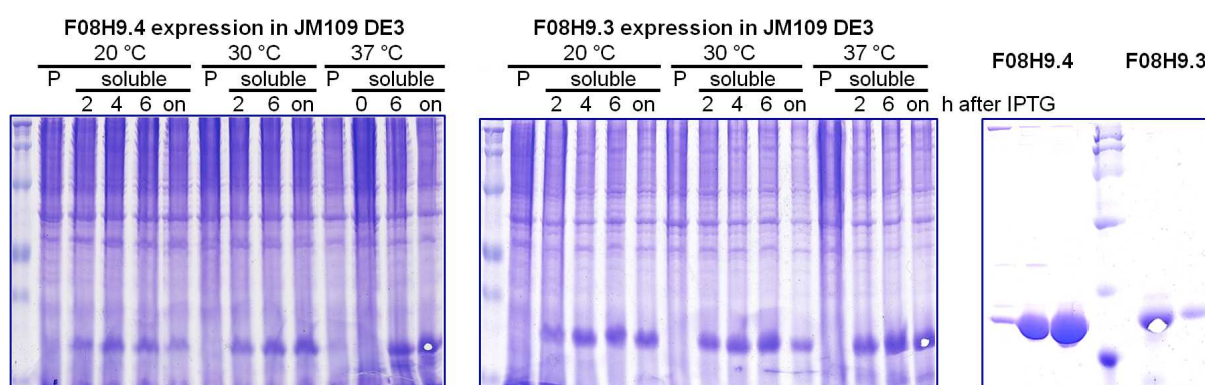


Fig. 3.2: Expression and purification results of F08H9.4 and F08H9.3. Left, middle: Examples of expression test SDS-PAGE gels showing pellet (P) and supernatant (soluble) fractions of JM109 DE3 cells grown at the indicated temperatures, at 140 rpm, and harvested after the indicated time after induction of protein expression (on: over night).

Right: Pure fractions of F08H9.4 and F08H9.3, as eluted from the final column, to the left and the right, respectively, of the low molecular weight marker. Holes in the gels indicate where aliquots were excised for MS analysis. In all cases, a Mascot search correctly identified the proteins.

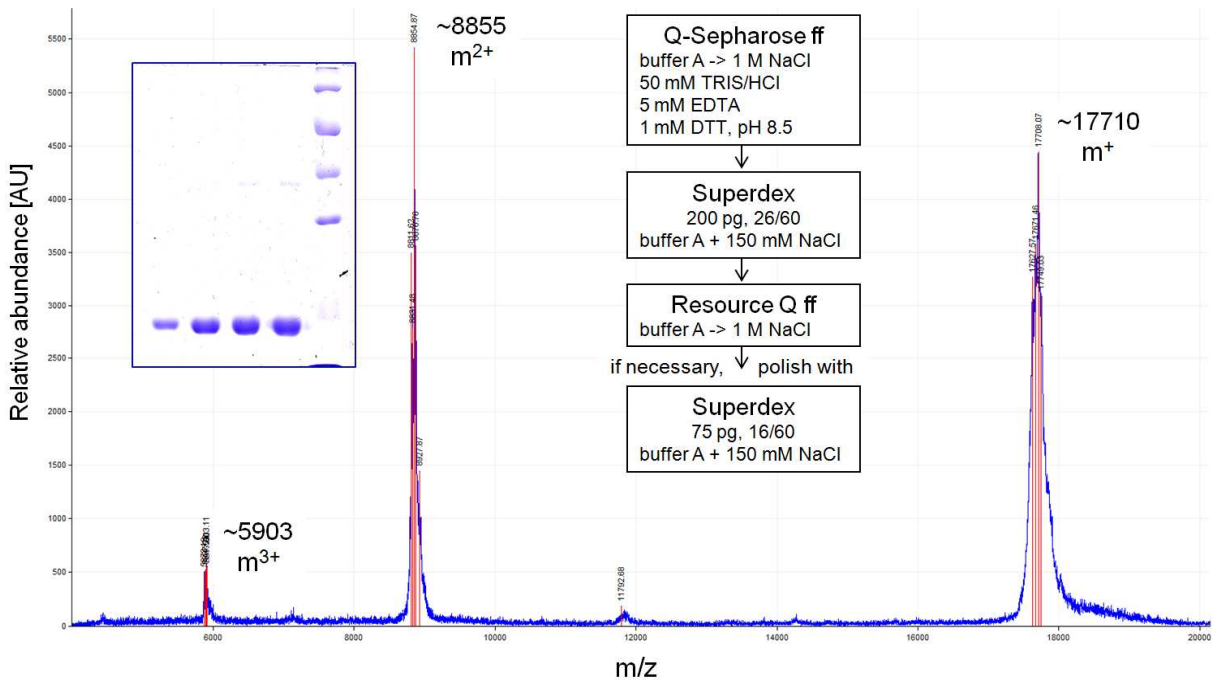


Fig. 3.3: Purification of Sip1. For crystal-grade purity, Sip1 from already quite pure fractions after Resource Q (see SDS-PAGE inset, mass spectrum) was subjected to a final polish by Superdex 75 pg size exclusion chromatography.

The proteins' identity, purity, intactness and correct folding were verified by a Mascot search of the tryptic digest MS patterns, MS of the full-length proteins, SDS-PAGE (Figs. 3.2, 3.3) and CD spectroscopy (Figs. 3.5, 3.6). Hsp16.1, Hsp16.2, Hsp16.41 and Hsp16.48 were available from previous purifications [220].

3.3 BUFFER SCREEN

To start the investigation into the Hsp16 proteins, a buffer was required in which all experiments could be conducted. All proteins needed to be stable also at elevated temperatures. The buffers' pH needed to be temperature-independent. While the pH_i in larval and adult nematodes was reported to be 7.5, an acidification to pH_i ≤ 6.3 in the worm was observed under certain circumstances (e.g., recovering dauers) [242]. Furthermore, eggs were shown to be largely acidic, and this acidification was reported to be essential for embryonic vitality [243]. Thus, it was possible that the embryonic Sip1 would behave differently at pH 7.5, which would represent the physiological pH of the other Hsp16s, than at a lower pH that might more accurately reflect its native conditions. For this reason, a buffer system with a wide buffer range and constant ionic strength was sought. Sip1 was found to be prone to aggregate in the standard PBS (phosphate-buffered saline) buffer. This might be explained by Sip1 binding calcium, which is

precipitated in the presence of phosphate. A total reflection X-ray fluorescence experiment (TXRF, a method for elemental composition analyses) by A. Kastenmüller had revealed no K, Zn or Fe, but a significant amount (3:1 molar ratio) of Ca in Sip1 dialyzed into ultra-pure water [244]. Therefore, a combination of MES and MOPS containing CaCl_2 (“MM”, buffering range pH 5.5 – 8.0) was tested in addition to a three-component buffer (“3C”, consisting of MES, TRIS and Na acetate) with buffer capacity from pH 3.7 - 9.0, and Teorell-Stenhagen buffer (“TS”, see [M&M 6.1.5](#)), a universal buffer over the pH range of 2.0 - 12.0 [245]. The listed buffer capacity ranges were experimentally confirmed by titration and parallel pH measurements.

To recreate the physiological condition, the ionic strength (I) was set to 150 mM by the addition of KCl, NaCl, or NaOH. The three buffers were also examined at an ionic strength of 50 mM ([M&M 6.1.5](#)).

First, protein stability was assessed by dialysis of test proteins into the buffers set to pH 6.3 and subsequent storage for two weeks at -20 °C , followed by thawing on ice. The least precipitation of Sip1, Hsp12.2 and Hsp12.3 (the latter two performed by M. Krause) was observed in the MM I = 150 mM buffer, as estimated visually during dialysis and again upon thawing, by pellet size after centrifugation (45 min at 14,000 g and 4 °C).

None of the six buffers displayed auto-absorption or fluorescence to interfere with spectroscopic measurements. However, both 3C buffers gave a rise in circular dichroism (CD) signal below 205 nm. The other solvents showed no ellipticity in the wavelength range of 260 – 190 nm and were thus best suited for CD experiments. The loss of secondary structure of Sip1 upon heating from 10 °C to 90 °C was followed in the CD polarimeter at 218 nm in all buffers. The melting temperature (T_m) was highest for the MM buffers (Table 3.1, Fig. 3.6).

Buffer (all pH 6.3), ionic strength		$T_m \pm 1\text{ °C}$
MES MOPS (MM)	I = 150 mM	60
MES MOPS	I = 50 mM	53
Teorell-Stenhagen (TS)	I = 150 mM	50
Teorell-Stenhagen	I = 50 mM	42
3-components (3C)	I = 50 mM	50
3-components	I = 150 mM	46

Table 3.1:
CD thermo-transition points of Sip1 in various buffers. 10 μg of Sip1 were heated from 10 °C to 80 °C , then cooled to the initial temperature. The change in ellipticity was followed at 218 nm and the melting temperature, T_m , was documented.

While F08H9.3 adopted the highest degree of β -folded secondary structure in MM buffer as opposed to TS or 3C buffer (Fig. 3.5A), the CD spectra of Sip1 and F08H9.4 were similar in all six buffers (shown for the MM I = 150 mM condition at different pH values in Figs. 3.5, 3.6). Like all core Hsp16 proteins [220], Sip1 displayed a pronounced minimum in ellipticity at 218 nm, which corresponded to the high amount of β -sheets typical for small heat shock proteins [72, 119]. In contrast, both F08H9 proteins always gave saddle-like CD spectra with an extreme minimum at 198-202 nm and a second local minimum at \sim 218 nm, indicating a significant content of random coils next to some β -sheets (Fig 3.5).

To determine the effect of the buffer on sHsp activity, their suppression of a stress-labile model substrate's aggregation was tested. However, one widely used substrate, citrate synthase (CS) proved too stable in all buffers to yield a sufficient aggregation signal when heated to 43 °C. Only when the MM buffer's ionic strength was reduced to 25 mM (by addition of just 17 mM KCl and 1 mM CaCl₂) was CS sufficiently destabilized, while Sip1 was still soluble and functional. Furthermore, all core Hsp16 protein were stable and chaperone-active in this buffer (see Chapter 3.6.1). The F08H9 proteins, however, displayed no chaperone activity in any buffer tested. This is in agreement with the literature [230], and correlated with the low amount of secondary structure elements seen by CD spectroscopy. Since no precipitation of the sHsp proteins had occurred, this lack of functionality was not attributed to low stability in the buffer system.

Many experiments for this Thesis were expected to require *C. elegans* lysate proteins. Therefore, the stability of worm lysate was tested in MM I = 150 mM pH 7.5. No increase in the aggregated, insoluble protein fraction was observed during incubation of lysed worms on ice for 2 h (Fig. 3.4), a duration deemed sufficient for any necessary

preparations following lysis.

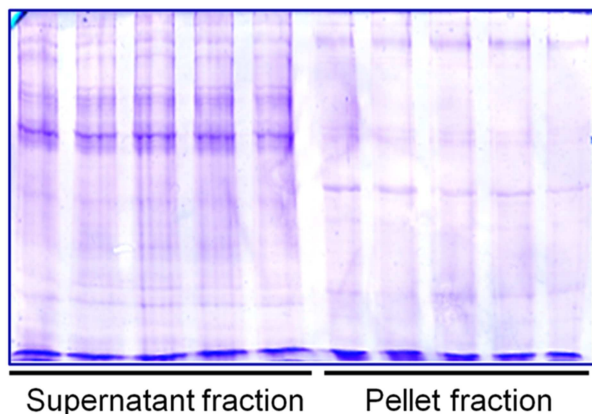


Fig. 3.4: *C. elegans* lysate stability in MM I = 150 mM buffer. An asynchronous worm culture was harvested, cleared of bacteria by repeated washing in MM buffer at pH 7.5, and lysed extensively in a microscale mortar followed by a bead mill (see M&M). After the indicated time on ice in standard buffer, the lysate was separated into soluble and precipitate fraction by centrifugation and analyzed by SDS-PAGE.

Because of the good performance of Sip1 and the core Hsp16s, the MES MOPS buffer with the physiological ionic strength of 150 mM was selected for subsequent analyses of the Hsp16 proteins (“standard buffer”), and all chaperone activity assays were performed in the MM I = 25 mM version (“aggregation buffer”).

MM buffer was also found to be optimal for Hsp12.2 and Hsp12.3. For instance, their melting temperatures in a thermostability assay were far higher in this solvent than in the other tested buffers. However, MM could not be used for characterization of the entire Hsp12 family, because Hsp12.1 and Hsp12.6 precipitated in this solvent [217].

3.4 STRUCTURAL CHARACTERIZATION

3.4.1 SECONDARY STRUCTURE AND STABILITY ANALYSES

Circular dichroism spectra of the Hsp16 proteins were recorded in order to determine whether they were correctly folded. This was true for the core Hsp16s and Sip1. In contrast, F08H9.3 and F08H9.4 displayed the aforementioned minimum at ~202 nm indicative of random coils under all tested conditions, along with the characteristic β -sheet signal at 218 nm. The high content of random coil observed only in the F08H9 proteins could either stem from unsuitable expression or purification steps, an intrinsic property of these proteins, or from the lack of a cofactor (although no such requirement had been reported for sHsps). Therefore, alternative purification protocols were tested (see [M&M 6.2.2](#)). His₆-tagged F08H9.3 and F08H9.4 produced in JM109 DE3 at only 30 °C yielded sufficient amounts of the pure proteins after tag cleavage. Their CD spectra, however, showed no improvement; the β -sheet content of F08H9.4 was even diminished (Fig. [3.5C](#), verified by CDNN calculation). When natively purified with the sole alteration of omitting DTT, F08H9.4 also showed a slightly more pronounced random coil signal (Fig. [3.5C](#)). Thus, the original native purification protocol yielded the highest β -sheet content. Moreover, the random coil signal at 202 nm was far less pronounced at pH 6.3 than at pH 8.2. To test the possibility of the F08H9 proteins requiring cofactors to adopt their full native fold, they were incubated in standard buffer supplemented with a range of possible candidates: 1 mM of Cu²⁺, Fe^{2+/3+}, Zn²⁺, Mg²⁺, Mn²⁺, Co²⁺, and 2 mM of ATP. Furthermore, various pH values were tested, as well as redox conditions by addition of 1 mM DTT_{ox} (*trans*-4,5-dihydroxy-1,2-dithiane) or DTT_{red} (dithiothreitol), since the F08H9 proteins and Sip1 all contain two Cys.

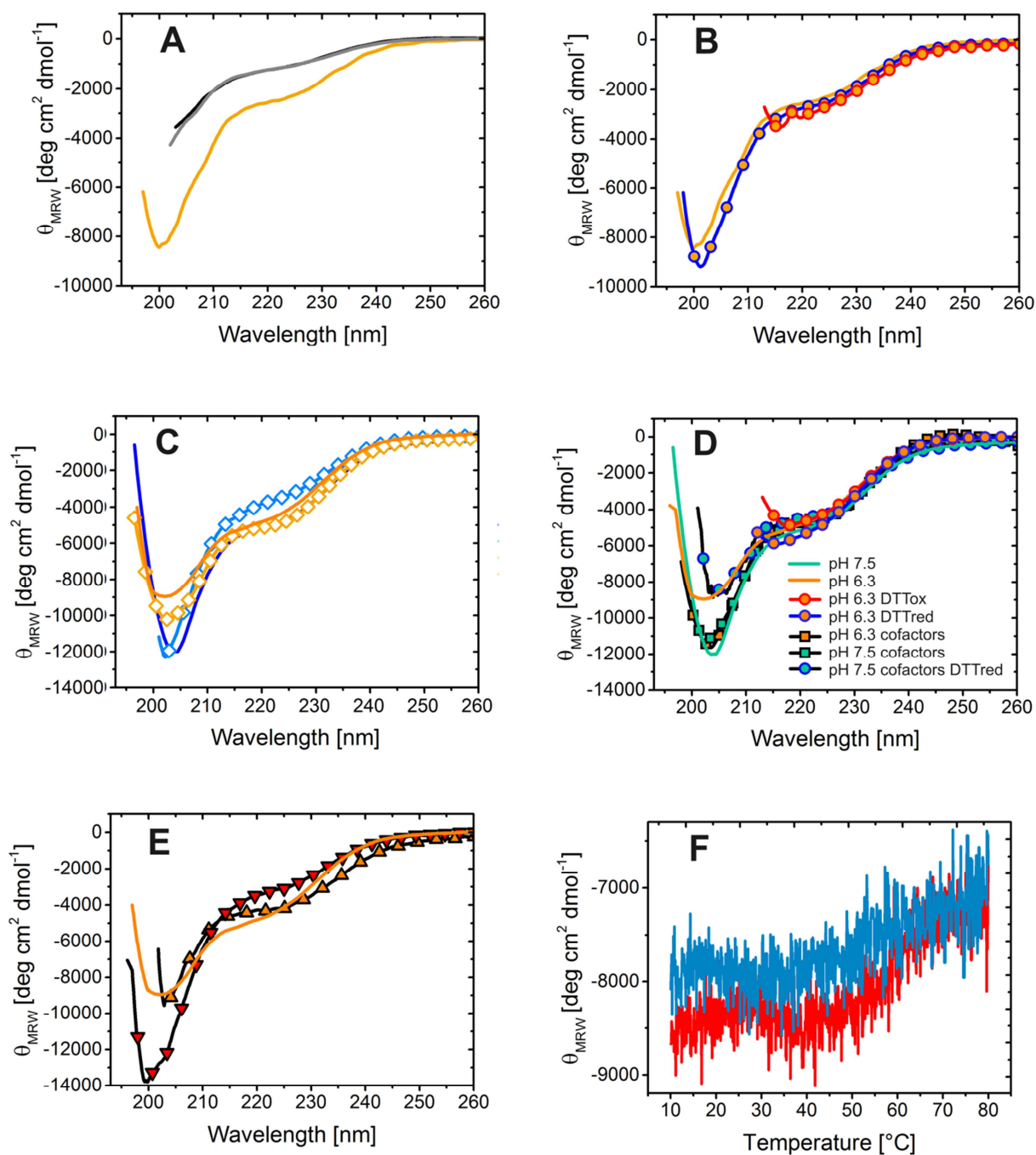


Fig. 3.5: CD spectra of F08H9.3 and F08H9.4 under various conditions.

A: CD spectra of natively purified F08H9.3 in standard MES MOPS buffer (—), 3 components buffer (—), or Teorell-Stenhagen buffer (—), all at pH 6.3. **B:** CD spectra of natively purified F08H9.3 in standard buffer at pH 6.3 (—) and upon addition of DTT_{ox} (—○—) or DTT_{red} (—●—). **C:** Comparison of F08H9.4 natively purified in the presence (—) or absence of DTT (—◇—), then dialyzed into standard buffer at pH 6.3, or F08H9.4HisTEV after cleavage of its His₆-tag in standard buffer at pH 8.2 (—◇—), in contrast to natively purified protein at the same pH value (—). **D:** Addition of possible cofactors (metal ions and ATP, see Text), DTT_{ox} and DTT_{red} to natively purified F08H9.4 in standard buffer at pH 7.5 and 6.3. Some measurements could not be conducted at lower wavelengths, since the DTT-containing buffer caused too high UV lamp voltage. **E:** CD spectra of F08H9.4 before (—), during (—▲—) and after (—▼—) heating from 10 °C to 80 °C and back. **F:** Thermotransition of F08H9.4 at 209 nm when heated from 10 °C to 80 °C (—) and back (—), at pH 6. All CD experiments were recorded at 10 °C (if not otherwise indicated) using 10 µg of protein in standard buffer.

None of the above, however, effected a change in the CD spectrum of F08H9.3 (shown for DTT_{ox} and DTT_{red}-containing buffer in Fig. 3.5B). In contrast, changes in the CD spectra were observed for F08H9.4 upon incubation in either DTT_{ox} or DTT_{red} (Fig. 3.5D). The curve recorded in standard buffer at pH 6.3 containing DTT_{red} seemed to indicate a more pronounced β -sheet signal.

However, both F08H9 proteins were chaperone-inactive at any pH value tested, even in standard buffer supplemented with DTT_{ox} or DTT_{red} (see Chapter 3.6.1).

The heat-destabilization of the F08H9.4 fold progressed in a relatively un-cooperative manner and was not finished at 80 °C (Fig. 3.5F). Therefore, the thermotransition curve could not be fitted with a two-state function. However, the CD signal did not change notably up to 40 °C, so the T_m of F08H9.4 would likely be above at least 60 °C. When cooling to 10 °C, the original ellipticity was not regained, showing the loss of secondary structure upon heating to 80 °C to be partially irreversible (Fig. 3.5E, F).

In the circular dichroism spectrum (Fig. 3.6), Sip1 showed the high β -sheet content evidenced by a single minimum at 218 nm and at an ellipticity of $\sim 6000 \theta_{MRW}$, which is typical for sHsps [72, 119, 246], and which was also observed for the core Hsp16 proteins [220]. In all Hsp16 spectra, this relatively low signal intensity suggested a low percentage of α -helices, which would cause two extensive minima at 208 and 220 nm. Sip1 was thus natively folded. Next, the pH-dependence of its secondary structure and its thermostability were to be assayed. Upon increase of the pH from 6.3 to 7.5, only a slight decrease in the CD signal at 218 nm was observed (Fig. 3.6A, B). CDNN calculated the β -sheet and β -turn content to be 29 % and 20 %, respectively, at pH 6.3, and 26 % and 20 % at pH 7.5. The melting temperature was significantly lower at pH 7.5 than at pH 6.3 (Fig. 3.6D).

In order to follow the pH-trend in more detail, additional pH values were tested in steps of 0.5 around pH 6.3. A summary of the T_m s upon heating of Sip1 is shown in Fig. 3.6D. Sip1 tended towards higher midpoints in thermotransition at low pH (Fig. 3.6C, D). Also, the loss in secondary structure was far less pronounced at acidic conditions (Fig. 3.6C). Thus, Sip1 appeared to be stabilized at slightly acidic conditions. In contrast, CD experiments to determine the stability against the denaturant guanidinium chloride (GdmCl, Fig. 3.6E, F) revealed the loss in native fold to progress slightly more steeply at pH 5.8 – 6.8 in comparison to pH 7.5.

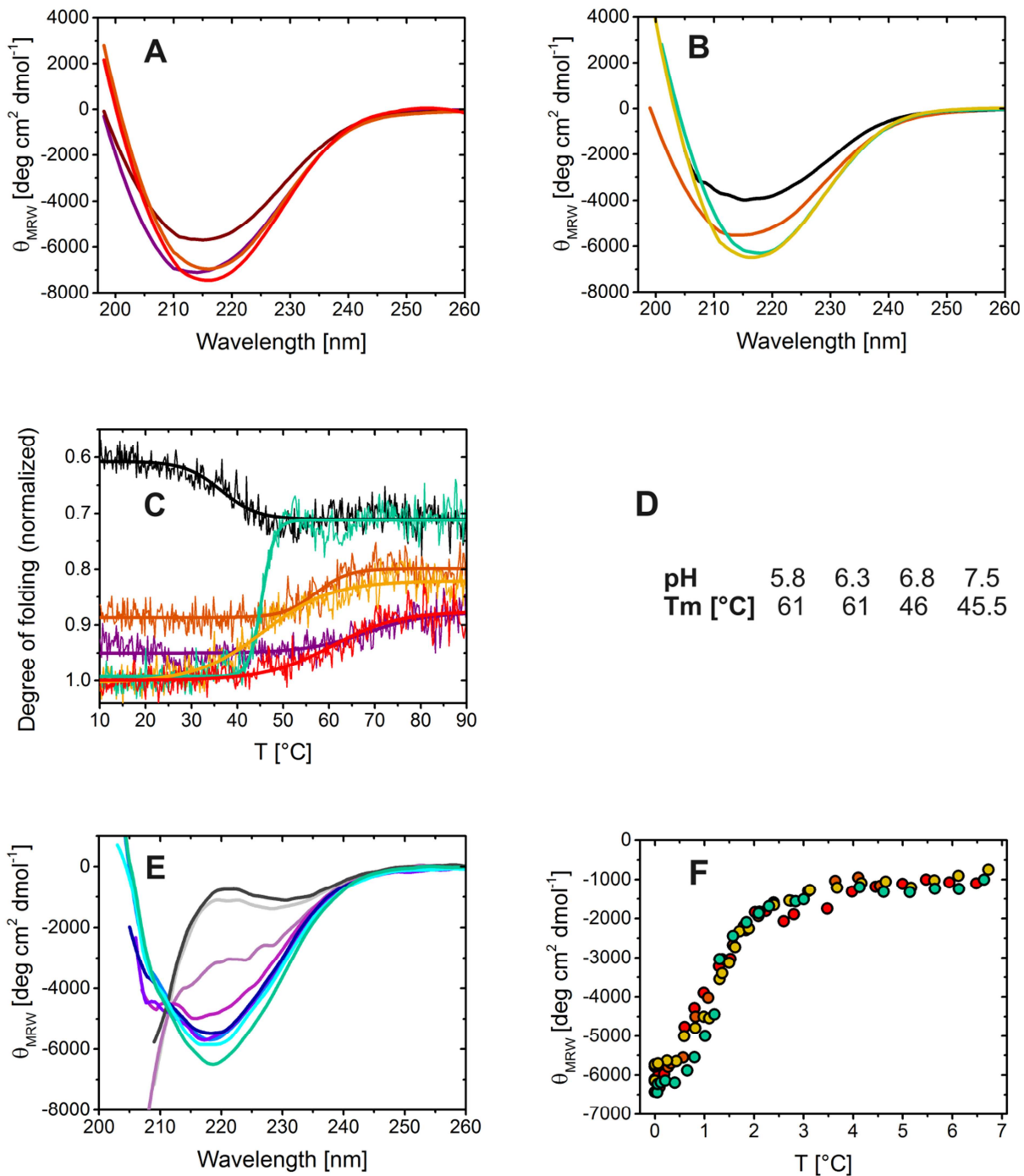


Fig. 3.6: Structure and stability of Sip1 under various conditions according to CD. **A:** CD spectra of natively purified Sip1: pH 5.8 (— and —, at 10 °C and after incubation at 90 °C, respectively), 6.3 (— / —), continued in **B** for Sip1 analyzed at pH 6.8 (— / —) and pH 7.5 (— / —). **C:** Thermal stability of Sip1 assayed by following the change in ellipticity at a wavelength of 218 nm upon heating. The Boltzmann-fitted thermotransition curves were recorded in standard buffer while heating to 90 °C and cooling back to 10 °C, at pH 5.8 (— and —, respectively), at pH 6.8 (— / —) and pH 7.5 (— / —). For clarity, the transitions at pH 6.3 have been omitted. **D:** Table of thermo-transition points calculated from **C** at different pH values. **E:** CD spectra of Sip1 incubated with mounting concentrations of GdmCl at pH 7.5. 0 M GdmCl: —, 0.06 M: —, 0.1 M: —, 0.2 M: —, 0.4 M: —, 0.8 M: —, 1.2 M: —, 2.3 M: —, 3 M: —. **F:** Ellipticity signals at 218 nm of the GdmCl titration series plotted against the GdmCl concentration, at pH 5.8: ●, pH 6.3: ●, pH 6.8: ●, pH 7.5: ●.

However, at all pH values, the midpoint of structural transition was calculated to be at ~ 1.25 M GdmCl. Independent of pH, 50 mM of GdmCl already effected a reduction in secondary structure content (Fig. 3.6E), and complete unfolding was observed at incubation with 3 M GdmCl, with no further loss in ellipticity signal up to 6 M GdmCl at pH 5.8 to pH 7.5.

3.4.2 QUATERNARY STRUCTURE OF SIP1

After the secondary structure analysis of Sip1 had revealed a β -sheet fold with pH-dependent thermostability, its quaternary structure was determined next. With the help of Dr. M. Krause, sedimentation velocity analytical ultracentrifugation (SV-AUC) was employed to find out whether Sip1 was monomeric or formed oligomers. The sedimentation coefficient analysis displayed only one relatively narrow peak at ~ 15.8 S at pH 7.5 (Fig. 3.7). Basically the same narrow peak was observed at pH 8.2. This alkaline pH value was elected to further expand the examined pH range, while not being too close to Sip1's isoelectric point of 7.9.

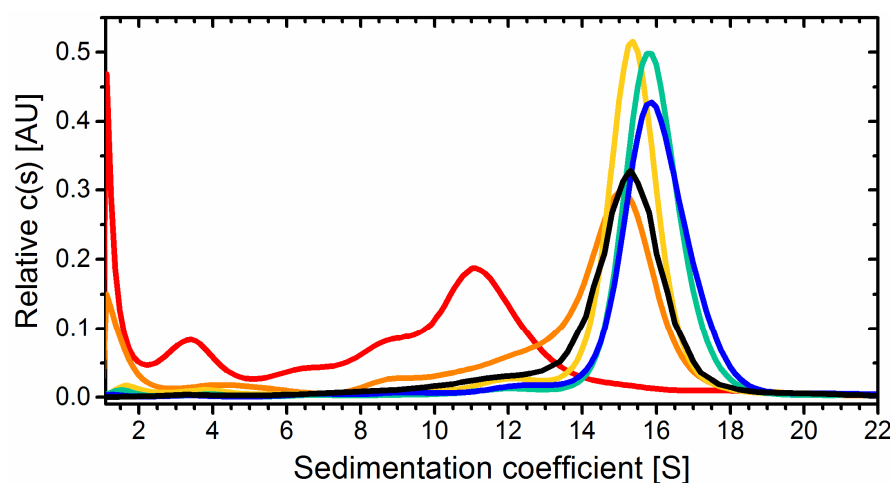


Fig. 3.7: Sedimentation velocity analytical ultracentrifugation analysis of Sip1 (79 μ M) at different pH values: pH 5.8: —, pH 6.3: —, pH 6.8: —, pH 7.5: —, pH 8.2: —. For direct comparison, the sedimentation equilibrium profile of Sip1 at pH 7.5 in the presence of 50 mM GdmCl is shown in this graph, as well: —.

Sip1 sedimented at pH 6.8 also showed a single, narrow maximum which, however, was shifted to 15.3 S. At pH 6.3, a rather broad peak emerged with a maximum at 15.1 S and a pronounced tailing towards small S-values, ending in a slight peak at ~ 9 S. Two additional diminutive peaks at ~ 4.3 and ~ 1 S indicated further small species. At pH 5.8,

the distribution of sedimentation coefficients was broader still than at pH 6.3, with local maxima at 11.1, 9.1, 6.8, 3.4 and ~ 1 S, while higher-order ensembles were missing.

The emergence of a multitude of broad peaks at small S-values was testament to the largest Sip1 complexes' collapse into a polydisperse ensemble of lower stoichiometries at acidic conditions. Sip1 dissociation could also be induced by GdmCl, because already the addition of 50 μM of this chaotropic agent to the pH 7.5 buffer resulted in a shift towards smaller sedimentation coefficients.

Previous AUC analysis of 45 μM of Sip1 in PBS at 20 $^{\circ}\text{C}$ had also yielded a single peak at ~ 16.5 S. Similarly, the core Hsp16 proteins had been found capable of oligomerization, with stoichiometries in the range 20 – 24 subunits according to AUC and EM analyses, and possibly up to 32 subunits according to size exclusion chromatography [220].

In contrast, F08H9.4 formed predominantly dimers and monomers at all tested pH values (Fig. 3.8), which might be due to their lower number of secondary structure elements.

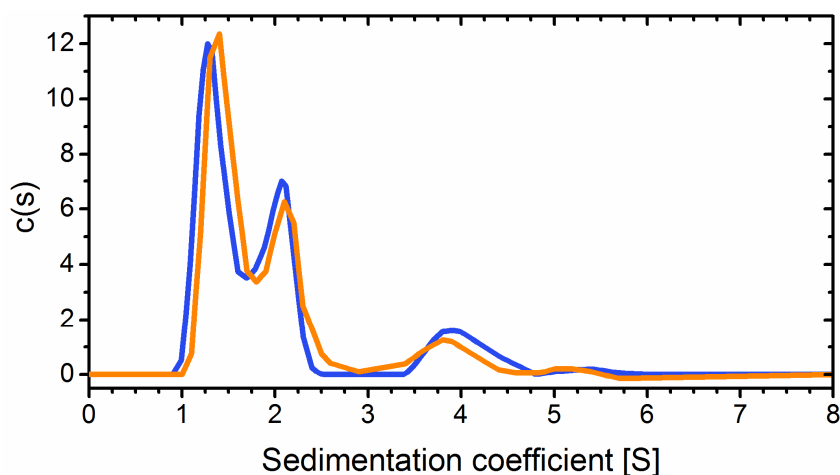


Fig. 3.8: SV-AUC profile of F08H9.4 in standard buffer at pH 6.3: —, and pH 8.2: —.

Thus, F08H9.4 was too small to attempt imaging by EM.

In cooperation with Dr. A. Kastenmüller and Dr. C. Peters from the Group of Prof. S. Weinkauf, transmission electron microscopy (EM) was employed for the visualization of the Sip1 oligomers and a more detailed analysis of their pH-dependent size distribution. First, Sip1 samples were negatively stained (NS, Fig. 3.9A). At pH 8.2, the uranyl acetate preparations showed mostly spherical ensembles with a relatively uniform average diameter of ~ 16 nm. These oligomers were not present at pH 5.8, instead, smaller and less well-defined particles prevailed. NS single particle images were recorded at pH 6.3

and 8.2, as well. Analogous to AUC data (Fig. 3.7), sorting by size revealed a predominance of large species at pH 7.5 and 8.2, and a trend towards smaller ensembles under acidic conditions (Fig. 3.9B). Clearly, the more monodisperse distribution of large oligomers at the slightly alkaline physiological pH of larvae and adult worms disintegrated into a heterogeneous mixture of smaller species upon acidification.

For further structural analysis, cryo-EM was employed. 12,075 projection images of ice-embedded Sip1 were collected at pH 6.5. 2D analysis showed the particles to vary considerably in size. When excluding species <10 nm, three subpopulations of different size and symmetry emerged, for which 3D models could be calculated. These most populated Sip1 oligomers were the 32-, 28-, and 24-mer. Fig. 3.9C shows the three-dimensional reconstructions of these species at a resolution of 12.8 Å, 10.2 Å and 16.7 Å, respectively, at Fourier shell correlation (FSC) = 0.5. The isosurface thresholds were set to enclose a molecular mass of 426 kDa for the 24-mer, 498 kDa for the 28-mer and 570 kDa for the 32-mer.

All three Sip1 assemblies depicted a barrel-like structure with a central pore. The hollow barrel consisted of two stacked, inverted identical subunits. These circular substructures were spanned, cage-like, by building units that stretched from the two subunits' interface to the barrel's hole, where they met with the neighboring "planks". Eight of these recurring units were found per symmetric half in the 32-mer, seven in the 28-mer, and six in the 24-mer. Thus, they were likely to consist of dimers and were indeed calculated to be large enough to accommodate the Sip1 dimer. Due to geometric constraints dictated by the different stoichiometries, dimensions, and general structures of the three reconstructions, minor variations in the spatial arrangement of the planks were observed. Strikingly, the increment between all species was four, which could most obviously be explained by a successive elimination or incorporation of one dimer from or into each inverted half-barrel. Accordingly, data sets of particles >10 nm collected at pH 7.5 and 8.2 also yielded 3D reconstructions of the 32-, 28-, and 24-mers.

These were almost identical to the 3D models described above, and no assemblies besides multiples of four could be identified. Like in the NS-EM results, the 32mer was the pre-eminent species at pH 8.2, whereas 28- and 24-meric states were more highly populated at more acidic conditions. In the course of this pH-driven dissociation process, the assemblies' diameter decreased from ~150 to 130 Å.

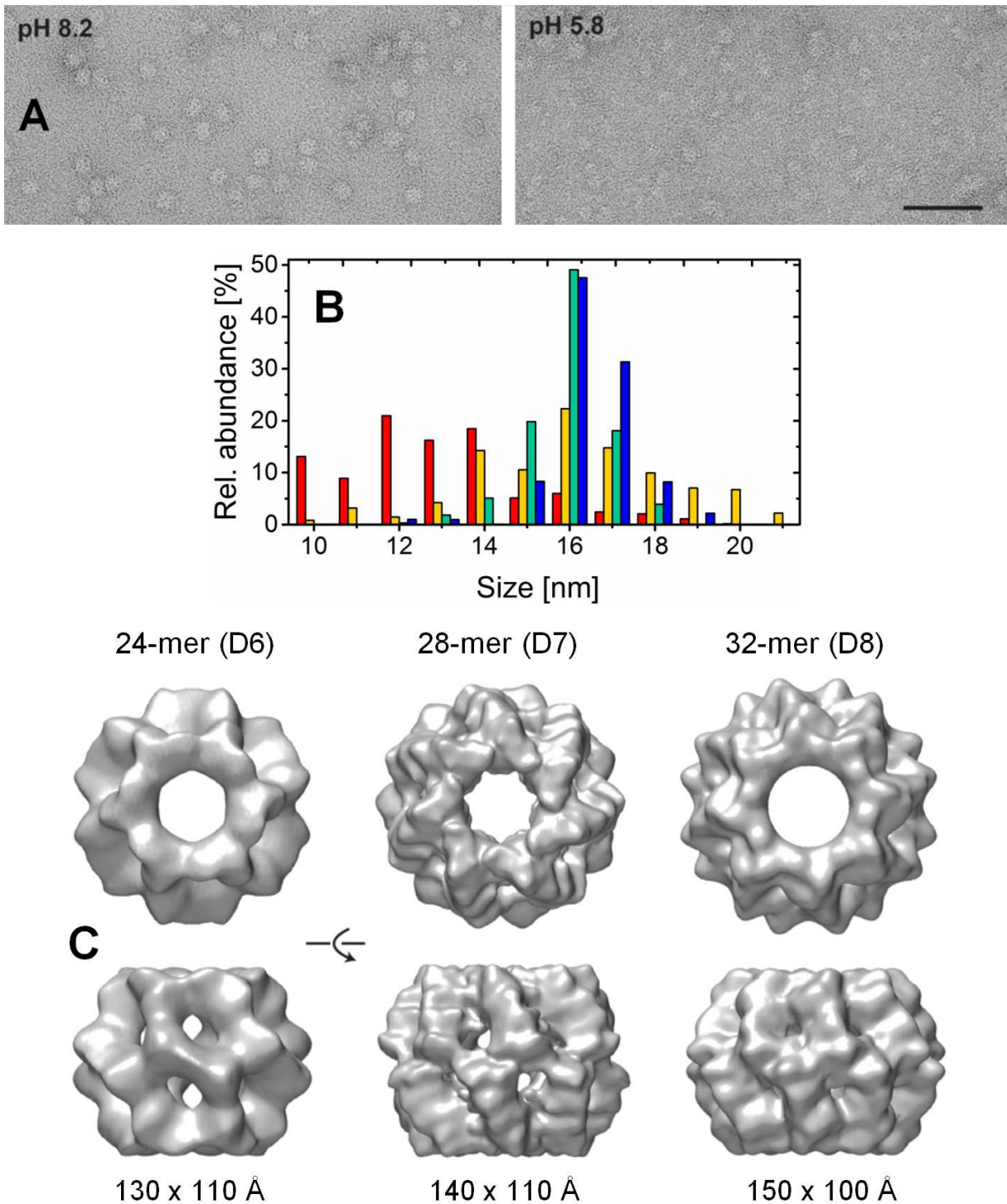


Fig. 3.9: Electron microscopic analyses of Sip1 oligomers. **A:** Negative-stain electron micrographs of Sip1 (25 $\mu\text{g/ml}$) at pH 8.2 and 5.8. Scale bar: 50 nm. **B:** Sip1 oligomer size distribution, as observed in negative stain-EM preparations at different pH values: pH 5.8: ■, pH 6.3: ■, pH 7.5: ■, pH 8.2: ■. **C:** Cryo-EM 3D-reconstructions of the Sip1 24-, 28-, and 32-mer. The D6, D7, and D8 symmetry is clearly visible in top view of the surface representations (top row), while the side view is directed along a two-fold axis through the hollow barrel structures' "middle". Data collection and analysis was performed by Dr. A. Kastenmüller and Dr. C. Peters in Prof. Weinkauf's Group.

The Sip1 24-mer notably differed from the NS-EM models of 24-meric Hsp16.2, Hsp16.41 and Hsp16.48 (Fig. 1.12).

3.4.3 CRYSTALLIZATION OF SIP1

3.4.3.1 SELENO-METHIONINE SUBSTITUTION

To obtain an atomic resolution structure of Sip1, its crystallization was attempted. Out of the several thousand crystallizing conditions tested, sufficiently large, refracting crystals of highly purified Sip1 only formed from 5 mg/ml of protein in 50 mM HEPES (4-(2-hydroxyethyl)-1-piperazineethanesulfonic acid), 50 mM MES (2-(*N*-morpholino)ethanesulfonic acid), 15 % PEG400 (polyethylene glycol), 50 mM sodium acetate, pH 7.1 (Fig. 3.10). Using synchrotron radiation from the Swiss Light Source (Paul-Scherrer-



Institut, Villingen, Switzerland), Dr. M Stein and Prof. M. Groll recorded a dataset to 3.6 Å in the P422 space group. From this, however, the Sip1 crystal structure could not be easily solved.

Fig. 3.10: Crystals of full-length Sip1 at the conditions specified in the text, in a sitting-drop well.

Somewhat surprisingly, the MR programme Phaser failed to find the Sip1 phases with the coordinates of truncated human CRYAB (PDB accession code: 2WJ7 [247]) as starting model. At 3.6 Å refraction, the data quality was insufficient for brute force testing of all possible phases. Other methods to recover lost phases depend on the distinct anomalous scattering factors of heavy atoms, from whose positions the other atoms' localization is inferred by interatomic vectors. In multiple isomorphous replacement (MIR), this is achieved by soaking crystals with heavy metals (Hg, Pb, Os), but for Sip1, no sufficient number of crystals was obtained.

To solve this problem, a mutant of Sip1 was generated in which all five Met were replaced by seleno-methionine (SeMet). Production of SeMet-substituted Sip1 was first

attempted by expressing Sip1 in the Met-auxotrophic *E. coli* strain B834. As detailed elsewhere [248], cells were grown in minimal medium containing Met, harvested and resuspended in medium without Met. Before induction, seleno-L-methionine was added. SeMet incorporation into Sip1 was successful judging by a slight increase in molecular weight seen in the SDS-PAGE band (235 Da). The protein yield of SeMet-labelled Sip1 was higher, however, when the Met biosynthesis of BL21 DE3+ was blocked. The Löwe protocol [249] achieved this by feedback-inhibiting aspartokinases in the presence of high concentrations of Ile, Lys and Thr, and adding seleno-L-methionine. SeMet-Sip1 was purified like the wt protein and crystallized from the same buffer conditions. The resulting crystals were of the same shape, and the absorption spectrum indicated the successful incorporation of SeMet into the protein. However, none of them yielded a sufficiently resolved dataset to serve as a starting model for the phase problem.

3.4.3.2 TRUNCATED SIP1

In consequence, a truncated version of Sip1 was created: Sip1-ACD. The construct encompassed aa 43 – 140, i.e. the ACD and part of the CTR up to two aa after the IXI motive. It was expressed in BL21 DE3+ and purified as described in M&M.

Crystals (Fig. 3.11) were obtained from 5 mg/mL of highly pure Sip1-ACD in 33 mM CAPS (*N*-cyclohexyl-3-aminopropanesulfonic acid), pH 6.9, 17 mM BIS-TRIS (bis(2-hydroxyethyl)-amino-tris(hydroxymethyl)-methane), 17 mM ammonium sulfate, 10 % pentaerythritol ethoxylate.

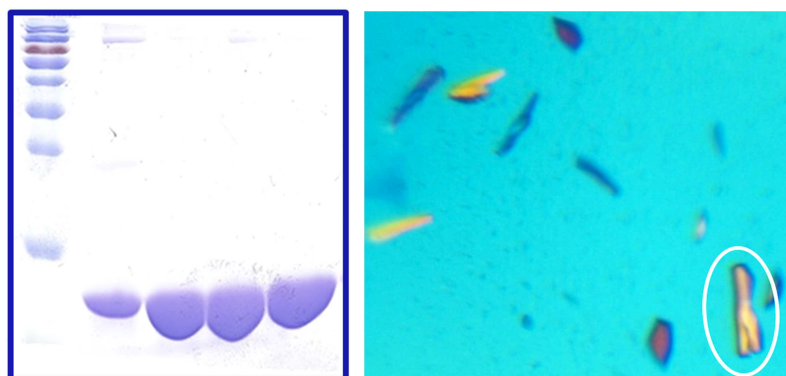


Fig. 3.11: Sip1-ACD.

Left: SDS-PAGE of pure fractions of Sip1-ACD. **Right:** Crystals of the Sip1 ACD construct in the buffer specified in the text, photographed through a polarization filter. The very crystal which gave the 2.1 Å diffraction data is circled.

Truncated Sip1 crystallized in the $P2_12_12_1$ space group. The 2.1 Å dataset could be refined to a final R_{free} value of 25.9 % by molecular replacement with the truncated hCRYAB structure (2WJ7, aa 67-157) and subsequent TLS refinement including the 2-

fold non-crystallographic symmetry. See Table 6.3 in M&M for the crystallographic parameters.

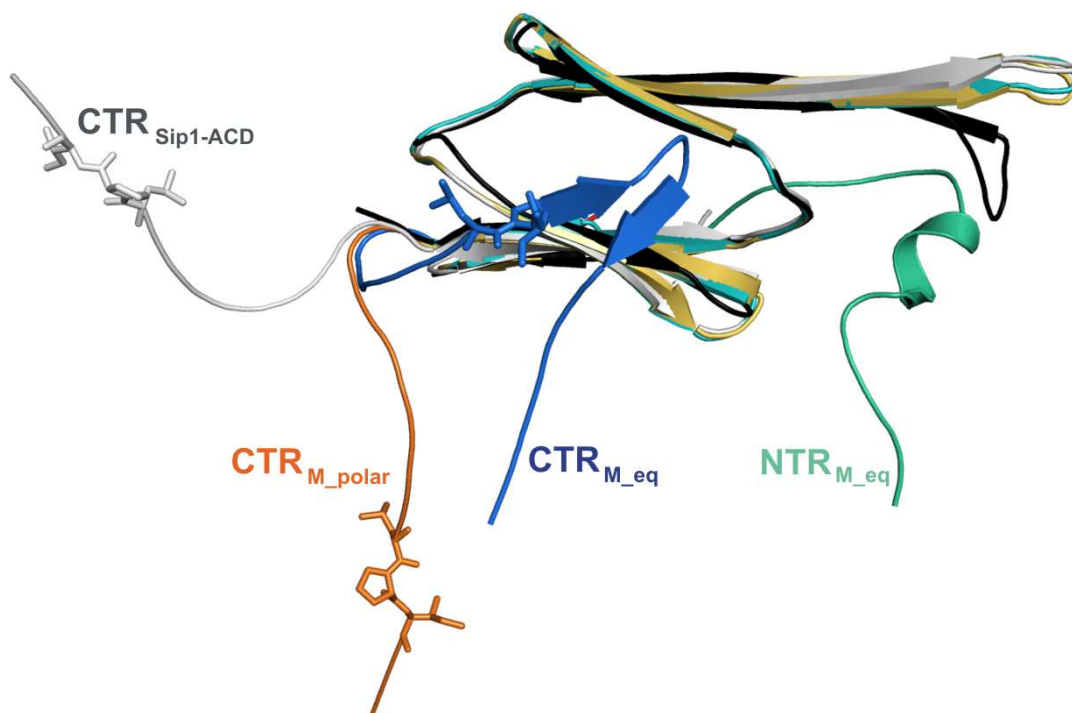


Fig. 3.12: Superposition of the crystal structures of monomeric Sip1-ACD (grey), the two full-length Sip1 conformers M_{polar} and M_{eq} (yellow-orange and green-blue, color coding according to the domain organization shown in Fig. 3.12C), and human αB -crystallin (2WJ7, black). While the ACD-domains of the protomers perfectly match (r.m.s.d of the C_{α} -atoms $< 0.43 \text{ \AA}$), the CTRs point to opposite directions, rendering the dimer asymmetric. The N- and C-terminal regions resolved in the crystal structures are indicated.

Strikingly, the Sip1 ACD fold clearly pertains to the mammalian-type category (Figs. 3.12, 1.6), rather than to the non-mammalian architecture which is also adopted by flatworm Tsp36 [93], the only other metazoan sHsp crystal structure available. In the crystal, the Sip1 ACDs are organized as dimers of two parallel layers of β -sheets formed from the antiparallel $\beta 2$ -9-strands, as usual for mammalian sHsps (shown for the full-length protein in Fig. 3.13A, B).

3.4.3.3 FULL-LENGTH SIP1

The full-length Sip1 crystal refracted to 3.6 \AA . This diffraction dataset in the P422 space group could finally be solved using the phases of the truncation construct. MR and isotropic TLS-refinement using the 2-fold symmetry axis in the asymmetric unit cell that contained 4 molecules yielded a final R_{free} value of 25.2 % (for the crystallographic parameters, see Table 6.3 in M&M).

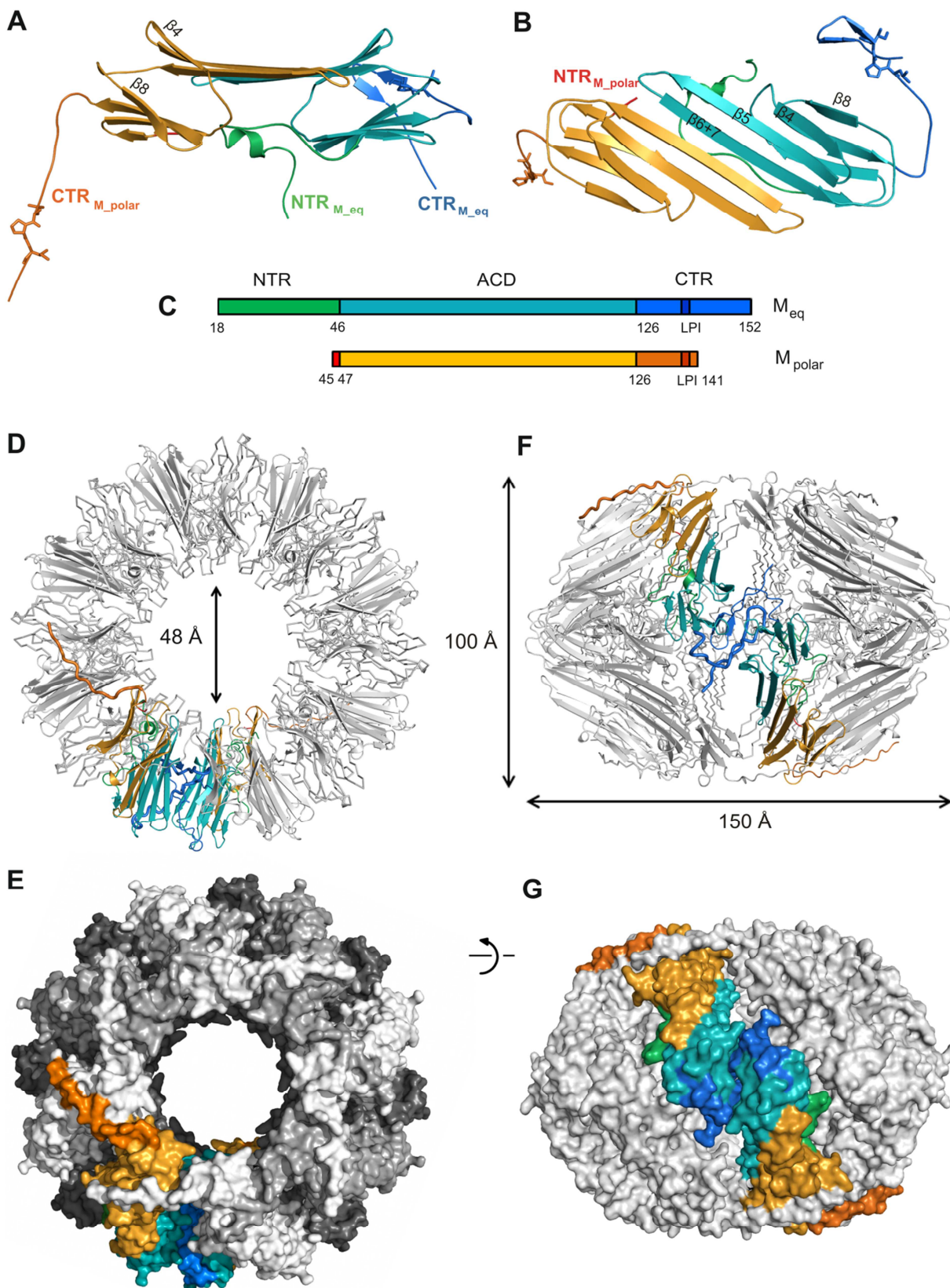


Fig. 3.13: Crystal structure of full-length, 32meric Sip1.

A: PyMOL cartoon representation of the Sip1 dimer viewed from the side and the top (**B**). The polar and equatorial monomers (M_{polar} and M_{eq} , colored according to the schematic shown in **C**) interact along their $\beta_6+\beta_7$ -strands within their ACDs to form an antiparallel homodimer. The side chains of C-terminal residues Leu136, Pro137 and Ile138 (IXI motive) are shown as sticks. Some β -strands as indicated as well. Loops are smoothed.

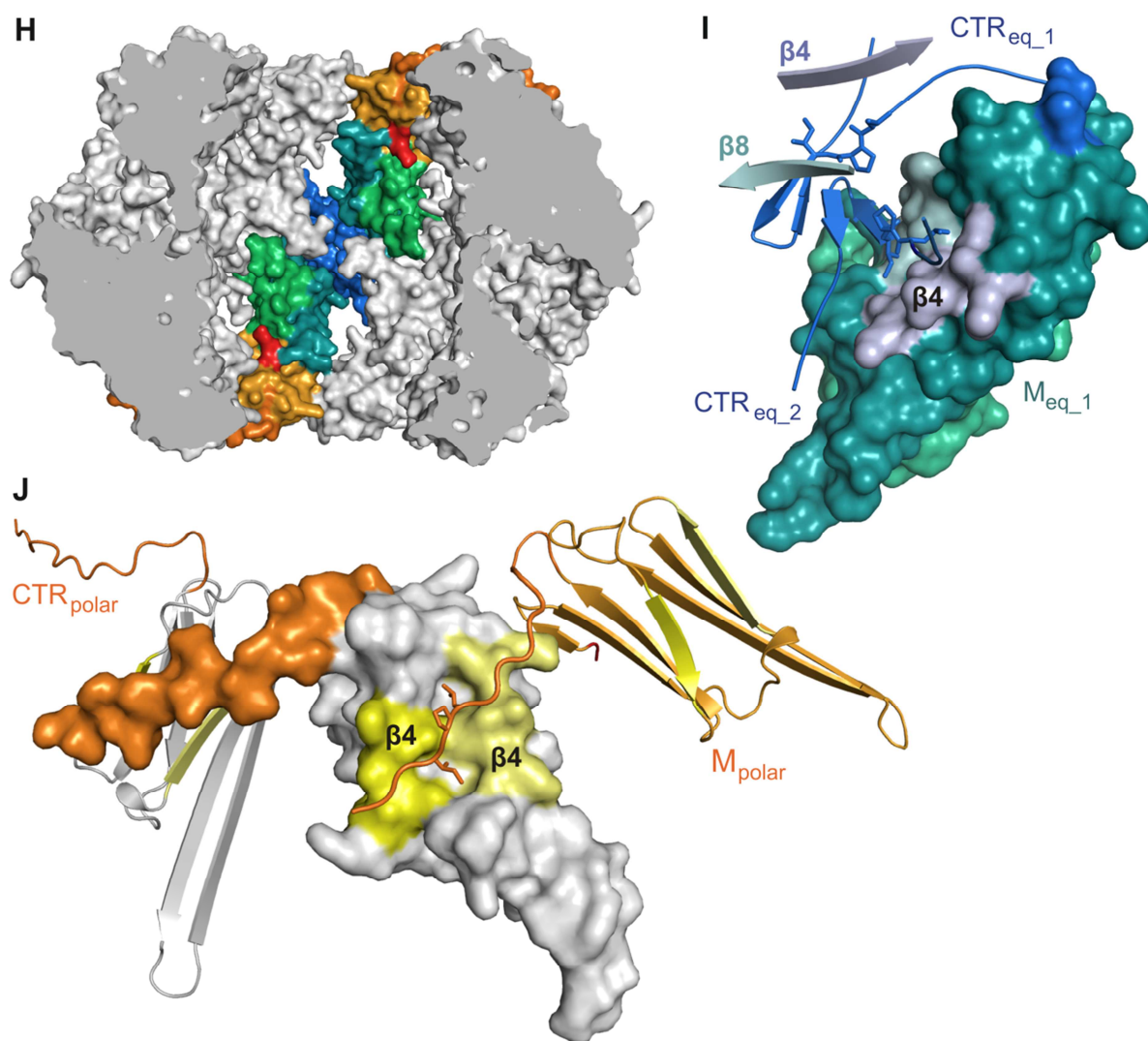


Fig. 3.13 (continued). **C:** Domain organization of Sip1: N-terminal region (NTR, residues 1–45, resolved from aa 18 or 45 in the equatorial or polar protomer, respectively): green or red, α -crystallin domain (ACD, residues 46-125): teal in M_{eq} and light orange in M_{polar} , C-terminal region (CTR, residues 126-159, resolved to aa 152 or 141, respectively): blue or orange.

D/E: Overall structure of the Sip1 32-mer viewed from top in cartoon (**D**) and surface (**E**) representation. Within each ring, one apical (M_{polar}) and one equatorial (M_{eq}) protomer is colored according to **C**. In **E**, the remaining subunits are shown alternately in light and dark grey.

F/G: Sip1 32-mer viewed from side in cartoon and surface representation. Dimensions are indicated in **F**.

H: Cross section through the middle of the 32-mer.

I: Inter-subunit contacts between two equatorial protomers stemming from opposite rings (*trans*-contacts). Shown is one monomer, M_{eq_1} , in surface representation with its β 4- and β 8-strands colored light purple and grey, respectively, and its CTR as cartoon. For clarity, only the β 4- and β 8-strands and the CTR of the second M_{eq} are shown. The protomers are intertwined on the one hand through binding of the IXI motive to the β 4/ β 8-groove, and on the other hand through formation of a β -sheet by the two short β -strands formed by the C-terminal residues downstream of the IXI motive (here LPI, shown as sticks).

J: Inter-subunit contacts between apical protomers within one ring (*cis*-contacts). The M_{polar} in the middle is shown in surface representation, while the flanking ones are represented as cartoons. The ring assembly is accomplished by binding of the C-terminal IXI motive of a M_{polar} into a hydrophobic groove formed by the β 4- and β 8-strands (highlighted in yellow) of the ACD of an adjacent M_{polar} .

The biological assembly under this condition was found to be the 32mer. The slightly flattened, hollow spheroid assembly has the dimensions 100 x 150 Å, an inner diameter of 60 Å and a central pore of 48 Å (Fig. 3.13D-H). The highly symmetrical structure can be likened to a barrel (like the EM structures) or to a globe with an equator and two poles. Employing the latter analogy, each hemisphere is spanned by eight dimers that radially emanate from the equator and group in a circle at the poles, leaving open an apical hole. The hemispheres are solely connected via the CTRs of the polar monomers. Two identical half-spheres are fused by the intertwining CTRs of two symmetrical, equatorial monomers across the equator interface. Mainly because of this distinct linkage motive, which forces the CTRs to stretch into different directions, the apical and equatorial monomers are non-equivalent, while among themselves, they are identical. In both cases, the IXI motive (LPI in Sip1) binds into the hydrophobic groove formed by the neighboring ACD's β 4- and β 8-strand, again pronouncing the important role of this structural determinant for oligomerization.

Intriguingly, the CTRs near the apical pore are resolved only to three residues after the IXI motive, whereas the last 17 residues are not resolved, indicating their flexibility (Fig. 3.13J). In contrast, the equatorial CTRs are almost fully resolved, revealing that contacts between half-spheres are conveyed by two extra β -strands that are formed by the additional ten resolved residues directly after the IXI motive (Fig. 3.13I).

Moreover, a large part of the equatorial NTR could be resolved, which points into the hollow sphere's cavity. No polar interactions between the NTRs and the surrounding monomers are detected, indicating that they likely contribute little to oligomer stabilization. The resolved aa that can be considered the very end of the polar NTRs are also oriented towards the 32-mer's center rather than its surroundings. The N-terminal 44 residues being unresolved again suggested their not being involved in long-lasting, stable interactions. However, with major parts of the NTRs invisible in the crystal structure, their real localization and potential function in oligomer stabilization or substrate binding can only be speculated at.

Structural disorder in the termini is common in sHsps, only few are fully resolved [72, 86, 89, 90, 95, 96]. In summary, aa 18 - 152 and 45 - 141 of the equatorial and polar Sip1 monomers are resolved, respectively.

See Fleckenstein, Kastenmüller *et al.* (in progress) for details and PDB accession numbers.

3.5 INVESTIGATION OF THE OLIGOMERIZATION SWITCH

3.5.1 SIP1 H111/139 DOUBLE MUTANT

The crystal structure allowed searching for the very amino acids that might play a role in the pH-induced dissociation of Sip1 oligomers which was observed in the AUC and EM experiments. EM results had suggested the step-wise de-oligomerization from the 32-mer to the 28- and 24-mer upon acidification to progress by the concerted expulsion of two dimers. Only histidine residues display a pKa at the relevant pH range, namely 6.7-7.1 within a polypeptide. Indeed, Sip1 is significantly enriched in His in comparison with its closest homologues.

His111 and His139 seemed promising candidates for pH sensing oligomerization switches, because they are located at the beginning of the β 8-strand and at the first β -strand immediately after the LPI motive in the CTR_{eq}, respectively (Figs. 3.1, 3.16B). Thus, they are situated within the very loop of the equatorial monomers which tethers the two halves of the Sip1 32-mer together. Both residues are close enough to the neighboring dimer as to facilitate interactions, such as π - π stacking. Also, a polar contact between H139 and T112 is indicated by PyMOL.

The two His were exchanged for Asn in order to generate a Sip1 mutant that would lose the wt's ability to react to a pH shift by changing its oligomerization state. After mutagenesis and transformation of the plasmid, the construct was produced and purified like wt Sip1 (Fig. 3.17A). The CD spectra at pH 5.8 and 7.5 were basically the same as for wt (Fig. 3.14). At a T_m of 52 °C and with a loss of 15 % in secondary structure upon heating from 10 °C to 90 °C, the His111/139Asn double mutant was more stable at pH 7.5 than the wt protein (compare Figs. 3.14, 3.6C).

In case the pH sensor had been rendered dysfunctional, the mutant would be expected to populate certain species at an inherent pattern of abundances, regardless of pH. No assemblies larger than the 16-mer would be expected if the alterations in the CTRs proved even grave enough that two halves could no longer combine to the globe-like structure. This was not the case, because the AUC profile of the Sip1 H111/139N double mutant quite closely mirrored the dissociation process evident in wt when shifted to lower pH values (compare Figs. 3.15, 3.7, and 3.9).

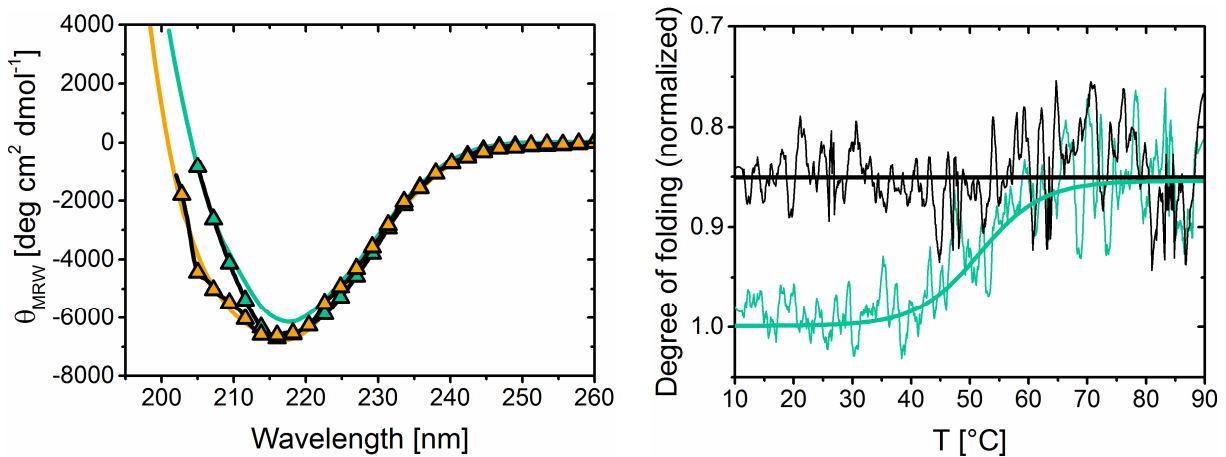


Fig. 3.14: CD spectra of Sip1 H111/139N mutant. **Left:** CD spectra were recorded at 10 °C for 10 μ g of wt Sip1 (lines) and His-Asn substituted Sip1 (triangles) at pH 6.3 (—) and 7.5 (—). **Right:** The thermal stability of the Sip1 H111/139N mutant was assayed by monitoring the change in ellipticity at a set wavelength of 218 nm upon heating (—) to 90 °C, and cooling back to 10 °C (—), at pH 7.5.

However, the single peak at alkaline conditions was far narrower than that for wt. At both pH 8.2 and 7.5, the maximum was shifted to \sim 15.1 S, as opposed to \sim 15.8 S for wt Sip1.

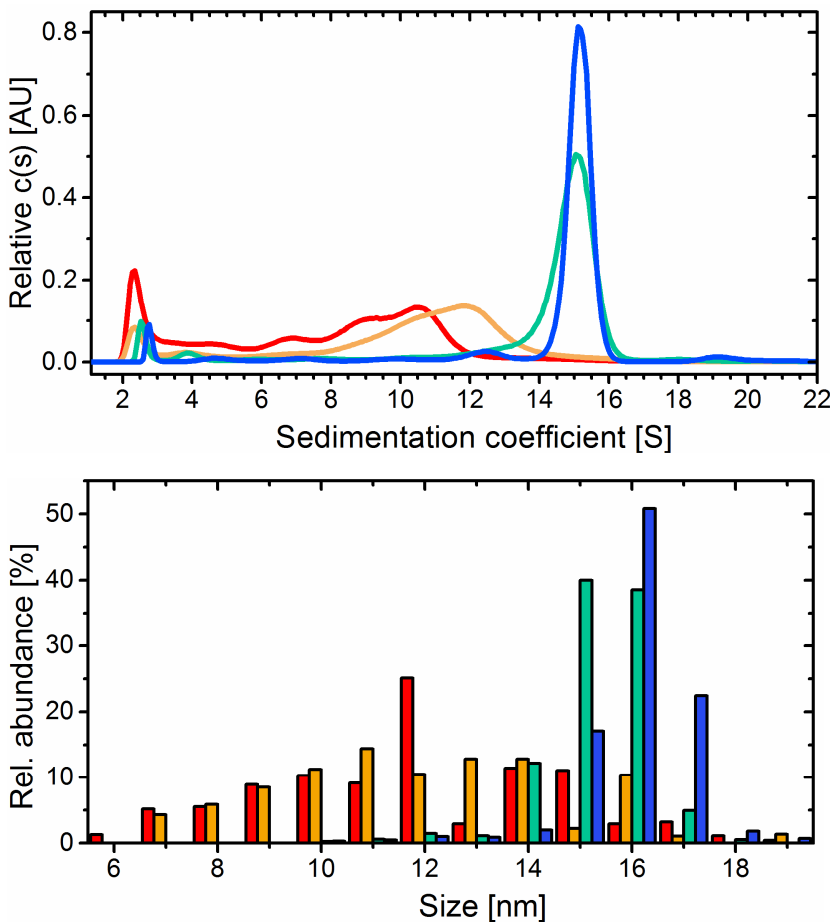


Fig. 3.15: Size distributions of Sip1 H111/139N double mutant.

Top: SV-AUC profile of the His mutant (70 μ M) at 10 °C, **Bottom:** Relative abundance of Sip1 H111/139N poly-disperse ensembles in NS-EM preparations (1.4 μ M). For both methods, the construct was analyzed in standard buffer at pH 5.8: —, pH 6.3: —, pH 7.5: —, pH 8.2: —, pH 8.2: —.

Moreover, the largest mutant oligomers started to dissociate at pH 7.5 already, as evidenced by a tailing towards smaller sedimentation coefficients, while the peaks at pH 8.2 and pH 7.5 were basically identical for wt protein. Most notably, the AUC profile at pH 6.3 showed a very broad population distribution peaking at ~ 12 S, which differed greatly from the more defined wt peak at ~ 15 S. At pH 5.8, peak patterns were comparable for the two proteins. An extremely similar size distribution was obtained by EM of Sip1 H111/139 negative stains prepared at the same four pH values (Fig. 3.15).

According to both methods, the onset of pH-induced deoligomerization thus occurred at more alkaline pH values if His111 and His139 were exchanged for Asn. Also, the largest ensemble found in wt Sip1, presumably the 32-mer, appeared to be missing. Since the construct's oligomeric state still showed a strong pH-dependence however, these two mutations proved insufficient to completely disrupt the pH sensor. More or different residues seem to be involved in the loss of inter-dimer contact and the ejection of dimers upon acidification.

3.5.2 SIP1-ACD AND SIP1/AB-CRYSTALLIN CHIMAERA

The Sip1-ACD construct which had been fundamental in solving the 32meric Sip1 crystal structure was further analyzed to evaluate the structural effect of the loss of NTR and part of the CTR. Since this truncated version still retained the CTR up to T140, i.e., two aa after the LPI motive, it would answer the question whether IXI alone was sufficient for oligomer formation. The Sip1 dimer had shown great similarity to α B-crystallin in the crystal structure, and their ACD sequences were highly homologous (Fig. 3.16B). Fusion of the unconserved CTR of human α B-crystallin to the Sip-ACD construct addressed whether a full CTR would allow oligomerization despite lack of the entire NTR, even if it was from another organism. Would the resulting oligomers behave more like Sip1 or α B-crystallin, or different altogether?

The sequence of this "chimaera" is shown in Fig. 3.16C. The fusion protein was expressed and purified like wt Sip1 (Fig. 3.17). CD spectroscopy (Fig. 3.18A, C) revealed both Sip1-ACD and chimaera to be natively folded. As expected, the minimum at ~ 218 nm grew more pronounced compared to the full-length protein as the relative percentage of β -sheets increased. Thus, the truncation mutant, which almost entirely consisted of the ACD, reached a θ_{MRW} signal of below $-11,000$ deg*cm²/dmol.

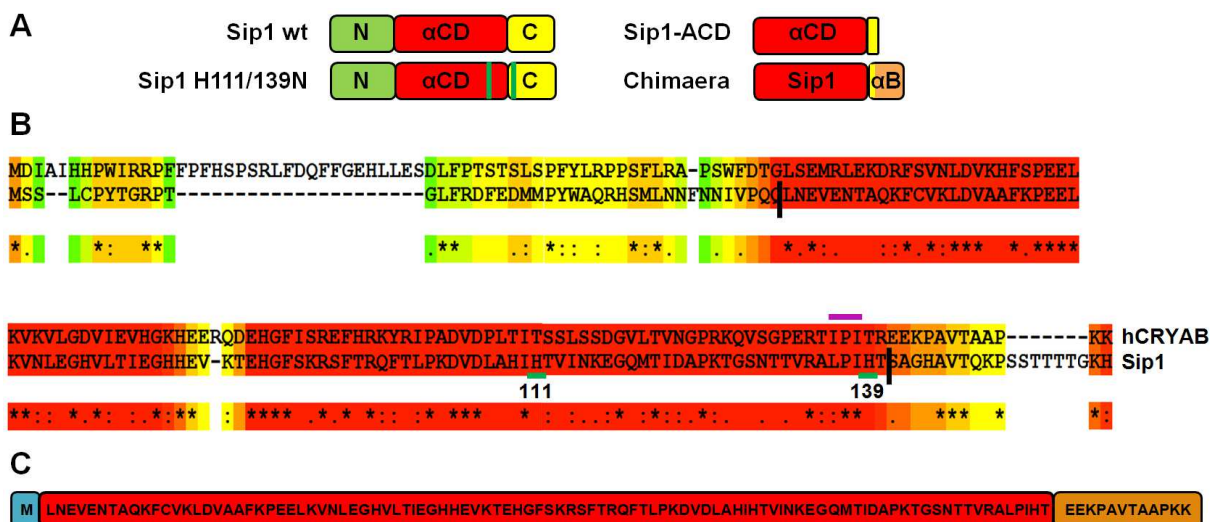


Fig. 3.16: Schematics and amino acid sequences of Sip1 mutants constructed in this work.
A: Schemes of domain architecture of wt Sip1 and its derivatives. N: N-terminal region, αCD: α-crystallin domain, C: C-terminus, αB: CTR of human αB-crystallin fused to the Sip1 ACD. His111 and His139 are indicated by green stripes in **A**, and underlined in **B**: Alignment of human αB-crystallin (hCRYAB) and Sip1. The IXI motive is over-lined in purple. The truncation limits for the Sip1 ACD (which corresponds to the Sip1-ACD mutant) are depicted as black bars. The sequence of the fusion protein consisting of the Sip1 ACD and the CRYAB CTR is given in **C**.

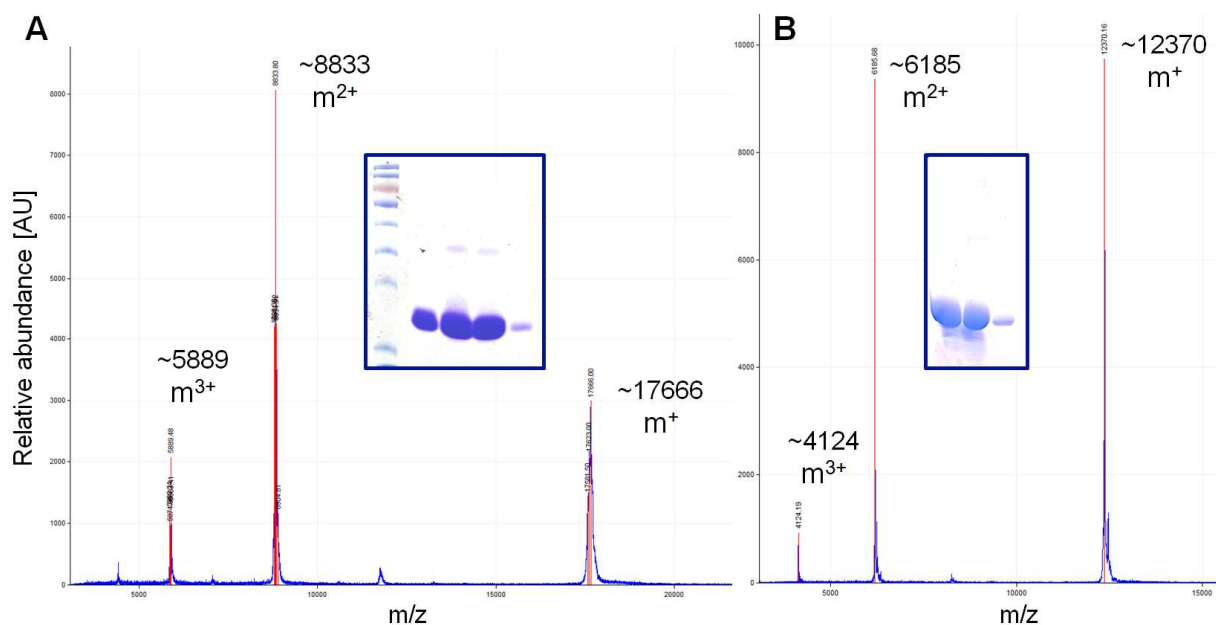


Fig. 3.17: SDS-PAGE and full-length MS showed the H111/139N mutant (A) and the Sip1-CRYAB fusion protein (B) to be ≥95 % pure and not degraded after native purification from BL21 DE3+.

CDNN calculations predicted the secondary structure of Sip1-ACD to consist of 36 % of β-sheets and 20 % of β-turns, which is still too low considering the crystal structure. The ellipticity signal changed within the examined pH range, with a minimum at pH 5.8. Sip1-ACD adhered to the trend set by wt Sip1, with highest thermostability under acidic conditions and increased heat-sensitivity of the secondary structure at neutral to alkaline

pH values (Fig. 3.18B). In detail, Sip1-ACD T_m was found to be $65 \pm 1.5^\circ\text{C}$ at pH 5.8 (with a 25 % decrease in native fold), $59 \pm 1^\circ\text{C}$ (39 %) at pH 6.9, and $44 \pm 1^\circ\text{C}$ (43 %) at pH 10. In contrast, with a T_m of $59 \pm 1^\circ\text{C}$, the chimaera was almost as stable at pH 7.5 as wt Sip1 at its preferred acidic pH values. 28 % of secondary structure was lost during heating of the fusion protein (Fig. 3.18C, D).

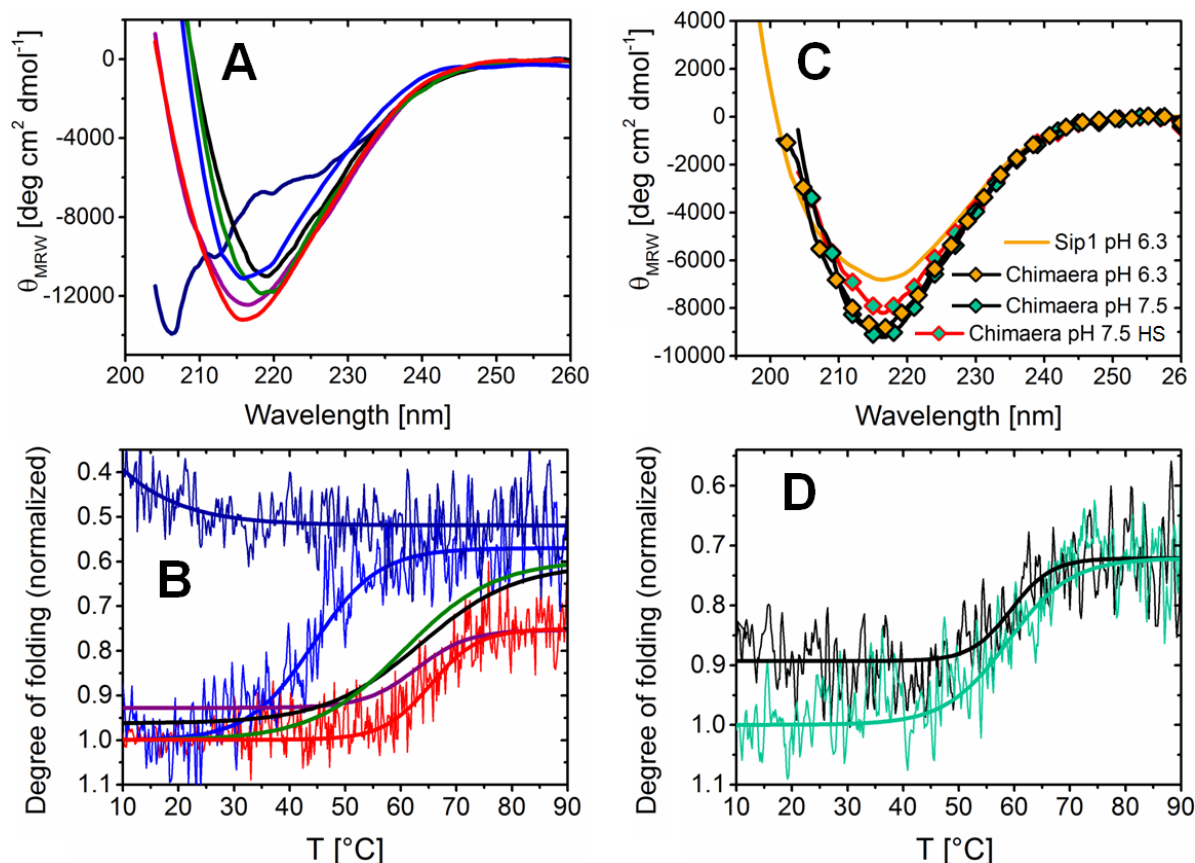
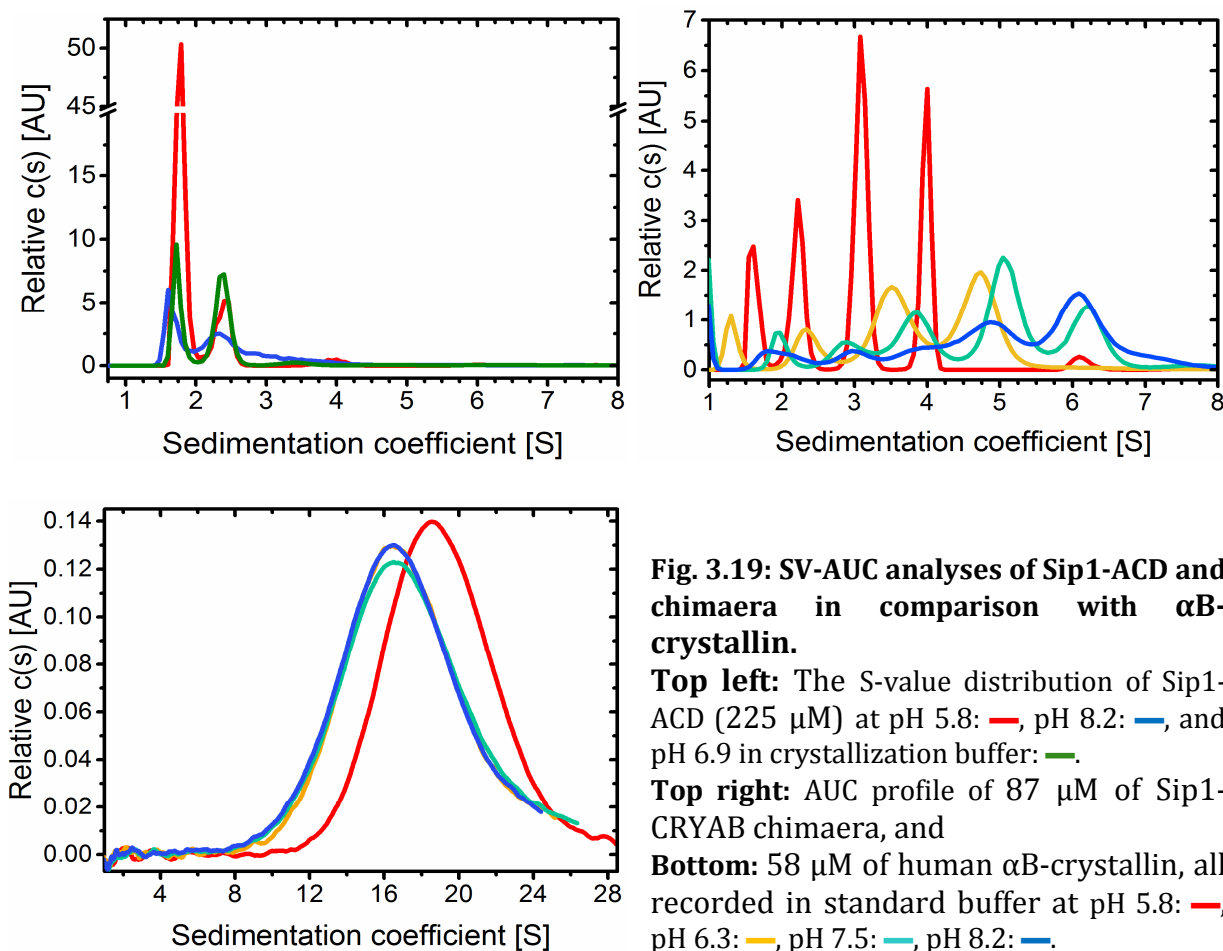


Fig. 3.18: CD spectra of Sip1-ACD and Sip1/ αB -crystallin chimaera. **A:** 10 μM of Sip1-ACD at 10 $^\circ\text{C}$ and after heating to 90 $^\circ\text{C}$, in standard buffer at pH 5.8 (— and —, respectively), in crystallization buffer at pH 6.9 (— / —), and in 50 mM CAPS, pH 10.0 (— / —). **B:** Thermal stability of Sip1-ACD upon heating to 90 $^\circ\text{C}$ and cooling back to 10 $^\circ\text{C}$, recorded at 218 nm in standard buffer at pH 5.8 (— and —, respectively), in crystallization buffer at pH 6.9 (— / —), and in 50 mM CAPS, pH 10.0 (— / —). For clarity, only the Boltzmann fit is shown for the pH 6.9 conditions.

C: CD spectra recorded at 10 $^\circ\text{C}$ for 10 μg of wt (line) and Sip1/ αB -crystallin fusion protein (diamonds) at pH 6.3 (orange) and 7.5 (green). The red line denotes chimaera at pH 7.5 after thermotransition. **D:** Thermotransition curve of chimaera as assayed by monitoring the change in ellipticity at a set wavelength of 218 nm upon heating (—) to 90 $^\circ\text{C}$, and cooling back to 10 $^\circ\text{C}$ (—), at pH 7.5.

A SV-AUC experiment of the Sip1-ACD fragment identified two dominant species at ~ 1.4 and ~ 2.2 S, (Fig. 3.19), corresponding to the monomer and the dimer. A slight peak at ~ 3.1 S most likely represented the tetramer. This result remained the same for Sip1-ACD

analyzed at pH 5.8 or 6.9, or at pH 10, in the CAPS buffer from which the truncation mutant was crystallized. Thus, the truncated ACD was sufficient to facilitate dimerization, as seen in the crystal structure. The remaining LPI motive might allow for some inter-dimer interaction, but the lack of NTR and the missing 19 C-terminal aa prevented higher order oligomerization, as displayed by wt Sip1 at these pH values.



The presence of a full CTR in the chimaeric construct conveyed the capability of oligomer formation, albeit at smaller stoichiometries than wt Sip1 (Fig. 3.19). Four to at least six species were observed by SV-AUC at the four examined pH values ranging from pH 8.2 to 5.8. Again, the assemblies tended to be larger under alkaline conditions. At pH 8.2, six peaks could be distinguished, with S-values ranging from \sim 7 S to \sim 1.7 S and the most intense signal at \sim 6.1 S. This indicated the presence of 16-mers, possibly 20-mers, down to di- and monomers, with various ensembles in between, presumably including 12-mers, octamers and tetramers. At pH 7.5, the size distribution was shifted to smaller sedimentation coefficients, with a maximum at \sim 5 S and an absence of particles sedimenting at \sim 7 S. This shift continued at pH 6.3 and 5.8, where four distinct particles emerged, most likely monomeric, dimeric, tetrameric and hexa-octameric chimaera,

according to SedFit calculations. The AUC peak at ~6.1 S was notably diminished at pH 5.8. The undefined $c(s)$ distribution at pH 8.2 and 7.5, as well as the slight changes in maxima of peaks that probably correspond to particles of the same stoichiometries suggested that these oligomers could adopt differently shaped, interchanging assemblies. Unfortunately, the fusion protein could not be visualized by Dr. C. Peters because NS-EM micrographs at various pH values failed to yield sufficiently homogenous particles within the expected size range.

Intriguingly, SV-AUC characterization of native human α B-crystallin showed the protein to adopt an ample range of different oligomers (spanning 8 S to at least 26 S), but their relative population was identical over a pH range of 8.2 to 6.3. Only at pH 5.8 did the ensemble shift to larger sizes, as the maximum changed from 16.5 S to 18.5 S (Fig. 3.19).

This meant that α B-crystallin, although a close homologue in sequence and ACD dimerization architecture, was Sip1's opposite in pH-dependency of size, with a tendency to form higher-order oligomers at low pH. In the fusion protein, it was the Sip1 ACD rather than the CRYAB CTR, which dictated the direction of size pH-dependency.

3.6 FUNCTIONAL CHARACTERIZATION

The structure of Sip1 had thus been investigated with the use of circular dichroism spectroscopy, electron microscopy and X-ray crystallography, and found to depend on pH in both oligomerization state and thermostability. Next, the function of Sip1 and whether it, too, was modulated by pH, were to be elucidated.

3.6.1 CHAPERONE ACTIVITY ASSAYS – COMPARISON OF SHSPS

Starting with an *in vitro* approach, chaperone assays were employed to ascertain whether Sip1 was active as a holdase as expected of, but not proven for all reported small heat shock proteins. As mentioned before, no member of the Hsp12 family of *C. elegans* has been shown to be functional as a molecular chaperone [83]. Also, neither F08H9.3 nor F08H9.4 could suppress the unspecific aggregation of a stress-labile, unfolding model substrate upon heat-shock. Both F08H9 proteins were inactive within the pH

range from pH 5.8 to 8.2, even at a 24-fold excess of sHsp to citrate synthase (CS), the precipitating substrate. Neither could they be activated upon pre-incubation in buffer containing DTT_{ox} or DTT_{red}, which had resulted in the highest regain of secondary structure for F08H9.4 (Fig. 3.5D). Only the results from the CS assay in standard buffer at pH 6.3 are shown in Fig. 3.20, as the aggregation curves recorded for the other conditions mentioned were similar.

At pH 7.5 and 8.5, Sip1 effected no significant alleviation of substrate aggregation, either (Figs. 3.20, 3.23C, D). Interestingly, Sip1 gained activity if the aggregation experiment was repeated under the acidic conditions that presumably better reflect the intracellular pH of nematode embryos [243], rather than larval and adult worms [241].

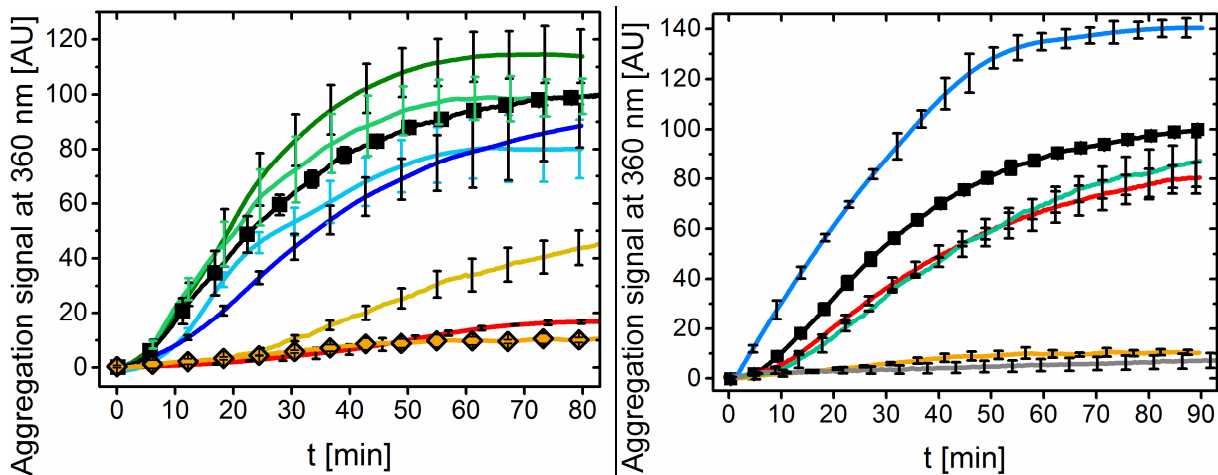


Fig. 3.20: Chaperone assays. Left: Comparison of the chaperone activities of all *C. elegans* Hsp16 proteins. The sHsps were mixed with citrate synthase at a ratio of 4:1 [Hsp16:CS]. The experiments were performed at 43 °C in aggregation buffer at pH 6.3. CS: ■, Sip1: ◆, Hsp16.1: —, Hsp16.2: —, Hsp16.41: —, Hsp16.48: —, F08H9.3: —, F08H9.4: —.

Right: pH-dependency of Sip1 *in vitro* chaperone activity. 0.5 μM of CS were incubated at 43 °C in the presence of a 4-fold molar excess of Sip1. CS: ■, Sip1: —, CS + Sip1 [1:4] at pH 5.8: —, pH 6.3: —, pH 7.5: —, pH 8.2: —. Pure CS and pure Sip1 are only shown at pH 7.5 as the changes in CS aggregation curves at the other three pH values were negligible.

All protein concentrations correspond to monomers. CS aggregation was monitored by measuring the increase in turbidity at 360 nm. The aggregation curves were normalized so that the maximum signal of pure CS was set to 100. All error bars correspond to standard deviation (SD).

At pH 6.8, 6.3 and 5.8, Sip1 inhibited the thermally induced aggregation of CS in a concentration-dependent manner (Figs. 3.20, 3.23A, B). Within this range, Sip1 demonstrated highest holdase efficiency at pH 6.3. There, the lowest amount of Sip1, less than three Sip1 monomers per CS monomer, was needed to reduce the aggregation to

50 % of the maximum aggregation signal recorded for pure CS (Fig. 3.21). Also at pH 6.3, only an 8:1 molar ratio of Sip1:CS was required to completely suppress CS aggregation. Besides citrate synthase, which is a dimeric protein of 104 kDa, malate dehydrogenase (MDH, dimer, 72 kDa) [37, 104, 250, 251] was assayed as another aggregation model substrate for Sip1. Sip1 was even more active towards MDH than CS (Figs. 3.22, 3.23Q-T). With MDH, the pH optimum of Sip1's chaperone activity was shifted to pH 5.8, where even an $\frac{1}{8}$ sub-stoichiometric ratio of Sip1 completely inhibited MDH aggregation (i.e. 0.125:1 [Sip1:MDH] relating to the monomeric proteins, Fig. 3.23Q). Moreover, Sip1 suppressed MDH aggregation (albeit not entirely) at all four examined pH values, in contrast to only chaperoning CS at pH 5.8 and 6.3.

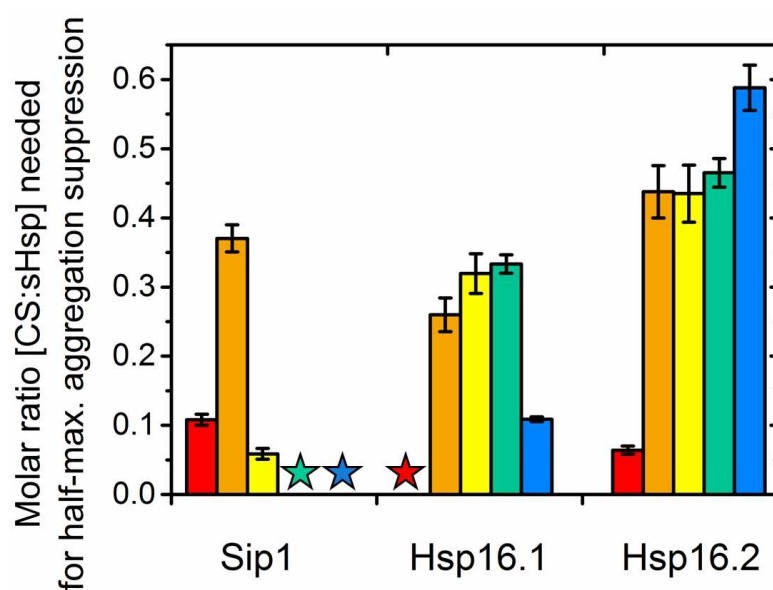


Fig. 3.21: Graphical summary of the pH optima of the chaperone activities of Sip1, Hsp16.1 and Hsp16.2. Molar ratio of CS to Sip1, Hsp16.1 and Hsp16.2 necessary for half-maximum inhibition of substrate aggregation at pH 5.8: ■, pH 6.3: ■, pH 6.8: ■, pH 7.5: ■, pH 8.2: ■. Stars denote that no half-maximum aggregation suppression was achieved by the sHsp at that pH value. See Fig. 3.21 for the complete aggregation curves at 43 °C.

The tendency towards an activity optimum at acidic conditions was confirmed when using Sip1 to reduce the chemically-induced aggregation of CS. For this experiment, CS was rapidly diluted from a stock solution supplemented with 6 M of GdmCl into aggregation buffer containing Sip1. Due to the instantaneous loss of chaotropic agent, the denatured CS spontaneously aggregated even at ambient temperatures. A ratio of 4:1 [Sip1:CS] resulted in a half-maximum suppression of aggregation at pH 6.3, the optimal pH condition (Fig. 3.22). Sip1 had been demonstrated to be chaperone-active towards GdmCl-denatured glutamate dehydrogenase at pH 6.3, at 20 °C as well [220]. Thus,

elevated temperatures were not necessary for Sip1 activation. Additionally, Sip1 could chaperone both the early unfolding intermediates and the almost completely unfolded substrates generated by the two different ways of inducing CS aggregation [37], [252].

All core Hsp16s exhibited chaperone activity at pH 6.3 (Fig. 3.20) and pH 7.0 [220]. Fig. 3.20 summarizes the relative chaperone efficiency of all *C. elegans* Hsp16 proteins towards heat-stressed CS at pH 6.3.

Under these conditions, the Hsp16.41/Hsp16.48 pair was less active than Sip1. However, the observed chaperone activity of Hsp16.2 and, to a lesser degree, Hsp16.1 was found to be comparable to that of Sip1 at pH 6.3 (see also Fig. 3.21). Thus, Hsp16.1 and Hsp16.2 were elected for a more detailed comparison with Sip1 in regard to pH dependency.

The two core Hsp16 proteins were able to operate comparably well over a broad pH range. Strikingly, Hsp16.1 and Hsp16.2 performed best at pH 7.5 and pH 8.2, respectively, where Sip1 was found to be inactive towards heat-stressed CS. Interestingly, Hsp16.1 was unable, and a 32-fold excess of Hsp16.2 was required, to completely suppress CS aggregation at pH 5.8 - diametrically opposed to Sip1 (Fig. 3.21).

Was Sip1 irregular just among *C. elegans* sHsps, or also among sHsps from other organisms in regard to becoming chaperone-active at a pH which was significantly lower than the physiological pH of 7.5 common to most living beings? In order to answer this question, the pH activity optima of two human sHsps, α B-crystallin and HspB1, wheat Hsp16.9, and *Saccharomyces cerevisiae* Hsp26 were determined. The respective aggregation curves at pH 5.8, 6.3, 7.5, and pH 8.2 are summarized in Fig. 3.22.

Strikingly, only α B-crystallin exhibited maximum chaperoning efficiency towards heat-stressed CS at pH 5.8. All other sHsps displayed a tendency towards operating best under neutral to alkaline conditions. This was astounding because AUC analysis had shown CRYAB to shift to larger oligomeric species at this very pH value (Fig. 3.19). CRYAB was functional as a chaperone at all four pH values, with medium efficiency at pH 7.5 and 6.3. The gain in activity upon changing to pH 5.8 was sudden and significant, representing the third best chaperoning ratio required for half-maximum aggregation suppression after Sip1 paired with MDH at pH 5.8 and 6.3.

Moreover, the Sip1 H111/139N mutant, which had displayed a comparable pH-dependency in adopting different oligomerization states (Fig. 3.15), closely mirrored wt Sip1 in the chaperone assay, as well. Like the native protein, the His-mutant was found to be incapable of reducing the CS aggregation to 50 % of the maximum signal at pH 7.5 and 8.2, but active at pH 6.3 and 5.8, with lowest stoichiometry required at pH 6.3. In absolute values, however, it was less active than wt Sip1 (Fig. 3.22).

Both truncated derivatives of Sip1, Sip1-ACD and chimaera showed no holdase activity within the tested pH range, which suggests a role for the NTR in substrate binding.

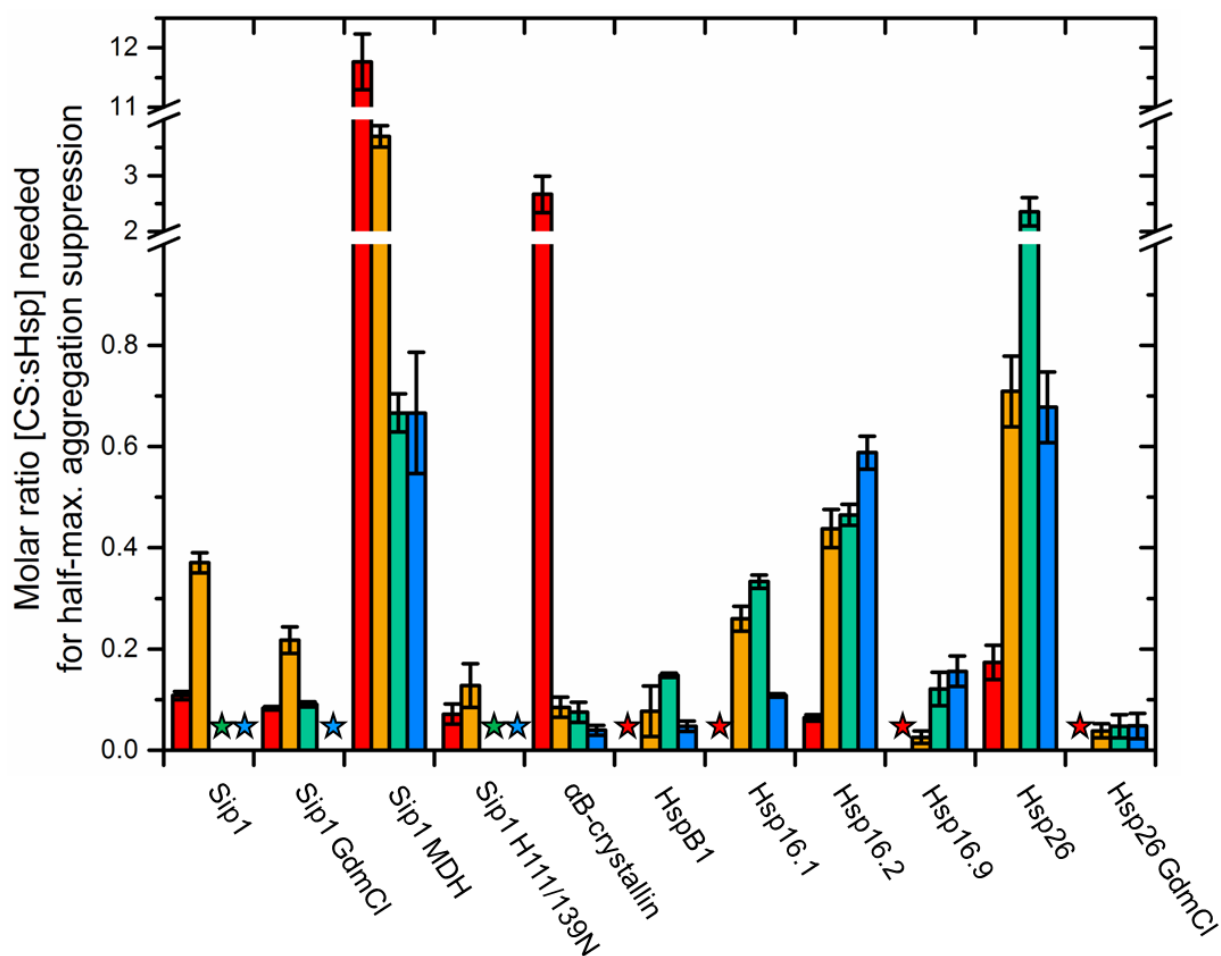
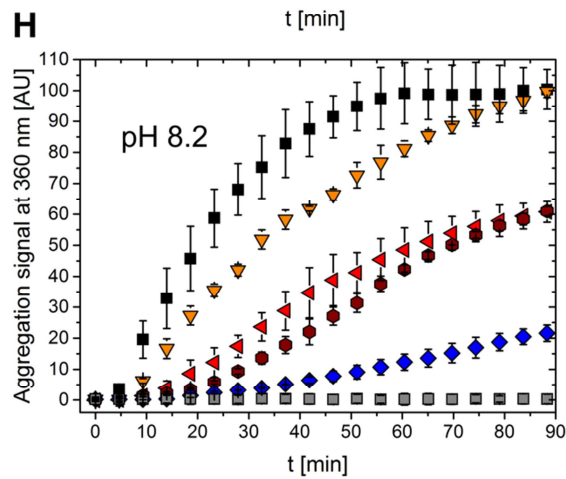
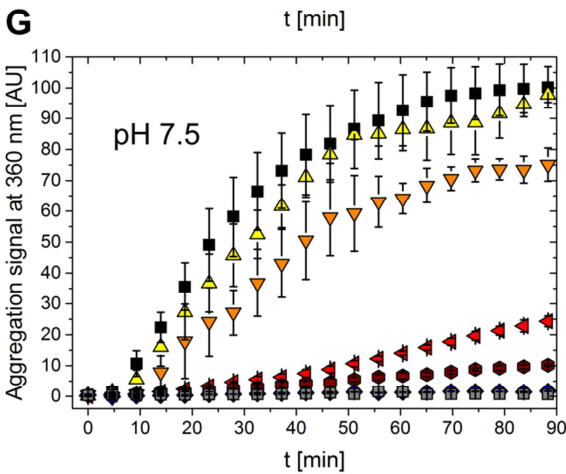
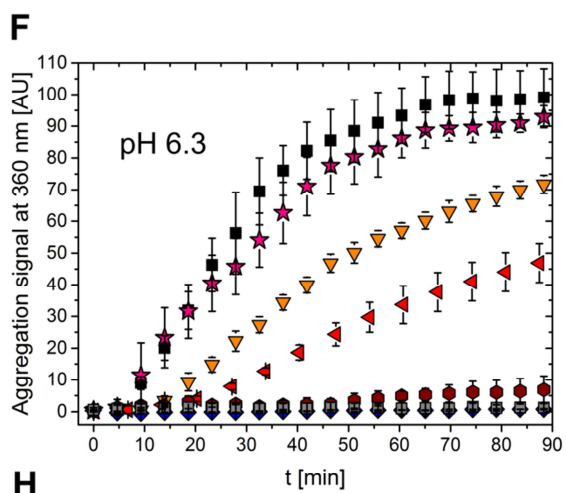
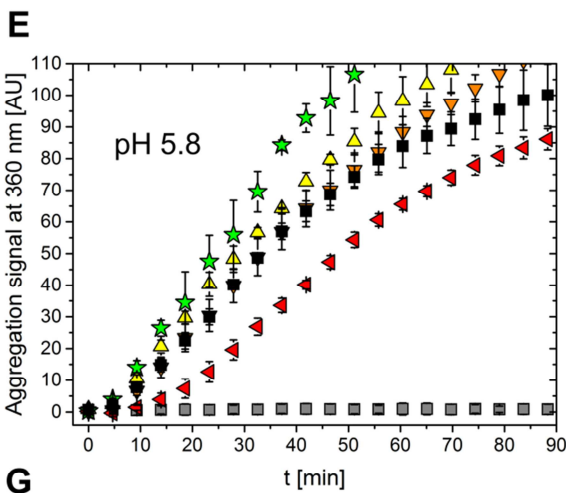
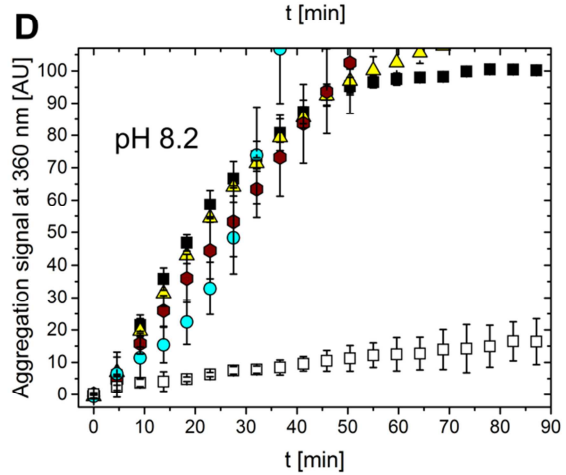
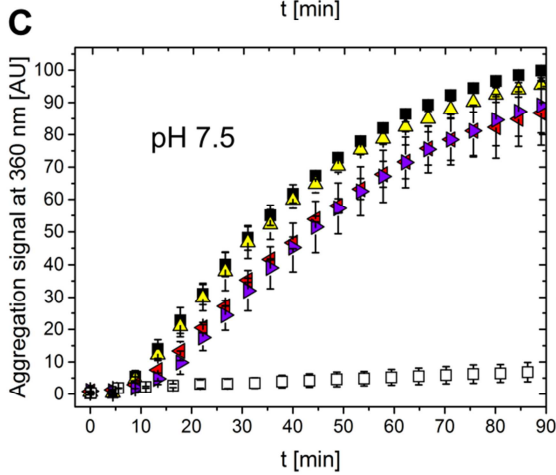
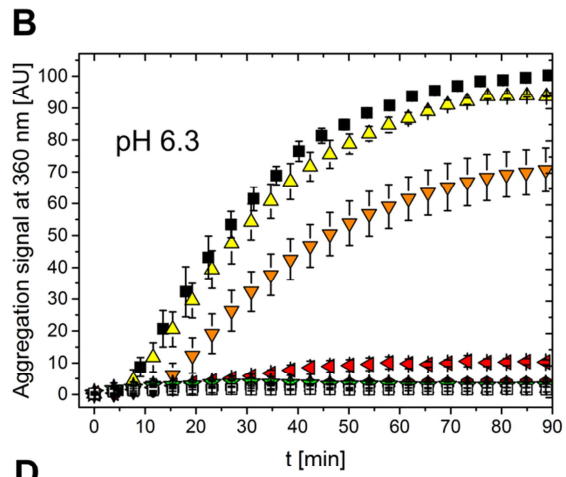
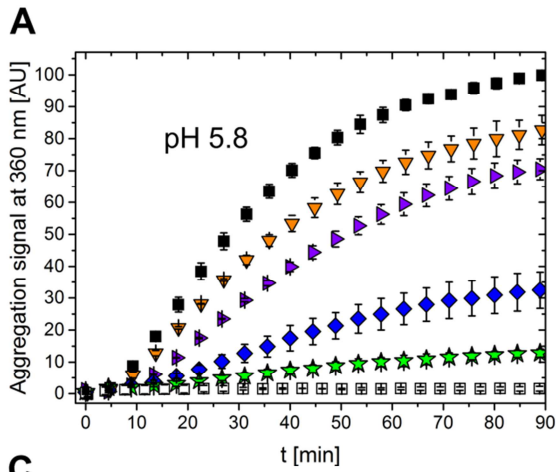
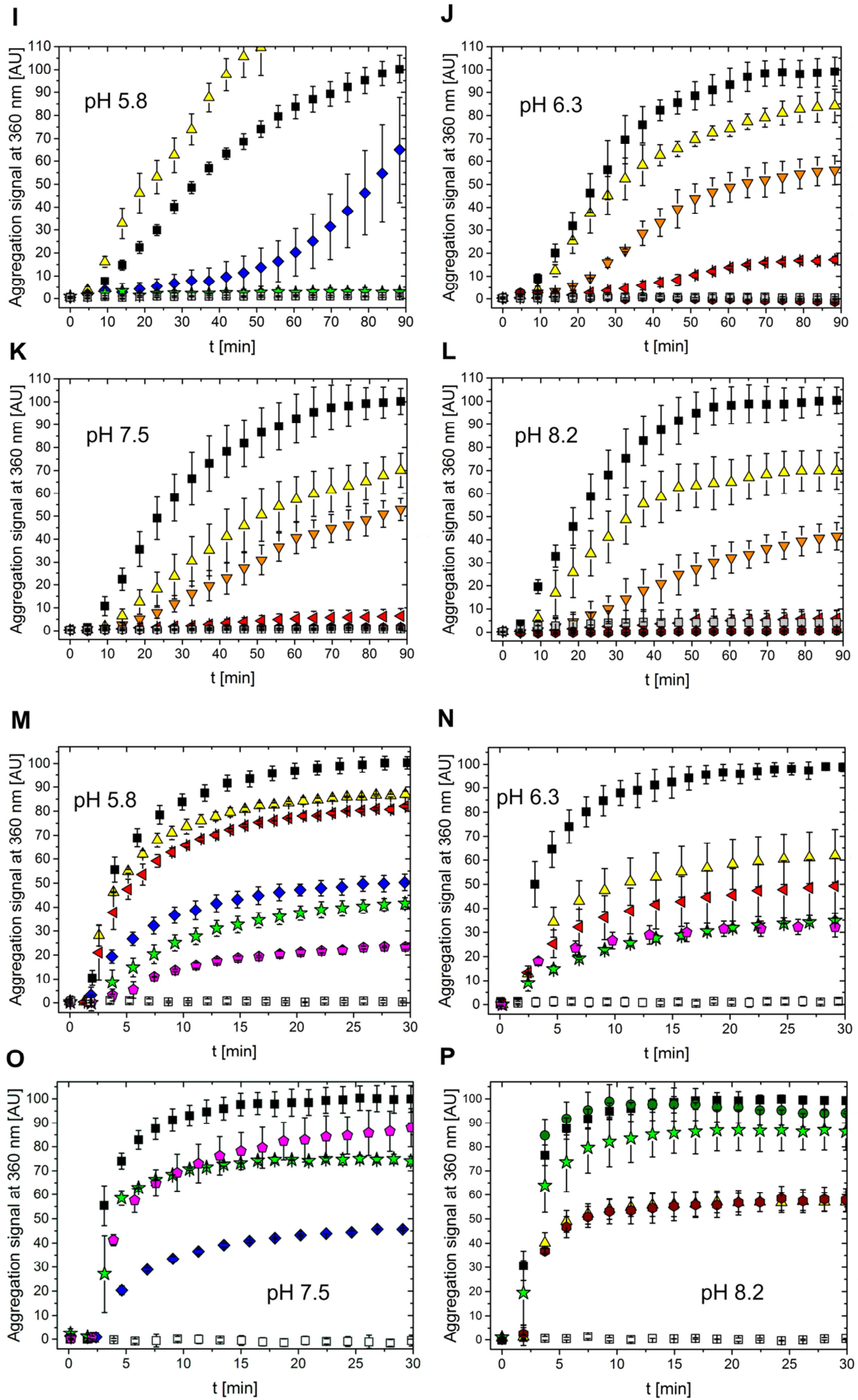


Fig. 3.22: Graphical summary of chaperone efficiencies of various sHsps at four different pH values: pH 5.8: ■, pH 6.3: ■, pH 7.5: ■, pH 8.2: ■. To the left, sHsps with an optimum at acidic conditions are grouped: Sip1 assayed with heat-stressed CS or MDH, or GdmCl-denatured CS, and the Sip1 H111/139N double mutant paired with heat-stressed CS, as well as αB-crystallin. Sip chimaera and the Sip1-ACD construct were found to be chaperone-inactive at any tested pH value. On the right half, all examined sHsp with an optimal pH of either pH 7.5 or 8.2 are depicted. Except for SchSp26, which was also combined with GdmCl-stressed CS, the sHsps' functionality was assayed towards CS at 43 °C.

Star symbols signify that the sHsp in question could not lower the substrate aggregation to half-maximum at this pH value. Error bars represent standard deviation (SD).





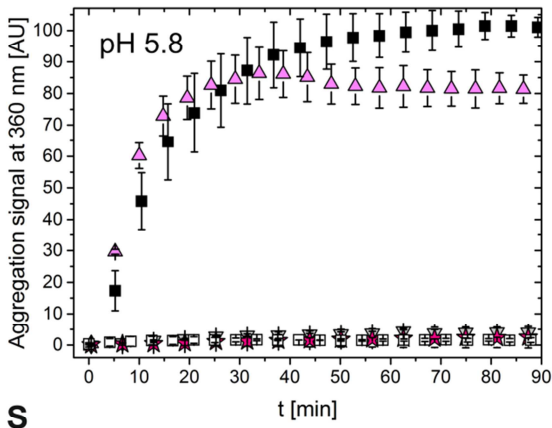
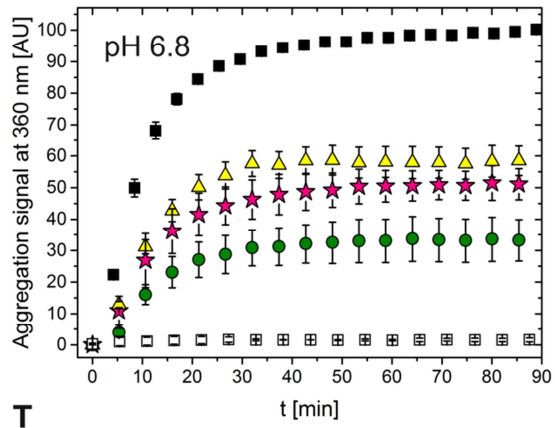
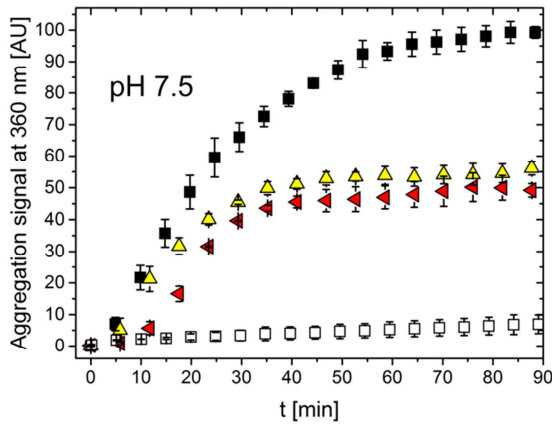
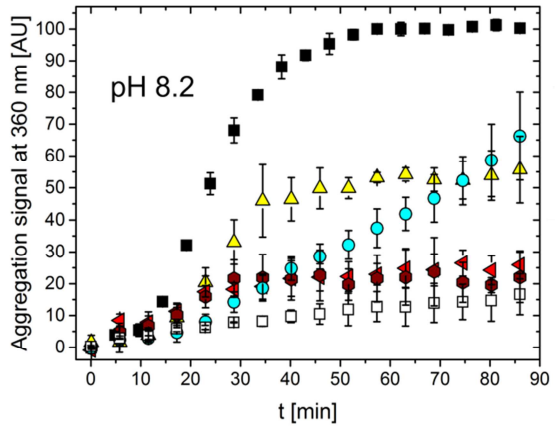
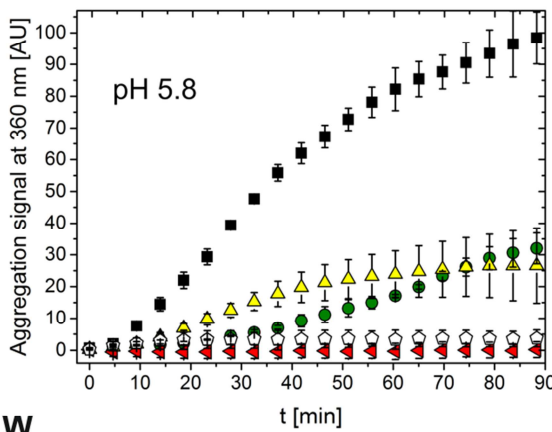
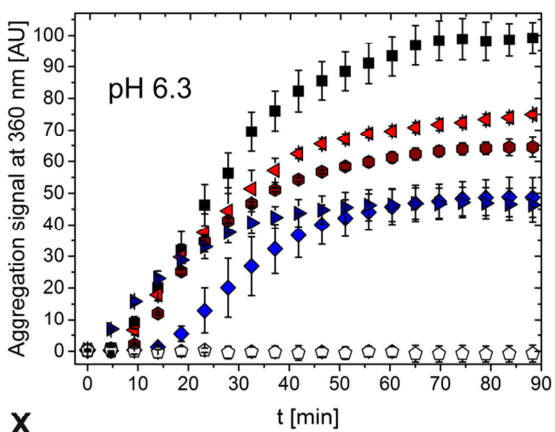
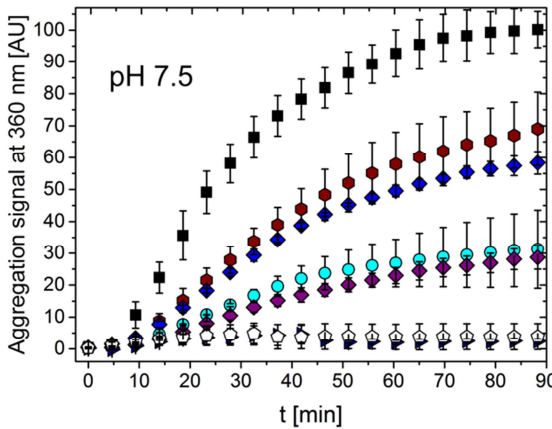
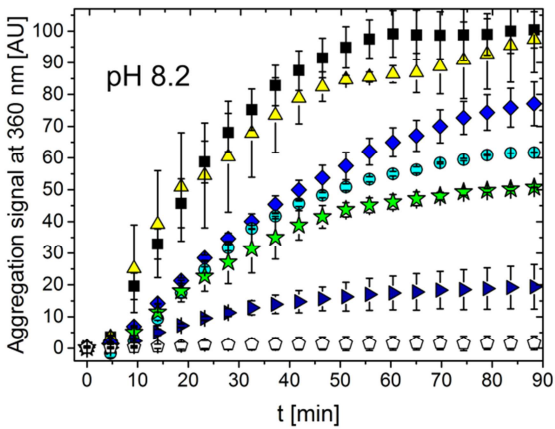
Q**R****S****T****U****V****W****X**

Fig. 3.23 A-D: Aggregation assay of Sip1 with heat-stressed CS, at pH 5.8, 6.3, 7.5, and 8.2. CS was incubated with increasing concentrations of Sip1 at 43 °C for 90 min, and the aggregation signal was surveyed at 360 nm. CS: ■, [CS:Sip1] 1:1: ▲, 1:2: ▼, 1:4: ◀, 1:6: ▶, 1:8: ◆, 1:12: ◇, 1:16: ●, 1:24: ☆, Sip1: □. Error bars correspond to standard deviation.

E-H: Aggregation assay of **Hsp16.11** with heat-stressed CS, at pH 5.8, 6.3, 7.5 and 8.2.

I-L: Aggregation assay of **Hsp16.2** with heat-stressed CS, at pH 5.8, 6.3, 7.5 and 8.2.

M-P: Aggregation assay of **Sip1** with **GdmCl**-denatured **CS**, at pH 5.8, 6.3, 7.5 and 8.2.

Q-T: Aggregation assay of **Sip1** with heat-stressed **MDH**, at pH 5.8, 6.8 (MDH is too stable at pH 6.3 to give a sufficient aggregation signal), 7.5 and 8.2.

U-X: Aggregation assay of **αB-crystallin** with heat-stressed CS, at pH 5.8, 6.3, 7.5 and 8.2.

Legend for the above: Pure CS or MDH: ■, [CS:Sip1] 16:1: ▲, 8:1: ▼, 4:1: ★, 2:1: ●, 1:1: ▲, 1:2: ▼, 1:4: ◀, 1:6: ▶, 1:8: ◆, 1:12: ◇, 1:16: ●, 1:24: ☆, 1:32: ◆, 1:48: ★, 1:64: ▶, pure Sip1: □, Hsp16.1: ■, Hsp16.2: ■, αB-crystallin: ◊.

In order to verify that Sip1 could keep its substrates in solution, CS and MDH were heat-shocked in the presence of Sip1, then centrifugated. At concentrations that were sufficient for half-maximum or complete suppression of aggregation, increasing amounts of the stressed proteins were retained in the soluble fraction. In contrast, almost all of CS and the majority of MDH precipitated in the absence of Sip1 (Fig. 3.24).

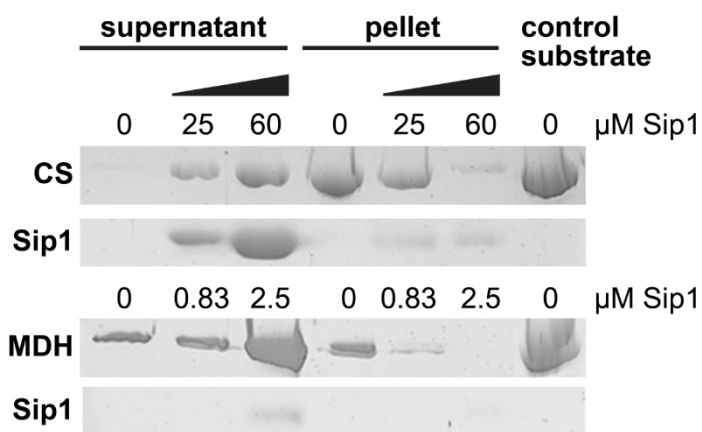


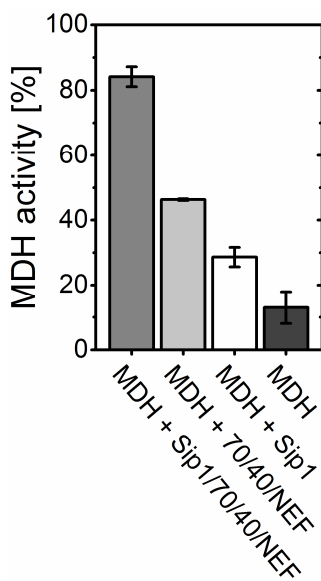
Fig. 3.24: Holdase function of Sip1. 10 μg of CS or MDH were heat-stressed at 43 °C for 1 h. Afterwards, soluble and aggregated components were separated by centrifugation and subjected to SDS-PAGE. Substrate solubility was greatly in the presence of Sip1 at a ratio that had conveyed half-maximum or total aggregation suppression in the chaperone assay (see Fig. 3.23), i.e., 12:1 and 4:1 [MDH:Sip1] at pH 5.8; and 1:2.5 and 1:6 [CS:Sip1] at pH 6.3, in aggregation

buffer. In the absence of Sip1, most of the substrate was detected in the sediment fraction. Control substrate was 10 μg of unstressed CS or MDH.

3.6.2 REFOLDING OF MDH BY SIP1

Small heat shock proteins must hand over their bound, unfolding substrates to ATP-dependent foldases for reconstitution [37, 65, 75, 84, 253, 254]. To determine whether Sip1, too, could cooperate with the *C. elegans* Hsp70/40 system, MDH was thermally inactivated together with Sip1 concentrations sufficient for complete aggregation inhibition at pH 6.3. The recovered activity was far higher (29 % of the activity of unstressed control MDH) than the activity retained and spontaneously regained by MDH

that was heat-shocked in the absence of Sip1 and then incubated for 4 h in refolding buffer (Fig. 3.25). When mixed with Hsc70, Dnj13 and Bag1, a nucleotide exchange factor (NEF) in refolding buffer, MDH regained 46 % of its original activity. Notably, this



percentage was almost doubled to 84 % if Sip1 had been present during the heat shock, followed by addition of the Hsp70/40 system.

Fig. 3.25: Cooperation of Sip1 with the CeHsp70/40 system for refolding of heat-denatured MDH. 2 μ M of MDH were heat-shocked for 45 min at 43 °C in the absence and presence of 0.5 μ M Sip1, sufficient for complete aggregation suppression according to the aggregation assay at pH 6.3. Refolding was started by the addition of *C. elegans* Hsc70, Dnj13 (Hsp40), and Bag1 (NEF, nucleotide exchange factor) in refolding buffer. After 4 h, the recovered MDH activity was detected and compared to that of unstressed MDH in the presence of all components of the refolding system (set to 100 %). For controls, samples lacking one or more key components were included. Error bars again represent SD.

Taken together, Sip1 kept its stressed substrates soluble but was insufficient for the regain of significant activity. For efficient refolding of non-native proteins, Sip1 was able to cooperate with the Hsp70/40 system, which had also been shown for Hsp16.1 and Hsp16.2, but not Hsp16.41 or Hsp16.48 with luciferase as client [220]. In contrast to Hsp16.1 and Hsp16.2, Sip1 could also achieve this together with Hsc70 and Dnj12, another of the many Hsp40 homologues in *C. elegans* (data not shown).

Sip1 was thus revealed as a potent molecular chaperone towards several model substrates. Its activity optimum at acidic pH values distinguished it from other sHsps, both from *C. elegans* and from other organisms. The reason for an optimal performance at an unusually low pH is most likely attributed to Sip1 reportedly being expressed solely in nematode oocytes and eggs [228, 237, 238], which are largely acidic [243].

3.7 EXPRESSION PATTERNS OF SIP1 AND HSP16

3.7.1 WESTERN BLOT

Before addressing the specific function of Sip1 *in vivo*, its temporal expression pattern was to be confirmed by immunoblotting, using worm lysates from all developmental stages.

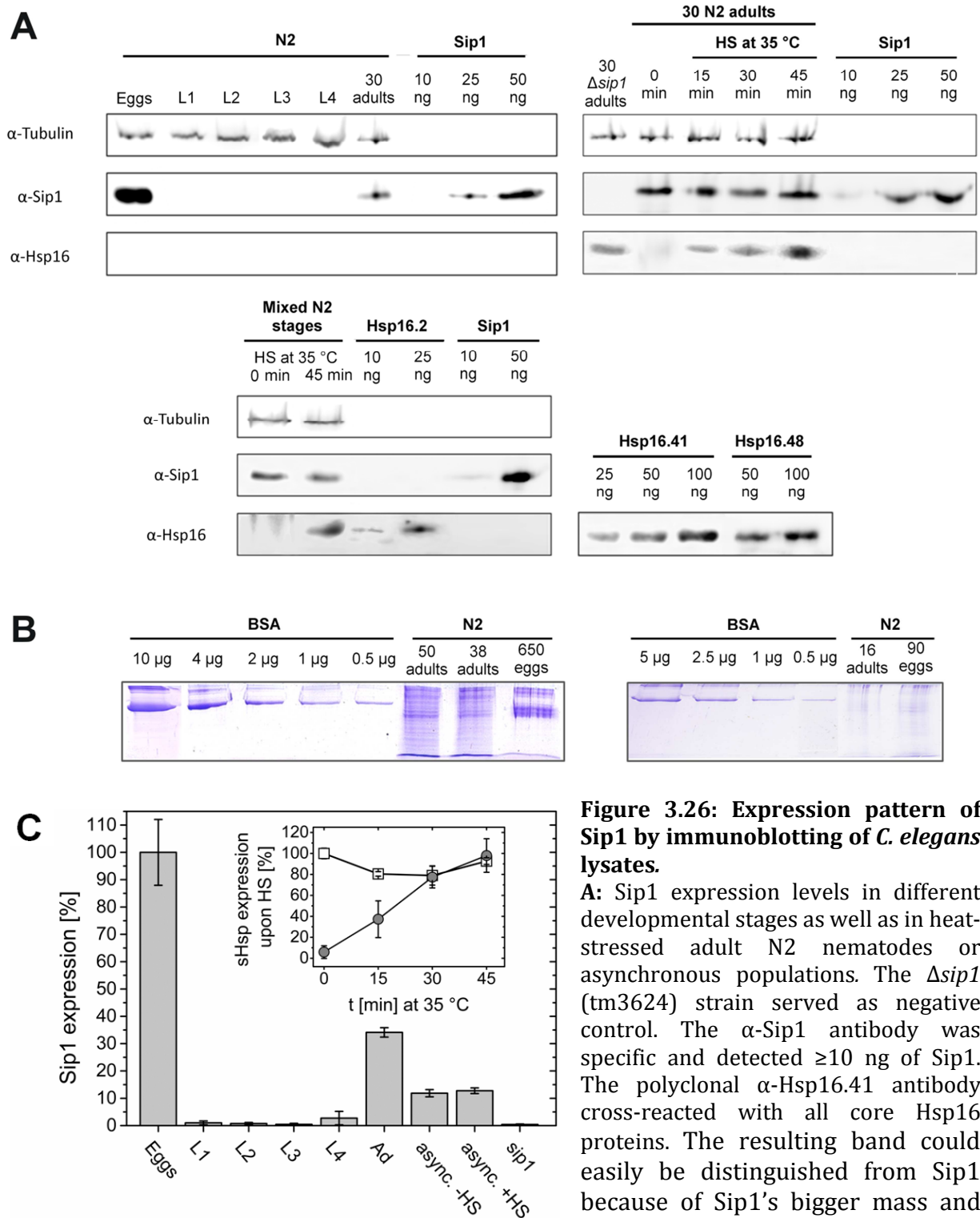


Figure 3.26: Expression pattern of Sip1 by immunoblotting of *C. elegans* lysates.

A: Sip1 expression levels in different developmental stages as well as in heat-stressed adult N2 nematodes or asynchronous populations. The $\Delta sip1$ (tm3624) strain served as negative control. The α -Sip1 antibody was specific and detected ≥ 10 ng of Sip1. The polyclonal α -Hsp16.41 antibody cross-reacted with all core Hsp16 proteins. The resulting band could easily be distinguished from Sip1 because of Sip1's bigger mass and consequently shorter migration

path in the SDS-PA gel. Tubulin was used as a loading control.

B: Determination of the total protein content in wild-type nematodes. A BSA concentration calibration line together with lysates of N2 adults and eggs were resolved briefly by SDS-PAGE, then stained with Coomassie Brilliant Blue.

C: Summary of **A**. Relative quantification by immunoblotting of Sip1 in different developmental stages of wt *C. elegans*, as well as in heat-stressed (HS) asynchronous cultures and adults. Sip1 is expressed in eggs and egg-laying adults (Ad). The amount of Sip1 in eggs was set to 100 %. The $\Delta sip1$ (tm3624) strain was used as negative control. Error bars are \pm SD.

Inset: Expression of Sip1 (□) and Hsp16 (●) in adult N2 worms that were stressed at 35 °C for 0, 15, 30 and 45 min, normalized to the Sip1 expression in unstressed nematodes. Sip1 protein amounts in egg-laying adults remained basically unaltered, and mixed stages of worms displayed no significant changes in Sip1 levels after 45 min at 35 °C, indicating that Sip1 is not heat-inducible at any developmental stage.

Sip1 was indeed found to be exclusively expressed in wild-type (N2) eggs and egg-producing adult *C. elegans* (Fig. 3.26A, C). At no stage was Sip1 inducible by heat-shock (35 °C for 45 min). The Hsp16 proteins, on the other hand, were only detected after heat-stress (Fig. 3.26C Inset) and, interestingly, in the unstressed *sip1* deletion strain (tm3624, see Fig. 3.26A).

Comparison of the Sip1 immunoblot signal from adult and egg lysate to the bands resulting from known amounts of the pure protein allowed for absolute quantification of Sip1 (Fig. 3.27A). One N2 egg contained ~0.14 ng, and one adult N2 worm ~2.14 ng of Sip1. This ratio is in good agreement with a reproducing adult containing 10 – 15 eggs at any given time [152]. Comparison with a BSA calibration line allowed for absolute quantification of the total protein content per egg and per adult worm (Figs. 3.27B). Thus, Sip1 could be estimated to account for ~2.1 % of one egg's total protein content and ~0.6 % of all proteins of a nematode at the first day of adulthood.

3.7.2 FLUORESCENCE MICROSCOPY

In a parallel approach, *sip1* promoter (and protein) were cloned in frame in front of enhanced yellow fluorescent protein, *eyfp*, encoded on a reporter plasmid designed for transformation of *C. elegans*. Promoter length was either 500 or 1000 bp upstream of the *sip1* gene. The resulting transcriptional *sip1-promoter::eyfp* or translational *sip1-promoter::sip1-eyfp* vectors were microinjected in the gonads of young adult hermaphrodites, to be taken up into the forming eggs. Germline expression is notoriously hard to generate [255]. Various protocols for improving (embryonic) reporter expression were employed, like complex array (addition of fragmented *E. coli* DNA to reduce formation of transgene silencing tandem repeats [255]). The success of the injection procedure *per se* was repeatedly proven by progeny expressing a co-injected *pmyo-2::cfp* marker. However, no eYFP fluorescence could be detected under a fluorescence microscope in most of these CFP-expressing nematodes.

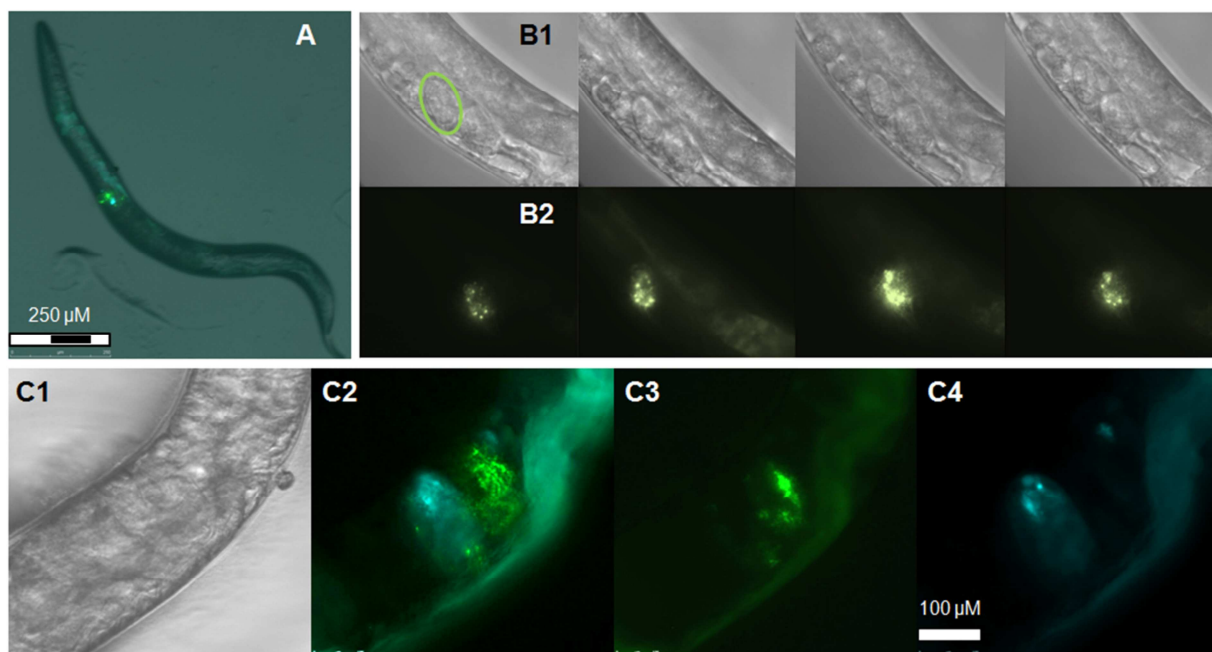


Fig. 3.27: Fluorescence microscope images of hermaphrodites injected with a translational 1000 bp *sip1-promoter::sip1-eyfp* reporter.

The reporter plasmid was mixed 1:1 with 75 ng/ μ L of *pmyo-2::cfp* pharynx marker and 20 ng/ μ L of *ScaI*- and *PvuII*-cut *E. coli* DNA. **A:** Merged DIC, YFP, and CFP channel image of a motile, feeding $\Delta sip1$ young adult hermaphrodite carrying two fluorescing eggs, taken on a Leica MZ 16 FA at 10x zoom. **B:** z-axis stacked images of another normally behaved $\Delta sip1$ young adult worm, fixed on a Zeiss Axiovert200 on day 3 after injection. **B1** row: DIC filter, 0.01 s exposure, the fluorescent egg is marked. **B2** row: YFP, 0.35 s exposure.

C: Images of the same worm as in **A**, 2 days after injection on the Axiovert200 at 63x zoom. **C1:** DIC, **C2:** YFP-CFP merge, intestine displays some auto-fluorescence, **C3:** YFP, **C4:** CFP. Exposure lasted for 0.1 s for DIC and 3 s on the fluorescence channels.

Repetition of the injection by two other experimenters, one of them with access to a gene bombardment device, failed to yield any transgenes. Thus, the fusion protein was most likely toxic. The inability to establish a transgenic *C. elegans* line, also with a reporter encoding a pH-sensitive GFP variant, precluded an investigation into the exact intracellular pH at the Sip1 expression locus.

Despite these difficulties, a number of eYFP-expressing individuals could be obtained (Fig. 3.27). Consistent with the immunoblot results, Sip1-eYFP fluorescence was only observed in eggs. Most of these were still contained within the hermaphrodite, one had been laid. No larvae hatched from these eggs, presumably because of the forced toxic reporter expression. In the fluorescence microscope images of the transformed eggs, some of the Sip1 reporter appeared to be distinctly localized and focused in spots, next to some diffuse fluorescence.

Some CFP fluorescence was detected at times besides eYFP, presumably in the developing pharynx.

PCR with *sip1*-specific primers on one hermaphrodite amplified the *sip1* sequence, proving that the plasmid was present.

3.8 IN VIVO IMPORTANCE OF SIP1

3.8.1 THERMOTOLERANCE IN *E. COLI*

Having verified the exclusively embryonic expression of Sip1, the next question to be addressed was whether Sip1 had an important organismal role - possibly specific to that early stage in development. As small heat shock protein, a function in stress tolerance suggested itself. So far, the only hint in this direction was Sip1 conveying heat resistance onto *E. coli* [228]. This could be verified for heat-, and additionally for cold-stressed BL21 DE3 transformed with the *sip1* or *hsp16.1*-encoding pET21a vector. Cells carrying these two plasmids showed the same growth curves at permissive temperatures as *E. coli* transfected with the empty vector. However, after incubation of a pre-culture at 50 °C for just 15 min, control cells used to inoculate fresh medium at 28 °C only grew to a stationary phase density of ~70 %, while the sHsp-expressing bacteria continued to propagate unimpededly even after the pre-cultures had been heat-shocked for 120 min at 50 °C (Fig. 3.28).

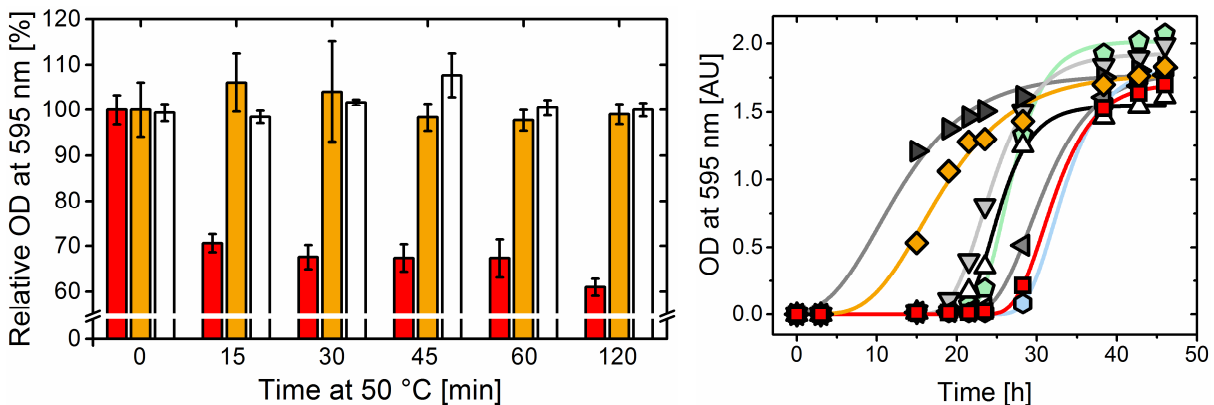


Fig. 3.28: Influence of Hsp16 overexpression on heat stress survival in *E. coli*. **Left:** BL21 DE3 cells expressing Sip1 (orange) or Hsp16.1 (white), or carrying the empty pET21a vector (control, red) were grown to OD_{595 nm} 0.4, then diluted into LB medium that had been pre-heated to 50 °C. After the time indicated, the cultures were used to inoculate fresh LB medium at 28 °C. After 1 h at 28 °C, the ODs were measured. **Right:** Similarly, BL21 DE3 bacteria transformed with empty vector or a plasmid containing one *hsp16* gene were heat-shocked at 58 °C for 1 h after having grown to OD 0.5. Fresh media were inoculated to OD 0.06 and the propagation at 28 °C was followed in the spectrophotometer. Control (■), Sip1 (◆), Hsp16.1 (△), Hsp16.2 (▽), Hsp16.41 (◀), Hsp16.48 (▶), F08H9.3 (●), F08H9.4 (◆).

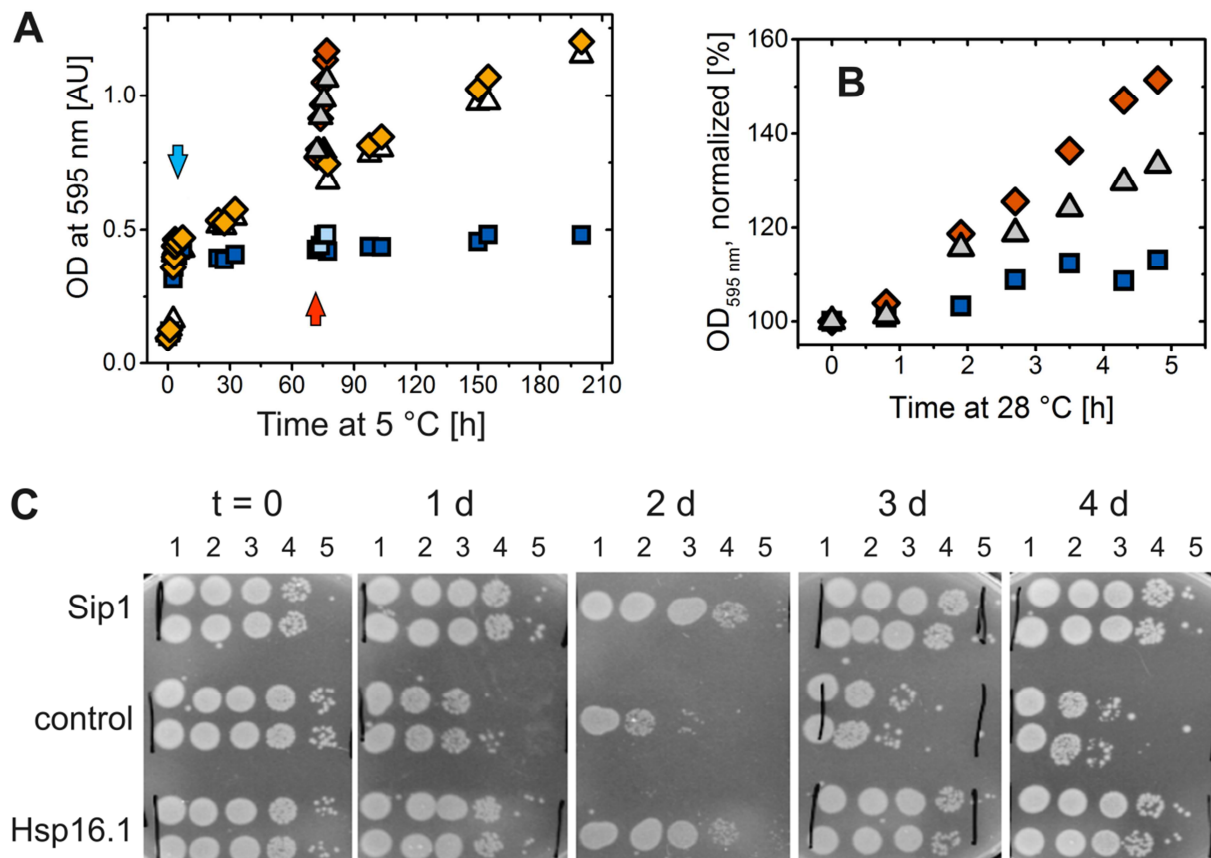


Fig. 3.29: Sip1 and, to a lesser degree, Hsp16.1 convey cold-resistance onto *E. coli*. BL21 DE3 cells expressing Sip1 (orange diamonds), Hsp16.1 (triangles) or carrying empty pET21a vector (blue boxes) were grown at 28 °C to OD = 0.5, then shaken at 5 °C for four days. The blue arrow indicates the beginning of the cold shock. OD_{595 nm} was measured both at 5 °C for the cold-shocked cultures (**A**) and at 28 °C for flasks retrieved in intervals of one day for recovery. The growth curves of cultures returned to 28 °C after 3 days at 5 °C (red arrow) are depicted in detail in **B**, where the starting ODs were set to 100 %. In parallel, viability after every day was determined by plating dilution series (**C**): 1. OD = 0.4; 2. 1:20; 3. 1:400; 4. 1:8,000; 5. 1:16,000.

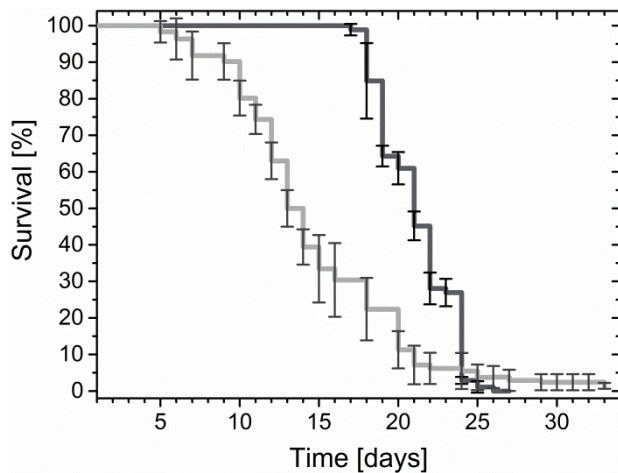
In a similar experiment, *E. coli* over-expressing Hsp16.41, Sip1, Hsp16.2, Hsp16.1 and F08H9.4 were significantly quicker than the control strain to resume growth after a heat shock at 58 °C for 1 h (Fig. 3.28).

Moreover, Sip1 allowed BL21 DE3 bacteria to continue growth during four days of incubation at 5 °C, and to rapidly resume growth after being placed at 28 °C again (Fig. 3.29). Control bacteria were significantly slower in their recovery. This was evident from both OD measurements and plating dilutions series of liquid cultures. Interestingly, Hsp16.1 was less effective than Sip1 in promoting development under cold shock conditions.

Sip1 had thus been demonstrated to increase survival at extreme temperatures when introduced to a foreign organism. Now, its phenotype in *C. elegans* was to be assessed.

3.8.2 LIFESPAN DETERMINATION OF *SIP1* DELETION NEMATODES

The *sip1* (tm3624) deletion mutant was examined for phenotypes. To begin with, its life span (commencing at the L4 stage) was determined at 20 °C (Fig. 3.30) and, with an



average of 13.4 ± 0.6 days, was found to be significantly shorter than that of the wt strain. N2 mean life time was 20.2 days ± 0.2 (s.e.m.), in good agreement with the 20 days observed by other groups [161].

Fig. 3.30:
***C. elegans* life span determination at 20 °C.**
N2 worms: —, *sip1*-deletion strain: —.

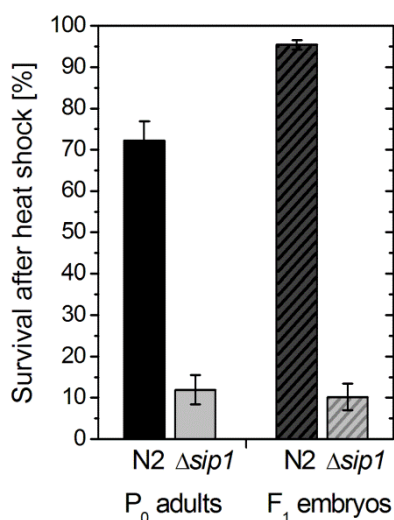
Thus, deletion of *sip1* resulted in a short-lived phenotype. This was in keeping with the notion that the longevity of *daf2* mutants was due partly to the unrestricted transcription of *shsps* by Daf16 (see Chapter 1.4.2).

3.8.3 THERMOTOLERANCE ANALYSIS

To assess the *in vivo*-function of Sip1 under stress conditions, as well, the survival of both wt and *sip1* deletion worms after heat shock was observed. L4 larvae were incubated for a total of 1.5 hours at 37 °C (see M&M 6.2.12). Survivors were counted after one day. Furthermore, the total number of F1 larvae that had hatched until day 4 after the heat stress was documented. Only ~12 % of $\Delta sip1$ adults survived, compared to ~72 % of wt adult worms (Fig. 3.31). Concomitantly, the total brood size, which had been comparable between the two strains at ambient temperatures, declined to ~5.8 eggs per surviving $\Delta sip1$ worm, in contrast to ~7.7 eggs within four days after heat shock per N2 hermaphrodite. Most disparately, of these few *sip1*-deleted embryos, only ~10 % proved actually viable, while more than 95 % of the wt eggs laid after heat shock hatched.

The absence of Sip1 thus greatly diminished the stress survival rate of *C. elegans* adults and -even more so - embryos.

In contrast, the same heat shock thermoprofile had not caused a significant drop in $\Delta hsp16.2$ (gk249) or $\Delta hsp16.41$ (tm1093) adult survival, compared to N2 (~77 %, in agreement with the result presented here) [220]. Both Hsp16.1 and Hsp16.2, or the



Hsp16.41 and Hsp16.48 pair had to be downregulated for a grave deterioration in thermotolerance to be observed [220]. This was interpreted as one partner of a Hsp16 pair being able to compensate for the loss of the other.

Fig. 3.31: Heat survival of *sip1* deletion worms. The thermotolerance assay screened the survival of wt (black) and $\Delta sip1$ (grey) young adult nematodes (left), and hatching of their offspring (right, shaded columns), 1 and 4 days, respectively, after a 37 °C heat shock for a total of 1.5 h.

Immunoblotting had shown the core Hsp16 proteins to be upregulated upon heat shock, but also at ambient temperatures in $\Delta sip1$ (tm3624) adults, presumably in an attempt to compensate for the loss of *sip1*. The significantly short-lived and thermo-sensitive phenotypes of $\Delta sip1$ nematodes, however, proved the other CesHsps to be poor substitutes for Sip1 function under both favorable and stress conditions.

3.9 *IN VIVO* SUBSTRATES OF SIP1 AND HSP16.2

Sip1 was thus demonstrated to be essential upon heat stress, without any of the other 15 *C. elegans* small heat shock proteins representing an efficient substitute. Was this due to Sip1's being produced constitutively and in a unique developmental expression pattern, or did Sip1 also have a specific set of substrates which differed from the other Hsp16s'? In order to identify the *in vivo* substrates of Sip1, *C. elegans* lysate proteins bound by Sip1 were co-immunoprecipitated by α Sip1 antibody. These pull-down experiments were performed in duplicate at pH 7.5 and 6.3, using tm3624 lysates which had either been kept at ambient temperatures or which had been subjected to heat stress, in the presence or absence of Sip1 (Fig. 3.32). To assess its overlap with another sHsp's individual sets of substrates, co-immunoprecipitation was also performed with Hsp16.2 as bait. Additionally, Sip1 co-immunoprecipitation (CoIP) was performed on the lysate of pre-purified tm3624 eggs.

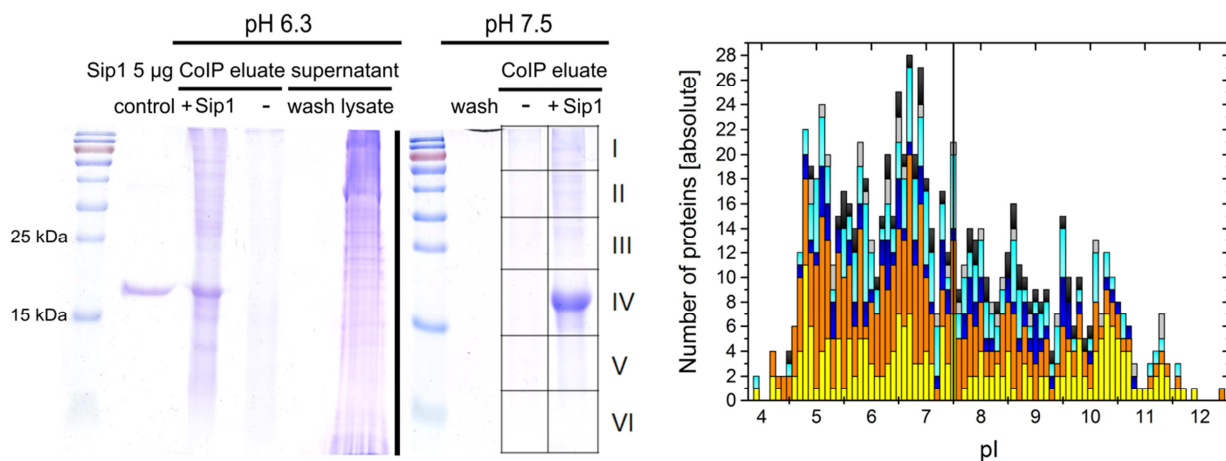


Fig. 3.32: Co-Immunoprecipitation of Sip1- and Hsp16.2 substrates.

Left: Exemplary SDS-PAGE-gels of the Sip1 pull-down. At pH 6.3 or 7.5, ~110 µg of asynchronous *Δsip1* (tm3624) worm lysate per sample were incubated for 45 min at 15 or 37 °C, with 10 µg of Sip1 (or Hsp16.2), or without sHsp in case of controls. Proteins bound to the sHsp were co-immunoprecipitated by the respective antibody, and the protein G-sepharose eluates separated by SDS-PAGE. Each gel lane was cut into six pieces, as indicated for the CoIP at pH 7.5 by Roman numerals, and analyzed by LC-MS-Orbitrap.

Right: Identified Sip1- or Hsp16.2-interacting proteins clustered by their pI. pI 7.5 is indicated by a black line. Sip1 substrates at pH 6.3, 15 °C: ■; 37 °C: ■; at pH 7.5, 15 °C: ■; 37 °C: ■. Hsp16.2 substrates at 15 °C, pH 6.3: ■; pH 7.5: ■.

After identification by liquid chromatography coupled to mass spectrometry (LC-MS), proteins were counted as potential substrates if they were pulled down from Sip1- or Hsp16.2-containing probes but not from the respective controls without sHsp.

This resulted in a significantly higher number of substrates for Sip1 than for Hsp16.2 (Fig. 3.33A, B). As might have been inferred from the *in vitro* chaperone activity, Hsp16.2 interacted with more proteins at pH 7.5 than at pH 6.3, while Sip1 showed the opposite trend. At both pH values, Sip1 bound more substrates if the lysate had been heat-stressed. Compared to the total proteome pI distribution [256], proteins of weakly acidic and neutral pI were slightly overrepresented especially among the Sip1 substrates at pH 6.3 (Fig. 3.32). Moreover, ≥60 % of all substrates were below 50 kDa in mass. A similar size distribution had been reported for the substrates of *E. coli* IbpB and *Deinococcus radiodurans* Hsp20.2 substrates [72, 257].

The identified proteins were classified according to their biological process, molecular function, pathway, and protein class using the gene ontology (GO) database PANTHER. Because of the sheer size of the CoIP data evaluation, the resulting spreadsheets could not be depicted in this thesis. Lists of all pulled-down proteins and over-representation

analyses (ORA) according to PANTHER of all performed co-immunoprecipitation experiments were deposited online instead, see the online Supplement to Fleckenstein, Kastenmüller *et al.*, (in progress). ORA reported the following GO categories to be enriched in both sHsp interactomes in comparison to their incidence in the *C. elegans* proteome: RNA binding and translation regulation, ribosome, primary and protein metabolism, catalytic activity (e.g. dehydrogenases, oxidoreductases), cytoskeletal components, and chaperones (Fig. 3.33).

Interestingly, certain protein categories were over-represented among the Sip1-, but not the Hsp16.2 interactome: TCA cycle and pyruvate metabolism, glycolysis, generation of precursor metabolites and energy, respiratory electron transport chain, H⁺-transporting ATP synthases, storage, but also proteolysis and ubiquitin-proteasome pathway components. For details, see Discussion.

According to wormbase, the majority of sHsp-interacting proteins was expressed in embryos at least at a low level. Beyond that, many Sip1 substrates were particularly linked or essential to embryos. The storage proteins that are significantly over-represented in the Sip1 pull-downs as opposed to the Hsp16.2 CoIPs are all vitellogenins. The yolk proteins Vit1 – 6 deliver fats and cholesterol from intestinal cells to the developing embryo [176, 258] (Fig. 1.9).

(m)RNA binding and -regulating proteins represented another functional category which featured more prominently within the substrate set of Sip1 than that of Hsp16.2. Vig1, a translation regulator and RISC complex component [259], was retrieved as Sip1 substrate under all conditions. See Chapter 4.3 for further examples.

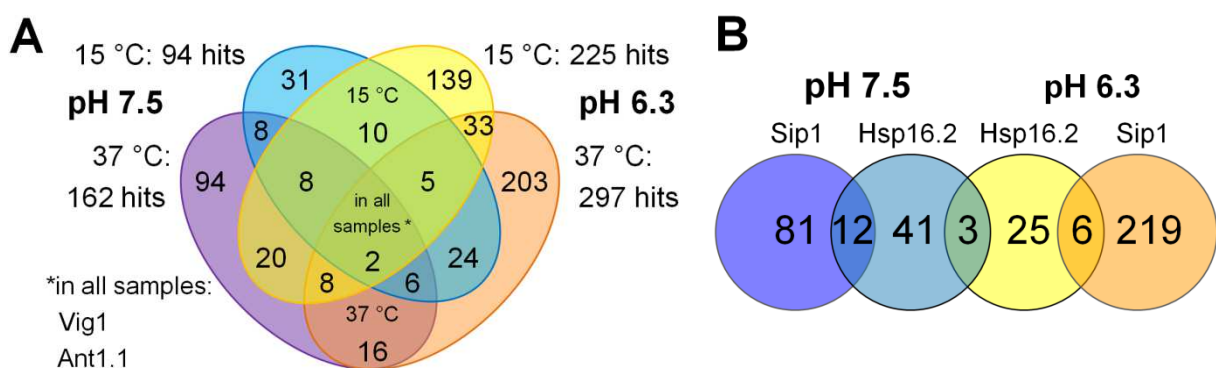


Fig. 3.33: *in vivo* substrates of Sip1 and Hsp16.2.

A: Venn diagram of all Sip1 CoIPs at the indicated conditions. Yellow: CoIP at pH 6.3, 15 °C, orange: CoIP at pH 6.3 at 37 °C, blue: CoIP at pH 7.5 at 15 °C, or at 37 °C (purple).

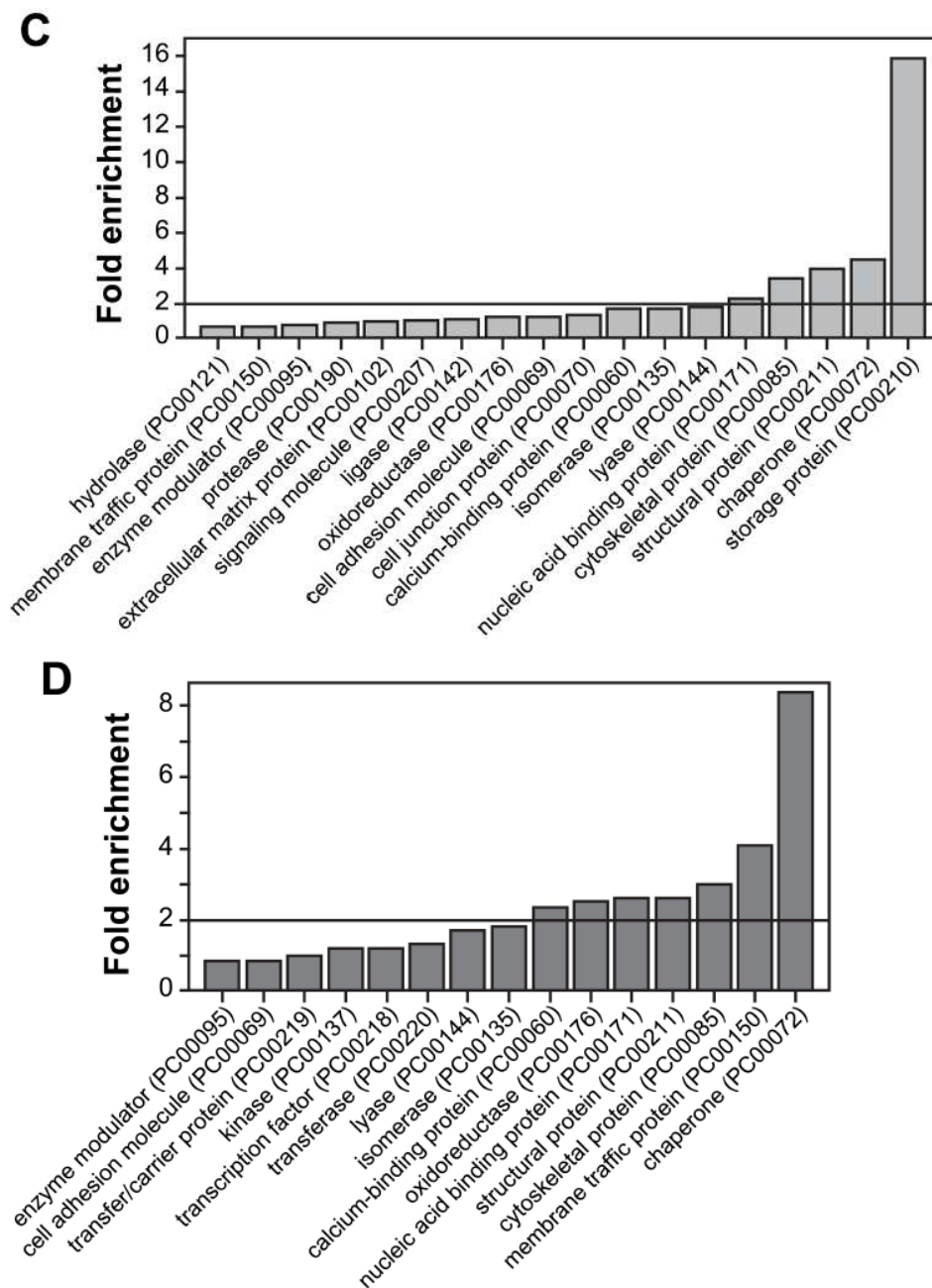


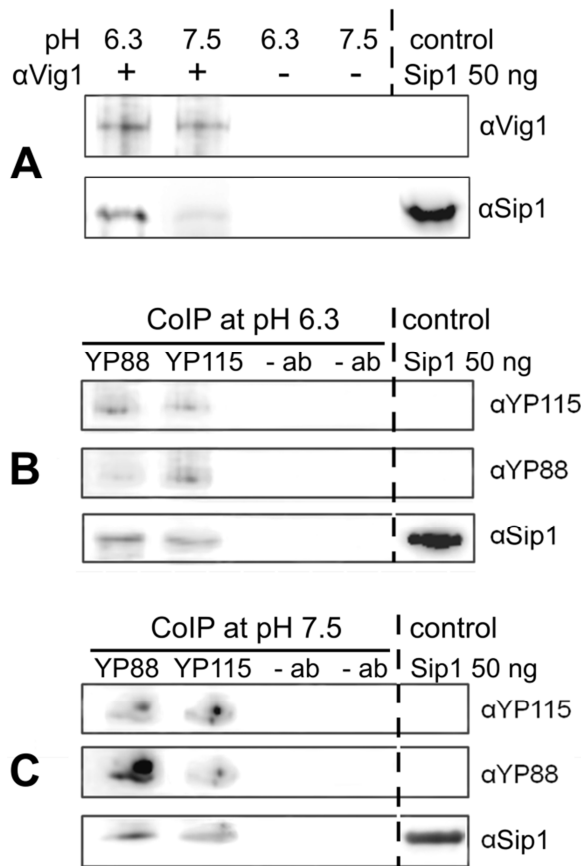
Fig. 3.33 (continued). B: Venn diagram displaying the overlap between substrates identified in Sip1 and Hsp16.2 CoIPs at pH 6.3 and 7.5.

C: Enrichment of PANTHER Protein Classes of Sip1 substrates pulled-down at pH 6.3, 15 °C referenced against the *C. elegans* proteome. A significance cutoff at 2-fold enrichment is indicated by a line, categories underrepresented <0.5-fold are not displayed.

D: PANTHER Protein Classes of Hsp16.2 substrates from the pH 7.5, 15 °C CoIP enriched in comparison to the *C. elegans* proteome.

All pulled-down proteins are listed in the online supplement to Fleckenstein, Kastenmüller *et al.* (in progress).

In order to verify some exemplary potential substrates and thus confirm the specificity of the co-immunoprecipitation, the pull-down was repeated with two substrates as bait. Endogenous Sip1 was detected alongside the antigens when performing the CoIP with



either an α -Vig1-antibody or two antibodies directed against the two cleavage products of the Vit6 yolk protein precursor, YP115 and YP88 (Fig. 3.34).

Figure 3.34: Co-Immunoprecipitation of Sip1. **A:** CoIP verification using Vig1. Endogenous Vig1 was pulled down from heat-stressed N2 lysate at pH 6.3 and 7.5 using an α -Vig1 antibody, and co-precipitated Sip1 was detected via α -Sip1 immunoblotting. Control: 50 ng of Sip1. **B, C:** CoIP verification of Vit6 at pH 6.3 and 7.5. Using α -YP88 and α -YP115 antibodies, the two cleavage products of Vit6 were pulled down from N2 lysates that had been pre-incubated for 45 min at 37 °C. Co-precipitated Sip1 was detected via α -Sip1 immunoblotting.

Thus, the substrate spectra of Sip1 and Hsp16.2 overlapped to a certain degree, more so when comparing protein families and functional classes rather than looking at individual proteins. However, Sip1 interacted with a range of proteins of critical importance to embryos, such as egg yolk proteins, which were not among the Hsp16.2 substrates.



4. DISCUSSION

4.1 PH-DEPENDENT STRUCTURE OF SIP1

As a fundamental class of molecular chaperones, small heat shock proteins assist an ample spectrum of substrates in retaining or regaining their native conformations, especially during proteotoxic stress which induces unfolding and aggregation. Despite decades of research in this clinically relevant field, key questions regarding their regulation, substrate specificity and functional mechanism remain unanswered. In this context, the characterization of the embryonic small heat shock protein Sip1 from the model organism *Caenorhabditis elegans* proved a fascinating topic and provided remarkable, new perspectives.

Of the Hsp16 family in *C. elegans*, only the four “core” Hsp16 proteins, Hsp16.1, Hsp16.2, Hsp16.41 and Hsp16.48, had been characterized structurally and functionally in detail. So far, little data has been published on the remaining three family members, F08H9.3, F08H9.4 and Sip1. To close this gap, the three sHsps were expressed, natively purified and analyzed *in vitro*.

Compared to the other Hsp16s, the F08H9 proteins contained less of the β -sheet secondary structure elements that are a hallmark of sHsps, but a substantially higher amount of random coils. Neither buffer and pH change, nor alternative purification protocols, nor addition of possible cofactors caused F08H9.3 to adopt the fold displayed by the other Hsp16 proteins. F08H9.4 was found to gain in β -sheet content by incubation with dithiothreitol. Still, both proteins did not form oligomers larger than dimers, and were therefore too small to be visualized by EM. F08H9.4 also failed to crystallize in a sitting drop buffer screen. In accordance with the literature [230], they displayed no chaperone activity under any condition tested.

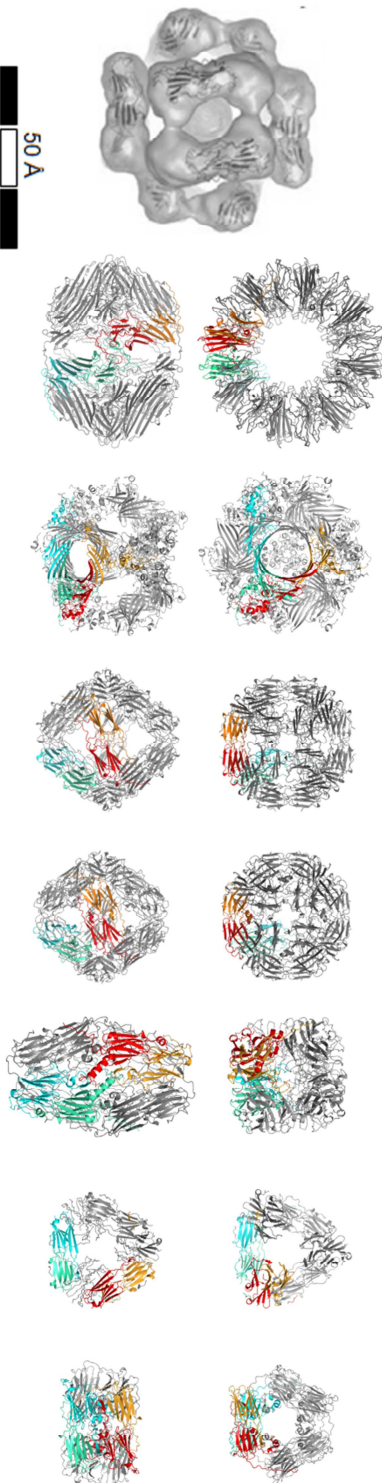
In contrast, for Sip1, the crystal structure of the 32-mer could be solved. Additionally, the 3D-structures of the 28- and 24-mer were reconstructed by cryo-electron microscopy. In those large oligomeric structures, Sip1 forms a highly symmetrical, hollow sphere, which in the case of the 32mer is slightly flattened along the C_8 axis, and in the 24mer is prolonged along the C_6 axis, resulting in a barrel-like shape. Sip1 dimers are the building units that make up the two identical, inverted halves of the spheroid structure. Within these dimers, two non-equivalent monomers combine along the $\beta_6+\beta_7$ -strands in the

typical mammalian ACD dimerization mode (Fig. 1.6) [88, 91, 92, 94]. At the apex, the dimers are held together by one apical monomer's long N-terminal region binding to its neighbour's ACD, which causes eight dimers (in the case of the 32-mer crystal structure) to group in a circle, leaving open a central pore of 48 Å. The equatorial monomers' CTRs intertwine with the C-terminal extensions of their counterpart across the globe-like 32-mer's equator, linking the two hemispheres.

With a size of 100 x 150 Å, the Sip1 32-mer represents not only the first crystal structure of a mammalian-like sHsp oligomer, but also the second largest sHsp crystal structure available to date (Fig. 4.1).

Comparison with the 11 other sHsps for which the full-length protein or truncated ACD could be crystallized so far allows for the classification into two structural types at the level of the dimer (cf. Chapter 1.2.2.2). Sip1 is the only sHsp of metazoan origin so far to share the architecture of the mammalian sHsps α A- and B-crystallin, HspB1, and HspB6. In contrast, the „non-mammalian type“ is adopted by sHsps from archaea, bacteria, plants and also by the only other metazoan sHsp which could be crystallized, Tsp36 from the parasitic flatworm *Taenia saginata*.

While the Sip1 dimer reveals high structural similarity to the mammalian sHsps like human α B-crystallin, its oligomers can best be compared to Hsp16.0 from *Schizosaccharomyces pombe*. In this ellipsoid 16-mer, the 2x four dimers are only oriented from the interface between the two identical, inverted halves to the apical hole. As in Sip1, two SpHsp16.0 dimers (green-cyan and orange-red in Fig. 4.1) connect at the interface at an angle of almost 180°. In contrast, *Triticum aestivum* Hsp16.9 crystallizes as a 12-mer of two stacked triangles [96], *Mycobacterium tuberculosis* Acr1 forms a tetrahedron, and the 24-meric *Methanocaldococcus jannaschii* Hsp16.5 [86] and *Sulfolobus tokodaii* Hsp14.0 [89] are octahedral. The angle between dimers is either 0° or 120°.



	SchHsp26 (2H50)	Sip1	HsCRYAB (2YGD)	MjHsp16.5 (1SHS)	StHsp14.0 (3VQK)	SpHsp16.0 (3W1Z)	MtAct1 (2BYU)	TaHsp16.9 (1GME)
Oligomer	24-mer	32-mer	24-mer	24-mer	24-mer	16-mer	12-mer	12-mer
Height [Å]	195	100	146	117	115	120	99	55
Width [Å]	195	151	146	117	115	95	99	75 / 102
Inner diameter [Å]	130	62	70	74	58	12	52	33
Largest pore diameter [Å]	45	48	33	30	19	11	36	33
Resolution [Å]	10.8	3.6	9.4	2.9	4.5	2.4	16.5	2.7
Poly-disperse	n	y	y	y	n	n	n	n
Method	cryo-EM	X-ray	cryo-EM	X-ray	X-ray	X-ray	ns-EM	X-ray
Termini resolved	-	NTR and CTR not fully resolved	-	NTR not resolved	NTR not resolved	some NTRs fully resolved	-	half of the NTRs fully resolved
Citation	White et al. Structure, 2006	Fleckenstein et al., in progress	Braun et al. PNAS, 2011	Kim et al. Nature, 1998	Hanazono et al. JMB, 2012	Hanazono et al. Structure, 2013	Kenaway et al. JBC, 2005	v. Montfort et al. Nat Str Biol, 2001

Fig. 4.1: sHsp oligomer structures at atomic resolution, from PDB, all full-length, ordered by size. The largest sHsp crystal structure, 36-meric *Xanthomonas axonopodis* XaHspA (3GLA) was omitted here because of its incomparable architecture of a quintuple sandwich [95].

In the 24-mers visualized by a cryo-EM triple hybrid approach (2YGD), human CRYAB dimers are arranged on a spherical surface without one preferred direction [112] in a

way that is far more reminiscent of the 24-meric Hsp16.2, Hsp16.41 and Hsp16.48 EM reconstructions (Fig. 1.12) [220] than of the Sip1 24-mer with its D6 symmetry and its defined “equator”.

Previously, SV-AUC of Hsp16.41 in PBS at pH 7.0 had resulted in a monodisperse distribution at 13.2 S, interpreted to correspond to the 22-mer, and sedimentation equilibrium AUC analyses of Hsp16.2 and Hsp16.48 in PBS had indicated 22- and 20-mers, respectively. NS-EM class-averaged images of Hsp16.2, Hsp16.41 and Hsp16.48 had only shown the 24-mers [220]. However, according to size exclusion chromatography, which was less exact than AUC and tended to give larger stoichiometries in this set of experiments, the core Hsp16 proteins might be able to form 32mers, as well [220].

Comparable to the results for 79 μM Sip1 in standard buffer at pH 7.5, a previous AUC run of 45 μM Sip1 in PBS had yielded a single peak at ~ 16.5 S, then thought to represent the 24-mer [220]. However, the AUC calculations and EM size distribution data would suggest that the 15 – 17 S range corresponds to the Sip1 28- to 32-mer.

The oligomerization state of Sip1 does not appear to be dependent on concentration over a range of 1.4 μM (EM) to 79 μM (AUC), because the assembly size distribution resulting from both methods is basically identical. However, pH decisively influences the range and relative abundance of oligomeric states that Sip1 populates at equilibrium. Acidification from pH 7.5 to 5.8, which is within the range of pH values reported in *C. elegans* [242], effectuates a dissociation of the largest species observed into a broad spectrum of ensembles of smaller stoichiometries. Presumably, the smaller particles interact and interchange subunits, possibly adopting variable shapes, which would serve to explain the progressively undefined $c(s)$ distribution of the AUC peaks at low pH values.

Intriguingly, the assembly principle of the transition from one large oligomer to the next smaller species is based on the reversible loss of two dimeric subunits, as evidenced by the EM reconstitutions of the 32-, the 28-, and the 24-mer. This of course raises questions as to the exact mechanism and the residues involved in sensing and reacting to pH changes. Various mutants of Sip1 were generated to address these points.

Half of the NTR are not resolved in the 32-meric crystal structure, and the equatorial monomers' NTR are missing the first 17 aa in the electron density map, meaning they are

flexible and do not form strong interactions. The resolved part of the equatorial NTR is packed underneath the ACD's extended β -sheet and then reaches into the central cavity. Thus, the NTRs possibly do not contribute to stabilization of the oligomer. In contrast, the CTRs have an obvious role in tethering the dimers together, by binding into the hydrophobic β_4/β_8 -grove of an adjacent dimer via their IXI motive (LPI in Sip1). Within the apical monomers, this CTR-ACD interaction builds up one hemisphere, while such a contact between equatorially localized monomers fuses two hemispheres together.

When searching for the specific amino acids involved in disrupting or forming these contacts for the intake/expulsion of dimers into/from the oligomer, histidines were an obvious choice because they alone have a pK_a in the relevant pH range. His111 and His139 were judged promising candidates since they were close enough for interacting, localized just after the LPI motive and within an extra β -strand that formed an extended β -sheet with the adjacent monomer's CTR across the equatorial interface, respectively. However, rendering these two His unable to de-/protonate by mutation to Asn resulted in NS-EM and SV-AUC size distribution profiles that still largely coincided with the wt oligomer dispersion patterns. Notable changes were the narrowing and shift to smaller S -values or particle sizes of the single peak observed at pH 8.2 and 7.5. This indicated that the largest oligomerization state adopted by wt Sip1, most likely the 32-mer judging by the combined X-ray, EM, and AUC data, was significantly less populated in favor of the next smaller species, probably the 28-mer, in the Sip1 His111/139Asn double mutant. Also, somewhat counter-intuitively, the His mutant was sensitive to a drop in pH already when shifted from pH 8.2 to pH 7.5, as opposed to a dissociation into multiple smaller assemblies requiring a change to pH 6.3 for the wt protein.

The most intuitive dissociation mechanism of Sip1 would arguably be the expulsion of two dimers that are linked across the equatorial interface between hemispheres. For this, the contacts at the poles would have to be interrupted, but not necessarily the equatorial interaction between the two expelled dimers. The additional β -sheet spanned by two β -strands per equatorial CTR stabilizes this contact in comparison to the simple IXI-grove binding of the apical CTR. Disruption of the latter interaction while maintaining the former would thus be feasible. The CTR region after the LPI motive is more important for the equatorial interlinkage than for apical contacts, where one of the two histidines is not even resolved. Dissociation by successive loss of tetramers (instead of

two dimers) would therefore explain why mutations of His111 and His139 proved insufficient to disrupt the pH-triggered changes in size distribution of Sip1 oligomers. Stable *trans*-interactions would also explain why the globe-like structure did not break into two hemisphere, which would have caused a second, intense peak corresponding to the 16-mer in the sedimentation coefficient curve at acidic pH.

In any case, more, or different residues are likely involved in the loss of inter-dimer contact and the ejection of dimers upon acidification.

A truncation mutant of Sip1 lacking the NTR and part of the CTR (the ten aa following the IXI motive) was found to be mono- and dimeric, with low levels of the tetramer, by AUC. The mere LPI could thus only facilitate some dimer-dimer interaction, but no higher oligomers. A fusion of the CTR of human α B-crystallin to Sip1's ACD and LPI motive (Fig. 3.16) was again able to form transient oligomers, up to presumably the 16-meric species. Possibly, the C-terminal extension of α B-crystallin is able to provide enough contact area to form the semi-spherical species (via the apical monomers' interlinkage), but seems to lack the ability to generate the equatorial contact zone required for conjunction of two half-spheres to one hollow sphere. This chimaeric protein also displayed a shift towards smaller particles at lower pH values, like wt Sip1 and unlike CRYAB. In summary, the CTR beyond the IXI motive is required for formation of higher oligomers, and the ACD dictates the pH-dependency of de-/oligomerization, rather than the CTR.

An alignment of the ACDs of all existing sHsps [35] indicated HspB1, followed by α B-crystallin, to be the closest relatives to Sip1 in humans (with a pairwise distance of 1.14 and 1.35, respectively). Incidentally, pH has also been described as a trigger for structural shifts and activation of human HspB1 and α -crystallin (see Chapter 4.2, [85, 106, 260, 261]).

In contrast to Sip1, however, which shifts to smaller species upon acidification, both HspB1 and α B-crystallin populate smaller assemblies under neutral to alkaline conditions in comparison to acidic pH values (this work, [85, 116]). CRYAB and a number of other sHsps from higher eukaryotes have also been demonstrated to dissociate into smaller oligomers when phosphorylated [84, 85, 122].

A further common trigger for conformational rearrangements and concomitant activation is heat [114, 120, 262]. This was shown to apply to Sip1 and the core Hsp16

proteins, as well, because a rise in temperature by 5 °C or less effected an increase in smaller species in the proteins' elution profile [220]. However, neither Sip1 nor the other four Hsp16 proteins require elevated temperatures in order to be active, as demonstrated by their ability to chaperone GdmCl-denatured substrates at 20 °C (this work, [220]).

Sip1 was found to be more thermostable than the core Hsp16 proteins. As expected, the thermotransition of the quaternary structure dissociation occurred at lower temperatures than the onset of secondary structure disintegration, which at ~61 °C for Sip1 at pH 5.8 and 6.3 was comparable to the T_m of Hsp16.1 and Hsp16.2 at pH 7.0 (~63 and ~60 °C, respectively, [220]). According to CD and SEC results, Sip1 was stabilized against heat stress at acidic pH values. Structural disintegration of Sip1 on the quaternary, but also on the secondary structure level was further observed to be induced by GdmCl. Again, the unfolding curves of the CD spectra and the transition midpoints were similar for all Hsp16 proteins (~1.25 M GdmCl for Sip1 at all pH values tested, ~1 M GdmCl for the Hsp16.1/Hsp16.2 pair, and ~ 1.8 M GdmCl for Hsp16.41 and Hsp16.48) (this work, [220]).

4.2 FUNCTION OF SIP1, pH-DEPENDENCY, AND COMPARISON WITH OTHER SHSPS

Importantly, the pH-triggered conformational rearrangement to assemblies of lower stoichiometries was shown to have immediate consequences for the chaperone activity of Sip1.

Measurements were routinely performed at pH 5.8 to 7.5, which represents the reported physiological pH range in *C. elegans* [241, 242]. Sip1 can exhibit chaperone activity up to the most alkaline pH examined, pH 8.2. Intriguingly, however, Sip1 is most effective as a chaperone towards varied unfolding substrates at both ambient and heat-stress temperatures at pH 5.8 - 6.3. The correlating trend towards smaller particles and higher activity under acidic conditions indicates that it is likely the smaller oligomers that can function as holdases. In keeping with current models (see Chapter 1.2.2.2), this would implicate that the larger Sip1 assemblies, like the 32-mer, are storage forms which can only be activated by dissociation.

Table 4.1: Properties of proteins tested for *in vitro* chaperone activity. v.s.: see above

Protein	MM [kDa] / AA	Oligomeric size	Optimum activity at pH	pI
sHsps:				
Sip1	17.839 / 159	AUC, EM: polydisperse, max. 32mer; smaller at low pH	5.8 – 6.3	7.9 (verified)
Sip1 His111/139Asn	17.793 / 159	AUC: like wt Sip1 but max. 28mer; more sensitive to acidification	6.3	7.9
Sip1-ACD	11.129 / 100	AUC: monomer, dimer at all pH values tested	not active	6.7
Sip1/ α B-crystallin chimaera	12.366 / 111	AUC: polydisperse, max. 16 - 20mer; smaller at low pH	not active	7.1
human α B-crystallin	20.159 / 175	AUC: polydisperse; larger at pH 5.8	5.8	6.8
human HspB1	22.783 / 205	Polydisperse; smaller at alkaline pH [85, 116]	7.5	6.0
CeHsp16.11	16.253 / 145	SEC: 27-32mer, possibly polydisperse [220]	7.5	5.4
CeHsp16.2	16.242 / 145	EM: probably 24mer, AUC, SEC: probably polydisperse [220]	8.2	5.3
CeHsp16.41	16.252 / 143	v.s.	n.d.	5.9
CeHsp16.48	16.299 / 143	v.s.	n.d.	5.5
CeF08H9.3	16.747 / 147	n.d.	not active	4.7
CeF08H9.4	16.418 / 147	AUC: monomer, dimer at all pH values tested	not active	5.2
wheat Hsp16.9	16.878 / 151	12mer	8.2	5.8
bakers' yeast Hsp26	23.880 / 214	max. 24mer	7.5 – 8.2	5.3
Substrates:				
Citrate synthase, pig heart	51.629 / 464	dimer	n.a.	8.1
Malate dehydrogenase 2, pig heart	35.596 / 338	dimer	n.a.	8.9

In any case, neither the dimeric Sip1-ACD construct including the LPI motive, nor the Sip1-ACD/CRYAB-CTR chimera, which form smaller oligomers than wt Sip1, exhibit chaperone activity at any condition tested. Thus, lack of the NTR abolished the capacity for binding and keeping soluble an unfolding substrate (as would be expected from analogy of other sHsps' NTRs pivotal role in substrate binding [108-110, 263]), while the formation of smaller to middle-sized oligomers was still feasible. The replacement of the CTR with the one of CRYAB would presumably not be the decisive factor in the loss of chaperone activity, because CRYAB was not only active, but showed the same trend of optimum activity at acidic pH as Sip1.

Compared to wt Sip1, the H111/139N mutant starts to dissociate into small species already at neutral pH values. This is not, however, reflected in augmented chaperone activity at pH 7.5. Instead, the mutant closely mirrors the pH trend of wt Sip1, albeit at a generally lower effectivity.

Remarkably, this activity optimum at pH 5.8 – 6.3 is specific to Sip1. Its closest relatives in *C. elegans*, the Hsp16 proteins, are in fact deactivated by acidic pH. Their expression is stress-inducible only after the early embryonic stages (i.e. 12 cell-stage at the soonest), with highest expression reported for L1 larvae [141, 142, 221, 226], which have an intracellular pH of 7.5 [241]. Fittingly, the core Hsp16 proteins display a rather acidic pI (5.3 – 5.9 as opposed to 7.9 for Sip1) and exhibit a pH optimum, broader than Sip1, at pH 6.8 – 8.2.

The physiological, cytoplasmic pH in most organisms is around 7.0 - 7.5 [264]: 7.0 in yeast cytosol [265], pH 7.5-7.7 in wheat and rice [266], 7.4-7.7 in *Aspergillus niger* [267], and 7.2 in human cytoplasm [268]. Thus, it is unsurprising that all cytosolic sHsps from other organisms examined here (Table 4.1) shared the *C. elegans* Hsp16s' tendency of optimum activity at neutral to alkaline pH values – save CRYAB.

Although functional over the entire pH range tested, α B-crystallin exhibited a vastly higher chaperoning efficiency towards heat-stressed CS at pH 5.8. This was somewhat surprising as AUC analysis showed CRYAB, unlike Sip1, to shift to larger oligomers at this very pH value, in accordance with the literature [116].

α B-crystallin is expressed in the developing embryo and various tissues relevant to human reproduction, heart, skeletal muscle, brain, lung, kidney, as well as lens [136]. In

human, rat and frog eye lenses, the intracellular pH is 6.8 – 7.0, and lens proteins are stable upon acidosis of the cytoplasm [269]. pH plays a role in the osmotic regulation of the lens, which is of prime interest in cataract development [269]. Moreover, fluctuations of intracellular pH occur physiologically during skeletal muscle contractions, changes in cardiac workload and heart rate, and high brain activity [270]. Dramatic deviations in pH are required for controlling cellular activities, such as egg division after fertilization [271]. On the other hand, local or systemic shifts in pH also accompany pathological conditions, and can become lethal for cells. For instance, even slight aberrations from the painstakingly maintained pH 7.35 - 7.45 of human blood would result in coma and death (at pH 6.95), or convulsions and muscle spasms (pH 7.7) [272]. Also, local acidification can be seen in malignant tumors, and myocardial ischaemia is associated with a major fall of pH_i from a steady-state value of ~ 7.2 to 6.5 or lower because of increased levels lactic acid, the product of glycolytic respiration [270]. Furthermore, stroke induces extracellular acidosis in mammals [266].

Activation of CRYAB at low pH values has been reported in context with some of these examples of acidified tissues. For instance, α B-crystallin binding to cardiac-muscle proteins (actin, desmin) is enhanced at pH 6.0 – 6.5 in ischaemic hearts [270, 273]. Myocytes are also protected from stiffening by α B-crystallin preventing titin aggregation at pH 6.6 [261]. Furthermore, α B-crystallin was shown to exert its protective in myocytes of metabolically and exercise-stressed skeletal muscle, where the mean resting pH_i drops from pH 7.05 to pH 6.7 [274].

Thus, the activity optimum at acidic pH most likely reflects an evolutionary adaptation to the tissues and stress conditions in and under which the holdase function of α B-crystallin is most needed. A similar concept is applicable to Sip1.

4.3 *IN VIVO* SUBSTRATES OF SIP1 VS. HSP16.2

The sHsp's constitutive expression has been shown here and elsewhere [228, 238] to be restricted to developing oocytes and embryos, large parts of which are acidic [243]. The low pH is caused by vacuolar H^+ -ATP synthases, Vhas, and is essential for the embryo because it facilitates protein sorting and receptor-mediated endocytosis [243, 266]. The ATP-dependent proton pumps are localized at membranes of intracellular

acidic organelles, including the numerous storage granules in intestinal cells of the *C. elegans* embryo [243]. These endocytotic compartments take up and store yolk proteins, i.e. vitellogenins (Vits) carrying primary nutrients [258].

Vits are egg yolk precursors in invertebrates and egg-laying vertebrates, and homologues to mammalian apolipoprotein Apo B-100 [258, 275]. In the sterol-auxotroph nematode, six Vit proteins transport cholesterol absorbed from food in the intestine to the oocytes, thus providing energy for the developing embryos and triggering the growth-promoting steroid signalling pathway (Fig. 1.9) [258]. Vits have been shown to enhance the response to various stresses and prolong lifespan [201, 216].

Both Vha subunits and Vits are among the Sip1 substrates identified by co-immunoprecipitation.

Conceivably, the spotted pattern of *sip1* reporter fluorescence, which is reminiscent of the dot-like staining when detecting Vha subunits, could indicate a tendency of Sip1 to cluster to such acidic compartments. Partition of cytosolic sHsps to certain compartments has been reported before. For instance, CeHsp16.1 localizes in the Golgi, where it functions together with the Pmr1 pump, a Golgi-specific Ca^{2+} - and Mn^{2+} -transporting ATPase, to prevent cytoplasmic Ca^{2+} overload under stress [276]. Similarly, overexpressed α A-crystallin co-localizes with the Golgi marker α -mannosidase II and the PMR1 ATPase and protects mammalian neurons from necrosis during heat-stroke [276]. Without repeat analyses and co-localization studies at a microscope rigged with computer software for the identification of single cells and compartments within the embryo, this, however, must remain speculation.

In any case, since they are not among the Hsp16.2-interacting proteins, Vit and Vha proteins could be Sip1-specific substrates. This also applies for a number of other proteins that are fundamental for the embryo. For instance, down-regulation of the glycolysis and electron transport chain components *Cyc1*, *Cco1/-2*, *Ucr1/-2*, as well as ATP synthase subunits like *Atp2* is lethal for embryos, and RNAi of TCA cycle genes like *cts1* results in arrested eggs [277]. Another potential Sip1 substrate, *Cpg2* forms part of the chondroitin proteoglycan-containing inner layer of the trilaminar eggshell, and Perm enzymes are required for the eggshell's permeability barrier [278].

Binding to embryonic proteins both under stress and non-stress conditions would be consistent with a special role for Sip1 in protecting proteostasis as the only sHsp present at a time of skyrocketing protein biosynthesis.

In contrast, many of the potential substrates that are shared with or unique to the Hsp16.2 CoIP are not particularly associated with the embryo, such as ribosomal subunits, metabolic enzymes and cytoskeleton components. For instance, Mdh1 and Cts1, the *C. elegans* homologues of MDH and CS were pulled-down in both the Sip1 and Hsp16.2 CoIP. For both, interaction with the two sHsps has been established by *in vitro* chaperone assays, see Chapter 3.6.1. A preference for binding metabolic enzymes and translation-related proteins (ribosome constituents, amino-acyl tRNA synthases, initiation/elongation factors) has also been observed in two of the few previous investigations into *in vivo* sHsp substrate spectra: CoIP of heated cell extract with *Deinococcus radiodurans* Hsp20.2 [72], and photo crosslinking of *E. coli* lysates with IbpB [279]. Also, other sHsps have been described to interact with nucleic acids and cytoskeletal proteins such as actin, as well [280]. Thus, these categories seem to be predisposed as sHsp substrates in general.

Strikingly, many Sip1-specific substrates are not only associated with the embryo, but also form part of the Daf16 transcriptome. There is a significant overlap of both, individual substrates as well as overrepresented categories identified in the Sip1 CoIP with two lists of Daf16-regulated genes. Murphy (2006) lists confirmed Daf16 transcriptional targets, ~25 % of which also are Sip1 CoIP hits [206]. Of the Sip1 interactome, genes associated with DNA replication (*pcn1*, *mcm* genes), RNA-binding (ribosomal *rpl* and *rps* genes), and protein degradation (*skr* genes), as well as the *vit* genes are repressed by Daf16. Many Sip1 substrates that are positively regulated by Daf16 pertain to the functional categories oxidative stress response (superoxide dismutases Sod1/-2, glutathione S-transferases Gst1/-6/-7), carbohydrate and lipid metabolism (acyl coenzyme A dehydrogenases *Acdhs*), as well as glycolysis/glyoxylate and TCA cycle (e.g., *Icl1*, a isocitrate lyase required for embryonic morphogenesis) [206].

The Sip1 substrate candidates also greatly mirror a list of genes found to be differentially expressed in a long-lived *daf2* mutant of *C. elegans* [208]: Proteasome-ubiquitin constituents, chaperones, ribosomal subunits, translation factors and (m)RNA processing proteins, e.g., Xpo1, and Vig1. Poly(A)-Binding, Pab1, regulates mRNA levels of germline genes and stimulates translation together with Sup26 and Car1 (Cytokinesis, apoptosis, and RNA-binding-1), which also co-precipitated with Sip1 [281]. Car1, which is of critical

importance for oogenesis, associates with Y-box proteins such as Cey4, another strong candidate for the Sip1 substrate spectrum [282].

Thus, a significant number of genes suppressed by Daf16 in a *daf2* mutant strain [208], and of a compilation of established Daf16 targets (Murphy, 2006) are also substrates of Sip1, which itself is induced by Daf16. Daf16 tends to regulate certain key players, rather than all members of a relevant process or pathway [206]. This makes the high incidence of assured Daf16 targets among the Sip1 substrates all the more remarkable.

There may be an interesting correlation involving Sip1 on the translational level, as well as the transcriptional level. DEAD box RNA helicases have been reported to contribute to the regulation of sHsp expression, indirectly or through mRNA stabilization and translation [283]. *Drosophila melanogaster* Vasa co-immunoprecipitates with the mRNA of eight chaperones including α -crystallin, *Synechocystis* CrhR is known to modulate chaperonins, and *sip1* mRNA levels are downregulated if a Vasa homologue in *C. elegans*, *vbh1*, is silenced [283]. Like other RNA helicases, Vbh1 and the Sip1 substrates Pab1 and Car1 are constitutive component of P granules, i.e. large ribonucleoprotein complexes that occupy much of the germ line cytoplasm of most animals [284]. Germ granules mainly function in posttranscriptional regulation, especially the control of maternally-transcribed mRNAs [283, 284]. Vbh1 was found to be important for the nematode's survival of heat and oxidative stress, which might result from its protecting *sip1* mRNA from degradation [283]. A yeast-two-hybrid screen further identified the germline-expressed DEAD box RNA helicase Mut14 as Sip1 interaction partner [285], which is presumably involved in RNA processing and translation [286]. Thus, Sip1 acting as a chaperone for RNA helicases and other translation regulators such as Vig1 (Vasa intronic gene-1) may well constitute a positive feedback loop. Control of Sip1 production at the translational level could far outweigh transcriptional modulation, since embryonic germline blastomeres are largely kept transcriptionally quiescent by maternal repressors [287], and *sip1* mRNA could be maternally provided [236].

Sip1 is special among the *C. elegans* sHsps in its oocyte- and embryo-restricted expression. It is produced even in the absence of stress conditions, binds a large number of substrates already without heat shock, and is active as a chaperone at ambient temperatures. Sip1 operates most effectively at acidic pH values which might reflect the physiological pH in nematode eggs. While able to function as a holdase at pH 7.5, the p*H*_i of larval to adult worms, Sip1 gains activity and co-immunoprecipitates more lysate proteins at pH 5.5 – 6.3, in contrast to the core Hsp16 proteins. While there is some overlap with the substrate spectrum of Hsp16.2, Sip1 preferentially interacts with embryonic proteins.

With this combination of unique features, it is unsurprising that the other 15 small heat shock proteins in *C. elegans* are insufficient to present an alternative to Sip1, even though the Hsp16s are expressed in the non-stressed $\Delta sip1$ mutant. This is evidenced by the decreased survival under both ambient and heat stress conditions. Contrarily, RNAi experiments indicate that depletion of one partner of the Hsp16.11/2 or Hsp16.41/48 pairs can be compensated by the remaining one [220].

On a similar note, a yeast artificial chromosomes hybridization approach identified no Hsp16 proteins as interaction partners of Sip1, as opposed to the core Hsp16s themselves, which either bind or hetero-oligomerize with each other [285].

Taken together, Sip1 has been optimized to function during a single period of worm development, be it to ensure high fidelity folding of the large quantities of nascent polypeptides produced during the intense biosynthetic phase in early embryos, or to preserve embryonic homeostasis during rapid cell division and growth.

As Sip1 is constitutively expressed and activated directly by its physiological surroundings, Sip1 is available to also prevent, as well as respond to, stressful situations at a time when the demand for accurate and efficient protein folding is intrinsically extremely high.

5. SUMMARY AND OUTLOOK

Almost all organisms depend on small heat shock proteins for efficient, high fidelity folding of polypeptides and prevention of unfolding and aggregation. As part of the stress response, the holdase function of these molecular chaperones towards non-native proteins is quite well described. However, many details about sHsp regulation and substrate specificity remain elusive. The analysis of an embryonic sHsp from the nematode *Caenorhabditis elegans*, Sip1, afforded new insights in this context.

Among the 16 sHsps found in *C. elegans*, Sip1 is special in that its expression is constitutive, but restricted to developing oocytes and embryos [228]. In contrast, Sip1's closest relatives, the four core Hsp16 proteins, are absent in the early embryo. In all other stages, they are also only produced after stress [83].

On a molecular level, Sip1 is set apart from the Hsp16 family by a higher molecular mass (17.8 kDa), and pronounced alkalinity (pI = 7.9).

In keeping with this, characterization of Sip1 revealed an intriguing subjection to pH. While the secondary structure remains basically unchanged, its thermostability is augmented at acidic pH values, as observed by circular dichroism. According to analytical ultracentrifugation and negative stain-electron microscopy, the oligomerization state with the 32- and 28-mer as the predominant species at pH 8.2 - 7.5 changes to a polydisperse ensemble of smaller structures when lowering pH to 6.3 and 5.8.

Cryo-EM reconstructions of the Sip1 32-, 28-, and 24-mers in combination with the crystal structure of the 32-mer revealed the sHsp's oligomeric architecture to be a hollow sphere, which, in the case of the 32-mer, is slightly flattened along the C_8 axis, and in the 24-mer is prolonged along the C_6 axis, resulting in an ellipsoid shape. The 32-mer resembles a globe made up of two identical hemispheres, with an equator and two poles that are each marked by a hole. The structures are spanned by dimeric building blocks, 2x 8 in the case of the 32-mer, 2x 7 in the 28-mer, and 2x 6 in the 24-mer. Dissociation to the next smaller oligomer thus progresses via the successive loss of two dimers. With its higher order D6 symmetry, the cryo-EM-derived model of the Sip1 24-mer displays an orientation of the dimers that substantially differs from that seen in the NS-EM reconstructions of Hsp16.2, Hsp16.41, and Hsp16.48 [220].

Rather, the quaternary structure of Sip1 resembles that of *S. pombe* Hsp16.0 [90]. On the level of the dimer, Sip1 shares the archetypical mammalian dimerization mode of human sHsps, as opposed to the crystallin domain architecture displayed by the metazoan Tsp36 (from flatworm), or sHsps from archaea, bacteria, or plant [72, 86, 88-96].

pH is pivotal in modulating not only the relative abundance of the polydisperse ensemble of different Sip1 stoichiometries, because the tendency for dissociation of the larger oligomers into smaller species at lower pH values is accompanied by a gain in chaperone activity.

Similar to other sHsps, Sip1 is acting as a holdase and can work in concert with the *C. elegans* Hsp70/40 system, which facilitates the active refolding of the non-native substrates in an ATP-dependent manner. The four core Hsp16 proteins also exhibit chaperone activity, but they operate most efficiently at around pH 7.5, which is the pH_i reported for larval and adult nematodes [241]. In contrast, the acidic milieu which represents the optimum conditions for Sip1 characterizes large parts of the embryo [243].

No other sHsp tested shares Sip1's narrow optimum pH range of pH 5.8 - 6.3 except for human α B-crystallin, which has been shown to function in tissues suffering from acidosis *in vivo*.

CoIP-MS analysis reveals that Sip1 interacts promiscuously with non-native proteins. While there is an overlap of the substrate spectra of Sip1 and Hsp16.2, many substrates appear to be specific to Sip1. These include proteins that are intimately associated with pivotal functions in the embryo, such as vitellogenins and vacuolar H⁺ ATP synthases, which effect the acidic pH that is essential for the embryo.

Thus, Sip1 is uniquely suited to protect the embryonic proteome from unspecific aggregation and assist in refolding of proteins by cooperating with the Hsp70/40 system. The importance of this function for the developing egg is reflected by the dramatic drop in heat stress survival of $\Delta sip1$ embryos in comparison to wild type.

The function of one core Hsp16 proteins can be substituted by another, because loss of a single representative does not evoke a phenotype [220]. In contrast, none of the remaining 15 sHsps of *C. elegans* can compensate for the deletion of *sip1*, as apparent from the significantly short-lived and thermo-sensitive phenotypes of $\Delta sip1$ nematodes, even though immunoblotting shows the normally only stress-inducible Hsp16 proteins to be upregulated at ambient temperatures in the *sip1* deletion strain.

The combined results indicate physiological roles of Sip1 that are singular among all CesHsps.

Sip1 has adapted to protect the cell in its earliest stages of development, when rapid cell division and growth mean protein biosynthesis is markedly elevated and proteostasis is especially precarious - even without external stresses.

In the course of this Thesis, the developmentally regulated sHsp Sip1 was analyzed *in vivo* and *in vitro* in respect to its expression, function, substrate spectrum, regulation, and structure. Sip1 is the first sHsp to afford insight into the importance of a promiscuous molecular chaperone dedicated to one specific developmental stage. In the context of sHsps in general, results for Sip1 reveal novel aspects of structural organization and expand the repertoire of regulatory principles. For the first time, 3D structures of varying stoichiometries are presented for one sHsp. They allow explaining how the architecture of large oligomers is modulated by environmental alterations, facilitating fine-tuning of chaperone activity according to cellular need independent of transcriptional control.

Of course, with these findings, new questions have arisen.

Determining the expression of Sip1 within the embryo on a (sub-)cellular level, as well as co-localization studies with P granules or acidic yolk storage granules would certainly prove interesting.

The search for the pH-sensitive oligomerization switch as well as the role of the C- and N-terminal extensions in oligomer stabilization and substrate recognition represent another wide field for future experiments. In this context, modeling of the NTR into so far unoccupied density within the EM structures using data from the crystal structure is under way. Cross-linking approaches would also provide useful information. For analysis of substrate binding sites on the Sip1 oligomer, a heat-shocked mixture of Sip1 and its preferential substrate MDH could be subjected to EM.

When further pursuing the involvement of histidine residues in oligomerization, His 81 and His82 could represent another pair of likely pH sensor candidates. They are located within the β 5-strand, with the residue moieties pointing into opposite directions, perpendicular to the β -sheet 2. Thus, they could conceivably alter the curvature of the

strand, and possibly the entire sheet, which might create enough tension to “bust free” a dimer.

Also, truncation variants of Sip1 missing either the NTR or the CTR would clarify the termini's role in structural support or substrate binding. Since Sip1 shares some interesting properties and tendencies with human α B-crystallin, further fusion constructs with permutations of the two sHsps' NTR, ACD and CTR would be expected to show which domains are interchangeable and which dictate behavior.

6. MATERIALS AND METHODS

6.1 MATERIALS

6.1.1 CHEMICALS

Chemicals of analysis grade purity were acquired from the following companies: Merck (Darmstadt, GER), VWR (Darmstadt, GER), Roth (Karlsruhe, GER), Serva (Heidelberg, GER) and Sigma-Aldrich (St. Louis, MO, USA).

All media and solutions were prepared from bi-distilled water (TKA GenPure, Thermo Scientific, Niederelbert, GER), and were pH-adjusted using a calibrated pH-meter (WTW, Weilheim, GER) at the intended temperature of use. Sterilization was achieved by filtration or autoclaving for 30 min at 121 °C and 200 kPa. Plates were stored at 4 °C.

6.1.2 *C. ELEGANS* STRAINS AND MEDIA

C. elegans strains utilized in this work were the wild-type (wt) N2 and $\Delta sip1$ (tm3624) strains from the *C. elegans* Gene Knockout Consortium at the University of Minnesota's *Caenorhabditis* Genetics Center and the National Bioresource Project for the Experimental Animal *C. elegans* at Tokyo Women's Medical University (S. Mitani), respectively. The deletion in *sip1* was verified by PCR.

C. elegans were maintained on NGM (nematode growth medium) agar plates carrying a lawn of *Escherichia coli* OP50, an uracil auxotroph strain with limited growth on NGM plates that is routinely used for feeding nematodes [153], using standard handling techniques [288].

NGM plates:	NaCl	3 g
	Agar	17 g
	Bacto peptone	2.5 g
	H ₂ O	970 ml

Autoclave, cool to 55 °C, add sterile-filtered:

Cholesterol (5 mg/ml in EtOH)	1 ml
1M MgSO ₄	1 ml
1M CaCl ₂	1 ml
1M K ₂ HPO ₄ /KH ₂ PO ₄ , pH 6.0	25 ml

M9 medium:	Na ₂ HPO ₄	5.8 g
	KH ₂ PO ₄	3.0 g
	NaCl	0.5 g
	NH ₄ Cl	1.0 g
	H ₂ O	ad 1 l
S-Basal:	K ₂ HPO ₄	1 g
	KH ₂ PO ₄	6 g
	NaCl	5.85 g
	Cholesterol (5 mg/ml in EtOH)	1 ml
	H ₂ O	ad 1 l
Potassium citrate: 1 M, pH 6.0	citric acid x 1 aq	20 g
	tri-potassium citrate x 1 aq	293.5 g
	H ₂ O	ad 1 l
Trace metal soln.:	di-sodium EDTA	1.86 g
	FeSO ₄ x 7 aq	0.69 g
	MnCl ₂ x 4 aq	0.2 g
	ZnSO ₄ x 7 aq	0.29 g
	CuSO ₄ x 5 aq	0.025 g
	H ₂ O	ad 1 l
S medium:	S Basal	1 l
	1 M potassium citrate, pH 6.0	10 ml
	trace metals soln.	10 ml
	1 M CaCl ₂	3 ml
	1 M MgSO ₄	3 ml
Bleaching soln.:	1M NaOH : Chlorix 1 : 2	1.5 ml per 3.5 ml worm suspension

6.1.3 *E. COLI* STRAINS AND MEDIA

LB ₀ medium:	Bacto Trypton	10 g
	Yeast extract	5 g
	NaCl	5 g
	H ₂ O	ad 1 l
For LB ₀ plates, add:	Agar Agar	15 g
<i>E. coli</i> selection:	Ampicillin	100 µg/ml
	Kanamycin	35 µg/ml
	Chloramphenicol	35 µg/ml
	Tetracyclin	12.5 µg/ml

Table 6.1: *E. coli* strains

Strain	Genotype	Source
Cloning:		
XL1 Blue	recA1 endA1 gyrA96 thi-1 hsdR17 supE44 relA1 lac [FproAB lacI ^q ZΔM15 Tn10 (Tet ^R)]	Agilent, Santa Clara, USA
Expression:		
BL21 DE3	F ⁻ ompT gal dcm lon hsdS _B (r _B ⁻ m _B ⁻) λ(DE3 [lacI lacUV5-T7 gene 1 ind1 sam7 nin5])	Agilent
BL21 DE3 CodonPlus-RIL	F ⁻ ompT hsdS(r _B ⁻ m _B ⁻) dcm+ Tet ^R gal λ(DE3) endA Hte [argU ileY leuW Cam ^R]	Agilent
Rosetta	F ⁻ ompT hsdS _B (r _B ⁻ m _B ⁻) gal dcm λ(DE3 [lacI lacUV5-T7 gene 1 ind1 sam7 nin5]) (Cam ^R)	Merck
JM109(DE3)	recA1 endA1 gyrA96 thi hsdR17 (r _k ⁻ m _k ⁺) supE44 relA1 λ-Δ(lac-proAB) [F' traD36 proAB lacI ^q ZΔM15], IDE3	Promega, Mannheim, GER
<i>C. elegans</i> feeding:		
OP50	Ura ^r , derived from <i>E. coli</i> B	CGC

6.1.4 CLONING

1kB DNA Ladder		Peqlab (Erlangen, GER)
Pfu DNA polymerase and reaction buffer		Promega (Fitchburg, USA)
Taq DNA polymerase and reaction buffer		Promega
Restriction enzymes		Promega, NEB (Ipswich, USA)
dNTP mix		Promega
Alkaline phosphatase		Roche (Basel, CH)
T4 DNA ligase		Promega
Wizard Miniprep kit,		Promega
Wizard PCR Product Purification & Gel Extraction kit		Promega
PCR Thermocycler Primus 25		MWG Eurofins (Ebersberg, GER)
Agarose gel Wide Mini-Sub Cell GT system		BioRad (Hercules, USA)
Electrophoresis power supply 601, 1001		GE Healthcare (Chalfont St. Giles, UK)
TAE buffer (50x):	TRIS/acetate, pH 8.0 EDTA	2 M 50 mM
BJ (10x):	Glycerol, pH 8.0 EDTA Bromophenol blue Xylene cyanol	50 % (v/v) 10 mM 0.2 % (w/v) 0.2 % (w/v)
Agarose soln. 1 %	Agarose TAE (1x) Stain G	1 g 100 mL, dissolve by boiling, cool, 1 μL

Quick ligation buffer:	TRIS/HCl, pH 7.6	132 mM
	MgCl ₂	20 mM
	DTT	2 mM
	ATP	2 mM
	PEG 6000	15 % (v/v)

Table 6.2: Primers

Amplicon and intended plasmid	Restriction	Primer obtained from MWG Eurofins (restriction site or mutation in capital letters)
Sip1 wt pET21a	fw. NdeI	gagatcCATATGtcttctctgcccatacact
	rev. XhoI	gagatcCTCGAGtttagtgctttccggtggt
Sip1-CRYAB chimaera pET21a	fw. NdeI	ttcataCATATGctcaacgaggtcgagaacaccgcccagaagtctg
	rev. XhoI	actagtCTCGAGtatttttccggagcagcggtaacagccggttttcttcagtgaggattggaagagcacgaacggtggtggtggag
Sip1 H111/139N pET21a	His111Asn	cgctgactggctcacatcAACaccgtcatcaacaaggaaggacag
	His139Asn	gttcgtgctctccaatcAACacttctgctggacacgc
Sip1-ACD pQE30	fw. BamHI	tcagtcGGATCCtcaacgaggtcgagaacaccgcccagaag
	rev. PstI	atcgatCTGCAGtcaagtgtggattggaagagcacgaacggtggtggtg
1.5 kb promoter Sip1 eYFP transcriptional reporter, pPD95.79	fw. NotI	atctgtGCGGCCGctgtactgcagctgaagcgagcgattcgagacgaggacg
	rev. NheI	actagtGCTAGCcaaagttgagtgaatagggttaagaatgaggtgaaaaacg atgaacgtctgagg
" translational	fw. NotI	atctgtGCGGCCGctgtactgcagctgaagcgagcgattcgagacgaggacg
	rev. NheI	caacgtGCTAGCgtgctttccggtggtggtggtgctggatggcttctg
1 kb promoter Sip1 eYFP transcriptional reporter, pPD95.79	fw. NotI	atctatGCGGCCGctgtactgcagctgaagcgagcgattcgagacgaggacg
	rev. NheI	actagtGCTAGCaaagttgagtgaatagggttaagaatgaggtgaaaaacga tgaacgtctgagg
" translational	fw. NotI	atctatGCGGCCGctgtactgcagctgaagcgagcgattcgagacgaggacg
	rev. NheI	caacgtGCTAGCtgcctttccggtggtggtggtgctggatggcttctg

6.1.5 PROTEIN PURIFICATION AND BUFFERS

Cell disruptor Basic Z

ÄKTA FPLC / Prime

FPLC Columns:

Q-Sepharose fast flow (ff)

Constant Sys. (Warwick, UK)

GE Healthcare

all GE Healthcare

Resource Q ff (6 ml)

HiLoad Superdex 200 prep grade (pg), 26/60 column volume

HiLoad Superdex 75 pg, 16/60

Ni-Sepharose HisTrap HP (5 ml)

Buffer A / B:	TRIS/HCl, pH 8.5	50 mM
	EDTA	5 mM
	DTT	1 mM
	Protease inhibitor mix HP	(Serva)
	DNase I	(Roche)
	(B: NaCl	1 M)
Buffer C:	TRIS/HCl, pH 8.5	50 mM
	NaCl	150 mM
	EDTA	5 mM
Buffer D / E:	TRIS/HCl, pH 8.3	50 mM
	NaCl	300 mM
	Imidazole	20 mM / E: 500 mM

Standard buffer for all measurements except if stated otherwise, at indicated pH:

“MES MOPS buffer” (pH 5.5 – 8.0 buffer range) I = 150 mM	MES /KOH, pH 5.8 – 8.2	10 mM
	MOPS	10 mM
	KCl	141 mM
	CaCl ₂	1 mM
MES MOPS buffer I = 50 mM	MES	10 mM
	MOPS	10 mM
	KCl	41 mM
	CaCl ₂	1 mM
Teorell-Stenhagen (pH 2 – 12 range) I = 150 mM	Citrate	9.9 mM
	H ₃ PO ₄	9.9 mM
	H ₃ BO ₃	17.1 mM
	NaOH 1N	103 ml per l
Teorell-Stenhagen I = 50 mM	Citrate	3.3 mM
	H ₃ PO ₄	3.3 mM
	H ₃ BO ₃	5.7 mM
	NaOH 1N	34.3 ml per l
3-components buffer (pH 3.7 – 9.0 range) I = 150 mM / 50 mM	MES	25 mM
	TRIS	5 mM
	NaOAc	25 mM
	NaCl	110 mM / 10 mM

6.1.6 PROTEINS

C. elegans Hsc70, Dnj13/12, Bag1 and pig heart citrate synthase (CS) had been purified at the Institute as described elsewhere [25, 289]. Malate dehydrogenase (Mdh2, mitochondrial, from pig heart) was purchased from Roche. Yeast Hsp26, wheat Hsp16.9,

human α B-crystallin and HspB1 were available at the Institute. All protein concentrations correspond to monomers.

6.1.7 GEL-ELECTROPHORESIS AND IMMUNODETECTION

Low Range Molecular Weight Standard (SDS-PAGE)		BioRad	
Hoefer Mighty Small II Gelelectrophoresis Unit		GE Healthcare	
Gel documentation system		GE Healthcare	
Immobilon nitrocellulose membrane		Millipore (Bedford, USA)	
Fast Blot B44 blotting device		Biometra (Göttingen, GER)	
Electrophoresis power supplies 601, 1001		GE Healthcare	
ImageQuant LAS 4000		GE Healthcare	
WesternBright enhanced chemiluminescence spray		Advansta, CA, USA	
SDS running buffer (10x):	TRIS/HCl pH 6.8	250 mM	
	Glycine	2 M	
	SDS	1 % (w/v)	
Laemmli sample buffer (5x):	TRIS/HCl pH 6.8	315.5 mM	
	SDS	10 % (w/v)	
	Glycerol	50 % (v/v)	
	2-mercaptoethanol	2.5 % (v/v)	
	Bromophenol blue	0.05 % (w/v)	
Separating gel buffer (4x):	TRIS/HCl pH 8.8	250 m M	
	SDS	0.8 % (w/v)	
Stacking gel buffer (2x):	TRIS/HCl pH 6.8	250 m M	
	SDS	0.4 % (w/v)	
SDS-PA gels:	Separating gel, 12.5 % (v/v)	Stacking gel	
H ₂ O	4.2 ml	1.9 ml	
Acrylamide/bisacrylamide 19:1 40 % (w/v)	3.1 ml	0.6 ml	
Gel buffer	2.5 ml	2.5 ml	
Ammonium persulfate 10 %	100 μ l	50 μ l	
Tetramethylethylenediamine	10 μ l	5 μ l	
Fairbanks staining buffer:	Coomassie B. Blue R250	2.5 g	
	Ethanol	250 mL	
	Acetic acid	80 mL	
	H ₂ O	ad 1 l	
De-staining:	Acetic acid	10 % (v/v)	
Transfer buffer:	Glycin	36 g	
	TRIS	7.6 g	
	Methanol	500 ml	
	SDS	0.3 % (w/v)	
	H ₂ O	ad 2.5 l	

PBS(-T) buffer:	NaCl	5.84 g
	Na ₂ HPO ₄	11.5 g
	NaH ₂ PO ₄	2.96 g
	H ₂ O	ad 1 l
	(Tween-20	1 ml)

6.1.8 LIQUID CHROMATOGRAPHY - MASS SPECTROMETRY

Ultraflex II MALDI ToF/ToF mass spectrometer	Bruker Daltonics (Bremen, GER)
LTQ Orbitrap XL mass spectrometer with	Thermo Scientific
Proteome Discoverer 1.4 software	Thermo Scientific
Speed vac DNA120	Thermo Scientific
0.22 µm centrifuge filter	VWR
Acclaim PepMap RSLC C18 trap column	both Thermo Scientific
PepMap RSLC C18 column (75 µm x 150mm, C18, 2 µm, 100 Å)	

6.1.9 CRYSTALLOGRAPHY

96-3 well Intelli-Plates for sitting drop	Art Robbins Instr. (Sunnyvale, USA)
Crystal Phoenix Liquid Handling System	Art Robbins Instruments
Cooled Incubator Series 3000	RUMED Rubarth (Laatzen, GER)
Crystal Cap HT for CryoLoop	Hampton (Aliso Viejo, USA)
Crystal Cap HT Vial	Hampton
Magnetic Caps, Pins and Vials	Mol. Dimensions (Newmarket, UK)
MICROLAB STARlet Workstation pipet robot	Hamilton (Reno, USA)
Micro Tool Box	Molecular Dimensions
Mounted CryoLoop	Hampton
NeXtal Suites	Qiagen (Hilden, GER)
Zoom stereo microscope SZX10/KL1500LCD	Olympus (Tokyo, JP)

Crystallization buffer for Sip1-ACD: (from a Sip1-ACD stock in CAPS 50 mM, pH 10)	CAPS, pH 6.9	33 mM
	BIS-TRIS	17 mM
	Ammonium sulfate	17 mM
	Pentaerythritol ethoxylate	10 %

Crystallization buffer for wt Sip1:	HEPES, pH 7.1	50 mM
	MES	50 mM
	Sodium acetate	50 mM
	PEG400	15 %

6.1.10 MICROSCOPY

Transmission electron microscopes:	
CM100X (100kV), for negative stain-EM	both Jeol (Tokyo, JP)
JEM 2011 for cryo-EM	

Light microscopes:

Stemi SV11	Zeiss (Jena, GER)
Axiovert 200 fluorescence microscope	Zeiss
with HAL100, HBO100, injection needle manipulator	
MZ 16 FA fluorescence microscope	Leica (Wetzlar, GER)

6.1.11 SPECTROSCOPY

Circular dichroism spectropolarimeter J-715 with PTC 343 Peltier temperature unit	both Jasco (Groß-Umstadt, GER)
UV quartz cuvettes QS 1 mm, 340 µL, with stopper	Hellma (Müllheim, GER)
Refractometer Abbe MARK II	Leica Mikrosysteme
UV-VIS spectrophotometry:	
Varian Cary 50 Bio	Agilent (Santa Clara, USA)
UV/Vis V-550	Jasco
NanoDrop	Thermo Fisher (Waltham, USA)
Plastic cuvettes, 1 mL and half-micro	Brand (Wertheim, GER)
UV quartz cuvettes QS ultra micro, 160 µL	Hellma

6.1.12 CENTRIFUGES

Table top centrifuge 5415 C	Eppendorf (Hamburg, GER)
Rotina 46R	Hettich (Tuttlingen, GER)
Avanti J25 and J2-HS with rotors JA-10, JA-25.50	Beckman Coulter (Brea, USA)
Analytical ultracentrifuges Optima XL-I,	both Beckman
ProteomeLab XL-A (equipped with FDS)	

6.1.13 FURTHER EQUIPMENT AND MATERIALS

Mx3000P qPCR system	Agilent
Balances BP 121 S, BL 310, BL 1500S, 1601 004	Sartorius (Göttingen, GER)
MM400 beadmill	Retsch (Haan, GER)
Polystyrol Petri dishes	Greiner (Nürtingen, GER)
15 / 50 ml plastic Greiner tubes	Greiner
200µl / 1.5 ml / 2 ml Eppendorf reaction tubes	Eppendorf
Pipetman pipettes	Gilson (Middleton, USA)
Ultrafiltration membrane	Amicon Millipore (Bedford, USA)
Stirred filtration chamber and membranes 30 MW	Amicon Millipore
Centricon 10 / 30 MW	Amicon Millipore
Slide-A-Lyzer dialysis cassettes	Pierce (Rockford, USA)
Sterile filter (0.22 µm)	Merck (Darmstadt, GER)
Membrane filter (0.22 µm)	Sartorius
pH indicator paper	Merck
pH meter Multical pH 538	WTW (Weilheim, GER)

6.1.14 SOFTWARE AND ONLINE DATABASES

Microsoft Windows 2007	Microsoft (Redmond, USA)
Endnote X5	Thomson Reuters (NYC, USA)
OriginPro 9.1 USA)	Microcal Software (Northampton, USA)
CDNN Spectra Deconvolution, Vers 2.1	Dr. Gerald Böhm, Universität Halle, GER
ApE Plasmid	M. W. Davis
CorelDraw	Corel Corporation (Ottawa, CAN)
ImageJ	http://rsb.info.nih.gov/ij/
PyMOL Schrödinger, LLC	http://pymol.sourceforge.net/
Oligo Calculator oligocalc.html	http://mbcf.dfc.harvard.edu/docs/
ExpASy Prot Param tool	http://web.expasy.org/protparam/
[GdmCl] and [Urea] Calculator	http://sosnick.uchicago.edu/gdmcl.html
TCoffee	http://www.tcoffee.org/
CLUSTAL W2	http://www.clustal.org/
MMass	http://www.mmass.org/
Mascot peptide database	http://www.matrixscience.com
PANTHER	http://www.pantherdb.org/
Wormbase	http://www.wormbase.org/
Wormbook	http://www.wormbook.org/
Wormatlas	http://www.wormatlas.org/
UniProt	http://www.uniprot.org/
ProtParam	http://web.expasy.org/protparam/
BLAST	http://blast.ncbi.nlm.nih.gov/Blast.cgi
PDB	http://www.rcsb.org/pdb/home/home.do
PubMed	http://www.ncbi.nlm.nih.gov/pubmed

6.2 METHODS

6.2.1 MOLECULAR BIOLOGY METHODS

pET21a(+) plasmids (Novagen, Gibbstown, USA) of all *hsp16* genes (cDNA transcribed from total *C. elegans* mRNA) were available at the Institute. The *sip1* plasmid was used as template for all *sip1* mutants created. DNA was amplified by polymerase chain reaction (PCR) [290]. For primer design, the *C. elegans* gene sequence was obtained from wormbase.org. Primer length was optimized using OligoCalc, and restriction sites selected according to the intended plasmid. Primers are indicated in Table 6.2. Hot start PCR amplification was performed according to standard lab protocols [291], employing

Taq polymerase for usual PCR reactions, and Pfu polymerase for long, genomic DNA amplicons. The successful amplification of the target DNA was judged by agarose gel-electrophoresis. Likewise, intact or restricted vectors were separated on agarose gels for subsequent isolation or analysis of DNA size and restriction efficiency, employing standard lab protocols [291] and the Promega PCR cleanup system kit. DNA was stored, nuclease-free, at -20 °C. Purified PCR products and empty vector were restricted by endonucleases and the plasmid's ends were de-phosphorylated by alkaline phosphatase in order to prevent re-ligation, following the supplier's instructions. Restricted plasmid and insert were then ligated by T4 DNA ligase in Quick ligation buffer, see 6.1.4.

His-to-Asn (H111/139N) mutations were introduced into wt Sip1 in pET21a(+) by following the QuikChange mutagenesis protocol (Agilent).

E. coli XL-1 Blue (Agilent) cells that had been made transfection-competent by the Sambrook or Inoue methods [291, 292] were transformed with the target plasmid and grown on LB plates containing the respective antibiotic for selection. Single colonies to be tested were propagated in liquid culture, harvested and lysed for plasmid purification using the Promega Miniprep Wizard Plus SV kit. All constructs were verified by sequencing by MWG Eurofins.

For microinjection of transcriptional or translational *sip1* expression reporters into worms, the *sip1* promoter (a 1,000 or 1,500 bp long fragment) with or without the *sip1* gene were amplified from genomic *C. elegans* DNA and subcloned in frame into the fluorescent protein-encoding vector pPD95.79 (eYFP version, based on the original GFP-encoding vector from Andrew Fire's lab), following the wormbase protocol [293]. For primers, see Table 6.2.

6.2.2 PROTEIN EXPRESSION AND PURIFICATION

Several *E. coli* strains were tested for recombinant protein production. The well-established BL21 strain is deficient of Lon and OmpT proteases to prevent protein digestion. In both BL21 and JM109-derived strains, the "DE3" designation indicates IPTG-inducibility of expression, as the strain encodes the T7 RNA polymerase under control of the *lacUV5* promoter. Since some tRNAs are rarer in *E. coli* than in the heterologous protein's original organism, Codon+ cells contain extra copies of tRNA genes (e.g., for R, I, L in BL21-CodonPlus-RIL). Similarly, Rosetta, another tested derivative of BL21 DE3,

supplies tRNA genes for rare R, I, L, P, and G codons to overcome the different codon usage between organisms and thus ensure unlimited translation.

Expression parameters were optimized for maximum soluble protein yield. 50 mL LB medium containing the appropriate antibiotic were inoculated with 1 mL of a pre-culture of different *E. coli* strains carrying the plasmid of interest. During incubation at 25, 30 or 37 °C at 120 rpm agitation, cell growth was followed by measuring the optical density (OD) at 595 nm. At OD = 0.5, expression was induced by addition of isopropyl 1-thio- β -D-galactopyranoside (IPTG, 1 mM) to all cultures. OD was noted and 1 mL samples were taken, and the completely pelleted cells were frozen at 0, 1.5, 3, 4, 5, and ~15 hours after induction. All samples were normalized to OD = 10 by adding the required volume of PBS and lysis buffer:

BugBuster® Protein Extraction Reagent (Merck Millipore)	1x
MgCl ₂	2.5 mM
Lysozyme	0.25 mg/ml
Protease inhibitor (Roche)	both as instructed
DNase (Roche)	by manufacturer

After lysis for 30 min, the samples were centrifuged at 20,8000 g, at 4 °C, for 45 min. The separated soluble and insoluble protein fractions were boiled in Laemmli sample buffer and evaluated by SDS-PAGE, following standard lab protocols [291, 294].

Bacteria were grown according to the parameters optimized in the expression test for maximum overproduction of the target protein, in the case of wt Sip1: *E. coli* BL21 DE3 Codon+ cells (Agilent) transfected with the pET21a(+) vector, in LB_{amp}, shaken at 130 rpm over night at 37 °C. F08H9.3 and F08H9.4 were expressed in the pET21a(+) in JM109 DE3 cells and grown under the same conditions as for Sip1. *E. coli* were harvested by centrifugation (15 min, 6,300 x g), resuspended in chilled buffer A (see 6.1.5) and lysed in a cooled cell disruptor at 1.8 kbar. After centrifugation (30 min, 24,000 x g, 5 °C), the clarified lysate was loaded onto a Q-Sepharose column equilibrated in buffer A and bound proteins were eluted by ≥ 4 column volumes of buffer A followed by a shallow NaCl gradient (buffer A \rightarrow B). Target protein-containing fractions were further purified by gel filtration (Superdex 200 pg 26/60, equilibrated in buffer C) and anion exchange chromatography (Resource Q, buffer A \rightarrow B without DNase I and protease inhibitor). In order to obtain ultra-pure Sip1 for crystallography, another size exclusion chromatographic run (Superdex 75 pg 16/60, equilibrated in buffer C) was used for a

final polish. All purification steps were performed at 5 °C, and assessed by SDS-PAGE. The pure protein was concentrated and aliquots were stored at -80 °C in standard buffer. The Sip1 mutants H111/139N and the Sip1/ α B-crystallin fusion protein were found to be highly overexpressed in *E. coli* BL21 DE3 Codon+ transfected with the pET21a(+) vector carrying the respective insert under the same conditions as for wt Sip1, and were natively purified like the wt protein. The truncated Sip1-ACD construct was expressed in BL21 DE3 Codon+ in pQE30 vector (Quiagen) and purified using a protocol modified from native protein purification: The clarified lysate in buffer D was loaded onto a Ni-HisTrap column and washed with several column volumes of buffer D. This was repeated with 95 % buffer D, 5 % buffer E, again until the chromatogram showed a stable baseline. The tagged protein was eluted by increasing the percentage of buffer E. The buffer was then exchanged for buffer A, and Q-Sepharose and Superdex 200 pg chromatography were performed as described above. The His₆ tag was removed by TEV protease cleavage, over night on ice. The protein eluted from a final Ni-column was pure.

For an alternate production and purification route, F08H9.3 tagged with a TEV-cleavable His₆ stretch in pET21a(+) was found to be most highly and solubly produced at only 30 °C in JM109 DE3, over night after IPTG induction at OD = 0.7 and shaking at 130 rpm. F08H9.3 HisTEV was purified in the same way as Sip1-ACD.

To demonstrate that the proteins were pure and had not been partially degraded during the purification process, the full-length molecular mass per charge (m/z) was determined by mass spectrometry (MS), using the soft ionization afforded by Matrix-assisted laser desorption/ionization - Time of Flight (Maldi ToF/ToF) MS (operated at linear mode). Digestion by trypsin before MS allowed for identification of the protein by comparison of the resulting characteristic peptide pattern to the Mascot database.

6.2.3 CRYSTALLOGRAPHY

Crystal structure determination of Sip1 was undertaken in cooperation with Prof. Dr. M. Groll and Dr. M. Stein. Crystals of the Sip1-ACD and full length protein were grown at 20 °C from 5 mg/ml of protein in the listed buffers (6.1.9), using the sitting drop vapour diffusion method. Using synchrotron radiation at the Swiss Light Source, Paul-Scherrer-Institut, Villigen, Switzerland, datasets to 2.1 and 3.6 Å were obtained for truncated and native Sip1 in the P2₁2₁2₁ and the P422 space groups, respectively. The Sip1-ACD

structure was refined by molecular replacement using the coordinates of α B-crystallin (PDB accession code: 2WJ7 [88]). Two dimerizing molecules were contained in the ASU (asymmetric unit). Model building and anisotropic TLS-refinement including the 2-fold noncrystallographic symmetry (NCS) resulted in a final R_{free} value of 25.9 %.

The high resolution Sip1 ACD dimer was subsequently used as a starting model for molecular replacement of the full length Sip1 dataset. Here, the ASU contained 4 molecules arranged in two NCS-related dimers. The biological assembly was found to be the 32mer. Model building mainly affected the N- and C-termini, whereas the high resolution ACD-domains showed little difference between the two crystal structures. Isotropic TLS-refinement gave a R_{free} value of 25.2 %. Both crystal structures are to be deposited in the Protein DataBase.

Table 6.3: Crystallographic data collection and refinement statistics of Sip1-ACD (truncated dimer) and wild type Sip1 (32mer).

Crystallographic data	Sip1 ACD*	Sip1 full-length*	
Crystal parameters Space group Cell constants (Å/°)	P2 ₁ 2 ₁ 2 ₁ a = 36.39 b = 50.82 c = 130.17	P422 a = 142.59 b = 142.59 c = 100.57	*Dataset has been collected on a single crystal.
Data collection Beamline Wavelength, Å Resolution range, Å No. observations No. unique reflections‡ Completeness, %† $R_{\text{merge}}^{\dagger,\S}$ $I/\sigma(I)^{\dagger}$	X06SA, SLS 1.0 47-2.1 78467 14754 99.7 (99.7) 6.0 (52.7) 16.32 (2.92)	X06SA 1.0 25-3.6 179075 12495 99.5 (100) 11.4 (67.5) 20.14 (5.48)	†Values of completeness, R_{merge} , and $I/\sigma(I)$ in parentheses correspond to the last resolution shell. ‡Friedel pairs were treated as identical reflections. § $R_{\text{merge}}(I) = \frac{\sum_{\text{hkl}} \sum_j I(\text{hkl})_j - I(\text{hkl}) }{\sum_{\text{hkl}} I(\text{hkl})}$, where $I(\text{hkl})_j$ is the measurement of the intensity of reflection hkl and $\langle I(\text{hkl}) \rangle$ is the average intensity.
Refinement Resolution range, Å No. reflections working set No. reflections test set No. nonhydrogen No. of ligand atoms Water $R_{\text{work}}/R_{\text{free}}$ %¶ Rmsd bond (Å)/(°)** Ramachandran plot, %***	15-2.1 13947 734 1624 10 37 23.0/25.9 0.005/1.08 97.4/2.6/0.0	15-3.6 11869 625 3668 0 0 22.6/25.2 0.004/0.788 92.8/7.2/0.0	¶ $R = \frac{\sum_{\text{hkl}} F_{\text{obs}} - F_{\text{calc}} }{\sum_{\text{hkl}} F_{\text{obs}} }$, where R_{free} is calculated without a sigma cut off for a randomly chosen 5% of reflections, which were not used for structure refinement, and R_{work} is

calculated for the remaining reflections.

**Deviations from ideal bond lengths/angles.

***Number of residues in favored region/allowed region/outlier region.

6.2.4 ELECTRON MICROSCOPY

Electron microscopy was performed in the Group of Prof. Dr. S. Weinkauf. To assess the oligomer ensemble distribution of Sip1 by negative stain-EM, the concentrated protein in standard buffer was diluted to 0.2 mg/ml into standard buffer at the indicated pH, incubated for at least one hour and then further diluted to 25 µg/ml. for 30 sec. 5 µl of sample were adsorbed onto carbon-coated, glow-discharged EM-grids. 5 µl 2 % (w/v) uranyl acetate stain was added. Electron micrographs were recorded using a Jeol CM100X operating at 100kV.

For cryo-EM structure determination, 0.25 mg/ml of Sip1 in 10 mM HEPES, 1 mM CaCl₂, pH 6.5 on EM-grids were vitrified by rapid freezing in liquid ethane. Images were collected in low dose mode on a Jeol JEM 2011 at 120 kV. 12.075 CTF-corrected protein particles were selected semi-automatically. Images were centred and sorted into three subsets differing in size by Multivariate Statistical Analysis (MSA). Initial starting models were generated from class averages for each subset and refined by iterations of projection matching and MSA for every reference-class. Three-dimensional structures were generated by exact filtered backprojection. Resolution was determined by Fourier Shell Correlation (0.5 criterion).

6.2.5 ANALYTICAL ULTRACENTRIFUGATION

Analytical ultracentrifugation (AUC) allows for tracing a protein's movements within a centrifugal field of up to 300,000 g. By AUC, information about the approximate shape (the deviation of the analyte's frictional ratio from that of a sphere), molar mass, and (if the protein is polydisperse) oligomerization states can be gleaned. Two kinds of experiments are commonly performed: In sedimentation velocity experiments, an applied gravitational field creates a boundary between sedimenting proteins and supernatant buffer from a previously homogenous mixture. This interface moves along the sedimentation path with constant speed because of the balanced gravitation and friction, which depend on the analytes' mass, density and volume, and particle shape and solvent viscosity, respectively. The velocity of the boundary layer's movement defines the sedimentation coefficient (s). This sedimentation rate is expressed in the unit of Svedberg [S] = 10⁻¹³ sec.

Sedimentation equilibrium experiments use a rotational frequency at which gravitation and diffusion compensate each other. At this steady-state, the analyte's time-independent concentration profile is Gauss-distributed and correlates to the angular velocity. This directly reports on the molar mass of any species independently of shape or hydrodynamic radius.

Sedimentation velocity samples contained 79 μM of F08H9.4, 79 μM of Sip1, 70 μM of Sip1 H111/139N, 87 μM of Sip1-CRYAB chimaera, 225 μM of Sip1-ACD, or 58 μM hCRYAB ($\text{OD}_{280\text{ nm}, 1\text{ cm}} = 0.8$) in standard buffer at pH 5.8, 6.3, 7.5, or 8.2. Additionally, 225 μM of Sip1-ACD were assayed in the crystallization buffers at pH 6.9 or 10. The samples were analyzed in an Optima XL-A centrifuge (Beckman Coulter). Sedimentation was carried out at 42,000 rpm and 20°C, and detected with interference optics at 645 nm or absorbance at 280 nm in the continuous scanning mode. Data were analyzed with Sedfit v. 12.1 [295], using a non-model based continuous Svedberg distribution method ($c(s)$).

In order to monitor the oligomer stability in the presence of a denaturant, 79 μM of Sip1 were incubated in standard buffer at pH 7.5 containing 50 and 100 μM of GdmCl, and examined by sedimentation equilibrium AUC. All experiments were conducted in cooperation with Dr. Maike Krause.

6.2.6 *IN VITRO* PROTEIN ANALYSES

6.2.6.1 UV/VIS-SPECTROSCOPIC ANALYSES

Concentration of proteins as well as nucleic acids was determined via UV/Vis spectroscopy at 230 nm (the wavelength at which the peptide bonds of the protein backbone absorb light) and 280 nm (detecting Trp, Tyr and Phe), or 260 nm, respectively. The extinction coefficients listed in Table 6.4 were used in the Beer-Lambert law (Eq. 6.1) for calculating protein concentrations:

$$A = \epsilon \cdot c \cdot d \quad (6.1)$$

A: absorption at 280 nm [AU], ϵ : molar extinction coefficient at 280 nm [$\text{M}^{-1}\text{cm}^{-1}$], c: protein concentration [M], d: pathlength of the cuvette [cm]

In the case of low extinction coefficients (Sip1-ACD, Sip1-CRYAB chimaera and F08H9.4), protein concentration was estimated by comparison to a BSA standard curve, in a Bradford assay.

Table 6.4: Extinction coefficients.

Protein	ϵ [$M^{-1}cm^{-1}$] (ProtParam)
Sip1	8480
Sip1-ACD	0
Sip1-CRYAB Chimaera	0
Sip1 H111/139N	8480
Hsp16.1	4470
Hsp16.2	4470
Hsp16.41	9970
Hsp16.48	8480
F08H9.3	2980
F08H9.4	0
Citrate synthase	75770
Malate dehydrogenase	7450
hCRYAB	13980

6.2.6.2 CIRCULAR DICHROISM ANALYSES OF SECONDARY STRUCTURES

Chiral molecules such as the L-amino acids (except Gly) are optically active. One such enantiomer absorbs left- and right circularly polarized light by varying degrees. The difference in the two extinction coefficients at any given wavelength gives the ellipticity. The asymmetric chemical environment created by a folded protein

imparts a strong circular dichroism (CD) even on mostly achiral aromatic rings like those of Tyr. Thus, the sum of all distinct secondary structure elements elicits a CD spectrum which is characteristic for the protein and allows for an estimation of relative α -helix, β -sheet, and random coil content. For instance, β -sheets display a minimum at 218 nm. Far-UV-CD spectroscopy (scanning from 190 to 260 nm) was used to verify the correct fold of newly purified Hsp16 proteins, to compare their secondary structure and to assess conformational changes as a function of temperature or concentration of denaturants.

Far-UV-CD spectra of F08H9.3, F08H9.4, as well as Sip1 and its mutants at different pH values or in the presence of increasing concentrations of GdmCl were measured on a J-710 spectropolarimeter. 10 μ M of protein were analyzed in stoppered quartz cuvettes with 1 mm pathlength at the following settings: 20 $^{\circ}$ C, scan speed = 20 nm/min, band width = 1 nm, data pitch = 0.1 s, response time = 4 s, with 16 accumulations. The heat-stability of Sip1 secondary structure was examined by heating from 10 $^{\circ}$ C to 90 $^{\circ}$ C and back, at a heating rate of 10 $^{\circ}$ C/h and λ = 218 nm (209 nm for F08H9.4). For determination of its stability towards chemical denaturants, Sip1 was incubated overnight in standard buffer containing different concentrations of the chaotropic agent guanidinium chloride (GdmCl) to allow for equilibrium formation. GdmCl concentration

was verified by refraction measurements, using the [GdmCl] Calculator tool. Per sample, the mean of the CD signal measured at 218 nm for 60 s was recorded.

After buffer correction, the measured “machine units” ellipticity θ [mdeg] were converted into per residue molar absorption units (Eq. 6.2). This protein length-independent mean residual weight ellipticity, θ_{MRW} , is historically expressed in units of [deg·cm²/dmol]:

$$\theta_{MRW} = \frac{\theta}{10 \cdot c \cdot d \cdot N_{aa}} \quad (6.2)$$

c: protein concentration [M], d: cuvette pathlength [cm], N_{aa} : number of amino acids

All spectra were buffer-corrected. If possible, the transitions were fitted with a Boltzmann function using Origin. Thermotransition data were normalized by setting the signal of the folded protein to 1.

6.2.6.3 CHAPERONE ACTIVITY ASSAYS

In order to compare the chaperone activity of the CeHsp16s with sHsps available at the Institute, two stress-labile model substrates were assayed as described previously [37, 252].

CS (500 nM) or MDH (1 μ M) were mixed with one sHsp (yeast Hsp26, wheat Hsp16.9, human α B-crystallin and HspB1, CeHsp16.1, Hsp16.2, Hsp16.41, Hsp16.48, F08H9.3, F08H9.4, or Sip1) at different molar ratios in quartz cuvettes (Hellma QS 10 mm pathlength). In order to facilitate aggregation of CS and MDH at 43 °C, the ionic strength of the standard assay buffer was reduced from 150 mM to 25 mM by addition of 17 mM KCl, but otherwise left unchanged (“aggregation buffer”). The pH ranged between pH 5.8 and 8.2. Aggregation caused progressive turbidity, which was measured at 360 nm in a Cary50 spectrophotometer. CS that had been denatured in 6.0 M GdmCl and 100 mM TRIS/HCl, pH 8.0 was rapidly diluted into aggregation buffer to a final concentration of 500 nM CS and 60 μ M GdmCl at 20 °C, in the presence or absence of a sHsp. This instantaneous loss of chaotropic agent resulted in fast aggregation of the unfolded CS. Each experiment was at least performed twice, in most cases three times. The mean saturation region of the substrate-only control curve was normalized to 100 AU.

6.2.6.4 HOLDASE FUNCTION OF SIP1

To ascertain whether Sip1 could keep its substrate soluble, 10 µg of CS or MDH were incubated for 1 h at 43 °C in the presence or absence of the sHsp. The substrate-to-sHsp ratio reflected the conditions that had conveyed half-maximum or complete aggregation suppression in the chaperone assay: 12:1 and 4:1 [MDH:Sip1] at pH 5.8; and 1:2.5 and 1:6 [CS:Sip1] at pH 6.3, in aggregation buffer. Aggregates were precipitated at 20,800 g for 10 min, and the repeatedly washed sediment fraction was contrasted to the supernatant by SDS-PAGE. 10 µg of CS or MDH were loaded as controls.

6.2.6.5 INTERACTION OF SIP1 AND THE HSP70/40 SYSTEM

Cooperation between holdases and foldases can be assessed as previously described [37, 84]. 2 µM of MDH were heat-stressed at 43 °C for 45 min in the absence or presence of 0.5 µM Sip1, in 60 µL of standard buffer containing 5 mM MgCl₂ at pH 6.3 (“refolding buffer”). Afterwards, the samples were kept on ice. Refolding of the still soluble MDH fraction by the Hsp70/40 chaperone machinery was started by mixing with 60 µL of refolding buffer containing 2 µM Hsc70, 0.5 µM Dnj13, and 0.25 µM Bag1, as well as 20 µg/ml pyruvate kinase, 3 mM phosphoenol pyruvate, and 5 mM ATP.

MDH reversibly catalyzes the reduction of oxaloacetate to L-malate by oxidizing NADH to NAD⁺. Thus, the enzymatic activity that had been regained after a certain duration could be measured by adding 10 µl of the refolding mix to 190 µl of 0.5 mM oxaloacetate and 0.2 mM NADH in HKM buffer (20 mM HEPES/KOH pH 7.4, 125 mM KAc, 5 mM MgAc₂, 1 mM DTT). The increasing consumption of NADH was detected at 340 nm for 15 min for each time point. As controls, key factors (HS, Hsp70/40/NEF, Sip1) were omitted in certain experiments.

6.2.7 CO-IMMUNOPRECIPITATION

Possible *in vivo*-substrates of Sip1 and Hsp16.2 were identified by co-immunoprecipitation (Co-IP) from nematodes lysates. For this, *sip1* (tm3624) animals were grown to high densities in S-medium, harvested and cleaned (as detailed in “*C. elegans* handling”) for an asynchronous aliquot. Embryos were obtained by disruption of

larvae and adults by NaOH treatment, removal of worm debris and concentration of eggs by gentle centrifugation through 30% sucrose. The resulting worm preparations were checked microscopically for purity. The pellets were suspended in an equal volume of IP buffer 1: 15 mM MES, 15 mM MOPS, 150 mM NaCl, 1% Nonidet P40 (NP40), 0.5% Na deoxycholate, 0.7 µg/ml pepstatin, protease inhibitor mix G, at pH 6.3 or 7.5. They were then frozen in liquid N₂ and stored until lysis at -80 °C. For quick lysis, the thawed nematodes were ground by 40 strokes in a chilled glass mortar, then transferred to an 1.5 mL Eppendorf tube and again frozen in liquid N₂. The barely thawed pellet was then broken up in a bead mill at 30 Hz for a total of 3 min, with pauses to prevent overheating. After centrifugation (10 min at 20,800 g), the supernatant was transferred to a fresh tube and the last traces of cell debris were removed by spinning. In order to subduct unspecifically binding lysate components, the supernatant (440-480 µl of ≤18 mg/ml protein for ~0.5 g wet weight of worms) was then pre-incubated with 50 µl of protein G-sepharose (GE Healthcare), by rocking for 4 h at 5 °C. To facilitate sHsp binding of lysate proteins at physiological or heat shock temperatures, 50 – 75 µl (~ 1 mg) of the pre-cleared lysate were incubated with 10 µg of Sip1 or Hsp16.2, or pure buffer for controls, shaking for 45 min at 15 °C or 37 °C. 10 µl of the corresponding α-sHsp antibody were added and all samples were rocked for 1 h at 5 °C, and then overnight with 50 µl of protein G-sepharose. The supernatant was discarded, and the gently pelleted sepharose was extensively washed by rocking for 5x 20 min at 5 °C, following Roche's protein G-agarose IP manual: twice with 1 ml IP buffer 1; twice with high salt buffer (15 mM MES, 15 mM MOPS, 500 mM NaCl, 0.1% NP40, 0.05% Na deoxycholate); once with low salt buffer (15 mM MES, 15 mM MOPS, 0.1% NP40, 0.05 Na deoxycholate, each at pH 6.3 or 7.5. The wash supernatant was removed completely. The sepharose-coupled protein complexes were dissociated by boiling for 5 min in 25 µl of Laemmli sample buffer and separated by SDS-PAGE. The Coomassie-stained gel lanes were cut into six parts, and individually prepared for liquid chromatography-mass spectrometry (LC-MS) by M. Daake.

In detail, the proteins in the gel slices were reduced, alkylated and digested over night with trypsin. The resulting peptides were extracted by sequentially adding 50 µl of 0.1 % formic acid in water, ACN, 0.1% formic acid, ACN, and again ACN. The collected supernatants of these five steps were combined, concentrated in a speed vac to approximately 20 µl end volume and filtered through a 0.22 µm centrifuge filter.

Peptides were loaded onto an Acclaim PepMap RSLC C18 trap column with 5 μ l/min and separated on a PepMap RSLC C18 column at a flow rate of 0.2 μ l/min. A linear gradient from 5 % to 35 % of acetonitrile containing 0.1 % formic acid eluted the peptides in 60 min to a LTQ Orbitrap XL. Full scans and 5 dependent MS2 scans (5 CID or 3 CID and 2 HCD spectra) were recorded in each cycle. The mass spectrometry data derived from the gel slices was searched against a *C. elegans* database downloaded from NCBI using the SEQUEST algorithm implemented into the Proteome Discoverer software. The search was limited to tryptic peptides containing a maximum of two missed cleavage sites, monoisotopic precursor ions, and a peptide tolerance of 10 ppm for precursors and 0.8 Da for fragment masses. Proteins were identified with two distinct peptides with a target false discovery rate for peptides below 1 % according to the decoy search.

Hits from at least two biological replicates were contrasted to the list of proteins that had been pulled down in the sHsp-free controls. These were reasoned to bind unspecifically to the sepharose matrix and thus were subtracted from the respective sHsp-containing probes. The candidate substrates were classified using the PANTHER GO database. The PANTHER binomial statistics overrepresentation analysis (ORA) tool was employed to find the protein classes that were enriched in the sHsp CoIP lists compared to the *C. elegans* proteome.

Two strong candidates for Sip1 chaperoning were to be re-tested for Sip1 binding by repeating the CoIP in the opposite direction. The fraction of endemic Sip1 in heat-stressed, asynchronous N2 lysates that was bound to Vit6 or Vig1 was pulled down at pH 6.3 and 7.5 using α -Vit6 (YP88 and YP115) or α -Vig1 antibody, as detailed above. Instead of MS analysis, the SDS-PA gels were blotted and developed against Sip1, Vit6 and Vig1 as described in 6.2.9. Controls contained all CoIP components except primary antibody and were performed three times.

6.2.8 *C. ELEGANS* HANDLING

C. elegans were maintained according to standard protocols [153, 157], at 20 °C on nematode growth medium- (NGM) plates or in liquid culture in agitated S-medium with OP50 *E. coli* as food source. Propagation, harvesting and synchronization of large worm populations by NaOH/hypochlorite treatment were performed employing the Stiernagle methods from wormbook [288, 296]. If only some animals were required, worms were

age-synchronized by timed egg-laying, i.e. individual nematodes were removed from a fresh NGM plate after having laid sufficient eggs, usually after 3 hours. Contaminating bacteria and dead worms were removed by repeated centrifugation in cold M9 buffer and through a sucrose gradient (flotation on cold 30% sucrose [296]). Correct staging and purity of *C. elegans* were confirmed by light microscopy, on a Zeiss Stemi SV 11 binocular.

C. elegans were maintained on NGM (nematode growth medium) agar plates carrying a lawn of *Escherichia coli* OP50, an uracil auxotroph strain with limited growth on NGM plates that is routinely used for feeding nematodes [153], using standard handling techniques [288].

6.2.9 SDS-PAGE AND WESTERN BLOTS

To confirm the reported Sip1 and Hsp16 expression patterns, 30 synchronized *C. elegans* at day 1 of adulthood were cleaned of bacteria by briefly placing them in a drop of S-medium buffer, then collected into 15 μ l of S-medium and were either heat-shocked at 35 °C for 15, 30 or 45 min, or frozen directly in liquid N₂. Worms were then lysed by boiling at 95 °C for 5 min in Laemmli sample buffer. The total protein content of all samples was determined by Bradford assay (Serva), according to the supplier's instructions, and by comparison with a bovine serum albumin control. Equal amounts of lysates and purified sHsps serving as calibration controls were separated by SDS-PAGE (~40 min at 35 mA for a 12.5 % gel). Proteins were semi-dry blotted onto a nitrocellulose membrane in transfer buffer (90 min at 72 mA). The transfer efficiency was monitored by migration of the molecular weight marker and Ponceau Red-staining of the membrane. After blocking for 1 h in PBS-T containing 5 % (w/v) of milk powder, the Western Blot was incubated for at least 1 h with the primary antibody (all 1:2,000 – 1:5,000 dilution), such as a monoclonal α -tubulin antibody (from mouse, Sigma-Aldrich), polyclonal rat α -CeVit6 (α -YP88 and α -YP115), or rabbit α -CeVig1 (cf. [Acknowledgements](#)). Polyclonal antibodies against purified Sip1 and Hsp16.41 had been produced in rabbit by Dr. Pineda Antibody Service, Berlin. The former readily detected 10 ng of the recombinant protein at high dilution (1:5,000), while α -Hsp16.41 crossreacted with all core Hsp16 proteins. It also bound to Sip1 to some degree, but this can be distinguished from the other Hsp16s because of the Sip1 band's higher molecular weight. Following extensive washing steps,

the membrane was rocked for 1 h in milk-PBST with the appropriate secondary antibody at 1:10,000: horseradish peroxidase-conjugated goat α -rabbit/ α -mouse/ α -rat IgG, all from Sigma-Aldrich. After repeated washing, antibody binding was visualized by enhanced chemiluminescence detection on an ImageQuant LA S 4000. Bands were quantified with ImageJ.

6.2.10 FLUORESCENT REPORTER INJECTION

For a transcriptional reporter, the genomic sequence 500 and 1000 bp upstream of the *sip1* gene was fused to the sequence encoding enhanced yellow-fluorescing protein (eYFP). Likewise, translational *sip1 promoter::sip1-eYFP* vectors were generated [293]. The plasmids were mixed 1:1 (50 - 75 μ g/ml each) with the injection marker *pmyo-2::cfp*, which causes CFP expression in the pharynx. ScaI- and PvuII blunt-end cut *E. coli* DNA was at times added to increase the total DNA concentration to 100 - 150 μ g/ml. Adult hermaphrodites were fixed on agar-covered glass slides, and the DNA was microinjected into their gonads using glass capillaries in a needle holder of a Zeiss Axiovert200 fluorescence microscope, as described on wormbook [255]. Fluorescent worms were identified and images taken using a Leica MZ 16 FA fluorescence microscope.

6.2.11 LIFE SPAN ASSAY

At the L4 moult ($t = 0$), at least 25 synchronized N2 and *sip1*-deleted animals were transferred to each of three NGM plates containing ampicillin (100 mg/l) and 5'-fluoro-2'-deoxyuridine (FUDR, 5 mg/l). The thymidylate synthase inhibitor FUDR inhibits progeny development and thus, hatching of eggs without significantly influencing life span (as observed also by other groups [215, 297, 298]). A minimum of 77 adult nematodes per strain were available for analysis. All worms were transferred to fresh plates on the same day, before bacteria became depleted (usually every 7 days). By signs of pharyngeal pumping, movement in water droplets, and touch sensitivity, their survival was scored every 1 - 2 days. Life span at 20 °C was counted from L4 stage. Worms that crawled off the plate and were found dehydrated on the plastic wall were censored. As such events were equally likely to happen in both strains, and occurred rarely and only within the first 10 days of the experiment, censored worms were not included in the data set.

6.2.12 *C. ELEGANS* THERMOTOLERANCE ASSAY

Synchronized control (N2) and *Δsip1* (tm3624) young adult nematodes were heat-shocked in a water bath on shrink-wrapped, OP50-seeded NGM agar plates that were equal in agar height and weight, to ensure rapid and homogenous heating of the agar pads. The plates were incubated for 1 h at 37 °C, followed by 1 h at 20 °C, and 30 min at 37 °C again (i.e., a hormetic approach). Surviving adult worms were counted after one day, as described in 6.2.11, and the number of their viable progeny was determined 4 days after the heat shock. Counted F1 worms were removed from the plate before they became L3 larvae, to avoid their growing to adulthood and intermixing with their heat-stressed parents. A total of 66 N2 and 67 tm3624 nematodes were analyzed.

6.2.13 *E. COLI* THERMOTOLERANCE ASSAYS

E. coli BL21 DE3 cells were transfected with empty pET21+a vector or plasmid encoding *sip1*, *hsp16.1*, or any of the other *hsp16* genes. They were grown at 28 °C to OD = 0.4 – 0.5, induced and diluted to OD = 0.06 into 50 mL of LB_{amp, IPTG} medium that had been pre-heated to 50 °C. After 15 - 120 min of shaking at 50 °C, the flasks were returned to 28 °C and OD was measured at the indicated time points. For cold shock, likewise prepared bacteria were shaken at 5 °C for four days. After each day, the OD was measured immediately and during recovery at 28 °C. The resumed growth was also measured each day by plating in duplicate a dilution series onto LB_{amp, IPTG} plates: 1:20; 1:400; 1:8,000; and 1:16,000; starting from OD = 0.4. The colonies that had formed over night at 28 °C were counted.

7. ACKNOWLEDGMENTS

The present thesis was largely funded by grants from the Deutsche Forschungsgemeinschaft (SFB 1035 A06) and CIPSM to Prof. Dr. J. Buchner. I was the recipient of two stipends: "Chancengleichheit für Frauen in Forschung und Lehre", a Women Researchers' scholarship by the Technische Universität München, and the Bavarian Elite Advancement Stipend by Universität Bayern e.V. and Elitenetzwerk Bayern.

I thank S. Mitani of the Ntl. Bioresource Project for *C. elegans* (Women's Medical University, Tokyo) and the *Caenorhabditis* Genetic Center, U. Minnesota, for providing the nematode strains. The pHluorin vector was used by courtesy of G. Missenböck and K. Nehrke. The α -tubulin antibody was a gift from P. v. Oosten-Hawle, NU Evanstone, α -Vitellogenin antibodies were kindly provided by S. Strome, UCSC, and T. Blumenthal, CU Boulder, and the α -Vig1 antibody was sent by G. Hannon, CSHL. I also acknowledge K. Richter and K. Papsdorf for CeHsp70/40/NEF proteins.

I am very grateful to Prof. Michael Groll, Prof. Sevil Weinkauff, Dr. Andreas Kastenmüller and Dr. Carsten Peters for their excellent cooperation regarding the structural studies and their invaluable contributions to the publication. I would like to thank members of the Chair for Biotechnology, especially Dr. Maike Krause for her AUC expertise, Marina Daake and Helmut Krause for the preparation and analysis of MS samples, Margot Rubinstein and my supervisors Dr. Martin Haslbeck and Prof. Johannes Buchner, who originally conceived the project, for their continued support. My deep gratitude goes to my loving, supportive family, the Stein family, and the wonderful, talented Dr. Martin Stein for providing both insight and diversion.

8. PUBLICATION

The majority of the results from this Thesis will be published in *The development-specific small heat shock protein Sip1 is a pH-regulated molecular chaperone* (working title) by Tilly Fleckenstein, Andreas Kastenmüller, Martin Lorenz Stein, Carsten Peters, Marina Daake, Maike Krause, Daniel Weinfurtner, Martin Haslbeck, Sevil Weinkauf, Michael Groll, and Johannes Buchner.

9. REFERENCES

1. *Life expectancy variation over time*, http://en.wikipedia.org/wiki/Life_expectancy, Editor 2014.
2. CIA *Life expectancy at birth*. The World Factbook, 2014.
3. WHO *Life expectancy*. 2014.
4. Köhler, H. *Rede des Bundespräsidenten auf dem 8. Seniorentag*. 2006. Cologne.
5. Jopp, D.S., et al. *Zweite Heidelberger Hundertjährigen-Studie*. 2013.
6. Kenyon, C., *The genetics of ageing*. Nature, 2010. **464**(7288): p. 504-12.
7. Sun, Y. and T. MacRae, *The small heat-shock proteins and their role in human diseases*. FEBS J., 2005. **272**.
8. Nations, U., *Population distribution according to age scales*. <http://esa.un.org/unpp>, 2009.
9. Anfinsen, C.B., et al., *The kinetics of formation of native ribonuclease during oxidation of the reduced polypeptide chain*. Proc Natl Acad Sci USA, 1961. **15**(47): p. 1309-14.
10. Jaenicke, R., *Protein self-organization in vitro and in vivo: partitioning between physical biochemistry and cell biology*. Biol. Chem., 1998. **379**(3): p. 237-43.
11. Wetlaufer, D.B., *Nucleation, rapid folding, and globular intrachain regions in proteins*. Proc. Natl. Acad. Sci. USA, 1973. **70**(3): p. 697-701.
12. Morris, E.R. and M.S. Searle, *Overview of protein folding mechanisms: experimental and theoretical approaches to probing energy landscapes*, in *Curr. Protoc. Protein Sci.* 2012.
13. Tanford, C., et al., *Effect of ethylene glycol on the conformation of gamma-globulin and beta-lactoglobulin*. J Biol Chem, 1962. **237**: p. 1168-71.
14. E. A. Craig, H. C. Eisenman, and H.A. Hundley, *Ribosome-tethered molecular chaperones: the first line of defense against protein misfolding?* Curr Opin Microbiol, 2003. **6**(2): p. 157-62.
15. Hartl, F.U., A. Bracher, and M. Hayer-Hartl, *Molecular chaperones in protein folding and proteostasis*. Nature, 2011. **475**(7356): p. 324-332.
16. Kiefhaber, T., et al., *Protein aggregation in vitro and in vivo: a quantitative model of the kinetic competition between folding and aggregation*. Biotechnology (N Y), 1991. **9**(9): p. 825-9.
17. U. Schubert, et al., *Rapid degradation of a large fraction of newly synthesized proteins by proteasomes*. Nature, 2000. **404**(6779): p. 770-4.
18. Richter, K., M. Haslbeck, and J. Buchner, *The heat shock response: life on the verge of death*. Mol. Cell, 2010. **40**: p. 253-266.
19. R. Seckler and R. Jaenicke, *Protein folding and protein refolding*. FASEB J, 1992. **6**(8): p. 2545-52.
20. van Oosten-Hawle, P. and R.I. Morimoto, *Organismal proteostasis: role of cell-nonautonomous regulation and transcellular chaperone signaling*. Genes Dev., 2014. **28**(14): p. 1533-43.
21. S. Walter and J. Buchner, *Molecular chaperones-cellular machines for protein folding*. Angew Chem Int Ed Engl, 2002. **41**(7): p. 1098-113.
22. Buchner, J., *Supervising the fold: functional principles of molecular chaperones*. FASEB J, 1996. **10**(1): p. 10-19.
23. A. Mogk and B. Bukau, *Molecular chaperones: structure of a protein disaggregase*. Curr Biol, 2004. **14**(2): p. R78-80.
24. Jakob, U., et al., *Small heat-shock proteins are molecular chaperones*. J. Biol. Chem., 1993. **268**: p. 1517-1520.
25. Haslbeck, M., et al., *Some like it hot: the structure and function of small heat-shock proteins*. Nat. Struct. Mol. Biol., 2005. **12**(10).
26. Welch, W.J., *The mammalian heat shock (or stress) response: a cellular defense mechanism*. Adv. Exp. Med. Biol., 1987. **225**(287-304).

-
27. DiDomenico, B.J., G.E. Bugaisky, and S. Lindquist, *The heat shock response is self-regulated at both the transcriptional and posttranscriptional levels*. *Cell*, 1982. **31**(3): p. 593-603.
 28. Hightower, L.E. and L.M. Hendershot, *Molecular chaperones and the heat shock response at Cold Spring Harbor*. *Cell Stress Chaperones*, 1997. **2**(1): p. 1-11.
 29. Lindquist, S., *The heat-shock response*. *Annu Rev Biochem*, 1986. **55**: p. 1151-91.
 30. Velichko, A.K., et al., *Mechanisms of heat shock response in mammals*. *Cell. Mol. Life Sci.*, 2013. **70**(22): p. 4229-41.
 31. Welch, W.J. and J.P. Suhan, *Morphological study of the mammalian stress response: characterization of changes in cytoplasmic organelles, cytoskeleton, and nucleoli, and appearance of intranuclear actin filaments in rat fibroblasts after heat-shock treatment*. *J. Cell. Biol.*, 1985. **101**: p. 1198-1211.
 32. Kühn, N.M. and L. Rensing, *Heat shock effects on cell cycle progression*. *Cell Mol Life Sci*, 2000. **57**(3): p. 450-63.
 33. F. U. Hartl and M. Hayer-Hartl, *Molecular chaperones in the cytosol: from nascent chain to folded protein*. *Science*, 2002. **295**(5561): p. 1852-8.
 34. Herbst, R., U. Schafer, and R. Seckler, *Equilibrium intermediates in the reversible unfolding of firefly (*Photinus pyralis*) luciferase*. *J. Biol. Chem.*, 1997. **272**: p. 7099-7105.
 35. Kriehuber, T., et al., *Independent evolution of the core domain and its flanking sequences in small heat shock proteins*. *FASEB Journal* 2010. **24**.
 36. Georgopoulos, C. and W.J. Welch, *Role of the major heat shock proteins as molecular chaperones*. *Annu Rev Cell Biol*, 1993. **9**: p. 601-34.
 37. Haslbeck, M., et al., *Disassembling protein aggregates in the yeast cytosol: The cooperation of Hsp26 with Ssa1 and Hsp104*. *J. Biol. Chem.*, 2005. **280**(25): p. 23861-8.
 38. Liberek, K., A. Lewandowska, and S. Zietkiewicz, *Chaperones in control of protein disaggregation*. *EMBO J.*, 2008. **27**: p. 328-335.
 39. Smith, D.F. and D.O. Toft, *Steroid receptors and their associated proteins*. *Mol Endocrinol*, 1993. **7**(1): p. 4-11.
 40. A. Brychzy, et al., *Cofactor tpr2 combines two tpr domains and a j domain to regulate the hsp70/hsp90 chaperone system*. *EMBO J*, 2003. **22**(14): p. 3613-23.
 41. Buchner, J., *Hsp90 & co. - a holding for folding*. *Trends Biochem Sci*, 1999. **24**(4): p. 136-41.
 42. Catelli, M.G., et al., *The common 90-kd protein component of non-transformed '8S' steroid receptors is a heat-shock protein*. *EMBO J*, 1985. **4**(12): p. 3131-5.
 43. Pratt, W.B. and Y. Morishima, *Chaperoning of glucocorticoid receptors*. *Handb. Exp. Pharmacol.*, 2006. **172**(111-138).
 44. Zou, J., et al., *Repression of heat shock transcription factor HSF1 activation by HSP90 (HSP90 complex) that forms a stress-sensitive complex with HSF1*. *Cell*, 1998. **94**(4): p. 471-80.
 45. Martin, J. and F.U. Hartl, *Chaperone-assisted protein folding*. *Curr. Opin. Struct. Biol.*, 1997. **7**(1): p. 41-52.
 46. Hartl, F.U. and M. Hayer-Hartl, *Molecular chaperones in the cytosol: from nascent chain to folded protein*. *Science*, 2002. **295**(5561): p. 1852-8.
 47. Bukau, B., T. Hesterkamp, and J. Lührink, *Growing up in a dangerous environment: a network of multiple targeting and folding pathways for nascent polypeptides in the cytosol*. *Trends Cell Biol.*, 1996. **6**: p. 480-486.
 48. Mayer, M.P. and B. Bukau, *Hsp70 chaperones: cellular functions and molecular mechanism*. *Cell. Mol. Life Sci.*, 2005. **62**: p. 670-684.
 49. S. L. Schmid, W. A. Braell, and J.E. Rothman, *Atp catalyzes the sequestration of clathrin during enzymatic uncoating*. *J Biol Chem*, 1985. **260**(18): p. 10057-62.
 50. J. Song, M. Takeda, and R.I. Morimoto, *Bag1-hsp70 mediates a physiological stress signalling pathway that regulates raf-1/erk and cell growth*. *Nat Cell Biol*, 2001. **3**(3): p. 276-82.
 51. S. Wickner, J. Hoskins, and K. McKenney, *Function of dnaj and dnak as chaperones in origin-specific DNA binding by repa*. *Nature*, 1991. **350**(6314): p. 165-7.

-
52. Abravaya, K., M.P. Myers, and e. al., *The human heat shock protein hsp70 interacts with hsf, the transcription factor that regulates heat shock gene expression*. Genes Dev, 1992. **6**(7): p. 1153-64.
 53. Hupp, T.R., et al., *Regulation of the specific DNA binding function of p53*. Cell, 1992. **71**(5): p. 875-886.
 54. J. R. Glover and S. Lindquist, *Hsp104, hsp70, and hsp40: a novel chaperone system that rescues previously aggregated proteins*. Cell, 1998. **94**(1): p. 73-82.
 55. Haslbeck, M., et al., *Disassembling protein aggregates in the yeast cytosol. The cooperation of Hsp26 with Ssa1 and Hsp104*. J. Biol. Chem., 2005. **280**: p. 23861-23868.
 56. D. A. Parsell, et al., *Protein disaggregation mediated by heat-shock protein hsp104*. Nature, 1994. **372**(6505): p. 475-8.
 57. Rampelt, H., et al., *Metazoan Hsp70 machines use Hsp110 to power protein disaggregation*. EMBO J., 2012. **31**(21): p. 4221-35.
 58. Odunuga, O.O., et al., *Molecular characterization of C. elegans Hsp70-1 and the effects of polyhistidine tagging on purification yield and ATPase activity*. FASEB J., 2012. **26**(963.11).
 59. Narberhaus, F., *α -crystallin-type heat-shock proteins: socializing minichaperones in the context of a multichaperone network*. Microbiol. Mol. Biol. Rev., 2002. **66**(64-93).
 60. Stromer, T., et al., *Analysis of the interaction of small heat shock proteins with unfolding proteins*. J. Biol. Chem., 2003. **278**(20): p. 18015-21.
 61. Mchaourab, H., J. Godar, and P. Stewart, *Structure and mechanism of protein stability sensors: chaperone activity of small heat shock proteins*. Biochemistry, 2009. **48**: p. 3828-3837.
 62. Cheng, G., et al., *Insights into small heat shock protein and substrate structure during chaperone action derived from hydrogen/deuterium exchange and mass spectrometry*. J. Biol. Chem., 2008. **283**(39): p. 26634-42.
 63. Haslbeck, M. and J. Buchner, *Chaperone function of sHsps*. Prog. Mol. Subcell. Biol., 2002. **28**: p. 37-59.
 64. Lee, G.J. and E. Vierling, *A small heat-shock protein cooperates with heat shock protein 70 systems to reactivate a heat-denatured protein*. Plant Physiol., 2000. **122**: p. 189-198.
 65. Ehrnsperger, M., et al., *Binding of non-native protein to Hsp25 during heat shock creates a reservoir of folding intermediates for reactivation*. EMBO J., 1997. **16**(2): p. 221-9.
 66. Veigner, L., L. Diamant, and J. Buchner, *The small heat-shock protein IbpB from Escherichia coli stabilizes stress-denatured proteins for subsequent refolding by a multichaperone network*. J. Biol. Chem., 1998. **273**: p. 11032-11037.
 67. Lindner, B., A. Kapur, and M. Mariani, *Structural alterations of α -crystallin during its chaperone action*. Eur. J. Biochem., 1998. **258**: p. 170-183.
 68. Ehrnsperger, M., J. Buchner, and M. Gaestel, *Structure and Function of Small Heat-Shock Proteins*, ed. A.L. Fink and Y. Goto. 1998, New York: Marcel Dekker, Inc.
 69. Haslbeck, M., et al., *Hsp42 is the general small heat shock protein in the cytosol of Saccharomyces cerevisiae*. EMBO J., 2004. **23**(3): p. 638-649.
 70. Basha, E., et al., *The identity of proteins associated with a small heat shock protein during heat stress in vivo indicates that these chaperones protect a wide range of cellular functions*. J. Biol. Chem., 2004. **279**(9): p. 7566-75.
 71. Allen, S.P., et al., *Two novel heat shock genes encoding proteins produced in response to heterologous protein expression in Escherichia coli*. J Bacteriol, 1992. **174**(21): p. 6938-47.
 72. Bepperling, A., et al., *Alternative bacterial two-component small heat shock protein systems*. Proc. Natl. Acad. Sci. USA, 2012. **109**(50): p. 20407-12
 73. Haslbeck, M., et al., *A domain in the N-terminal part of Hsp26 is essential for chaperone function and oligomerization*. J. Mol. Biol., 2004. **343**(2): p. 445-55.
 74. Haslbeck, M., et al., *Hsp26: a temperature-regulated chaperone*. EMBO J., 1999. **18**(23): p. 6744-51.
 75. Lee, G.J., et al., *A small heat shock protein stably binds heat-denatured model substrates and can maintain a substrate in a folding-competent state*. EMBO J., 1997. **16**(3): p. 659-71.

-
76. Matuszewska, M., et al., *The small heat shock protein IbpA of Escherichia coli cooperates with IbpB in stabilization of thermally aggregated proteins in a disaggregation competent state*. J. Biol. Chem, 2005. **280**: p. 12292-12298.
77. Laskowska, E., A. Wawrzynów, and A. Taylor, *IbpA and IbpB, the new heat-shock proteins, bind to endogenous Escherichia coli proteins aggregated intracellularly by heat shock*. Biochimie, 1996. **78**(2): p. 117-22.
78. Jiao, W., et al., *Small heat-shock proteins function in the insoluble protein complex*. Biochem. Biophys. Res. Commun., 2005. **335**(1): p. 227-31.
79. Hamouda, M.A., et al., *The small heat shock protein B8 (HSPB8) confers resistance to bortezomib by promoting autophagic removal of misfolded proteins in multiple myeloma cells*. Oncotarget, 2014. **5**(15): p. 6252-66.
80. Caspers, G.J., A.M. Leunissen, and W.W. de Jong, *The expanding small heat shock protein family, and structure predictions of the conserved 'α-crystallin domain'*. J. Mol. Chem., 1995. **271**: p. 238-248.
81. de Jong, W.W., G.J. Caspers, and J.A. Leunissen, *Genealogy of the α-crystallin small heat-shock protein superfamily*. Int. J. Biol. Macromol., 1998. **22**(3): p. 151-162.
82. Kappé, G., W. Boelens, and W. de Jong, *Why proteins without an alpha-crystallin domain should not be included in the human small heat shock protein family HSPB*. Cell Stress Chaperones, 2010. **15**(4): p. 457-61.
83. Candido, E.P., *The small heat shock proteins of the nematode Caenorhabditis elegans: Structure, Regulation and Biology*, in *Small Stress Proteins*, A.P. Arrigo and W.E. Müller, Editors. 2002, Springer: Berlin.
84. Peschek, J., et al., *Regulated structural transitions unleash the chaperone activity of αB-crystallin*. Proc. Natl. Acad. Sci. USA, 2013. **110**(40): p. 3780-9.
85. Chernik, I.S., et al., *pH-induced changes of the structure of small heat shock proteins with molecular mass 24/27kDa (HspB1)*. Biochem Biophys Res Commun, 2004. **324**(4): p. 1199-203.
86. Kim, K.K., R. Kim, and S.H. Kim, *Crystal structure of a small heat-shock protein*. Nature, 1998. **394**: p. 595-599.
87. Van Montfort, R.L., et al., *Crystal structure and assembly of an eukaryotic small heat-shock protein*. Nat. Struct. Biol., 2001. **8**: p. 1025-1030.
88. Bagnéris, C., et al., *Crystal structures of alpha-crystallin domain dimers of alphaB-crystallin and Hsp20*. J. Mol. Biol., 2009. **392**: p. 1242-1252.
89. Hanazono, Y., et al., *Structural studies on the oligomeric transition of a small heat shock protein, StHsp14.0*. J. Mol. Biol., 2012. **422**(1): p. 100-8.
90. Hanazono, Y., et al., *Nonequivalence observed for the 16-meric structure of a small heat shock protein, SpHsp16.0, from Schizosaccharomyces pombe*. Structure, 2013. **21**(2): p. 220-8.
91. Hochberg, G.K., et al., *The structured core domain of αB-crystallin can prevent amyloid fibrillation and associated toxicity*. Proc. Natl. Acad. Sci. USA, 2014. **111**: p. E1562-70.
92. Laganowsky, A., et al., *Crystal structures of truncated alphaA and alphaB crystallins reveal structural mechanisms of polydispersity important for eye lens function*. Protein Sci., 2010. **19**: p. 1031-1043.
93. Stamler, R., et al., *Wrapping the alpha-crystallin domain fold in a chaperone assembly*. J. Mol. Biol., 2005. **353**(68-79).
94. Weeks, S.D., et al., *Molecular structure and dynamics of the dimeric human small heat shock protein HSPB6*. J. Struct. Biol., 2014. **185**(3): p. 342-354.
95. Hilario, E., et al., *Crystal structures of Xanthomonas small heat shock protein provide a structural basis for an active molecular chaperone oligomer*. J. Mol. Biol., 2011. **408**: p. 74-86.
96. van Montfort, R.L., et al., *Crystal structure and assembly of a eukaryotic small heat shock protein*. Nat. Struct. Biol., 2001. **8**: p. 1025-1030.
97. Stamler, R., et al., *Wrapping the α-Crystallin Domain Fold in a Chaperone Assembly*. J. Mol. Biol., 2005. **353**: p. 68-79.

-
98. Horwitz, J., *Alpha-crystallin*. Exp. Eye Res., 2003. **76**(2).
 99. Sobott, F., et al., *Subunit exchange of multimeric protein complexes. Real-time monitoring of subunit exchange between small heat shock proteins by using electrospray mass spectrometry*. J. Biol. Chem., 2002. **277**: p. 38921-9.
 100. Lentze, N., et al., *Temperature and concentration-controlled dynamics of rhizobial small heat shock proteins*. Eur. J. Biochem., 2004. **271**: p. 2494-2503.
 101. Bova, M.P., et al., *Subunit exchange of small heat shock proteins - Analysis of oligomer formation of alpha A-crystallin and Hsp27 by fluorescence resonance energy transfer and site-directed truncations*. J. Biol. Chem., 2000. **275**: p. 1035-42.
 102. Matuszewska, M., et al., *The small heat shock protein IbpA of Escherichia coli cooperates with IbpB in stabilization of thermally aggregated proteins in a disaggregation competent state*. J Biol Chem, 2005. **280**(13): p. 12292-8.
 103. Datskevich, P.N., E.V. Mymrikov, and N.B. Gusev, *Utilization of fluorescent chimeras for investigation of heterooligomeric complexes formed by human small heat shock proteins*. Biochimie, 2012. **94**(8): p. 1794-1804.
 104. Basha, E., H. O'Neill, and E. Vierling, *Small heat shock proteins and alpha-crystallins: dynamic proteins with flexible functions*. Trends Biochem. Sci., 2012.
 105. Leroux, M.R., et al., *Structure-function studies on small heat shock protein oligomeric assembly and interaction with unfolded polypeptides*. J. Biol. Chem., 1997. **272**(39): p. 24646-56.
 106. Delbecq, S.P. and R.E. Klevit, *One size does not fit all: the oligomeric states of α B crystallin*. FEBS Lett., 2013. **587**(8): p. 1073-80.
 107. Narberhaus, F., *α -crystallin-type heat-shock proteins: Socializing minichaperones in the context of a multi-chaperone network*. Microbiol. Mol. Biol. Rev. , 2002. **66**.
 108. Shi, J., et al., *Cryoelectron microscopy analysis of small heat shock protein 16.5 (Hsp16.5) complexes with T4 lysozyme reveals the structural basis of multimode binding*. J. Biol. Chem., 2013. **288**(7): p. 4819-30.
 109. Jaya, N., V. Garcia, and E. Vierling, *Substrate binding site flexibility of the small heat shock protein molecular chaperones*. Proc. Natl. Acad. Sci. USA, 2009. **106**(37): p. 15604-9.
 110. Basha, E., K.L. Friedrich, and E. Vierling, *The N-terminal arm of small heat shock proteins is important for both chaperone activity and substrate specificity*. J. Biol. Chem., 2006. **281**(52): p. 39943-52.
 111. Morris, A.M., et al., *Glutamic acid residues in the C-terminal extension of small heat shock protein 25 are critical for structural and functional integrity*. FEBS J., 2008. **275**(23): p. 5885-98.
 112. Braun, N., et al., *Multiple molecular architectures of the eye lens chaperone alphaB-crystallin elucidated by a triple hybrid approach*. Proc. Natl. Acad. Sci. USA, 2011. **108**: p. 20491-6.
 113. Haslbeck, M., S. Walke, and T. Stromer, *Hsp26: A temperature-regulated chaperone*. EMBO J., 1999. **18**: p. 6744-6751.
 114. White, H.E., et al., *Multiple distinct assemblies reveal conformational flexibility in the small heat shock protein Hsp26*. Structure, 2006. **14**: p. 1197-1204.
 115. Kennaway, C.K., et al., *Dodecameric structure of the small heat shock protein Acr1 from Mycobacterium tuberculosis*. J. Biol. Chem., 2005. **280**(39): p. 33419-25.
 116. Shashidharamurthy, R., et al., *Mechanism of chaperone function in small heat shock proteins: dissociation of the HSP27 oligomer is required for recognition and binding of destabilized T4 lysozyme*. J. Biol. Chem., 2005. **280**: p. 5281-9.
 117. Aquilina, J.A., et al., *Subunit exchange of polydisperse proteins: mass spectrometry reveals consequences of alphaA-crystallin truncation*. J. Biol. Chem., 2005. **280**: p. 14485-91.
 118. Franzmann, T.M., et al., *The activation mechanism of Hsp26 does not require dissociation of the oligomer*. J. Mol. Biol., 2005. **350**: p. 1083-93.
 119. Stromer, T., et al., *Analysis of the regulation of the molecular chaperone Hsp26 by temperature-induced dissociation - The N-terminal domain is important for oligomer assembly and the binding of unfolding proteins*. J. Biol. Chem., 2004. **279**: p. 11222- 8.

-
120. Franzmann, T.M., et al., *Activation of the chaperone Hsp26 is controlled by the rearrangement of its thermosensor domain*. Mol. Cell, 2008. **29**(2): p. 207-16.
 121. Aquilina, J.A., et al., *Phosphorylation of alphaB-crystallin alters chaperone function through loss of dimeric substructure*. J. Biol. Chem., 2004. **279**(27): p. 28675-80.
 122. Rogalla, T., et al., *Regulation of Hsp27 oligomerization, chaperone function, and protective activity against oxidative stress/tumor necrosis factor alpha by phosphorylation*. J. Biol. Chem., 1999. **274**(27): p. 18947-56.
 123. Giese, K.C. and E. Vierling, *Changes in oligomerization are essential for the chaperone activity of a small heat shock protein in vivo and in vitro*. J. Biol. Chem., 2002. **277**: p. 46310-8.
 124. Yang, H., et al., *The Mycobacterium tuberculosis small heat shock protein Hsp16.3 exposes hydrophobic surfaces at mild conditions: conformational flexibility and molecular chaperone activity*. Protein Sci., 1999. **8**: p. 174-179.
 125. Lindner, R.A., et al., *Structural alterations of alpha-crystallin during its chaperone action*. Eur. J. Biochem., 1998. **258**: p. 170-183.
 126. Mchaourab, H.S., E.K. Dodson, and H.A. Koteiche, *Mechanism of chaperone function in small heat shock proteins. Two-mode binding of the excited states of T4 lysozyme mutants by alphaA-crystallin*. J. Biol. Chem., 2002. **277**: p. 40557-66.
 127. Lindner, R.A., et al., *Mouse Hsp25, a small shock protein. The role of its C-terminal extension in oligomerization and chaperone action*. Eur. J. Biochem., 2000. **267**: p. 1923-32.
 128. Goldberg, A.L., *Protein degradation and protection against misfolded or damaged proteins*. Nature, 2003. **426**(6968): p. 895-9.
 129. Shinohara, H., et al., *Alpha B crystallin and HSP28 are enhanced in the cerebral cortex of patients with Alzheimer's disease*. J Neurol Sci., 1993. **119**(2): p. 203-8.
 130. Renkawek, K., G. Bosman, and W. de Jong, *Expression of small heat-shock protein hsp 27 in reactive gliosis in Alzheimer disease and other types of dementia*. Acta Neuropathol., 1994. **87**(5): p. 511-9.
 131. Kappé, G., et al., *The human genome encodes 10 alpha-crystallin-related small heat shock proteins: HspB1-10*. Cell Stress & Chaperones, 2003. **8**(1): p. 53-61.
 132. Shinohara, H., et al., *Alpha B crystallin and HSP28 are enhanced in the cerebral cortex of patients with Alzheimer's disease*. Neurol Sci, 1993. **119**(2): p. 203-8.
 133. Shemetov, A., A. Seit-Nebi, and N.B. Gusev, *Structure, Properties, and Functions of the Human Small Heat-Shock Protein HSP22 (HspB8, H11, E2IG1): A Critical Review*. J. Neuroscience Res., 2008. **86**: p. 264-269.
 134. Fonte, V., et al., *Interaction of intracellular beta amyloid peptide with chaperone proteins*. Proc. Natl. Acad. Sci. USA, 2002. **99**(14).
 135. Fonte, V., et al., *Suppression of in vivo-amyloid peptide toxicity by overexpression of the Hsp16.2 small chaperone protein*. J. Biol. Chem., 2008. **283**(2).
 136. Delamere, N.A., *The Lens*, in *Duane's Ophthalmology 2006*, Lippincott Williams & Wilkins.
 137. Horwitz, J., *Alpha-crystallin*. Exp Eye Res, 2003. **76**(2): p. 145-53.
 138. Roelofs, M.F., W.C. Boelens, and J. LAB, *Identification of small heat shock protein B8 (HSP22) as a novel TLR4 ligand and potential involvement in the pathogenesis of rheumatoid arthritis*. J. Immunol., 2006. **176**: p. 7021-7027.
 139. Sax, C.M. and J. Piatigorsky, *Expression of the alpha-crystallin/small heat-shock protein/molecular chaperone genes in the lens and other tissues*. Adv. Enzymol. Relat. Areas Mol. Biol., 1994. **69**: p. 155-201.
 140. Jakob, U. and J. Buchner, *Assisting spontaneity: the role of Hsp90 and small Hsps as molecular chaperones*. Trends Biochem. Sci., 1994. **19**(5): p. 205-11.
 141. Stringham, E., et al., *Temporal and spatial expression patterns of the small heat shock (hsp16) genes in transgenic Caenorhabditis elegans*. Mol. Biol. Cell, 1992. **3**(2).
 142. Stringham, E.G. and E.P. Candido, *Transgenic hsp16-lacZ strains of Caenorhabditis elegans as biological monitors of environmental stress*. Environ. Toxicol. Chem., 1994. **13**: p. 1211-20.

-
143. Richmond, C., et al., *Genome-wide expression profiling in Escherichia coli K-12*. Nucleic Acids Res., 1999. **27**(19): p. 3821-35.
 144. González-Márquez, H., C. Perrin, and P. Bracquart, *A 16 kDa protein family overexpressed by Streptococcus thermophilus PB18 in acid environments*. Microbiology, 1997. **5**: p. 1587-1594.
 145. Harndahl, U., R.B. Hall, and K.W. Osteryoung, *The chloroplast small heat-shock protein undergoes oxidation-dependent conformational changes and may protect plants from oxidative stress*. Cell Stress Chaperones, 1999. **4**: p. 129-138.
 146. Kappé, G., J. Leunissen, and W. De Jong, *Evolution and diversity of prokaryotic small heat shock proteins*. Prog. Mol. Subcell. Biol., 2002. **28**: p. 1-17.
 147. Wood, W.B., *The nematode Caenorhabditis elegans*, ed. W.B. Wood. 1988, Cold Spring Harbor, New York: CSHL Press.
 148. Altun, Z.F. and D.H. Hall, *Handbook of C. elegans Anatomy*, WormAtlas, Editor 2012.
 149. Sulston, J.E., et al., *The embryonic cell lineage of the nematode Caenorhabditis elegans*. Dev. Biol., 1983. **100**: p. 64-119.
 150. von Ehrenstein, G. and E. Schierenberg, *Cell lineages and development of Caenorhabditis elegans and other nematodes*, in *Nematodes as biological models*, B.M. Zuckerman, Editor. 1980, Academic Press: New York. p. 2-68.
 151. Zarkower, D., *Somatic sex determination*, in *WormBook*, T.C.e.R. Community, Editor 2006.
 152. Schafer, W.R., *Egg-laying*, in *WormBook2005*, The *C. elegans* Research Community.
 153. Brenner, S., *The genetics of Caenorhabditis elegans*. Genetics, 1974. **77**(1): p. 71-94.
 154. Johnson, T.E., et al., *Arresting development arrests aging in the nematode C. elegans*. Mech. Age. Dev, 1984. **28**: p. 23-40.
 155. Riddle, D.L. and P.S. Albert, in *C. elegans II*, D.L. Riddle, et al., Editors. 1997, Cold Spring Harbor Laboratory Press: Cold Spring Harbor, NY. p. 739-768.
 156. Cassada, R.C. and R.L. Russell, *The dauer larva, a postembryonic developmental variant of the nematode Caenorhabditis elegans*. Dev. Biol, 1975. **46**: p. 326-342.
 157. Riddle, D.L., *The dauer larva*, in *The nematode Caenorhabditis elegans*, W.B. Wood, Editor. 1988, CSHL Press: Cold Spring Harbor, New York. p. 393-412.
 158. Klass, M. and D. Hirsh, *Non-ageing developmental variant of Caenorhabditis elegans*. Nature, 1976. **260**(5551): p. 523-5.
 159. Murphy, C.T. and P.J. Hu, *Insulin/insulin-like growth factor signaling in C. elegans*. WormBook, 2013.
 160. Guarente, L. and C. Kenyon, *Genetic pathways that regulate ageing in model organisms*. Nature, 2000. **408**(6809): p. 255-62.
 161. Kenyon, C., et al., *A C. elegans mutant that lives twice as long as wild type*. Nature, 1993. **366**(6454): p. 461-4.
 162. Maupas, E., *Modes et formes de reproduction des nematodes*. Archives de Zoologie Experimentale et Generale, 1900. **8**: p. 463-624.
 163. Dougherty, E.C. and H.G. Calhoun, *Possible significance of free-living nematodes in genetic research*. Nature, 1948. **161**(4079): p. 29.
 164. Sequencing Consortium, *Genome sequence of the nematode C. elegans: A platform for investigating biology*. Science, 1998. **282**(5396): p. 2012-2018.
 165. Kaletta, T. and M.O. Hengartner, *Finding function in novel targets: C. elegans as a model organism*. Nat Rev Drug Discov, 2006. **5**: p. 387-98.
 166. WUSTL, *The Genome Institute, Washington University School of Medicine*, 2014: <http://genome.wustl.edu/search/?page=10&keywords=roundworm§ions=genomes>.
 167. Holden-Dye, L. and R.J. Walker, *Antihelminthic drugs*, in *WormBook2007*, The *C. elegans* Research Community.
 168. Félix, M.A., *RNA interference in nematodes and the chance that favored Sydney Brenner*. Journal of Biology, 2008. **7**(9): p. 34-56.
 169. Feng, Z., et al., *A C. elegans model of nicotine-dependent behavior: regulation by TRP family channels*. Cell, 2006. **127**(3): p. 621-633.

-
170. Morgan, P.G., E.B. Kayser, and M.M. Sedensky, *C. elegans and volatile anesthetics*, in *WormBook2007*, The *C. elegans* Research Community.
171. Raizen, D.M., et al., *Lethargus is a Caenorhabditis elegans sleep-like state*. *Nature*, 2008. **451**(7178): p. 569-72.
172. Szewczyk, N.J., et al., *Caenorhabditis elegans survives atmospheric breakup of STS-107, space shuttle Columbia*. *Astrobiology*, 2005. **5**(6): p. 690-705.
173. BBC, *University sends worms into space*, in *BBC News2009*, http://news.bbc.co.uk/2/hi/uk_news/england/nottinghamshire/7835020.stm.
174. Rankin, C.H., *From gene to identified neuron to behaviour in Caenorhabditis elegans*. *Nat. Rev. Genet.*, 2002. **3**: p. 622-630.
175. de Bono, M., *Molecular approaches to aggregation behavior and social attachment*. *J. Neurobiol.*, 2003. **54**: p. 78-92.
176. Ashrafi, K., *Obesity and the regulation of fat metabolism*, in *WormBook2007*, The *C. elegans* Research Community.
177. Morley, J.F., et al., *The threshold for polyglutamine-expansion protein aggregation and cellular toxicity is dynamic and influenced by aging in Caenorhabditis elegans*. *Proc. Natl. Acad. Sci. USA*, 2002. **99**(16): p. 10417-22.
178. Reichert, K. and R. Menzel, *Expression profiling of five different xenobiotics using a Caenorhabditis elegans whole genome microarray*. *Chemosphere*, 2005. **61**(2): p. 229-37.
179. van Oosten-Hawle, P. and R.I. Morimoto, *Transcellular chaperone signaling: an organismal strategy for integrated cell stress responses*. *J. Exp. Biol.*, 2014. **217**(1): p. 129-36.
180. Garigan, D., et al., *Genetic analysis of tissue aging in Caenorhabditis elegans: a role for heat-shock factor and bacterial proliferation*. *Genetics*, 2002. **161**(3): p. 1101-12.
181. Pirkkala, L., P. Nykänen, and L. Sistonen, *Roles of the heat shock transcription factors in regulation of the heat shock response and beyond*. *FASEB J.*, 2001. **15**(7): p. 1118-31.
182. Akerfelt, M., R.I. Morimoto, and L. Sistonen, *Heat shock factors: integrators of cell stress, development and lifespan*. *Nat. Rev. Mol. Cell Biol.*, 2010. **11**: p. 545-555.
183. Sarge, K.D., S.P. Murphy, and R.I. Morimoto, *Activation of heat shock gene transcription by heat shock factor 1 involves oligomerization, acquisition of DNA-binding activity, and nuclear localization and can occur in the absence of stress*. *Mol. Cell. Biol.*, 1993. **13**(3): p. 1392-407.
184. An, J.H., et al., *Regulation of the Caenorhabditis elegans oxidative stress defense protein SKN-1 by glycogen synthase kinase-3*. *Proc Natl Acad Sci USA*, 2005. **102**(45): p. 16275-80.
185. An, J.H. and T.K. Blackwell, *SKN-1 links C. elegans mesendodermal specification to a conserved oxidative stress response*. *Genes Dev*, 2003. **17**(15): p. 1882-93.
186. Shore, D.E. and G. Ruvkun, *A cytoprotective perspective on longevity regulation*. *Trends Cell Biol.*, 2013. **23**(9): p. 409-20.
187. Glover-Cutter, K.M., S. Lin, and T.K. Blackwell, *Integration of the unfolded protein and oxidative stress responses through SNK-1/Nrf*. *PLoSGene*, 2013. **9**: p. e1003701.
188. Tullet, J.M., et al., *Direct inhibition of the longevity-promoting factor SKN-1 by insulin-like signaling in C. elegans*. *Cell*, 2008. **132**(6): p. 1025-38.
189. Leiser, S.F., et al., *Life-span extension from hypoxia in Caenorhabditis elegans requires both HIF-1 and DAF-16 and is antagonized by SKN-1*. *J Gerontol A Biol Sci Med Sci*, 2013. **68**(10): p. 1135-44.
190. Robida-Stubbs, S., et al., *TOR signaling and rapamycin influence longevity by regulating SKN-1/Nrf and DAF-16/FoxO*. *Cell Metab*, 2012. **15**(5): p. 713-24.
191. Lant, B. and K.B. Storey, *An Overview of Stress Response and Hypometabolic Strategies in Caenorhabditis elegans: Conserved and Contrasting Signals with the Mammalian System*. *Int. J. Biol. Sci.*, 2010. **6**(1): p. 9-50.
192. Mukhopadhyay, A., S.W. Oh, and H.A. Tissenbaum, *Worming pathways to and from DAF-16/FOXO*. *Exp. Gerontol.*, 2006. **41**(10): p. 928-34.
193. Furuyama, T., et al., *Identification of the differential distribution patterns of mRNAs and consensus binding sequences for mouse DAF-16 homologues*. *Biochem J.*, 2000. **349**(2): p. 629-34.

-
194. Murphy, C.T., et al., *Genes that act downstream of DAF-16 to influence the lifespan of Caenorhabditis elegans*. *Nature*, 2003. **424**(6946): p. 277-83.
 195. Tepper, R.G., et al., *PQM-1 complements DAF-16 as a key transcriptional regulator of DAF-2-mediated development and longevity*. *Cell*, 2013. **154**(3): p. 676-90.
 196. Takahashi, Y., et al., *Asymmetric Arginine Dimethylation Determines Life Span in C. elegans by Regulating Forkhead Transcription Factor DAF-16*. *Cell Metab*, 2011. **13**(5): p. 505-16.
 197. Chiang, W.C., et al., *C. elegans SIRT6/7 homolog SIR-2.4 promotes DAF-16 relocalization and function during stress*. *PLoS Genet*, 2012. **8**(9): p. e1002948.
 198. Hsin, H. and C. Kenyon, *Signals from the reproductive system regulate the lifespan of C. elegans*. *Nature*, 1999. **399**(6734): p. 362-6.
 199. Hsu, A.L., C.T. Murphy, and C. Kenyon, *Regulation of Aging and Age-Related Disease by DAF-16 and Heat-Shock Factor*. *Science*, 2003. **300**.
 200. Wolff, S., et al., *SMK-1, an essential regulator of DAF-16-mediated longevity*. *Cell*, 2006. **124**(5): p. 1039-53.
 201. Fischer, M., et al., *Vitellogenins increase stress resistance of Caenorhabditis elegans after Photorhabdus luminescens infection depending on the steroid-signaling pathway*. *Microbes Infect*, 2013. **15**(8): p. 569-78.
 202. Mak, H.Y. and G. Ruvkun, *Intercellular signaling of reproductive development by the C. elegans DAF-9 cytochrome P450*. *Development*, 2004. **131**(8): p. 1777-86.
 203. Murakami, M., M. Koga, and Y. Ohshima, *DAF-7/TGF-beta expression required for the normal larval development in C. elegans is controlled by a presumed guanylyl cyclase DAF-11*. *Mech Dev*, 2001. **109**(1): p. 27-35.
 204. Li, W., S.G. Kennedy, and G. Ruvkun, *daf-28 encodes a C. elegans insulin superfamily member that is regulated by environmental cues and acts in the DAF-2 signaling pathway*. *Genes Dev*, 2003. **17**(7): p. 844-58.
 205. Lithgow, G.J. and G.A. Walker, *Stress resistance as a determinate of C. elegans lifespan*. *Mech Ageing Dev*, 2002. **123**(7): p. 765-71.
 206. Murphy, C.T., *The search for DAF-16/FOXO transcriptional targets: Approaches and discoveries*. *Exp. Gerontol*, 2006. **41**(10): p. 910-921.
 207. Kenyon, C. and C.T. Murphy, *Enrichment of regulatory motifs upstream of predicted DAF-16 targets*. *Nat. Genet*, 2006. **38**(4): p. 397-8.
 208. Stout, G., et al., *Insulin/IGF-1-mediated longevity is marked by reduced protein metabolism*. *Mol. Sys. Biol.*, 2013. **9**(679).
 209. Puig, O. and R. Tjian, *Transcriptional feedback control of insulin receptor by dFOXO/FOXO1*. *Genes Dev.*, 2005. **19**(20): p. 2435-46.
 210. Kauffman, A.L., et al., *Insulin signaling and dietary restriction differentially influence the decline of learning and memory with age*. *PLoS Biology*, 2010. **8**(5): p. e1000372.
 211. Kurapati, R., et al., *Increased hsp22 RNA levels in Drosophila lines genetically selected for increased longevity*. *J Gerontol A Biol Sci Med Sci*, 2000. **55**(11): p. B552-9.
 212. Wadhwa, R., et al., *Pro proliferative functions of Drosophila small mitochondrial heat shock protein 22 in human cells*. *J. Biol. Chem.*, 2010. **285**(6): p. 3833-9.
 213. Walker, G.A. and G.J. Lithgow, *Lifespan extension in C. elegans by a molecular chaperone dependent upon insulin-like signals*. *Aging Cell*, 2003. **2**(2): p. 131-9.
 214. Lithgow, G.J., et al., *Thermotolerance and extended life-span conferred by single-gene mutations and induced by thermal stress*. *Proc Natl Acad Sci USA*, 1995. **92**(16): p. 7540-4.
 215. Morley, J.F. and R.I. Morimoto, *Regulation of Longevity in Caenorhabditis elegans by Heat Shock Factor and Molecular Chaperones*. *Mol. Biol. Cell*, 2004. **15**(2): p. 657-64.
 216. Halaschek-Wiener, J., et al., *Analysis of long-lived C. elegans daf-2 mutants using serial analysis of gene expression*. *Genome Res*, 2005. **15**: p. 603-15.
 217. Krause, M., *Structural and functional characterization of small heat shock proteins of the nematode Caenorhabditis elegans*, in *Lehrstuhl für Biotechnologie, Technische Universität München 2013*, Doctoral Thesis.
 218. Kohara, Y., <http://nematode.lab.nig.ac.jp/>, in *The Nematode Expression Pattern DataBase 2005*.

-
219. Russnak, R., D. Jones, and E. Candido, *Cloning and analysis of cDNA sequences coding for two 16 kilodalton heat shock proteins (hsps) in Caenorhabditis elegans: homology with the small hsps of Drosophila*. *Nucleic Acids Res.*, 1983. **11**(10).
220. Weinfurtnner, D., *Strukturelle und funktionelle Charakterisierung einer Familie kleiner Hitzeschockproteine*, in *Lehrstuhl für Biotechnologie, Technische Universität München* 2008, Doctoral Thesis.
221. Jones, D., et al., *Transgenic strains of the nematode C. elegans in biomonitoring and toxicology: effects of captan and related compounds on the stress response*. *Toxicology*, 1996. **109**(2-3): p. 119-27.
222. Shin, H., et al., *Gene expression profiling of oxidative stress response of C. elegans aging defective AMPK mutants using massively parallel transcriptome sequencing*. *BMC Research Notes*, 2011. **4**(34): p. 1756-72.
223. Jones, D. and E.P. Candido, *Feeding is inhibited by sublethal concentrations of toxicants and by heat stress in the nematode Caenorhabditis elegans: relationship to the cellular stress response*. *J. Exp. Zool.*, 1999. **284**(2): p. 147-157.
224. Shapira, M., et al., *A conserved role for a GATA transcription factor in regulating epithelial innate immune responses*. *Proc Natl Acad Sci USA*, 2006. **103**(38): p. 14086-91.
225. Junkersdorf, B., H. Bauer, and H.O. Gutzeit, *Electromagnetic fields enhance the stress response at elevated temperatures in the nematode Caenorhabditis elegans*. *Bioelectromagnetics*, 2000. **21**(2): p. 100-6.
226. Zhu, J., et al., *Reprogramming of early embryonic blastomeres into endodermal progenitors by a Caenorhabditis elegans GATA factor*. *Genes & Development*, 1998. **12**: p. 3809-3814.
227. Leroux, M., et al., *Unique structural features of a novel class of small heat shock proteins*. *J. Biol. Chem.*, 1997. **272**(19): p. 12847-53.
228. Linder, B., et al., *Molecular characterization of a novel, developmentally regulated small embryonic chaperone from Caenorhabditis elegans*. *J. Biol. Chem.*, 1996. **271**(47).
229. Hockertz, M.K., I. Clark-Lewis, and E.P. Candido, *Studies of the small heat shock proteins of Caenorhabditis elegans using anti-peptide antibodies*. *FEBS Lett*, 1991. **280**(2): p. 375-8.
230. Shim, J., S. Im, and J. Lee, *Tissue-specific expression, heat inducibility, and biological roles of two hsp16 genes in Caenorhabditis elegans*. *FEBS Lett.*, 2003. **537**.
231. Liu, T., K.K. Zimmerman, and G.I. Patterson, *Regulation of signaling genes by TGFbeta during entry into dauer diapause in C. elegans*. *BMC Dev Biol*, 2004. **4**(11): p. 1471-83.
232. Freedman, J., et al., *The Novel Metallothioneine Genes of Caenorhabditis elegans*. *J Biol Chem*, 1993. **268**(4): p. 2554-64.
233. Liang, V., et al., *Altered proteostasis in aging and heat shock response in C. elegans revealed by analysis of the global and de novo synthesized proteome*. *Cell Mol Life Sci*, 2014.
234. Cui, Y., et al., *Toxicogenomic analysis of Caenorhabditis elegans reveals novel genes and pathways involved in the resistance to cadmium toxicity*. *Genome Biol*, 2007. **8**(6): p. R122.
235. Reinke, V., et al., *Genome-wide germline-enriched and sex-biased expression profiles in Caenorhabditis elegans*. *Development*, 2004. **131**(2): p. 311-23.
236. Baugh, L.R., et al., *Composition and dynamics of the Caenorhabditis elegans early embryonic transcriptome*. *Development*, 2003. **130**(5): p. 889-900.
237. Levin, M., et al., *Developmental milestones punctuate gene expression in the Caenorhabditis embryo*. *Dev. Cell*, 2012. **22**(5): p. 1101-8.
238. Tabuse, Y., T. Nabetani, and A. Tsugita, *Proteomic analysis of protein expression profiles during Caenorhabditis elegans development using two-dimensional difference gel electrophoresis*. *Proteomics*, 2005. **11**: p. 2876-91.
239. Mohri-Shiomi, A., L. Vega, and D. Garsin, *The role of sHSPs and protein damage during bacterial infection in C. elegans*, in *16th International C. elegans Meeting* 2007: UCLA.
240. van Montfort, R., C. Slingsby, and E. Vierling, *Structure and function of the small heat shock protein/alpha-crystallin family of molecular chaperones*. *Adv. Protein Chem.*, 2001. **59**: p. 105-156.
241. Nehrke, K., *A reduction in intestinal cell pHi due to loss of the Caenorhabditis elegans Na/H-exchanger NHX-2 increases life span*. *J. Biol. Chem.*, 2003. **278**(45).

-
242. Wadsworth, W. and D. Riddle, *Acidic intracellular pH shift during Caenorhabditis elegans larval development*. Proc. Natl. Acad. Sci. USA, 1988. **85**(22).
243. Oka, T. and M. Futai, *Requirement of V-ATPase for Ovulation and Embryogenesis in Caenorhabditis elegans*. J. Biol. Chem., 2000. **275**: p. 29556-61.
244. Kastenmüller, A., *Elektronenmikroskopische Untersuchungen zur Assemblierung und Struktur von kleinen Hitzeschockproteinen*, in *Doctoral Thesis 2011*, Fachgebiet für Elektronenmikroskopie, Technische Universität München.
245. Teorell, I. and E. Stenhagen, *Ein Universalpuffer für den pH-Bereich 2.0-12.0*. Biochem. Z., 1938. **299**: p. 416-9.
246. Caspers, G., J. Leunissen, and W. De Jong, *The expanding small heat shock protein family*. J. Mol. Evol., 1995. **40**(3): p. 238-248.
247. Clark, A.R., et al., *Crystal Structure of R120G Disease Mutant of Human α B-Crystallin Domain Dimer Shows Closure of a Groove*. J. Mol. Biol., 2011. **408**: p. 118-134.
248. Walden, H., *Selenium incorporation using recombinant techniques*. Acta Crystallogr D, 2010. **66**(4): p. 352-7.
249. van den Ent, F. and J. Löwe *Expression of selenomethionine substituted proteins in non-methionine auxotrophic E. coli*. 2003.
250. Friedrich, K., et al., *Interactions between small heat shock protein subunits and substrate in small heat shock protein-substrate complexes*. J. Biol. Chem., 2004. **279**: p. 1080-1089.
251. Basha, E., et al., *Chaperone activity of cytosolic small heat shock proteins from wheat*. Eur. J. Biochem., 2004. **271**: p. 1426-36.
252. Buchner, J., H. Grallert, and U. Jakob, *Molecular Chaperones*, in *Methods in Enzymology*. 1998, Academic Press.
253. Mogk, A., et al., *Small heat shock proteins, ClpB and the DnaK system form a functional triade in reversing protein aggregation*. Mol. Microbiol., 2003. **50**: p. 585- 595.
254. Veinger, L., et al., *The small heat-shock protein IbpB from Escherichia coli stabilizes stress-denatured proteins for subsequent refolding by a multichaperone network*. J. Biol. Chem., 1998. **273**: p. 11032-11037.
255. Evans, T.C., *Transformation and microinjection*, in *WormBook*, T.C.e.R. Community, Editor 2006.
256. Schrimpf, S.P., et al., *Comparative Functional Analysis of the Caenorhabditis elegans and Drosophila melanogaster Proteomes*. PLoS Biology, 2009. **7**(3): p. 616-627.
257. Fu, X., et al., *Multilevel structural characteristics for the natural substrate proteins of bacterial small heat shock proteins*. Protein Sci., 2013. **23**(2): p. 229-237.
258. Grant, B. and D. Hirsh, *Receptor-mediated Endocytosis in the Caenorhabditis elegans Oocyte*. Mol. Biol. Cell, 1999. **10**: p. 4311-4326.
259. Caudy, A., et al., *A micrococcal nuclease homologue in RNAi effector complexes*. Nature, 2003. **425**(25): p. 411-4.
260. Bennardini, F., A. Wrzosek, and M. Chiesi, *Alpha B-crystallin in cardiac tissue. Association with actin and desmin filaments*. Circ Res., 1992. **71**(2): p. 288-94.
261. Kötter, S., et al., *Human myocytes are protected from titin aggregation-induced stiffening by small heat shock proteins*. J. Cell Biol., 2014. **204**(20): p. 187-202.
262. Haslbeck, M., et al., *Structural dynamics of archaeal small heat shock proteins*. J. Mol. Biol., 2008. **378**(2): p. 362-374.
263. Patel, S., E. Vierling, and F. Tama, *Replica exchange molecular dynamics simulations provide insight into substrate recognition by small heat shock proteins*. Biophys. J., 2014. **106**(12): p. 2644-55.
264. Smith, F.A. and J.A. Raven, *Intracellular pH and its regulation*. Ann. Rev. Plant Physiol., 1979. **30**: p. 289-311.
265. Orij, R., S. Brul, and G.J. Smits, *Intracellular pH is a tightly controlled signal in yeast*. Biochim. Biophys. Acta, 2011. **1810**(10): p. 933-44.
266. Kulichikhin, K., et al., *Effect of oxygen concentration on intracellular pH, glucose-6-phosphate and NTP content in rice (Oryza sativa) and wheat (Triticum aestivum) root tips: in vivo 31P-NMR study*. Physiologia Plantarum, 2007. **129**(3): p. 507-518.

-
267. Bagar, T., et al., *Live-cell imaging and measurement of intracellular pH in filamentous fungi using a genetically encoded ratiometric probe*. *Eukaryot Cell*, 2009. **8**(5): p. 703-12.
268. Boron, F., F. Walter, and E.L. Boulpaep, *Medical Physiology: A Cellular And Molecular Approach*. 2004: Elsevier/Saunders.
269. Duncan, G. and M. Wormstone, *Physiology of the Lens*, in *Duane's Ophthalmology* 2006, Lippincott, Williams & Wilkins.
270. Vaughan-Jones, R.D., K.W. Spitzer, and P. Swietach, *Intracellular pH regulation in heart*. *J. Mol. Cell. Cardiol.*, 2009. **46**(3): p. 318-31.
271. Waugh, A. and A. Grant, *Anatomy and Physiology in Health and Illness*. 2007: Churchill Livingstone Elsevier.
272. Darnell, J., H. Lodish, and D. Baltimore, *Molecular Cell Biology*. 1986, New York: Scientific American Books, Inc.
273. Bennardini, F., A. Wrzosek, and M. Chiesi, *α B-crystallin in cardiac tissue. Association with actin and desmin filaments*. *Circ. Res*, 1992. **71**: p. 288-294.
274. Khong, T.K., et al., *In-vivo intracellular pH at rest and during exercise in patients with essential hypertension*. *J Hypertens*, 2001. **19**(9): p. 1595-1600.
275. Schneider, W.J., *Vitellogenin receptors: oocyte-specific members of the low-density lipoprotein receptor supergene family*. *Int. Rev. Cytol.*, 1996. **166**: p. 103-137.
276. Kourtis, N., V. Nikolettou, and N. Tavernarakis, *Small heat-shock proteins protect from heat-stroke-associated neurodegeneration*. *Nature*, 2012. **490**(7419): p. 213-8.
277. Rahman, M.M., et al., *Down-regulation of tricarboxylic acid (TCA) cycle genes blocks progression through the first mitotic division in *Caenorhabditis elegans* embryos*. *Proc. Natl. Acad. Sci. USA*, 2014. **111**(7): p. 2602-7.
278. Olson, S.K., et al., *Hierarchical assembly of the eggshell and permeability barrier in *C. elegans**. *J. Cell Biol.*, 2012. **198**(4): p. 731-748.
279. Fu, X., et al., *In vivo substrate diversity and preference of small heat shock protein IbpB as revealed by using a genetically incorporated photo-cross-linker*. *J. Biol. Chem.*, 2013. **288**(44): p. 31646-54.
280. Sun, Y. and T.H. MacRae, *Small heat shock proteins: molecular structure and chaperone function*. *Cell. Mol. Life Sci.*, 2005. **62**: p. 2460-76.
281. Ko, S., I. Kawasaki, and Y.H. Shim, *PAB-1, a *Caenorhabditis elegans* poly(A)-binding protein, regulates mRNA metabolism in germline by interacting with CGH-1 and CAR-1*. *PLoS One*, 2013. **8**(12): p. 84798-810.
282. Boag, P.R., A. Nakamura, and T.K. Blackwell, *A conserved RNA-protein complex component involved in physiological germline apoptosis regulation in *C. elegans**. *Development*, 2005. **132**(22): p. 4975-86.
283. Paz-Gómez, D., E. Villanueva-Chimal, and R.E. Navarro, *The DEAD Box RNA helicase VBH-1 is a new player in the stress response in *C. elegans**. *PLoS One*, 2014. **9**(5): p. 97924.
284. Updike, D. and S. Strome, *P granule assembly and function in *Caenorhabditis elegans* germ cells*. *J. Androl.*, 2010. **31**(1): p. 53-60.
285. Vidal, M., *Worm Interactome Database vers. 8*, 2009: http://interactome.dfci.harvard.edu/C_elegans/index.php.
286. Tijsterman, M., et al., *Helicase MUT-14-dependent gene silencing triggered in *C. elegans* by short antisense RNAs*. *Science*, 2002. **295**(5555): p. 694-697.
287. Seydoux, G., et al., *Repression of gene expression in the embryonic germ lineage of *C. elegans**. *Nature*, 1996. **382**(6593): p. 713-6.
288. Stiernagle, T., *Maintenance of *C. elegans**, in **C. elegans: A Practical Approach**, I. Hope, Editor. 1999, Oxford University Press. p. 51-67.
289. Sun, L., et al., *The Lid Domain of *Caenorhabditis elegans* Hsc70 Influences ATP Turnover, Cofactor Binding and Protein Folding Activity*. *PLoS ONE*, 2012. **7**(3): p. 33980-93.
290. Mullis, K., et al., *Specific enzymatic amplification of DNA in vitro: the polymerase chain reaction*. *Biotechnology*, 1986. **24**: p. 17-27.
291. Sambrook, J. and D.W. Russell, *Molecular Cloning: A Laboratory Manual*. 3 ed. 2001, Cold Spring Harbor, New York, USA: CSHL Press.

-
292. Inoue, H., H. Nojima, and H. Okayama, *High efficiency transformation of Escherichia coli with plasmids*. *Gene*, 1990. **96**: p. 23-28.
293. Boulin, T., J.F. Etchberger, and O. Hobert, *Reporter gene fusions*, in *WormBook*, T.C.e.R. Community, Editor 2006.
294. Fling, S.P. and D.S. Gregerson, *Peptide and protein molecular weight determination by electrophoresis using a high-molarity tris buffer system without urea*. *Anal Biochem*, 1986. **155**(1): p. 83-8.
295. Schuck, P., *Size-distribution analysis of macromolecules by sedimentation velocity ultracentrifugation and lamm equation modeling*. *Biophys. J.*, 2000. **78**(3): p. 1606-19.
296. Hope, I.A., *C. elegans: A Practical Approach*. Practical Approach Series, ed. B.D. Hames. 1999: Oxford University Press.
297. Apfeld, J. and C. Kenyon, *Regulation of lifespan by sensory perception in Caenorhabditis elegans*. *Nature*, 1999. **402**(6763): p. 804-9.
298. Mitchell, D.H., et al., *Synchronous growth and aging of Caenorhabditis elegans in the presence of fluorodeoxyuridine*. *Journal of Gerontology*, 1979. **34**(1): p. 28-36.

DECLARATION

This Doctoral Thesis was conducted at the Chair for Biotechnology, Department of Chemistry, at the Technische Universität München from June 2010 to October 2014. I herewith declare that I wrote this Dissertation on my own and performed all experiments myself, unless explicitly indicated. All cooperation partners, resources and references are listed.

This Thesis has not been submitted to any other Board of Examiners.
Major parts of this work will be published in a scientific journal.

Garching, 10.09.2014

Tilly Fleckenstein